



307F

REPORT NO.
65008-00-04

OCTOBER
1964

STANDARD FORM 602

N 65 10372	(THRU)
(ACCESSION NUMBER)	
307	1
(PAGE)	(CODE)
CR 53336	38
(NASA CR OR TNX OR AD NUMBER)	(CATEGORY)

CR 53336

FINAL REPORT

CONTRACT NASw-615

OTS PRICE

XEROX \$ 2.00 FS
MICROFILM \$ 1.75 mf

PREPARED FOR
THE NATIONAL AERONAUTICS
AND SPACE ADMINISTRATION
CONTRACT NO. NASW-615
A CONTINUATION OF THE
PROGRAM ORIGINATED UNDER
CONTRACT NO. NAS5-664

LIQUID PROPELLANT
LOSSES DURING
SPACE FLIGHT

LIQUID PROPELLANT LOSSES DURING SPACE FLIGHT

FINAL REPORT [1965-1966] [1965]

ON

CONTRACT NO. NASw-615

Report No. 65008-00-04

1412702

(Arthur D.) Little, Inc.
Cambridge, Massachusetts

Approved for Distribution by:

Richard B. Hinckley
Richard B. Hinckley
Project Director

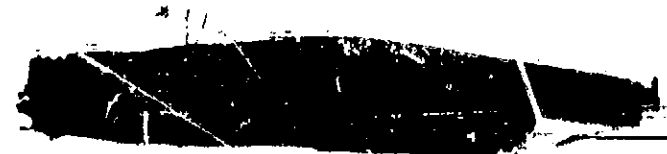
1965 10/7, 1965

Prepared

for

NATIONAL AERONAUTICS AND SPACE ADMINISTRATION
OFFICE OF LAUNCH VEHICLE PROGRAMS
LIQUID ROCKET ENGINES PROGRAM

(N/A) Contract Number NASw-615



ACKNOWLEDGEMENTS

The following personnel of Arthur D. Little, Inc., were associated with this program.

Charles Apt	Jere L. Lundholm
Richard P. Berthiaume	Max Mellner
Igor A. Black	Reed Moffitt
Jacques M. Bonneville	Robert R. Perron
Russell L. Bowen	Albert H. Rawdon, Jr.
Paul R. Doherty	Frank E. Ruccia
Alfred G. Emslie	Peter F. Strong
Arthur A. Fowle	Joseph P. Sullivan
Frank Gabron	Virginia R. Valeri
Peter E. Glaser	Ann J. Whittier
Richard B. Hinckley	Norman M. Wiederhorn
Reed H. Johnston	

We should like to acknowledge the assistance of the following university personnel who worked as consultants for us on this program.

Professor Sydney Goldstein, Chairman, Department of Applied Mathematics
Harvard University

Professor Robley D. Evans, Department of Physics—
Massachusetts Institute of Technology

Professor Gerald V. Bull, Department of Engineering Sciences
McGill University

We should also like to acknowledge the assistance of
Mr. Oscar Bessie and Mr. Jack Phillips of NASA Headquarters and
Dr. R. J. Brun, Mr. James Kramer and Mr. James Barber of the NASA
Lewis Research Center in the conduct of this work.

TABLE OF CONTENTS

Part I	Introduction
Part II	The Performance of Multilayer Insulations
Part III	The Insulation Tank Program
Part IV	Effect of Meteoroid-Bumper Debris on Multilayer Insulation
Part V	Mechanical Test Program on a Specific Multilayer Insulation System
Part VI	Abstracts of Reports on the Space Environment
Part VII	Abstracts of Reports on the Evaluation of Meteoroid Bumper Protection Systems

PART I

INTRODUCTION

I. INTRODUCTION

The work summarized herein was accomplished under Contract Nos. ~~NAS5-664~~ and ~~NASw-615~~ during the period September 1, 1960, through September 30, 1963. The original contract authorized Arthur D. Little, Inc., to obtain scientific information concerning the space environment and its effects on vehicle stored liquid propellants. Those influences found in the space environment, both individually and in combination, that tend to reduce the amount, the stability, and the energy content of the propellants as well as jeopardize the effectiveness of the surrounding structures were to be investigated.

General goals established for this effort were: (1) collecting existing data pertinent to the subject, (2) initiating the theoretical analyses of the interactions of the space environment for the liquid hydrogen-liquid oxygen system, (3) planning experiments for inclusion in satellites where theory indicated gaps that could not be filled by on-the-ground experiments, and (4) experimentally determining the thermal properties of probable structural and insulation materials at low temperature.

Modifications to the basic contract later established specific tasks which could be divided into the following areas: (1) space environment, (2) interaction of thermal radiation with the propellant and its storage system, (3) interaction of meteoroids with the propellant and its storage system, and (4) interaction of ionizing

radiation with the propellant and its storage system. The program objectives were to provide techniques, methodology, and data for the evaluation of liquid propellant storage system concepts and to provide a basis for the design of optimum systems for vehicles for any mission within the solar system.

Over the contract period, however, data has become available in increasing quantities from satellite and probe experiments, independent research reported in the literature, and other programs such as that at Arthur D. Little, Inc. Much of this data, especially that on meteoroids and ionizing radiation, indicates that these problems may be less severe (from the viewpoint of liquid propellants) than anticipated originally. Lately, it has been apparent that the U. S. space programs require engineering design data on the conservation of cryogenic propellants and/or cryogenics in use in ecological systems, together with methods for assimilating and using the available data and that which will be obtained in the near future. With the advent of Contract No. NASw-615, therefore, NASA reoriented the program to make it consistent with the existing need for acquiring data and design solutions for cryogenic propellant storage in space.

This report is submitted in partial fulfillment of our contractual responsibilities under Contract No. NASw-615 with the National Aeronautics and Space Administration. It presents a brief outline of the work accomplished by Arthur D. Little, Inc., under Contract Nos. NAS5-664 and NASw-615 in the areas of the space

environment and theoretical analyses of the interaction of meteoroids with the propellant and its storage system. Our reports on the space environment were published under the initial contract and, therefore, are treated only briefly herein.

Our supply of reports in these two areas has been exhausted. Accordingly, we have included a listing of the technical reports issued on these two subjects, together with an abstract of the contents of each report and the ASTIA number of the report as known to us. All reports, referenced herein, that were issued subsequent to April 1962 are available from:

Office of Scientific and Technical Information
National Aeronautics and Space Administration
Attn: Code AFSS-AD
Washington, D. C. 20546

The major portion of the theoretical work on the solution of the meteoroid problem has been conducted by McGill University under subcontract to Arthur D. Little, Inc. Consequently, this work is referenced herein but not described in detail.*

Development of successful insulation systems, installation on tankage, and collection and reduction of data necessarily will require longer periods of time than do analytical investigation. NASA and

*The McGill University final report is being prepared for publication and will be issued when available.

Arthur D. Little, Inc., therefore, by mutual agreement, plan to dispense with the distribution of quarterly reports and will issue a final contract report only. Topical reports, however, may be issued when data considered to be of particular significance to programs in being is available. _____

A continuing investigation of the problems associated with cryogenic storage presently is being negotiated with the Lewis Research Center. This investigation will be concerned primarily with the development of thermal insulation systems suitable for use in the space environment and the acquisition of experimental data supporting these developments.

In our earlier studies, a broader scope of investigation was undertaken and, consequently, quarterly reports were issued to an extensive group of interested contractors and Government agencies, to assure dissemination of the latest information at frequent intervals. Much of the data published was based on collations of published information, mathematical analyses of expected phenomena, and laboratory investigations of thermal performance. Such data was amenable to frequent publication.

The follow-on investigations, however, are centered around insulation development and experimental data obtained on small-scale tankage.

PART II

THE PERFORMANCE OF MULTILAYER INSULATIONS

<u>TABLE OF CONTENTS</u>		<u>PAGE</u>
I. SUMMARY		II-1
A. Purpose and Scope		II-1
B. Approach		II-1
C. Conclusions		II-2
D. Recommendations		II-3
II. INTRODUCTION		II-4
III. THEORETICAL INSULATION PERFORMANCE		II-7
A. Gas Pressure within Multilayer Insulations		II-7
1. Edge Pumping		II-8
2. Broadside Pumping of Perforated Radiation Shields		II-11
3. Effects of Static Gas Density		II-13
B. Radiation Transfer within Multilayer Insulations		II-15
1. Radiation Transfer Through Perforated Radiation Shields		II-15
2. Radiation Transfer by Closely Spaced Shields		II-17
3. Radiation Transfer Through Seams and Penetrations		II-18
a. Assumptions and Method of Calculation		II-20
b. Heat Input due to a Joint Between Two Radiation Shields		II-25
c. Heat Input due to the Penetration of a Pipe Through Radiation Shields		II-33
C. Gas Leakage From Cryogenic Fuel Tanks		II-36
1. Minimum Heat Flux Through a Stack of Perforated Radiation Shields		II-36
D. Conductive Heat Leaks at Discontinuities Due to Joints, Supports, and Piping Attachments		II-47
1. Weak-Thermal Shorts		II-48
2. Strong Thermal Shorts		II-50

	<u>PAGE</u>
3. Effect of Internal Radiation in Pipes	II-52
a. Pipe with Length-to-Diameter Ratio of 3	II-53
b. Pipe with Length-to-Diameter Ratio of 9	II-54
4. The Possibility of Scaling	II-54
a. Insulation Blanket	II-55
b. Penetrations	II-58
IV. INSULATION SYSTEMS	II-60
V. EXPERIMENTAL APPARATUS	II-68
A. Design Considerations	II-68
B. Description of the Apparatus	II-70
1. Guarded Cold Plate	II-70
2. Warm Plate	II-73
3. Sample Chamber	II-74
4. Liquid Nitrogen Guard Vessel	II-75
5. Bell Jar	II-75
C. Instrumentation	II-75
1. Vacuum System	II-75
2. Temperature Measurement	II-77
3. Gas Pressure Control Device	II-77
4. Automatic Boil-Off Rate Recorders	II-80
a. Low Boil-Off Rates	II-80
b. High Boil-Off Rates	II-80
D. Test Procedure	II-80

	<u>PAGE</u>
E. Calibration and Reproducibility	II-86
1. Electric Heater	II-86
2. Standard Sample	II-88
F. Effect of Discontinuity (Edge Effects)	II-89
1. Analysis of Edge Effects	II-90
2. Insertion of a Buffer Zone	II-93
a. Required Width of Buffer Zone	II-94
b. Interaction of Buffer Zone with Sample	II-96
VI. EXPERIMENTAL RESULTS	II-100
A. Density	II-100
B. Mechanical Load	II-103
C. Temperature	II-106
D. Residual Gas Pressure	II-115
E. Perforations	II-119
F. Discontinuities	II-121
G. Emissivity	II-127
H. Contact Resistance	II-128
I. Foam-Filled Honeycomb Insulation	II-130
J. Polyurethane Foam Insulation	II-138
K. Microfiber Glass Wool	II-143
L. Edge Effects	II-147
1. Turned-Up Edges	II-147
2. Emissivity of Edge Boundaries	II-147
3. Effect of Edge Wall Temperature Variation	II-149

	<u>PAGE</u>
4. Effects of Plate Separation —	II-151
5. <u>Effects of Sample Edge Treatments</u> ———	II-151
6. <u>Effectiveness of Buffer Zone</u> —————	II-157
7. <u>Conclusions</u>	II-160
M. <u>Spacer Material with 11% Support Area</u>	II-161
N. <u>Comparison of Two Radiation Shield Materials</u>	II-163
O. <u>Combination of Multilayer and Foam</u> —————	II-163
P. <u>Penetrations</u>	II-166
VII. <u>ABSTRACTS OF PREVIOUSLY ISSUED REPORTS</u> —————	II-169

LIST OF FIGURES

<u>FIGURE</u>		<u>PAGE</u>
II-III-1	Mean Free Path of a Molecule Confined Between Two Parallel Plates	II-9
II-III-2	Radiation Transfer Through Perforated Shield	II-15
II-III-3	One-Way Energy Flux Between Two Foils Versus Gap Width	II-19
II-III-4	Gap Between Two Panels of Multilayer Insulation	II-21
II-III-5	Effect of an Increment Δq in Heat Flux to an Interior Shield in an Insulation Panel	II-24
II-III-6	Reduced Variables Used to Describe the Radiation Transfer in the Gap	II-24
II-III-7	Plot of Equation II-III-37	II-28
II-III-8	Effective Gap δ in Units of the Insulation Thickness d , for Various Values of the Shielding Factor $n(\frac{2}{\epsilon} - 1)$	II-30
II-III-9	Relationship of Gap Width to Percentage Heat Leak at Seams	II-32
II-III-10	Vent Pipe Penetrating Multilayer Shields	II-34
II-III-11	Heat Flux Through 100 Perforated Shields as a Function of Perforation Factor for Various Hydrogen Gas Flow Rates	II-41
II-III-12	Direct Venting of Leaking Gas by Double-Walled Tank Construction	II-42
II-III-13	Gas Flow Pattern for Closely Spaced Perforations	II-44
II-III-14	Radiation Flow Pattern for Closely Spaced Perforations	II-44
II-III-15	Gas Flow Pattern for Widely Spaced Perforations	II-46
II-III-16	Radiation Flow Pattern for Widely Spaced Perforations	II-46
II-III-17	Maximum Width of Various Thermal Shock Materials Penetrating Multilayer Insulations	II-49

<u>FIGURE</u>		<u>PAGE</u>
II-III-18	Techniques for Decreasing the Effect of Thermal Shorts	II-51
II-IV-1	Enlarged View of Typical Spacer Materials	II-67
II-V-1	Double-Guarded Cold Plate Thermal Conductivity Apparatus	II-71
II-V-2	Cross-Section of Double-Guarded Cold Plate Thermal Conductivity Apparatus	II-72
II-V-3	Instrumentation for Double-Guarded Cold Plate Thermal Conductivity Apparatus	II-76
II-V-4	Gas Pressure Control Device	II-79
II-V-5	Apparatus for Recording Low Boil-Off Rates	II-81
II-V-6	Rotating Face Attachment to Wet-Test Meter for Recording	II-82
II-V-7	Variation of Boil-Off Rate with Electric Heater Input	II-87
II-V-8	Sample Between Circular Plates and Surrounded by Vertical Plates	II-90
II-V-9	Sample Width Annular Buffer Zone	II-93
II-V-10	Heat Flow Pattern in Buffer Zone	II-94
II-V-11	Interaction Between Buffer and Sample with No-Flux End Walls	II-96
II-VI-1	The Contribution of Solid Conduction and Radiant Heat Transfer to the Thermal Conductivity of Multilayer Insulations	II-101
II-VI-2	Effect of Density on Thermal Conductivity	II-102
II-VI-3	Effect of Mechanical Loading on Heat Flux of Multilayer Insulations	II-103
II-VI-4	Effect of Compressive Loading on Product of Thermal Conductivity and Density	II-107
II-VI-5	Effect of Warm Plate Temperature on Heat Flux	II-112

<u>FIGURE</u>		<u>PAGE</u>
II-VI-6	Effect of Boundary Temperature on the Mean Apparent Thermal Conductivity and on Heat Flux of Multiple-Layer Insulations	II-113
II-VI-7	Effect of Warm Boundary Temperature on Heat Flux and Thermal Conductivity	II-114
II-VI-8	Effect of Helium Gas Pressure on Thermal Conductivity	II-116
II-VI-9	The Dependence of Thermal Conductivity on Gas Pressure of Typical Powders, Fibers, and Multilayer Insulations	II-117
II-VI-10	Effect of Perforations on Heat Flux	II-119
II-VI-11	Effect of Diameter of Perforations on Heat Flux	II-120
II-VI-12	Configuration of Multilayer Sample Tested for the Effect of a Discontinuity on Thermal Conductivity	II-123
II-VI-13	Effect of a Discontinuity on Thermal Conductivity of Multilayer Insulation	II-124
II-VI-14	Sketch of Edge Treatments for Samples Used in Discontinuity Tests	II-125
II-VI-15	Effect of Discontinuities in the Radiation Shields of Multilayer Insulation	II-126
II-VI-16	Effect of Purge Gas on Thermal Conductivity of a Foam Insulation	II-136
II-VI-17	Suggested Purge Line Arrangement	II-137
II-VI-18	Diagram of Polyurethane Foam Samples	II-140
II-VI-19	Location of Mylar Disc	II-144
II-VI-20	Influence of T_{mean} of Sample on Mean Thermal Conductivity	II-145
II-VI-21	Configuration of Insulation Sample Using Crinkled, Aluminized Polyester Film, System C	II-148
II-VI-22	Edge Treatments	II-156

<u>FIGURE</u>		<u>PAGE</u>
II-VI-23	Effect of Slot Width on Heat Flux Through a Multilayer Insulation	II-159
II-VI-24	— Configuration of Spacer Used in Sample of 11% Support Area, Systems L & M	II-162
II-VI-25	Schematic Diagram of Arrangement of Sample and Pin for Penetration Test	II-167

THE PERFORMANCE OF MULTILAYER INSULATIONS

I. SUMMARY

A. Purpose and Scope

This report summarizes the work carried out on the analysis, experimental measurement, and design of thermal protection systems for liquid hydrogen tanks by Arthur D. Little, Inc., under Contract NAS-664 and continuation Contract NASw-615 at Cambridge, Massachusetts, and at NASA, Lewis Research Center, Cleveland, Ohio.

The purpose of the work was to increase the knowledge of the thermal behavior of multilayer insulations and obtain data on the performance of such insulations when they are exposed to a variety of conditions which are expected to be encountered in practical applications.

B. Approach

To achieve the stated purpose in this work, we proceeded as follows:

1. We placed the greatest emphasis on evaluating the performance of commercially available materials that are applicable to thermal protection systems for cryogenic fuel tanks for use in extended space missions;
2. We designed and constructed thermal conductivity apparatus to permit the measurement of insulation performance under conditions approximating those expected to occur in actual installations;
3. We investigated the effects of temperature, mechanical load, gas pressure, type of gas, perforations, and thermal shorts on the insulation performance; and

4. We analyzed the heat transfer mechanisms that control the performance of the insulations, so as to guide the experimental part of the program and provide information useful for design purposes.

C. Conclusions

The data obtained on the performance of thermal protection systems using various materials suitable for multilayer insulations have shown that high insulating effectiveness can be achieved under carefully controlled conditions. Even if the best performance cannot be achieved in practical installation, the insulating effectiveness of multilayer insulations is far superior to the effectiveness of any other thermal insulations available at this time. Thus, the application of multilayer insulations for large liquid hydrogen tanks appears to be highly desirable, provided that production and application techniques can be more fully developed so that predictable and reproducible performance is obtained.

The most profound effect on insulation performance is produced by mechanical load, gas pressure and type of gas, and thermal shorts. We conclude, therefore, that to counteract these effects, it will be necessary to:

1. Assure that the insulation is exposed as little as possible to the effects of outside forces, such as atmospheric or aerodynamic loads, by arranging a shroud to surround the liquid hydrogen tank wherever possible. Atmospheric loads of short duration can be tolerated, provided that no permanent deformation of the radiation shields or spacer materials takes place.

2. Permit any purging gas to vent to space in minimum time after
lift-off.

3. Assure the vacuum tightness of the cryogenic vessel or make
provision to duct leakage gas away from the insulation to prevent the
diffusion of gases into the insulation during prolonged space missions.

4. Pay very careful attention to the treatment of the edges of
multilayer insulations so as not to compromise the insulation perfor-
mance.

5. Eliminate or reduce the effects of thermal shorts insofar as
possible.

6. Prevent degradation of insulation reflectivity from the ambient
atmosphere during prolonged storage by purging with inert gas.

D. Recommendations

On the basis of the thermal performance data we have obtained for
multilayer insulations, we recommend:

1. Development of multilayer insulation systems capable of with-
standing mechanical loads without suffering a sharp increase in thermal
conductivity. This would greatly ease the solution of practical appli-
cation problems.

2. A thorough leak detection procedure for the hydrogen tank. This
procedure should be mandatory so as to assure that hydrogen will not
diffuse into the insulation during extended periods of space flight.

3. Development of suitable attachment techniques for the insulation.
These techniques will insure that the insulation will not suffer due to
imposed mechanical forces or vibration, and will permit faster and more
economical methods of laying up the individual layers.

4. Development of techniques for reducing boil-off rates during the ground hold period when inert purge-gas flow is used.

5. Elimination of the adverse effects of interplant handling procedures and atmospheric degradation of reflecting surfaces during assembly at the launch site.

6. A continuation of efforts to develop a thermal protection system which will have the high-insulating effectiveness of multilayer insulations but be less sensitive to lateral heat flow, less subject to deleterious effects of outside influences, and less costly.

II. INTRODUCTION

The fact that a brilliantly glowing nose cone can successfully resist the effects of aerodynamic heating while re-entering the earth's atmosphere is proof that thermal protection systems can be developed to meet conditions which only a few years ago were considered to be beyond technological feasibility. Less spectacular, but of equal importance to the continued progress of space exploration, is the availability of thermal protection systems for propellants, in particular liquid hydrogen, to meet the demands of the wide spectrum of space missions.

The development of multilayer insulations has had a profound influence on techniques for storing cryogenic liquids and, in particular, liquid hydrogen. Although terrestrial storage and transport vessels have made wide use of multilayer insulations, the difficulties that impede the development and application of these insulations to space vehicles have only recently been fully appreciated. The principal challenge lies in the integration of high performance insulations with the advancing state-of-the-art of thin-wall tank designs.

The high insulating effectiveness of multilayer insulations is achieved when a series of radiation shields of high reflectivity are separated by nearly nonconducting interleaving spacers while exposed to a pressure below 10^{-4} torr. In terrestrial cryogenic vessels, the multilayer insulations are assembled in an evacuated space bounded on one side by the liquid container and on the other side by a vacuum-tight outer pressure vessel capable of withstanding atmospheric loads or applied mechanical loads. The radiation shields and spacers, therefore, do not experience any compressive loads, and the achievement of the required high vacuum is within the state-of-the-art of vacuum engineering practice.

This approach is not feasible where a minimum weight system is required, as in liquid hydrogen tanks for space vehicles. The outer pressure vessel cannot be used because of its tremendous weight penalty; hence, the insulation is exposed to atmospheric pressures and imposed outside forces unless it is suitably shrouded. The attachment of the insulation to the tank walls is critical and has to be accomplished without introducing undesirable heat leaks or sacrificing structural integrity. In addition, substantial boil-off losses and weight penalties must be avoided during the prelaunch period by using techniques that prevent atmospheric gases from diffusing into the insulation and condensing on the tank wall. If flexible gas-tight outer skins are used, then the insulation has to be capable of withstanding atmospheric loads caused by cryopumping and of recovering its high insulating effectiveness after such loads are removed at altitude.

Because data on the performance of multilayer insulations under conditions expected to be encountered in actual service have not been obtained, adequate design solutions for integrated thermal protection systems are not available. As a result, multilayer insulations have not been widely used in space applications up to this time. The development efforts required before liquid hydrogen tanks can be adequately insulated to permit space vehicles to explore the regions beyond the vicinity of the earth appear to be at least equivalent to efforts already expended on the development of re-entry heat shield materials.

From the time a thermal protection system is assembled in the production plant to the successful completion of a desired space mission, a number of imposed environments will affect such a system. These environmental interactions need to be recognized and considered in the various design approaches and performance expectations. Of major importance to the performance of multilayer insulations are their thermal interactions with heat sources external to the vehicle and with heat sources on board the vehicle. Among the external heat sources are the thermal conditions existing on the ground prior to flight, the aerodynamic heating encountered during the boost phase, and the various radiation heat inputs such as direct solar radiation and planet shine, modified by possible vehicle orientation. On-board heat sources consist of radiative inputs from other portions of the vehicle and heat leaks to the cryogenic fuel tank from supports, pipes, and other structural members.

Damage caused by meteoroids of high kinetic energy can markedly reduce the effectiveness of multilayer insulations, unless suitable shields to mitigate these effects are incorporated in the over-all

thermal protection system. Finally, because a certain amount of handling and transportation of the insulated tanks is necessary prior to launch, the thermal protection system must be so designed that these actions will not cause a decrease in reliability or an increase in the complexity of maintenance procedures.

Accordingly, we have undertaken an analytical and experimental program to define the influence of such variables as temperature, mechanical load, gas pressure and type of gas, thermal shorts, and outgassing rates on the performance of typical state-of-the-art multilayer insulations. The following part discusses 1) the theoretical considerations which specifically govern the performance of multilayer insulations, 2) typical multilayer insulation systems we tested during this program, 3) the experimental thermal conductivity apparatus we constructed, 4) the test results we obtained, and 5) their implications.

III. THEORETICAL INSULATION PERFORMANCE

The simultaneous action of the combined heat transfer mechanisms in evacuated multilayer insulations has already been treated in considerable detail in the literature. However, a number of problem areas concern specifically the practical applications of multilayer insulations; these areas are illustrated in the following analytical approaches for idealized multilayer insulations that consist of floating radiation shields.

A. Gas Pressure Within Multilayer Insulations

Multilayer insulations must be evacuated to at least 10^{-4} torr for adequate performance. Two approaches are possible. The first method is to produce a pre-evacuated or cryopumped insulation by using a flexible

outside shield. There is considerable doubt that the required high vacuum could be maintained at the various joints during the severe vibration and acceleration of the launching. Unless the outside skin can be removed at altitude, any noncondensable gases which might diffuse through the outer skin or through the tank wall would increase the gas pressure within the insulation. Also, in view of the possible outgassing of metal surfaces as a result of bombardment by high energy radiation, it is questionable whether the required vacuum could be maintained in space, unless adequate means for venting were provided.

The second approach is to exclude atmospheric gases by purging with a noncondensable gas such as helium. In this case, the insulation is not subjected to atmospheric pressure; however, reliance must be placed on rapid venting at altitude.

Venting to the space environment is required in both approaches. Such venting will depend on the geometric arrangement of the insulation layers (e.g., exposure of the edges to the external vacuum or perforation of the shields) which will be designed to enhance the pumping speed for gas molecules.

1. Edge-Pumping

To determine the equilibrium pressure when a panel of multilayer insulation is pumped only at the edges, we must first calculate the mean free path of a molecule confined in the space between two parallel plates separated by a distance h . If the molecule leaves the lower plate (Figure II-III-1) with a cosine distribution in angle, then the mean radial distance that the molecule travels before

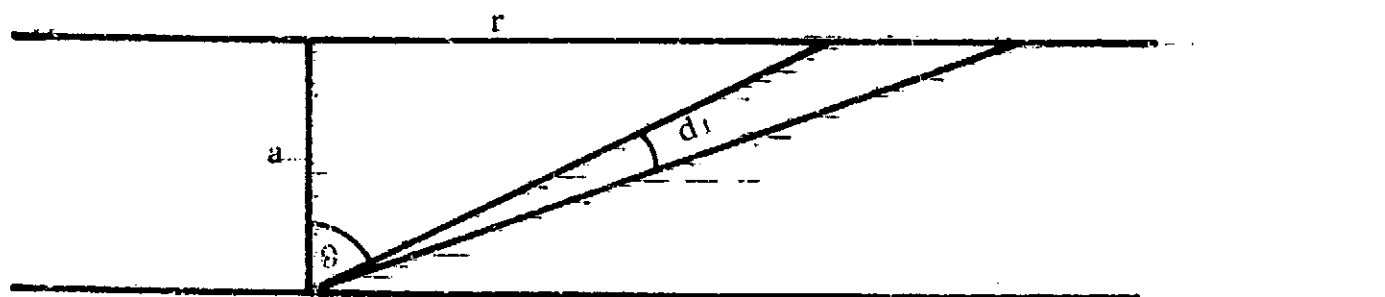


FIGURE II-III-1 MEAN FREE PATH BETWEEN TWO PLATES

hitting the other plate is

$$r = \frac{1}{\pi} \int_0^{\pi/2} r \cos \theta \, d\theta \quad (\text{II-III-1})$$

where $d\theta$ is an element of solid angle and θ is the angle of the path with respect to the normal to the plates.

Since $d\Omega = 2\pi \sin\theta \, d\theta$ and $r = a \tan\theta$, the integral can be evaluated to give

$$r = \frac{\pi}{2} a \quad (\text{II-III-2})$$

The corresponding two-dimensional diffusion coefficient for motion parallel to the plane of the plates is

$$D = \frac{1}{2} \bar{c} \bar{r} = \frac{\pi}{4} \bar{c} a \quad (\text{II-III-3})$$

Now assume that the two plates are in the form of a long strip of width l and that molecules are outgassing from the interior surfaces at a net rate of ν $\text{cm}^{-2} \text{sec}^{-1}$. Then the diffusion equation for the equilibrium density of molecules is

$$D \frac{\partial^2 N}{\partial x^2} = - \frac{2\nu}{a} \quad (\text{II-III-4})$$

where N is the density of the molecules and x is measured from the center of the strip.

The solution for the case of a perfect vacuum along each edge of the strip is

$$N = \frac{\nu}{Da} \left(\frac{l^2}{4} - x^2 \right) \quad (\text{II-III-5})$$

The maximum density occurs at the center of the strip and is

$$N_{\text{max}} = \frac{\nu l^2}{4Da} = \frac{\nu l^2}{\pi c a^2} \quad (\text{II-III-6})$$

If the pressure is to be less than 10^{-5} mm Hg at 25°K , the gas density must be less than 4×10^{12} molecules cm^{-3} . Now assume, as a typical example, that the shield consists of panels 1 meter wide composed of radiation shields 0.002 cm thick and stacked 40 to the cm, with spacers that occupy effectively 90% of the spaces between the foils.

Then we can substitute the following values in Equation II-III-6:

$$l = 50 \text{ cm}$$

$$\bar{c} = 3 \times 10^4 \text{ cm sec}^{-1}$$

$$A_{\text{effective}} = 0.0023 \text{ cm}$$

$$N_{\text{max}} = 4 \times 10^{12} \text{ cm}^{-3}$$

The maximum allowable outgassing rate is therefore

$$v = 8 \times 10^8 \text{ molecules cm}^{-2} \text{ sec}^{-1}$$

This corresponds to the removal of one monomolecular layer from all exposed surfaces every two weeks. Much higher outgassing rates than this are likely to be encountered if the radiation shields and spacers are exposed to atmospheric pressure at the time of launching. In which case, adequate venting must be provided to prevent destructive effects due to sudden pressure reduction.

Another difficulty with edge-pumping is that at the pumping areas, the innermost foils must be brought into contact with the vacuum outside. This provides places where solar radiation can bypass most of the shields and penetrate almost directly to the insulated tank.

2. Broadside Pumping of Perforated Radiation Shields

Let τ be the perforated fraction of the surface of each radiation shield, so that τ is the molecular transmission coefficient. Thus, if N is the density of molecules on one side of a shield and N' the density on the other side, the net flux F of molecules through the shield is

$$F = \frac{1}{4} N \bar{c} \tau - \frac{1}{4} N' \bar{c} \tau \quad (\text{II-III-7})$$

For a stack of shields, this equation can be written in the form

$$P = - \frac{\bar{c}\tau}{4} \frac{\partial N}{\partial n_s} \quad (\text{II-III-8})$$

where n_s is the series number of the shields.

As before, let v be the outgassing rate per cm^2 of actual shield surface. Then the number of molecules emitted per cm^2 per second into the space between two shields is $2v(1 - \tau)$. Thus, for steady-state flow,

$$\frac{\bar{c}\tau}{4} \frac{\partial N}{\partial n_s} = - 2v(1 - \tau) \quad (\text{II-III-9})$$

If the array of shields is in contact with a perfect vacuum on one side and an impervious wall on the other side, the boundary conditions are

$$\frac{\partial N}{\partial n_s} = 0 \text{ for } n_s = 0$$

$$N = 0 \text{ for } n_s = n$$

Equation II-III-9 gives for the maximum allowable molecular density:

$$N_{\text{max}} = \frac{4v(1 - \tau)n^2}{\bar{c}\tau} \quad (\text{II-III-10})$$

It is of interest to consider under what conditions broadside and edge-pumping are equally efficient. On equating the values of the outgassing rates given by Equation II-III-6 and II-III-10, we find for the required relationship

$$\frac{L}{a} = n \sqrt{\frac{4\pi\tau}{1-\tau}}$$

If $n = 100$, $\tau = 0.1$, and $a = 0.0023$ cm, we find that $L = 2.3$ cm. This means that for edge-pumping to be as efficient as broadside pumping with 10% perforated shields, the edge-pumping must be applied along lines separated by only 4.6 cm. The excessive exposure of the innermost foils in such a design appears to be quite impractical. We therefore conclude that the method of broadside pumping is much preferred.

The allowable outgassing rate with broadside pumping may be calculated from Equation II-III-10 with the following values:

$$N_{\max} = 4 \times 10^{12} \text{ cm}^{-3}$$

$$\tau = 0.1$$

$$n = 100$$

$$\bar{c} = 3 \times 10^4 \text{ cm sec}^{-1}$$

Then

$$Q = 1 \times 10^{11} \text{ cm}^{-2} \text{ sec}^{-1}$$

Actually, the allowable outgassing rate must be considerably less than this, because τ must be well below 0.1 to prevent excessive radiation transfer through the perforations in the shields.

3. Effects of Static Gas Density

Consider two adjacent radiation shields at temperatures T and $T + \Delta T$. The number of molecular impacts on each surface per unit area per second is $N\bar{c}/4$, where N is the number of molecules per unit volume and

\bar{c} is the mean molecular velocity. If the accommodation coefficient is unity and the mean free path of the molecules is large compared with the spacing of the shields, the average kinetic energy of the molecules striking one shield is $c_v T$ and that striking the other shield is $c_v (T + \Delta T)$. The heat transfer rate is therefore

$$\begin{aligned} q_c &= \frac{N}{l} \cdot c_v \Delta T & (II-III-11) \\ &= \frac{3}{8} N \bar{c} k \Delta T \end{aligned}$$

since c_v is approximately equal to the translational kinetic energy per degree at the low temperatures where conduction is important.

The radiation transfer rate is

$$q_r = \frac{\Delta(\sigma T^4)}{\frac{2}{\epsilon} - 1} \quad (II-III-12)$$

where ϵ is the emissivity of the surfaces.

The total heat flux is therefore

$$q = \frac{3}{8} N \bar{c} k \Delta T + \frac{\Delta(\sigma T^4)}{\frac{2}{\epsilon} - 1} \quad (II-III-13)$$

We must now sum this difference equation over the set of n successive gaps between the shields. In doing this, we assume that ϵ is constant and that $N \propto 1/T$ and $\bar{c} \propto \sqrt{T}$, since the pressure is constant. The result of the summation is:

$$nq = \frac{3}{4} N_1 \bar{c}_1 k (\sqrt{T_1 T_2} - T_1) + \frac{\sigma (T_2^4 - T_1^4)}{\frac{2}{e} - 1} \quad (\text{II-III-14})$$

where N_1 , \bar{c}_1 , T_1 refer to the low-temperature side of the shield and T_2 refers to the high-temperature side.

B. Radiation Transfer Within Multilayer Insulations

In addition to the transmission of heat by gas conduction through multilayer insulations, the following radiation transfer conditions arise:

1. Radiation Transfer Through Perforated Radiation Shields

Figure II-III-2 shows the radiation entering and leaving on the two sides—

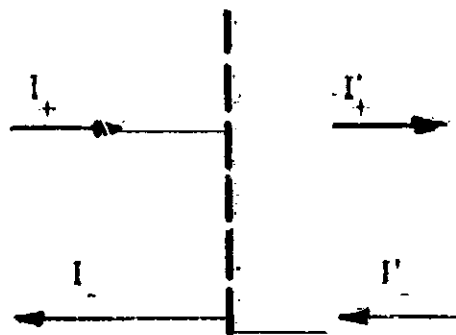


FIGURE II-III-2 RADIATION TRANSFER THROUGH PERFORATED SHIELD

of a perforated shield of emissivity ϵ , transmission coefficient τ , and temperature T . The energy balance equations are

$$I_+ = \tau I_+ + (1 - \tau)(1 - \epsilon)I'_+ + (1 - \tau)\epsilon \sigma T^4 \quad (\text{II-III-15})$$

$$I'_+ = \tau I_- + (1 - \tau)(1 - \epsilon)I'_- + (1 - \tau)\epsilon \sigma T^4 \quad (\text{II-III-16})$$

$$I'_+ - I'_- = I_+ - I_- = q_r \quad (\text{II-III-17})$$

Equations II-III-15, -16, and -17 are satisfied by relations of the form — —

$$I_+ = A - kn_s \quad (\text{II-III-18})$$

$$I_- = B - kn_s \quad (\text{II-III-19})$$

$$\sigma T^4 = C - kn_s \quad (\text{II-III-20})$$

where A, B, C, and k are constants and n_s , as before, is the series number of a given shield. To get I'_+ and I'_- we replace $n_s + 1$. The constant k is the gradient $\Delta(\sigma T^4)/\Delta n_s$.

On substituting Equations II-III-18, -19, and -20 into Equation II-III-15 and -16 and noting that $A - B$ is the net radiation flux q_r , we find that

$$q_r = \frac{\epsilon + (2 - \epsilon)\tau}{(2 - \epsilon)(1 - \tau)} \frac{\Delta \sigma T^4}{\Delta n_s} \quad (\text{II-III-21})$$

Now suppose that a stack of n shields is placed between two black sheets at temperatures T_2 and T_1 . Then, on adding the radiative impedances

of the two outer gaps to that given in II-III-21, we find for the flux:

$$q_r = \frac{\sigma (T_2^4 - T_1^4)}{1 + \frac{(2 - \epsilon)(1 - \tau)}{\epsilon + (2 - \epsilon)\tau}} n = \frac{\sigma (T_2^4 - T_1^4)}{1 + \left(\frac{2}{\epsilon'} - 1\right)n} \quad (\text{II-III-22})$$

where ϵ' is the effective emissivity of the perforated foils:

$$\epsilon' = \epsilon + (2 - \epsilon)\tau \quad (\text{II-III-23})$$

Note that (II-III-22) gives correct results for $\epsilon' = 0$ and 1.

Let $\epsilon = 0.05$ and $\tau = 0.1$. Then $\epsilon' = 0.245$. Thus, a transmission factor that is large enough to give an appreciable molecular pumping speed increases the effective emissivity of the shields by a factor of five.

2. Radiation Transfer by Closely Spaced Shields

The usual formula for radiation transfer through a stack of radiation shields does not apply when the spacing of the shields is less than the wavelength of the peak of the blackbody spectral distribution corresponding to the temperature of the shields. Two effects set in at these close spacings--wave interference and radiation tunneling. Wave interference of the emitted radiation occurs in the narrow gaps between the shields and may increase or decrease the energy transfer, depending on the spacing. Radiation tunneling allows transfer of radiation that ordinarily suffers total internal reflection inside the shield material; the resulting energy transfer increases exponentially as the spacing decreases. The two effects together give an energy transfer rate per unit area which becomes, in the limit of zero spacing,

$$q = \frac{n^4}{n^2 + k^2} \sigma (T_2^4 - T_1^4)$$

where n and k are the real and imaginary parts of the complex refractive index, σ is the Stefan-Boltzmann constant, and T_2 and T_1 are the temperatures on the two sides of a gap.

The formula implies that the radiation density c' and velocity of propagation c' in the shield material are:

$$c' = \frac{n^2 \sigma T^4}{c}$$

$$c' = \frac{n^2 c}{n^2 + k^2}$$

For moderate values of the absorption index k , the flux formula predicts a transfer rate between two close shields greater than that between two black surfaces.

In the case of metal shields, when the spacing between the two shields is increased from zero, the radiation transfer rate at first rises sharply to a high maximum and then falls below the usual value for widely spaced shields. The flux returns to the normal level when the spacing exceeds—about one-half of the wavelength of the blackbody peak. (See Figure II-III-3.)

3. Radiation Transfer Through Seams and Penetrations

With conventional insulation materials, such as foam or glass wool, one can easily seal a joint between panels by "caulking" the seams with

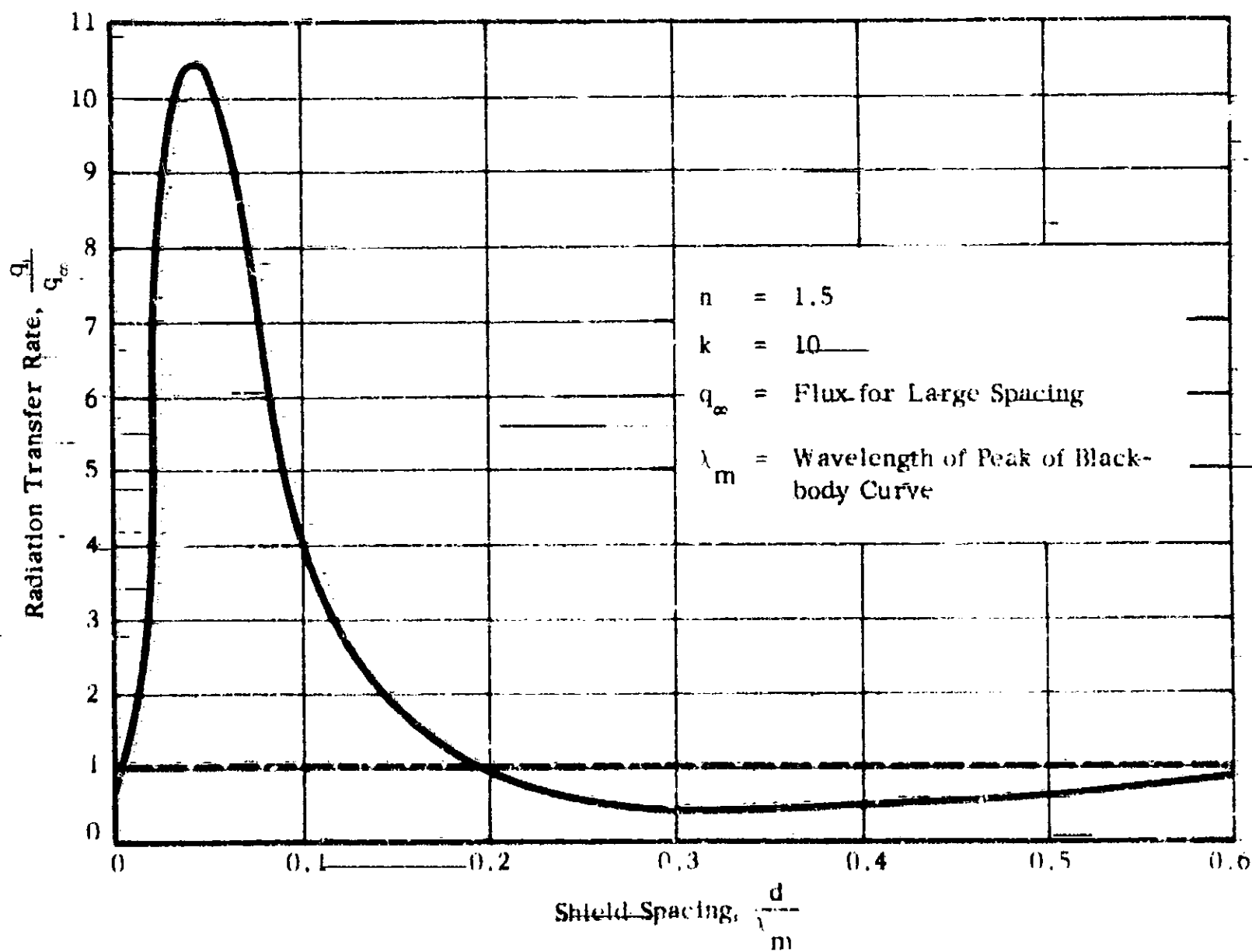


FIGURE II-III-3 — ONE WAY ENERGY FLUX BETWEEN TWO FOILS VS GAP WIDTH

the same material or by overlapping the panels. This is possible because these materials have isotropic thermal conductivity. But these simple methods cannot be used with metal radiation shields, since the conductivity of the shields is highly directional. The conductivity of multilayer insulations in the direction perpendicular to the plane of metal radiation shields is about 10^6 times lower than the conductivity within the plane. Overlapping of panels of multilayer insulations is therefore useless, since this ties high- and low-temperature points together. Filling the seams with pieces of the multilayer material fails for the same reason. The use of isotropic materials of higher conductivity, such as foam or wool, also partially short-circuits the high- and low-temperature sides of the shield, but does provide a significant improvement in insulation. One possible solution would be simply to leave a gap at the junctions between all panels and around all pipes and struts that penetrate the panels, if the extra heat input at the joints could be kept to a tolerably low level with gaps of practical width.

a. Assumptions and Method of Calculation

Figure II-III-4 shows two panels of multilayer insulation of thickness d , separated by a gap of width δ . The storage-tank wall at the bottom of the diagram is at a temperature T_0 . The outermost layer of shield is at temperature T_1 and is made to bridge the gap by attachment of an additional strip of shield after assembly of the panels.

We assume that all surfaces have the same emissivity ϵ . However, the stacked shields look black from an edge-on point of view because of the multiple reflections of the radiation in the narrow spaces between the individual shields and absorption by the spacer material. We assume

further that the effective conductance of the panels in the plane of the shields is so large compared with the radiative conductance across the gap that the temperature of each shield is uniform.

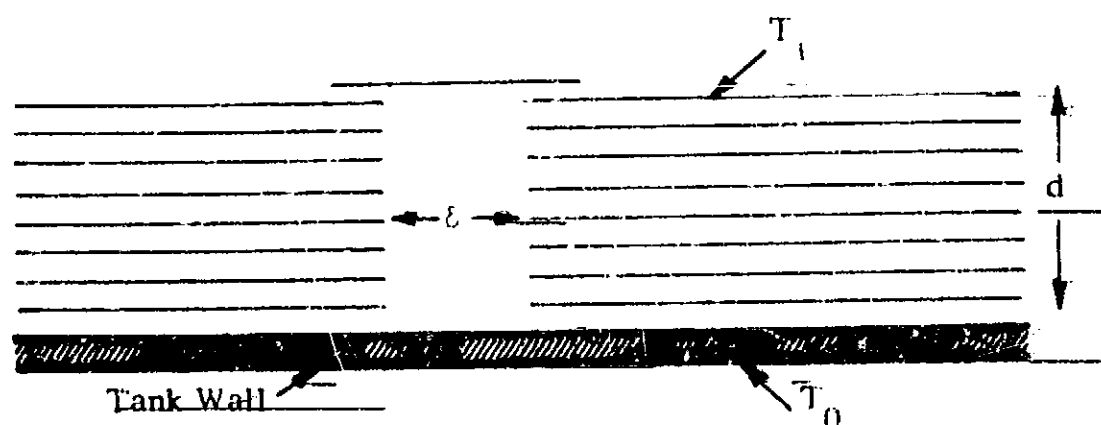


FIGURE II-III-4 GAP BETWEEN TWO PANELS OF MULTILAYER INSULATION

We wish to calculate the additional heat flux that reaches the storage tank because of the gap. The most important contribution to this flux arises from radiation interchange across the gap between the exposed edges of the two panels. For example, radiation from the outer, hotter layers of the right-hand panel can reach the inner, cooler layers of the left-hand panel. The heat transferred in this way immediately spreads over a large area of the left-hand panel, because of the high conductance in the plane of the shields. A certain fraction of this heat then finds its way to the tank. The remainder goes in the other direction, towards the outer layers of the shield.

The fraction of the heat that reaches the tank is easily found. Let an increment of heat flux Δq be received by a certain shield which is

located at a distance y from the tank wall, as shown in Figure II-III-5. Then the heat balance equation for the fluxes q_1' and q_0' above and below the shield is:

$$q_0' = q_1' + \Delta q \quad (\text{II-III-24})$$

If we ignore conduction through the spacers, we have for the radiation fluxes:_____

$$q_1' = k \frac{T_1^4 - (T + \Delta T)^4}{d - y} \quad (\text{II-III-25})$$

$$q_0' = k \frac{(T + \Delta T)^4 - T_0^4}{y} \quad (\text{II-III-26})$$

where ΔT is the small temperature rise due to Δq , and k is a constant.

In the undisturbed state when Δq is zero,

$$q_1 = q = k \frac{T_1^4 - T^4}{d - y} \quad (\text{II-III-27})$$

$$q_0 = q = k \frac{T^4 - T_0^4}{y} \quad (\text{II-III-28})$$

Thus the flux variations in the two directions are

$$\Delta q_1 = q_1 - q_1' = k \frac{(T + \Delta T)^4 - T^4}{d - y} \quad (\text{II-III-29})$$

$$\Delta q_0 = q_0' - q_0 = k \frac{(T + \Delta T)^4 - T^4}{y} \quad (\text{II-III-30})$$

From (II-III-29) and (II-III-30) we obtain the desired equation for the incremental heat flux to the tank:

$$\Delta q_0 = \left(\frac{d - y}{d} \right) \Delta q \quad (\text{II-III-31})$$

since

$$\Delta q_0 + \Delta q_1 = \Delta q \quad (\text{II-III-32})$$

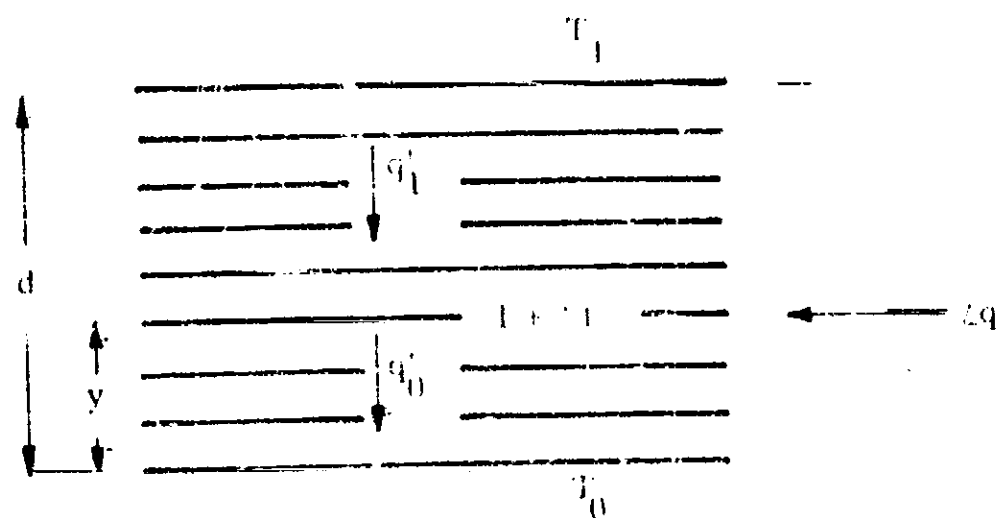


FIGURE II-III-5 EFFECT OF AN INCREMENT Δq IN HEAT FLUX TO AN INTERIOR SHIELD IN AN INSULATION PANEL

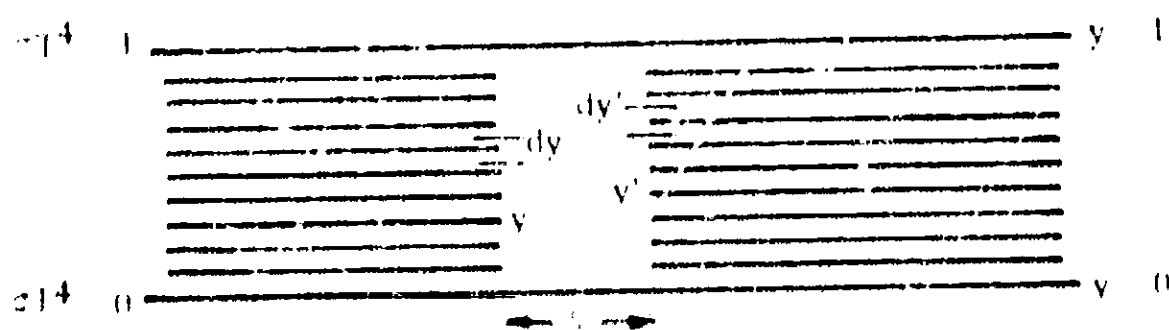


FIGURE II-III-6 REDUCED VARIABLES USED TO DESCRIBE THE RADIATION TRANSFER IN THE GAP

Equation II-III-31 states that the fraction of the heat that goes to the tank falls off linearly as the distance of the shield from the tank increases. This result is the key to the calculation of the additional input flux due to the gap at the junction between two panels or at a penetration.

b. Heat Input due to a Joint Between Two Multilayer Insulation Panels

The calculation of the radiation transfer for the geometry shown in Figure II-III-4 is greatly simplified by the requirement that the gap width δ must be made small compared with the panel thickness d if the extra heat input to the tank is to stay at a tolerable level. When $\delta \ll d$, the top and bottom sheets, which are at temperatures T_1 and T_0 respectively appear like blackbodies no matter what the true emissivity ϵ may be. The reason is that, for small δ , the radiation received by these surfaces comes predominantly from a few neighboring metal shields, which appear like blackbody radiators. Thus, the top surface receives only blackbody radiation at approximately its own temperature T_1 . The reflected radiation plus the emitted radiation from this surface therefore produce essentially blackbody radiation at the temperature T_1 . The same consideration applies to the bottom surface. Thus, in Figure II-III-4, all four surfaces surrounding the gap can be regarded as black.

In the calculations, it is convenient to express all distances temporarily in units of d , and all radiation flux density in units of $\sigma(T_1^4 - T_0^4)$. Also, since only the difference $T_1^4 - T_0^4$ is important, we can choose $T_0 = 0$ for simplicity. Figure II-III-6 shows the reduced variables. In terms of these variables, the flux emitted by the element dy , per unit length normal to the plane of the diagram, is simply ϵdy .

The net flux received by dy is

$$q_{\text{net}} = \frac{dy}{2} \int_0^1 \frac{(y' - y) \delta^2 dy'}{[\delta^2 + (y' - y)^2]^{3/2}} + \frac{dy}{2} (1 - y) \left\{ 1 - \frac{1 - y}{[\delta^2 + (1 - y)^2]^{1/2}} \right\} - \frac{dy}{2} y \left\{ 1 - \frac{y}{[\delta^2 + y^2]^{1/2}} \right\} \quad (\text{II-III-33})$$

In the first term the expression $\frac{1}{2} \delta^2 [\delta^2 + (y' - y)^2]^{-3/2}$ is the view factor between dy and dy' , while $y' - y$ represents the difference in the fourth powers of the temperatures of these two elements. The second term is the net radiation from the top surfaces to dy . The third term is the net radiation from the bottom surface to dy .

To obtain the total indirect heat input to the storage tank due to the net radiation entering the side-walls of the gap, we must multiply (II-III-33) by the redistribution factor $1 - y$, discussed in the previous section, then integrate over y , and finally multiply by 2 to allow for the two side walls. The result is

$$q_{\text{indirect}} = \int_0^1 \int_0^1 \frac{(1 - y)(y' - y) \delta^2 dy dy'}{[\delta^2 + (y' - y)^2]^{3/2}} + \int_0^1 (1 - y)^2 \left\{ 1 - \frac{1 - y}{[\delta^2 + (1 - y)^2]^{1/2}} \right\} dy - \int_0^1 y(1 - y) \left\{ 1 - \frac{y}{[\delta^2 + y^2]^{1/2}} \right\} dy \quad (\text{II-III-34})$$

The direct radiation to the bottom surface is

$$q_{\text{direct}} = [(1 + \delta^2)^{1/2} - 1] + \int_0^1 \left[1 - \frac{y}{(\delta^2 + y^2)^{1/2}} \right] y dy \quad (\text{II-III-35})$$

where the first term is the radiation from the top surface, and the second term is the net radiation from the two side walls.

The total extra flux due to the presence of the gap is the sum of (II-III-34) and (II-III-35), which simplifies to

$$q_{\text{total}} = (1 + \delta^2)^{1/2} - 1 + 2 \int_0^1 \left[1 - \frac{y}{(\delta^2 + y^2)^{1/2}} \right] y^2 dy - \delta^2 \int_0^1 \int_0^1 \frac{y(y' - y) dy dy'}{[\delta^2 + (y' - y)^2]^{3/2}} \quad (\text{II-III-36})$$

After some reduction, Equation II-III-36 becomes

$$q_{\text{total}} = \sqrt{1 + \delta^2} \left(\frac{1}{3} - \frac{2}{3} \delta^2 \right) + \left(\frac{2}{3} \delta^3 - \frac{1}{3} \right) + \delta^2 \ln \left(\frac{1 + \sqrt{1 + \delta^2}}{\delta} \right) \quad (\text{II-III-37})$$

This expression is plotted in Figure II-III-7.

Returning now to the original variable, we obtain for the heat flux per unit length of the seam:

$$q_{\text{total}} = d\sigma (T_1^4 - T_0^4) \left[\sqrt{1 + \frac{\delta^2}{d^2}} \left(\frac{1}{3} - \frac{2}{3} \frac{\delta^2}{d^2} \right) + \left(\frac{2}{3} \frac{\delta^3}{d^3} - \frac{1}{3} \right) + \frac{\delta^2}{d^2} \ln \left(\frac{1 + \sqrt{1 + \frac{\delta^2}{d^2}}}{\frac{\delta}{d}} \right) \right] = d\sigma (T_1^4 - T_0^4) f \left(\frac{\delta}{d} \right) \quad (\text{II-III-38})$$

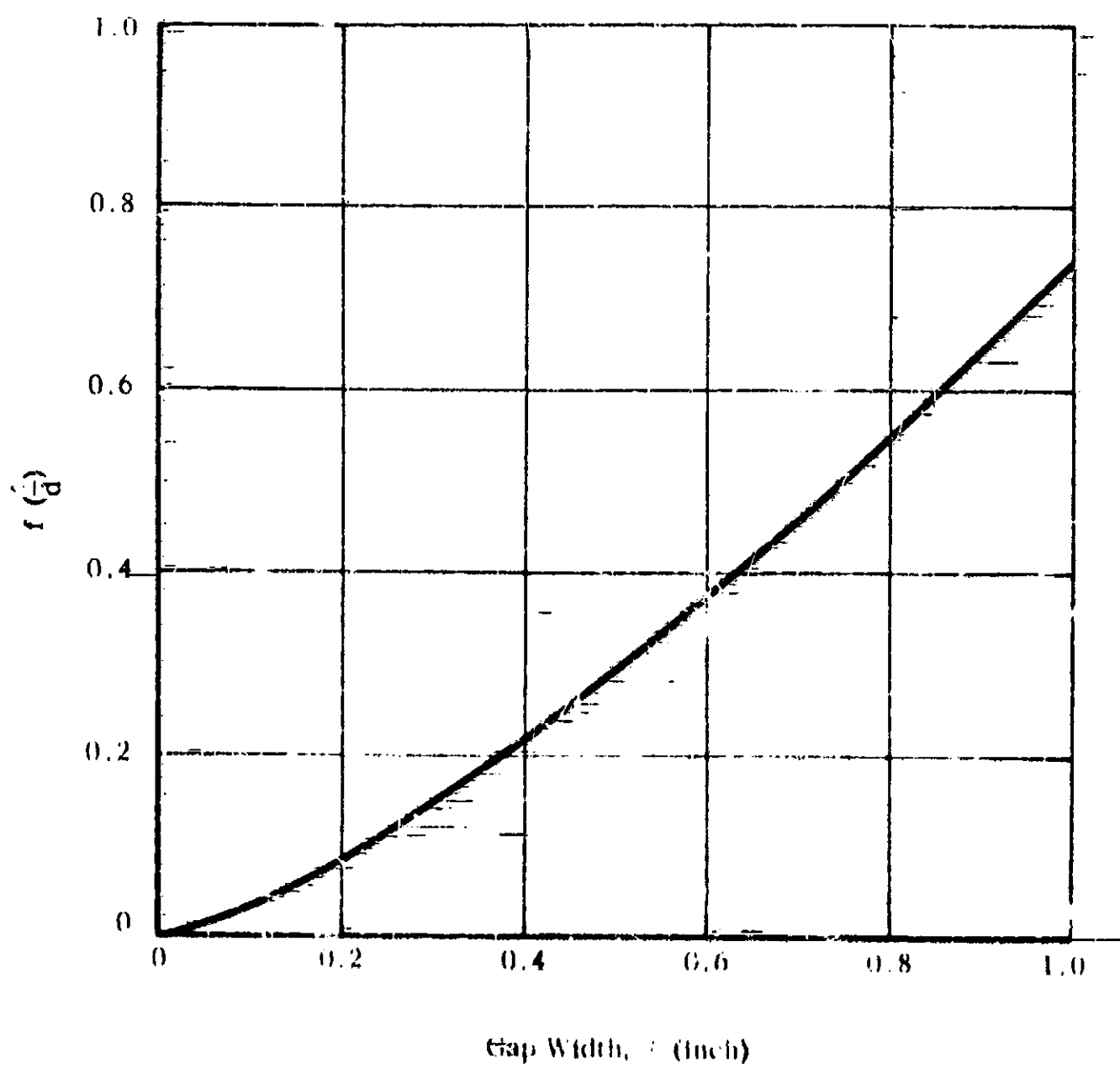


FIGURE II III-7 PLOT OF EQUATION II III-37

It is convenient to express this flux in terms of an equivalent width of the insulating panel that transmits the same flux for the same temperature difference. The width δ_{eff} that does this is given by the formula

$$q_{\text{total}} = \frac{\delta_{\text{eff}} \sigma (T_1^4 - T_0^4)}{\frac{2}{\epsilon} - 1)n} \quad (\text{II-III-39})$$

where n is the number of shields.

From Equations II-III-38 and II-III-39, we obtain the result

$$\frac{\delta_{\text{eff}}}{d} = \left(\frac{2}{\epsilon} - 1 \right) n f\left(\frac{b}{d}\right) \quad (\text{II-III-40})$$

where

$$f\left(\frac{b}{d}\right) = \frac{1}{1 + \frac{b^4}{d^4}} \left(\frac{1}{3} - \frac{2}{3} \frac{b^2}{d^2} \right) + \left(\frac{2}{3} \frac{b^2}{d^2} - \frac{1}{3} \right) + \frac{b^2}{d^2} \ln \left(\frac{1 + \sqrt{1 + \frac{b^4}{d^4}}}{\frac{b}{d}} \right) \quad (\text{II-III-41})$$

Figure II-III-8 shows how δ_{eff}/d varies with b/d for three different values of the shielding factor, $n(\frac{2}{\epsilon} - 1)$. For $b/d = 0.1$ Equation II-III-40 can be written in an approximate, simpler form:

$$\frac{\delta_{\text{eff}}}{d} \approx \left(\frac{2}{\epsilon} - 1 \right) n \left(\frac{b^2}{d^2} \ln \frac{2d}{b} - \frac{b}{2d} \right) \quad (\text{II-III-42})$$

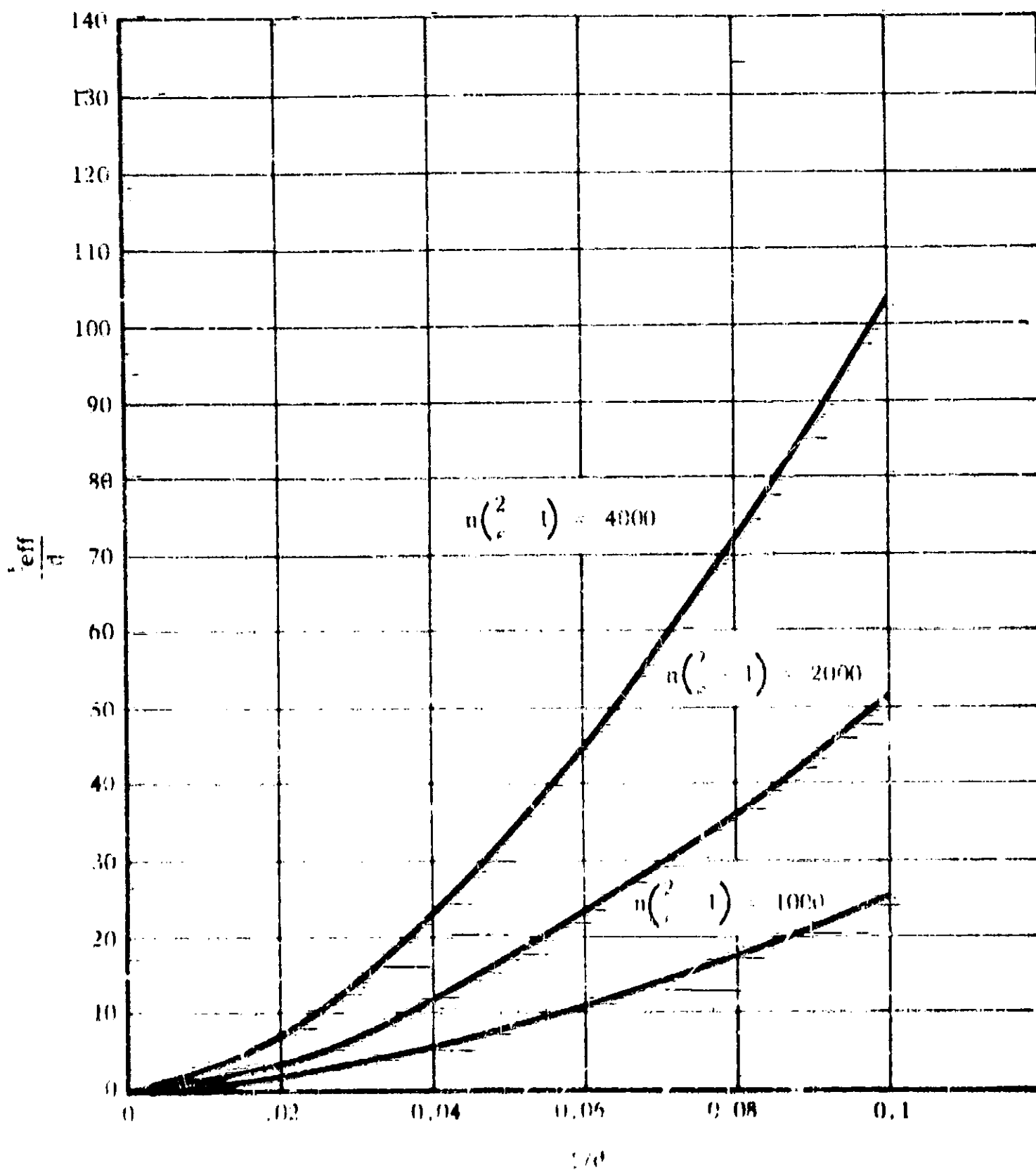


FIGURE II III-8

EFFECTIVE GAP l IN UNITS OF THE INSULATION THICKNESS d , FOR VARIOUS VALUES OF THE SHIELDING FACTOR $n(\epsilon^2 - 1)$

To obtain an estimate of the additional heat leak due to the seams, we consider the typical case of a cylindrical tank 10 feet long and 10 feet in diameter, with flat ends and insulated with 100 layers of metal shield having an emissivity of 0.05 and total thickness of 1 inch. If the insulation is applied in four sections--namely, two end disks and two halves of a cylindrical shell--the total length of seam is 80 feet. The total area of the tank surface is 450 ft^2 . The shielding factor $n(\frac{2}{\epsilon} - 1)$ is about 4000.

If we allow a gap width at the seams of $\delta = 0.1$ inch, then $\delta/d = 0.1$, and from the upper curve in Figure II-III-8 we find that $\delta_{\text{eff}}/d = 102$. Therefore, $\delta_{\text{eff}} = 102 \text{ inches} = 8.5 \text{ ft}$, and the effective area of the seams is $8.5 \text{ ft} \times 80 \text{ ft} = 680 \text{ ft}^2$. Since the total area of the tank is 450 ft^2 , the seams cause an additional heat input of 150%.

Figure II-III-9 shows the percentage heat leak as a function of the gap width. To reduce the leak at the seams to a reasonable value, such as 10%, one must make the gap no wider than 0.020 inch. In view of the much larger dimensional changes in the tank due to thermal contraction during filling, a gap of this size would seem to require impossible tolerances in the fabrication and installation of the insulation panels.

Apparently, the only solution to the problem is to eliminate the seams altogether. Two ways of doing this suggest themselves. In one method the insulation can be applied by wrapping the tank with a continuous narrow strip of the metal shield, interleaved with a strip of spacer material. Although in this method there would be a continuous metal path from the outside to the inside of the completed multilayer insulation, the path would be so long that the conductive heat leak would probably

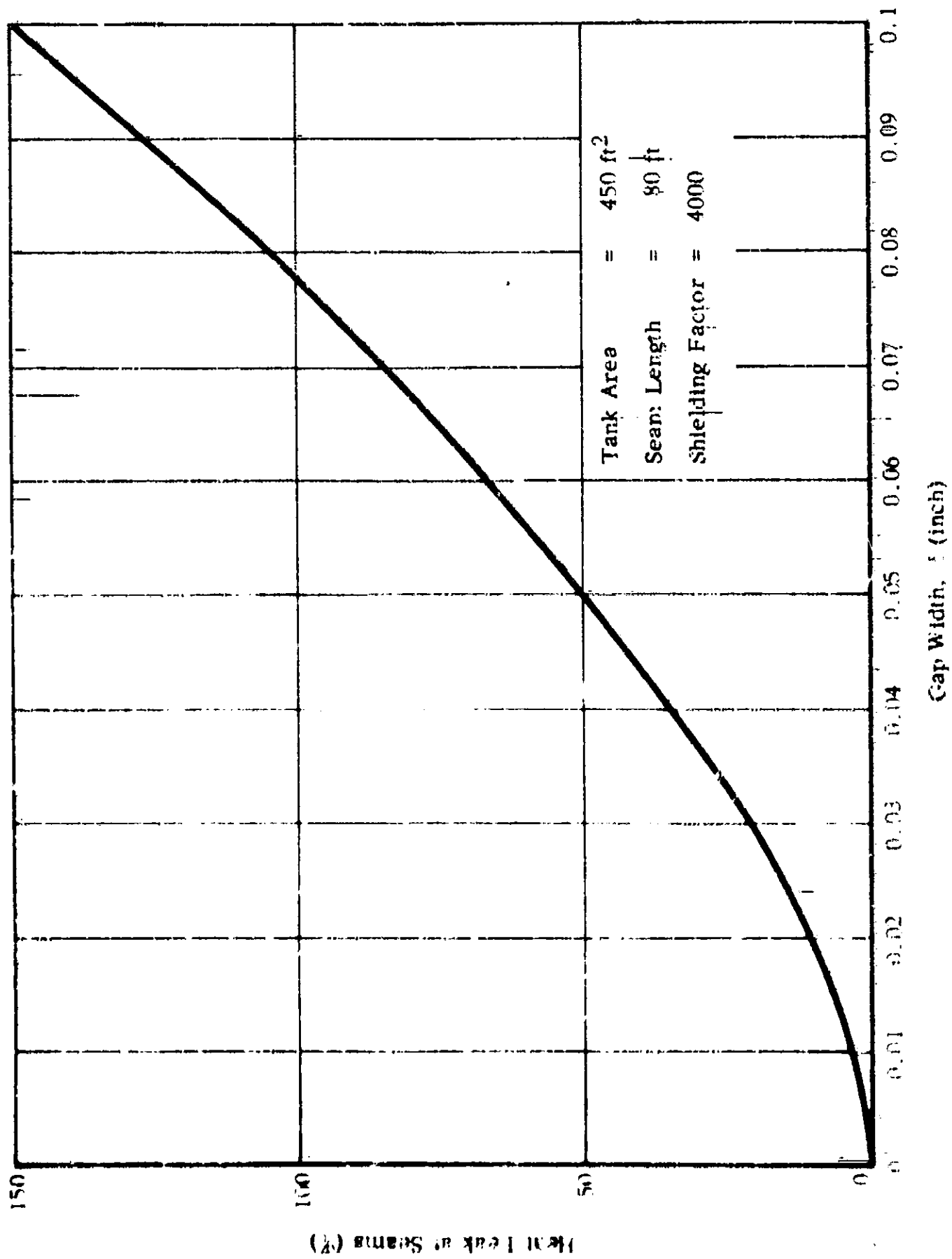


FIGURE II-II-9 RELATIONSHIP OF GAP WIDTH TO PERCENTAGE HEAT LEAK AT SEAMS

be negligible. In the other method, complete alternating layers of metal shield and spacer material can be applied to the tank by filament-winding or otherwise. In this way, no direct conductive path from outside to inside is permitted. In both methods, the shields must be perforated to allow gas to be pumped out.

An alternative plan is to give up the use of metal shields and substitute plastic film with a very thin reflective metallic coating. The conductivity of such material in its own plane is so low that the seam problem is much less severe.

c. Heat Input Due to the Penetration of a Pipe Through Radiation Shields

As an example of a penetration, consider the case shown in Figure II-III-10 of a vent pipe of radius r which penetrates the multilayer metal radiation shields. Assume that the pipe is at the temperature T_0 of the tank and is protected from direct sunshine by a single shield at temperature T_1 .

Let ϵ_0 be the emissivity of the outside surface of the pipe. Then the net radiation received by a length dy of the pipe from the black edges of the multilayer shield is

$$dq = 2\pi r d\epsilon_0 (T_1^4 - T_0^4) \quad (II-III-43)$$

According to the argument used previously, a fraction $(d - y)/d$ of this heat comes from the tank itself and should therefore not be considered. The remaining fraction, y/d , comes from the outside. Thus, the total heat entering the tank by way of the gap between the shield

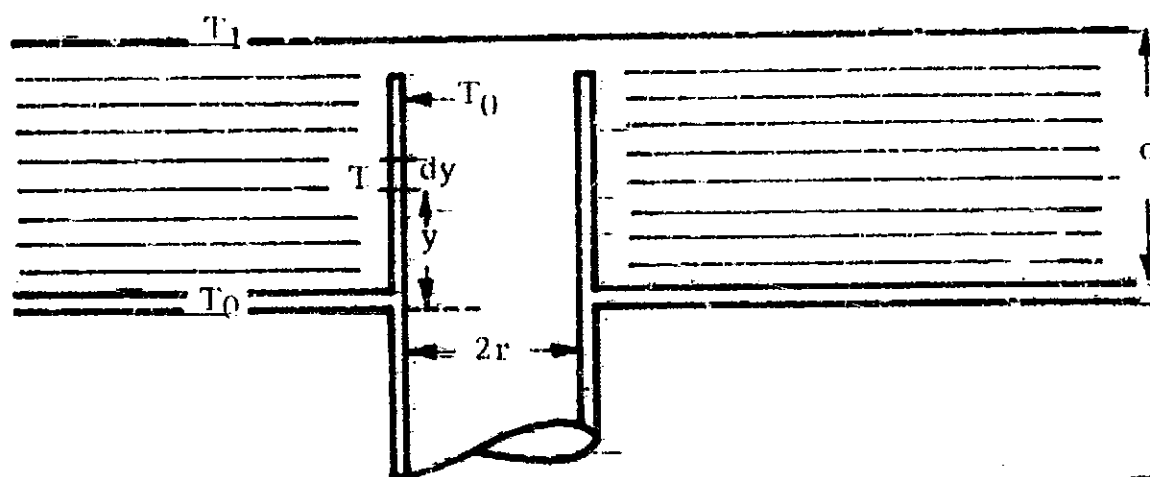


FIGURE II-III-10 VENT PIPE PENETRATING MULTILAYER SHIELDS

and the outside of the pipe is

$$q_{\text{indirect}} = \int_0^d \frac{y}{d} 2\pi r dy \epsilon_0'' (T^4 - T_0^4) \quad (\text{II-III-44})$$

Now

$$T^4 - T_0^4 = (T_1^4 - T_0^4) \frac{y}{d} \quad (\text{II-III-45})$$

Thus

$$q_{\text{indirect}} = \frac{2\pi r}{d^2} \epsilon (T_1^4 - T_0^4) \int_0^d y^2 dy = \frac{2\pi}{3} \epsilon_0 r d \epsilon (T_1^4 - T_0^4) \quad (\text{II-III-46})$$

The direct radiation from the outermost foil into the pipe is

$$q_{\text{direct}} = \pi r^2 \epsilon (T_1^4 - T_0^4) \quad (\text{II-III-47})$$

We have assumed here that the inside of the pipe is black. This is a conservative assumption which is approached when r/d is small.

The resultant heat flow to the tank due to the penetration is

$$q_p = (\pi r^2 + \frac{2\pi}{3} \epsilon_0 r d) \epsilon (T_1^4 - T_0^4) \quad (\text{II-III-48})$$

The total heat flow over the whole surface of the tank is

$$q_t = \frac{A}{n(\frac{2}{\epsilon} - 1)} (T_1^4 - T_0^4) \quad (\text{II-III-49})$$

Thus the fractional leak due to the penetration is

$$\frac{q_p}{q_t} = \frac{(\pi r^2 + \frac{2\pi}{3} \epsilon_0 r d) n(\frac{2}{\epsilon} - 1)}{A} \quad (\text{II-III-50})$$

If we assume the previous values $n = 100$, $d = 1$ inch, $\epsilon = \epsilon_0 = 0.05$, $A = 450 \text{ ft}^2$ and take $r = 1/2$ inch, we find that $q_p/q_t = 0.05$. Thus a single 1-inch diameter pipe increases the heat flux by only 5%. This is an extreme estimate, since the inside of the pipe was assumed to

be black. For a shiny inside surface, of moderate r/d, the input flux could be much less.

6. Gas Leakage from Cryogenic Fuel Tanks

With present technology, it is practically impossible to make large tanks for liquid hydrogen with gas-tight welds. The leak rates from large tanks may be so high that the performance of multilayer insulations will be seriously degraded unless proper allowance can be made in the design of the thermal protection system. Similar problems may arise when the helium-purged gas is vented.

1. Minimum Heat Flux Through a Stack of Perforated Radiation Shields

The analysis of the minimum heat flux through a series of perforated radiation shields can be based on the preceding calculations, and the heat transfer rates due to both conduction and radiation can be obtained for any given value of the perforation coefficient τ . It is clear that the total heat flux must pass through a minimum as τ varies from 0 to 1, since the radiation is very large when τ is near unity and the conduction is very large when τ is near zero. It is therefore of interest to find that best value of τ and the corresponding minimum value of the flux.

The flux due to gas conduction near the cold side of the stack of shields, where the gas density is highest, is, from Equations II-III-10 and II-III-11,

$$q_c = \frac{1}{2} \frac{\rho^2 \gamma (1 - \tau) k T^2}{\tau}$$

where T is the temperature difference across a single gap. We will

make no appreciable error in assuming that this expression holds over the whole set of shields, since the effect of conduction is negligible except near the cold side of the stack, due to the rapidity with which the radiation factor ϵT^4 rises with T .

The radiation rate can be written with sufficient accuracy, from Equation II-III-21, -22, and -23, as

$$q_r = \frac{\epsilon + (2-\epsilon)T_2}{T} \epsilon T^4$$

where ϵT^4 refers to one gap. We have omitted the 1 in the denominator of Equation II-III-22 to facilitate further calculations. Since n is large and ϵ small, this makes no appreciable difference.

The sum of these two expressions is the total flux q across a given gap and is a difference equation in T and T^4 . When this equation is summed over all the gaps and the result divided by n , we obtain for the total flux

$$q = \frac{\epsilon + (2-\epsilon)T_2}{(2-\epsilon)(1-\epsilon)} \frac{(T_2^4 - T_1^4)}{n} + \frac{3}{2} k(T_2 - T_1) \frac{(1-\epsilon)n}{n}$$

$$= \frac{\sigma(T_2^4 - T_1^4)}{(\frac{2}{\epsilon} - 1)n} + (\frac{2}{2-\epsilon}) \frac{(T_2^4 - T_1^4)}{(1-\epsilon)n} + \frac{3}{2} k(T_2 - T_1) \frac{(1-\epsilon)n}{n}$$

(II-III-51)

The first term in Equation II-III-51 is the radiation flux without perforations. The second term is the increase in radiation due to the perforations. The third term is the flux due to conduction by the gas molecules in the spaces between the shields.

For any fixed value of n , this expression goes through a minimum for a certain value of the perforation coefficient τ . The optimum value of τ is given by

$$\frac{\tau}{1-\tau} = n \left[\frac{\frac{3}{2} \nu k (T_2 - T_1)}{\sigma (T_2^4 - T_1^4)} \left(\frac{2-\epsilon}{2} \right) \right]^{1/2} \quad (\text{II-III-52})$$

The corresponding minimum value of q is

$$q_{\min}(n) = \frac{\sigma (T_2^4 - T_1^4)}{\left(\frac{2}{\epsilon} - 1 \right) n} + \left[6 \nu k (T_2 - T_1) \sigma (T_2^4 - T_1^4) \left(\frac{2}{2-\epsilon} \right) \right]^{1/2} \quad (\text{II-III-53})$$

Equation II-III-53 shows that, no matter how large n may be, the flux can never be less than the value

$$q_{\min}(\infty) = \left[6 \nu k (T_2 - T_1) \sigma (T_2^4 - T_1^4) \left(\frac{2}{2-\epsilon} \right) \right]^{1/2} \quad (\text{II-III-54})$$

Table II-III-1 shows how $q_{\min}(\infty)$ depends on the outgassing rate under the following conditions:

$$T_2 = 300^\circ\text{K}$$

$$T_1 = 25^\circ\text{K}$$

$$\epsilon = .05$$

$$k = 1.38 \times 10^{-16} \text{ erg deg}^{-1}$$

TABLE II-III-1

MINIMUM HEAT FLUX AS A FUNCTION OF
OUTGASSING RATE

<u>Outgassing Rate</u> <u>(molecules cm⁻² sec⁻¹)</u>	<u>q_{min}([∞])</u> <u>(erg cm⁻² sec⁻¹)</u>
10 ¹⁰	33
10 ¹¹	105
10 ¹²	330
10 ¹³	1,050

For comparison, when $n = 100$, the first term in Equation II-III-53 is $118 \text{ erg cm}^{-2} \text{ sec}^{-1}$. This value corresponds to the optimum heat flux for an interplanetary mission, with only radiation transfer through the shield. Table II-III-1 indicates that this optimum flux cannot be obtained with practical shielding if the outgassing rate is higher than $10^{10} \text{ molecules cm}^{-2} \text{ sec}^{-1}$.

The flux q , as given by Equation II-III-51, is plotted in Figure II-III-11 in $\text{Btu/ft}^2\text{-hr}$ as a function of the perforation factor τ for various assumed values of the hydrogen gas flow rate v_0 (expressed in both $\text{molecules/cm}^2\text{-sec}$ and $\text{lb/ft}^2\text{-hr}$). The graph refers to the case of 100 shields of emissivity 0.05, with outer and inner temperatures of 300°K and 25°K , respectively.

Figure II-III-11 shows that an optimum perforation factor exists for any given gas flow rate. Table II-III-2 gives the optimum value of τ and the corresponding minimum heat flux q for various values of the gas flow rate v_0 . The table shows that a hydrogen flow rate of $2.5 \times 10^{-7} \text{ lb/ft}^2\text{-hr}$ impairs the insulation by a factor of about two. This

leakage rate corresponds to only 1 lb per year from a tank of 500 ft² surface area.

TABLE II-III-2
OPTIMUM PERFORATION FACTOR τ_{opt} AND
MINIMUM HEAT FLUX q_{min} FOR VARIOUS
GAS FLOW RATES v_o

v_o (lb H ₂ /ft ² - hr)	τ_{opt}	q_{min} (Btu/ft ² - hr)
0	0	0.04
2.5×10^{-7}	0.01	0.07
2.5×10^{-6}	0.03	0.14
2.5×10^{-5}	0.11	0.38
2.5×10^{-4}	0.27	1.24

For the leakage rate of 2.5×10^{-4} lb/ft² - hr, which corresponds to a loss of 3 lb/day from the 500 ft² tank, the total heat input is 600 Btu/hr, which would boil off all the hydrogen in two months. Actual leak rates may be even larger than 3 lb/day.

These calculations indicate clearly that the gas leaking through the seams of the tank should not be pumped by the external vacuum through the insulating blanket. Instead, the gas should be vented directly to the external vacuum by means of a double-walled arrangement, shown schematically in Figure II-III-12. The leakage of gas into the insulating layers will be greatly reduced if the outer tank wall is reasonably gas-tight.

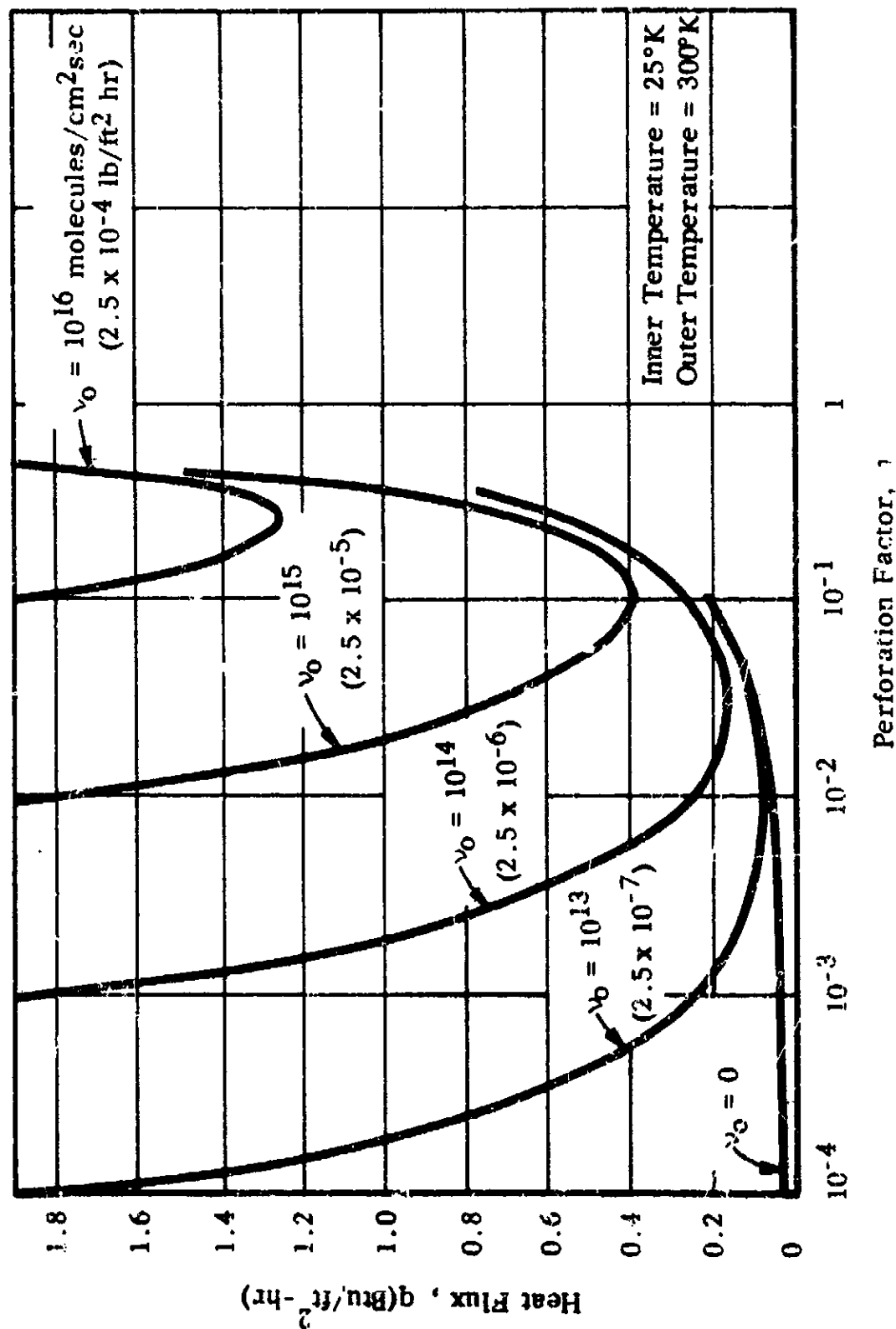


FIGURE II-III-11

HEAT FLUX THROUGH 100 PERFORATED SHIELDS AS A
FUNCTION OF PERFORATION FACTOR FOR VARIOUS
HYDROGEN GAS FLOW RATES

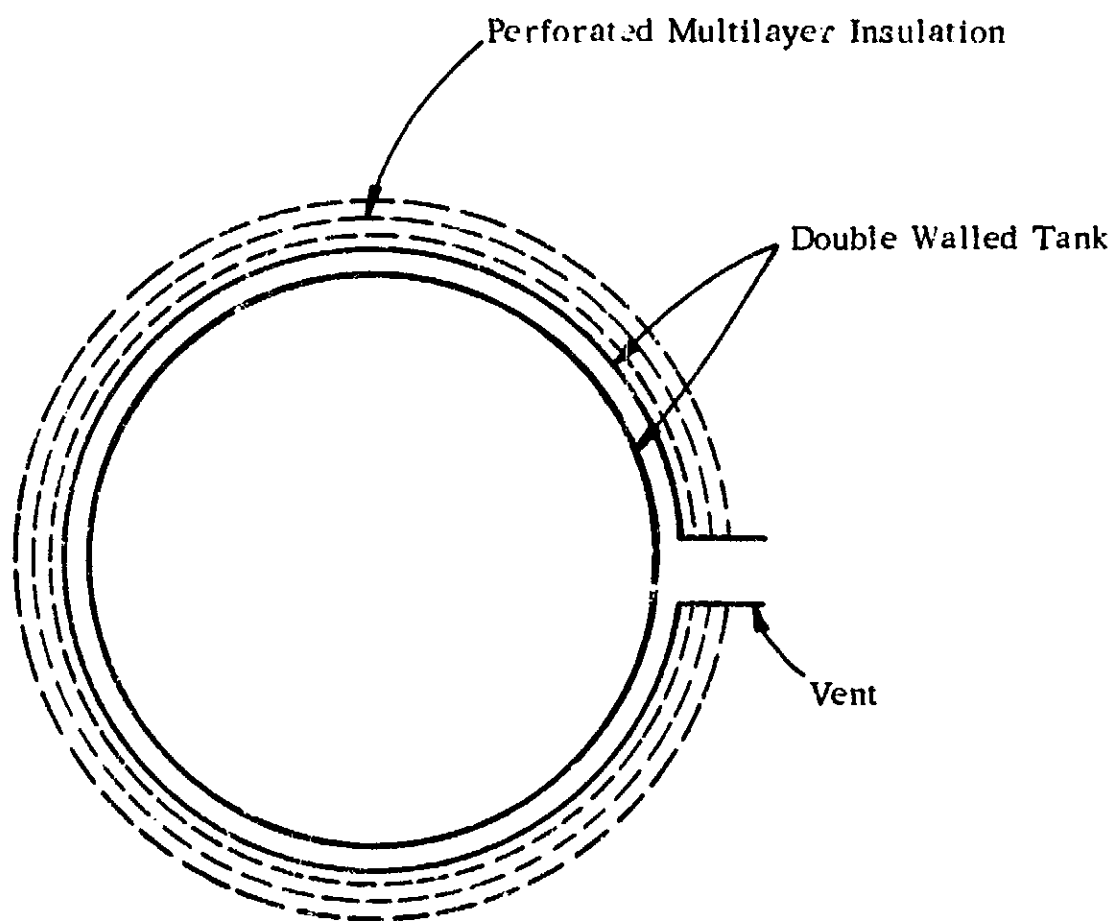


FIGURE II-III-12

DIRECT VENTING OF LEAKING GAS BY DOUBLE-WALLED TANK CONSTRUCTION

The vent pipe will probably have to extend well beyond the insulation to prevent diffusion of the vented gas back into the perforated shields from the outside. The static pressure at the exit of a pipe of cross section 1 cm^2 that transmits 3 pounds of hydrogen per day is about 5 mm Hg; thus, aerodynamic rather than free molecular flow occurs at the exit.

A much better solution to the gas conduction problem than the double-walled tank arrangement would, of course, be the development of a method for making vacuum-tight welds. It is likely that successful long-term cryogenic storage in space will depend on this development.

The configuration of the perforations in the multilayer insulation is of considerable importance. For a given perforation ratio, the highest gas-pumping performance, relative to the inward radiation leakage, is obtained with a large number of small holes with an average spacing much less than the shield separation. This perforation arrangement was assumed in the derivation of Equation II-III-51. The reason why this is the best arrangement is that the net flow pattern for both gas molecules and radiation is then in the form of straight lines perpendicular to the shields, except in the immediate vicinity of the shields themselves. The two flow patterns are illustrated in Figures II-III-13 and -14. The only difference is that some of the radiation flow lines start and terminate on unperforated parts of the shields, whereas the molecular flow lines cannot do this.

On the other hand, when the perforations are widely spaced relative to the shield separation, as in Figures II-III-15 and -16, the radiation flow is much more nearly perpendicular to the foils than is the gas flow.

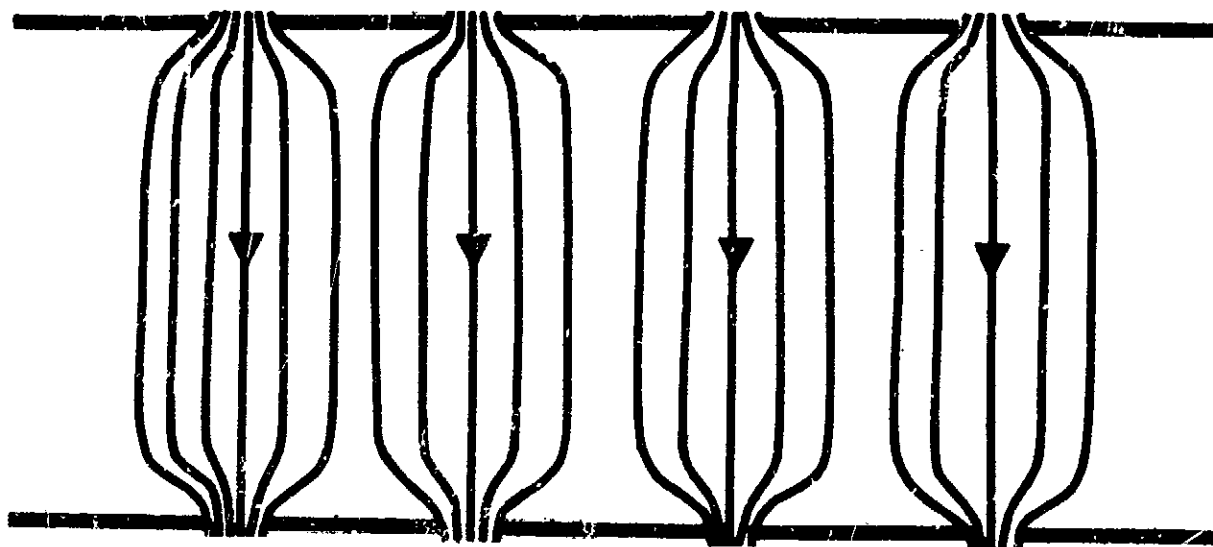


FIGURE II-III-13 GAS FLOW PATTERN FOR CLOSELY SPACED PERFORATIONS

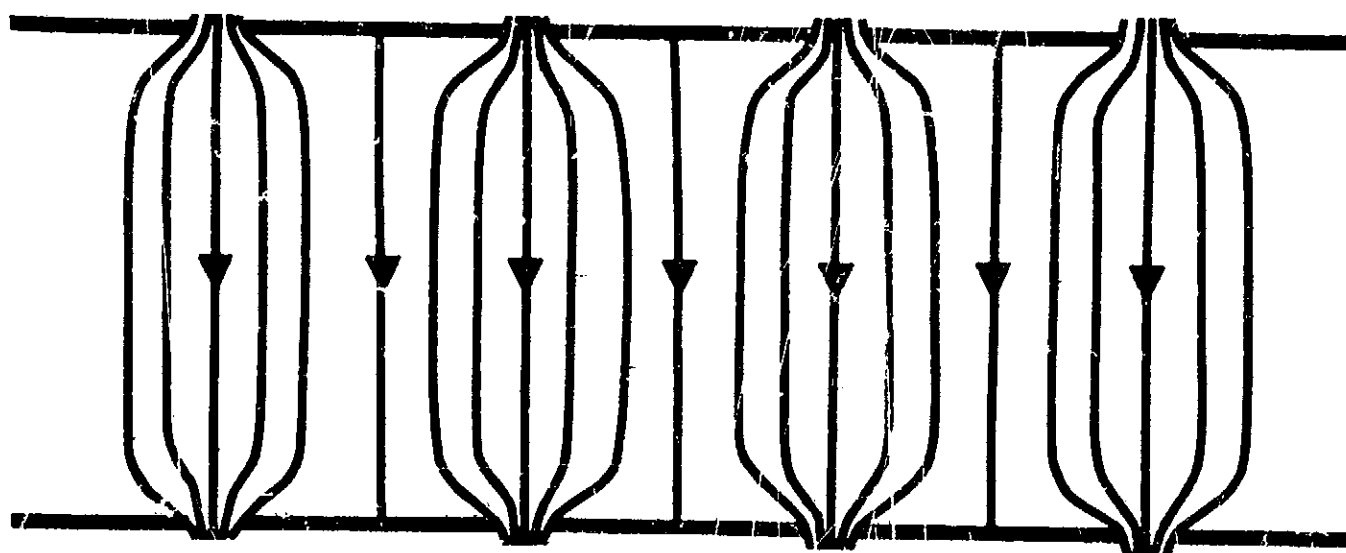


FIGURE II-III-14 RADIATION FLOW PATTERN FOR CLOSELY SPACED PERFORATIONS

The reason is that the gas can flow only through the holes, whereas the radiation can also flow directly through the nonperforated regions by the process of absorption on one side of a foil and re-emission on the other side. Since the gas must take longer paths through the foils than the radiation, the pumping efficiency, relative to the radiation leakage, is much less for very widely spaced holes.

Calculation of the flow patterns of Figure II-III-15 and -16 would be very difficult, but one can see qualitatively that not much change from the conditions of Figures II-III-13 and -14 will occur if the hole spacing is of the same order as the shield spacing. On the other hand, for very large hole spacings, the gas flow rate approaches zero, while the radiation rate drops to a limiting value. For the case of regularly spaced holes that are staggered from shield to shield as in Figures II-III-15 and -16, the radiation flux has the limiting value:

$$q = \frac{\sigma (T_2^4 - T_1^4)}{n \left(\frac{2}{\epsilon} - 1 \right) \left(\frac{1 - \tau}{1 + \tau} \right) + 1} \quad (\text{II-III-55})$$

For randomly distributed holes the limit is

$$q = \frac{\sigma (T_2^4 - T_1^4)}{n \left(\frac{2}{\epsilon} - 1 \right) \left(\frac{1 - \tau}{1 + \tau} \right) + 1} \quad (\text{II-III-56})$$

For small values of τ these two expressions are almost identical.

On the other hand, the radiation flux for closely spaced holes, as shown in Equation II-III-22 is:

$$q = \frac{\sigma (T_2^4 - T_1^4)}{n \left[\frac{2}{\epsilon + (2 - \epsilon) \tau} - 1 \right] + 1} \quad (\text{II-III-57})$$

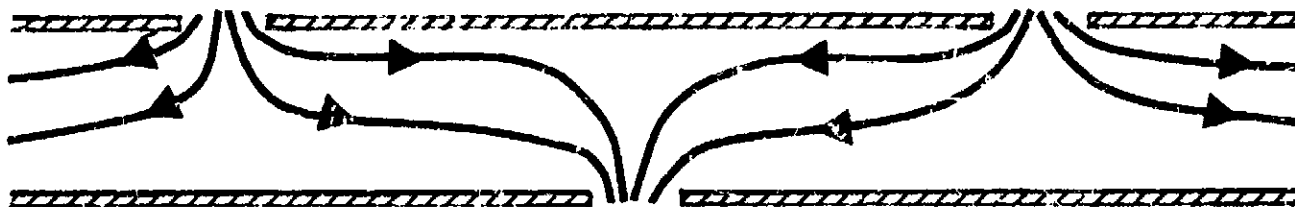


FIGURE II-III-15 GAS FLOW PATTERN FOR WIDELY SPACED PERFORATIONS

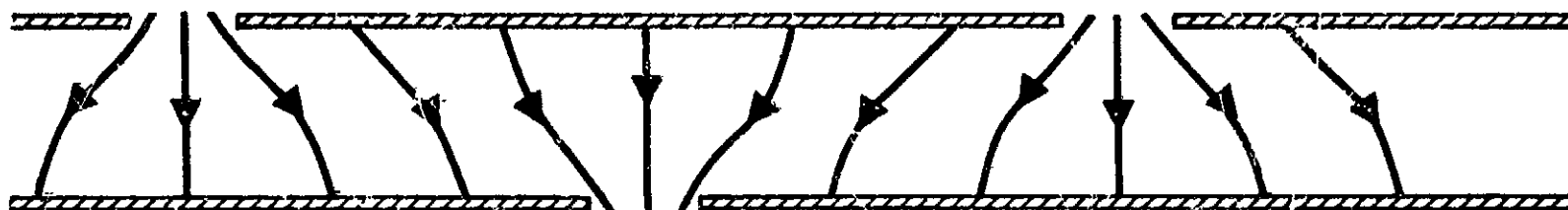


FIGURE II-III-16 RADIATION FLOW PATTERN FOR WIDELY SPACED PERFORATIONS

A comparison of (II-III-56) and (II-III-57) shows that, for constant T , the radiation flux increases considerably as the hole spacing is decreased, but the gas conduction flux increases by a still larger amount.

Production problems impose a practical lower limit on the diameter of the perforations as well as their spacing. New production techniques will have to be devised to obtain the desired perforations and thus increase the insulating performance of multilayer insulations in an actual installation.

D. Conductive Heat Leaks at Discontinuities Due to Joints, Supports, and Piping Attachments

Once the basic requirements for the payload and the weight of the cryogenic propellants to complete specific missions are known, the insulating effectiveness of the thermal protection system and the maximum allowable heat leak through discontinuities caused by joints, supports, and piping attachments can be specified. As a rough design guide, no more than 30% of the total heat leak into the tank should be caused by such discontinuities. If the proportion were higher than 30%, the effectiveness of the multilayer insulation would tend to be nullified, and its application might not be warranted.

Analyses have been carried out on the heat leaks due to insulation penetrations and discontinuities. These can be classified as:

(a) Weak thermal shorts, where a linearized radiation boundary condition can be applied with acceptable accuracy (e.g., where the surface temperature is within 10% of the adiabatic wall temperature).

(b) Strong thermal shorts, when the depression of the temperature at the outer surface of a foil exceeds 10% of the adiabatic wall

temperature and when the analytical solution of the problem is complicated by a nonlinear boundary condition.

(c) Absolute thermal shorts, where the penetration is so highly conductive that the tank wall and the outside surface of the short are nearly at the same temperature.

Conductive heat leaks are of particular concern after the space vehicle has left the earth's atmosphere and is subject to the various radiative heat inputs from the sun and other solar system bodies.

1. Weak Thermal Shorts

Multilayer insulations can be used with materials such as Teflon to meet structural requirements and to satisfy the weak thermal short condition. Steel or other separators would not fall into the category of weak thermal shorts unless an insulator could be installed between the multilayers and the penetration. In the case of aluminized film, weak thermal shorts can be obtained for reasonable thicknesses of very poor conducting structural materials when the thickness of the film assembly is greater than one inch.

Figure II-III-17 concerns the penetration of multilayer insulations by various materials and shows the maximum widths that these materials can have for the weak thermal short approximation to be applicable.

The design of the thermal protection system, even with weak thermal shorts, may have to be modified so that the over-all heat leak is within permissible limits. To illustrate this point, a cylindrical tank 10 feet in diameter and 20 feet long would contain about 5000 pounds of liquid hydrogen, and its cylindrical surface area would be 628 sq. ft. If there are two 10-mil plastic dividing strips around this tank, then it can be

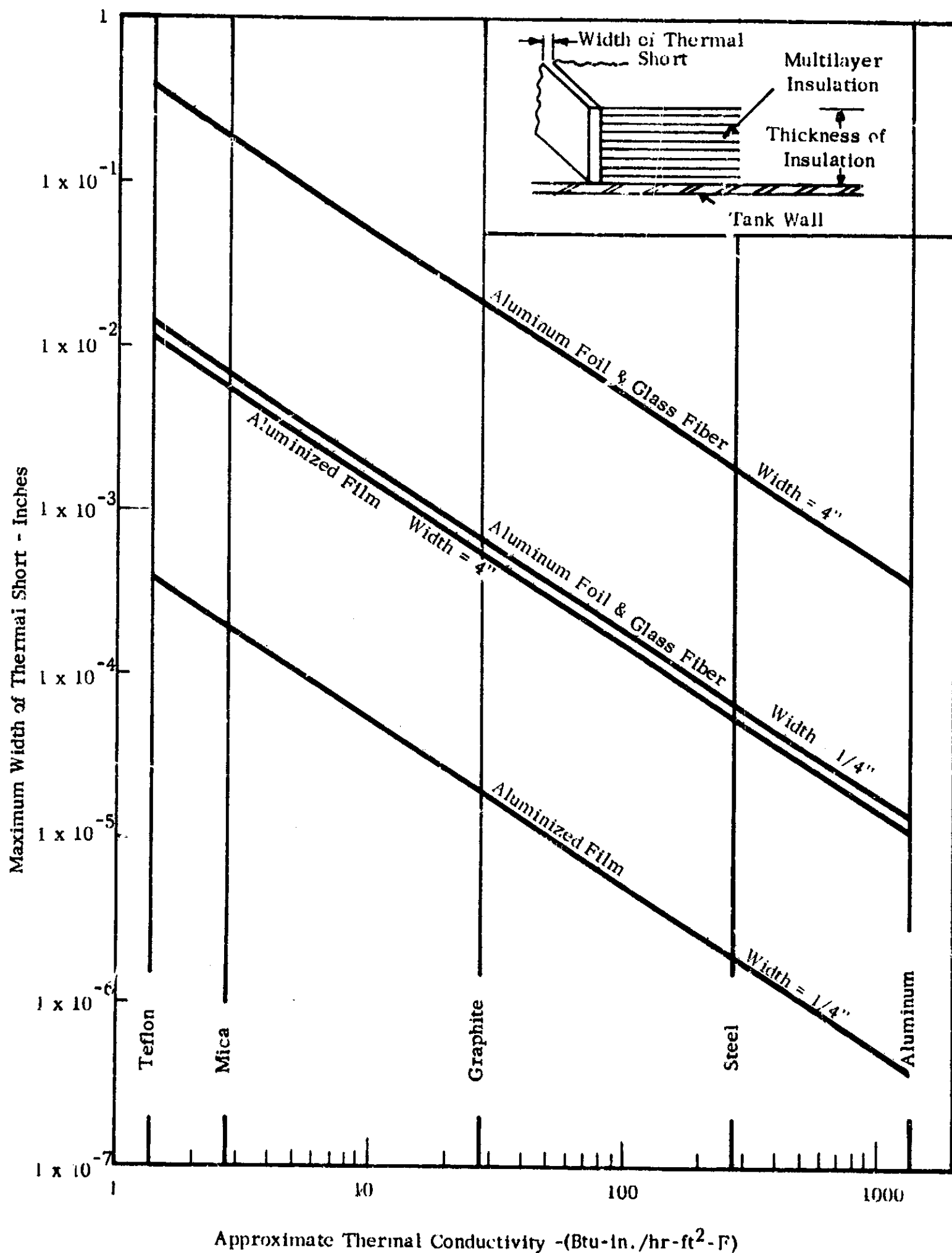


FIGURE II-III-17 MAXIMUM WIDTH OF VARIOUS THERMAL SHORT MATERIALS PENETRATING MULTILAYER INSULATIONS

shown that the heat leak through these strips would be equivalent to that of 520 sq. ft. of insulation. Therefore, the over-all heat leak would be increased by more than 80%.

2. Strong Thermal Shorts

Because heat leaks associated with strong thermal shorts are greater than would occur from weak thermal shorts, design approaches that convert strong shorts to weak ones must be used.

The approach in reducing the heat leak due to a strong thermal short is to separate the strong thermal shorts from the ends of the multilayer insulation, thus bringing them into the range of weak thermal shorts. Examples of the approach that can be followed to decrease the effect of a strong thermal short are shown in Figure II-III-18. This figure shows the following:

(a) A strip of evacuated insulation (fibers or foam) separating multilayer insulation from a thermal short.

(b) A square section of evacuated insulation placed in a corner to protect the shields in one direction from being shorted by those in the other direction when the radiant flux impinges equally on both surfaces of the insulation.

(c) A square section of evacuated insulation, the upper side of which is kept adiabatic to protect a joint between a tank wall and a large pipe or a structural support with negligible heat flow from the warm end to which these elements would be connected.

(d) A square section of evacuated insulation provided with a protective radiation shield, the upper side of which receives the same radiant flux as does the multilayer insulation.

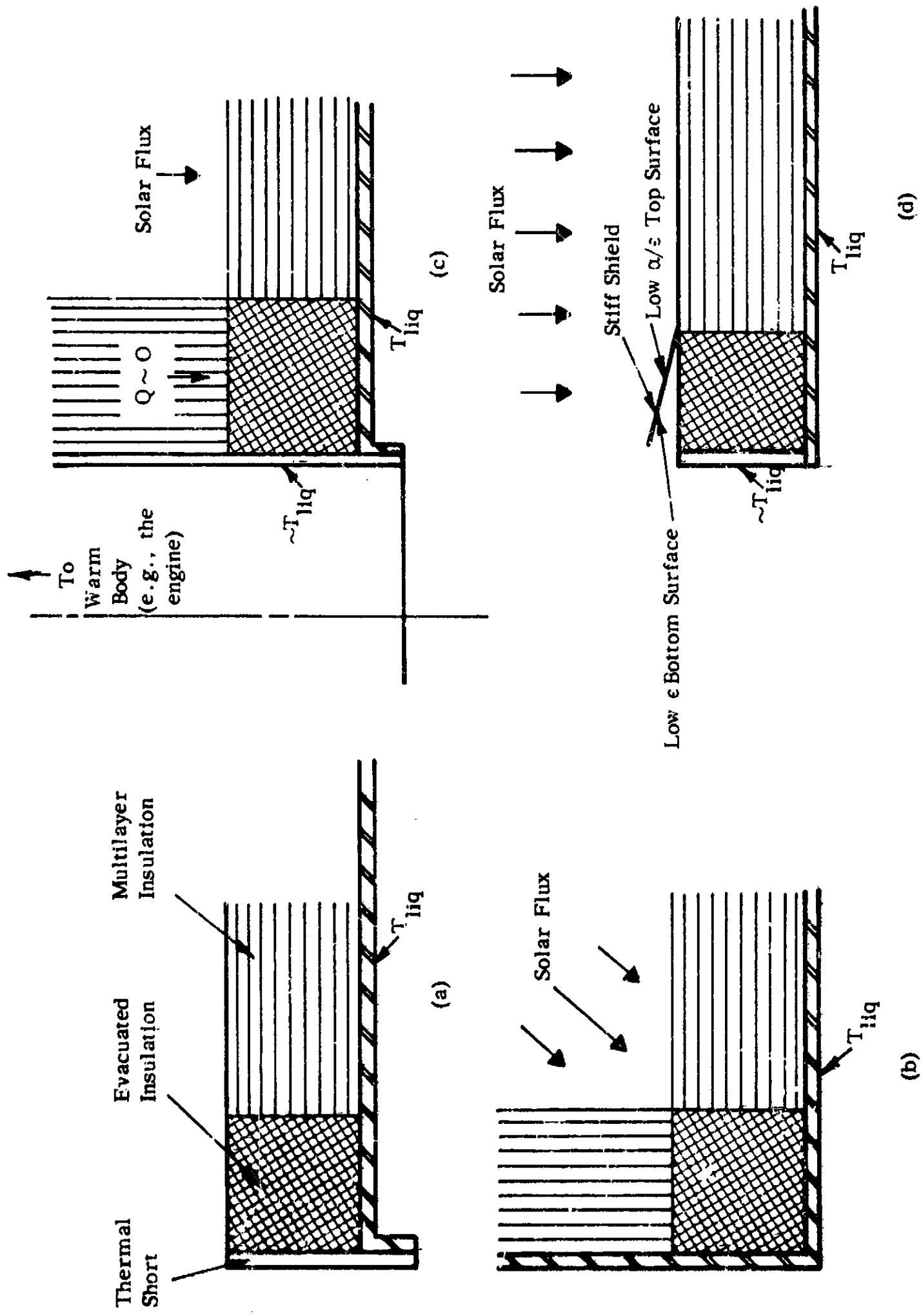


FIGURE II-III-18 TECHNIQUES FOR DECREASING THE EFFECT OF THERMAL SHORTS

Calculations have shown that, for a surface temperature of 300°K and a liquid temperature of 20°K , the heat leak due to the presence of a one-foot length of a square cross section of evacuated insulation is equivalent to from 0.5 to 1.5 sq ft of undisturbed multilayer insulation. The dimensions of the square cross section do not influence this result for insulation thicknesses in the order of one inch.

Splices and terminating insulation sections should be placed on the shady side of the tank or be protected by a shadow shield to reduce the possibility of edge effects at discontinuities.

Thus, joints, supports, and piping attachments must be given considerable attention. Special design techniques must be employed so that the heat leak can be kept to acceptable proportions.

3. Effect of Internal Radiation in Pipes

We have also analyzed the leakage of heat into cryogenic tanks through transfer lines. The thermal coupling through the transfer line that joins the cryogenic tank to the relatively warm engine involves internal heat radiation as well as conduction along the pipe walls. If thermal radiation were absent or negligible, the conductive heat flow to the tank could be kept within reasonable limits by proper selection of pipe wall materials and thicknesses. However, the thermal radiation energy emitted at the warm end is partly absorbed by the walls at points nearer the cold end; some of this energy is conducted and some re-radiated toward the cold end. The resulting radiation and increased pipe wall gradients can lead to heat leaks that are greater than the heat flow through the blanket of thermal insulation applied over the entire cryogenic tank.

We have analyzed the radiative-conductive effect in a pipe, to determine what heat inleakages might be expected and to provide a guide for the thermal design of the pipe.

a. Pipe with Length-to-Diameter Ratio of 3

First, we considered a pipe with an L/D ratio of 3. Gray, diffuse walls have been assumed. (The assumption of diffuse reflection is not conservative; specular reflection should lead to greater heat flow by radiation to the cold end.)

The results can be applied, for example, to a typical pipe 10 inches in diameter and 30 inches long, with its warm end at 300°K and its cold end at 20°K . At low end emissivities, with non-zero wall conductivity, the total heat leak will be affected by wall emissivity if the latter is between 0 and approximately 0.2. The heat leak is of the order of a few watts. At high end emissivities, again with non-zero wall conductivity, wall emissivity plays a minor role; the heat leak is quite high (between 7 and 9 watts) and almost independent of ϵ_{wall} . It is therefore necessary for such a pipe to have low emissivity at its ends. However, this may be difficult to achieve except with shiny baffles near the ends.

Some variations in pipe design to decrease the heat leak to values of the order of a watt or less are possible: higher L/D ratios, baffles at selected points, curved pipes. In addition, part of the outer surface of the pipe can be left bare near the warm end so that it can radiate to a cold environment; this will cause the temperature of the pipe to fall off to low values for most of its length. In such a case the cold end views only the distant circle of the warm end cross section, and the radiative interchange is effectively decoupled from the cryogenic tank.

b. Pipe with Length-to-Diameter Ratio of 9

We also considered a single case of a pipe with an L/D ratio of 9. In this case, the end emissivities were considered to be unity and the wall emissivity zero. The resulting radiative heat leak for a pipe 90 inches long and 10 inches in diameter is 2.7 watts, compared with 6.7 watts for a similar pipe only 30 inches long. The conductive leak depends on the wall conductivity and thickness; it can be added algebraically to the radiative component, since the two are decoupled. For a given wall thickness, the longer pipe will obviously conduct less heat. If the product (thermal conductivity) x (wall thickness) can be neglected for this long pipe, the heat leak will be purely radiative and will equal 2.7 watts regardless of wall emissivity, provided the end emissivities are unity. This again points to the importance of end emissivities and to the necessity for pipe design based on considerations of radiative heat transport.

4. The Possibility of Scaling

When the insulation on a cryogenic tank has been properly designed and applied, the penetrations of various types (weak shorts, strong shorts, pipes, strips, pins, etc.) will behave as follows: (1) they will not interfere with one another, in the sense that the temperature disturbance due to one penetration will not affect the behavior of any other penetration; (2) they will alter the temperature distribution in the insulation blanket (as imposed by external flux) only locally. Under such circumstances, the total heat inleakage to the tank can be predicted by superimposing the contributions of the insulation blanket and the penetrations, if each contribution is known separately.

The circumstances postulated above should occur frequently. Where they do not (i.e., where there is strong interference between various components), either the system has not been designed properly from a thermal point of view, or some overriding consideration (e.g., structural) has been imposed. In the ordinary case, what has been said about superposition applies; thus, it is important to be able to predict the behavior of the blanket itself.

a. Insulation Blanket

The total heat inleakage, Q_B , through the insulation blanket (considered without penetrations) will depend on the incident flux distribution, the shape and size of the tank, the number of foils and their optical and thermal properties. We will consider only the steady state. For a given tank shape and incident flux distribution (normalized by dividing by the maximum flux), the following three sets of variables must be kept constant if two tanks are to be considered similar:

$$\left(\frac{\alpha_o}{\epsilon_o} f_{\max} \right)^{3/4} \frac{\epsilon D^2}{k t n^2}$$

$$\frac{\epsilon_o n}{\epsilon}$$

and

$$\frac{\epsilon \epsilon_o (T_{\text{liq}})^4}{\alpha_o f_{\max}} = \left(\frac{T_{\text{liq}}}{T_{a, \max}} \right)^4$$

where

α_o = absorptivity of the outer surface of the outer foil for the incident radiation

ϵ_o = emissivity of that surface

f_{\max} = intensity of incident flux at the point where it is a maximum

ϵ = emissivity of the foils at the temperature

$$T_{a, \max} = \left[\alpha_o f_{\max} / \sigma \epsilon_o \right]^{1/4}$$

D = a typical dimension of the tank

k = thermal conductivity of the foils

t = thickness of a foil

n = number of foils

σ = the Stefan-Boltzmann constant

T_{liq} = temperature of the cryogenic liquid (and of the tank wall)

$T_{a, \max}$ = adiabatic wall temperature corresponding to the maximum incident flux.

If the third parameter, $T_{liq}/T_{a, \max}$, is small compared with unity, the condition that it be kept constant is not a very stringent one. The other two conditions are sufficient for similarity, provided that heat flows normal to the foils by radiation only and parallel to the foils by conduction only.

For self-similar cases, the total heat flow to the tank (no penetrations) is

$$Q_B = (\text{Constant}) (\alpha_o f_{\max} D^2) \frac{\epsilon}{\epsilon_o n}$$

provided that ϵ has the same dependence on temperature for similar cases (which will be true if the same foil material is used in each case), or that ϵ is not a function of temperature (we have seen that little error is incurred in assuming that the latter is true). Since $\epsilon_o n / \epsilon$ is presumed constant, we may rewrite Q_B as:

$$Q_B = (\text{Constant}) \alpha_o f_{\max} D^2$$

The condition that the first two parameters be kept constant leaves some choice in the selection of the remaining variables. This choice will determine the scaling factor to be used in computing Q_B for a particular tank from the results (test or computer) on a similar tank of different size. In the following two examples, ϵ and kt are kept constant and the same foils are used.

(1) If n/D is kept constant, then for similarity,

$\alpha_o f_{\max}$ must vary as $1/D$

and

ϵ_o must vary as $1/D$

If these relationships are adhered to, Q_B will vary as D . Suppose that, under direct solar radiation, 8 watts of heat flows into a cylindrical cryogenic tank 10 feet long, 4 feet in diameter, axis at 45° to the direction of the sun, and insulated with 20 layers of a certain foil. The outer foil absorbs 20% of the solar radiation ($\alpha_o = 0.2$) and has an emissivity ϵ_o of 0.9. With this information we can determine the heat input to a geometrically similar tank--one that is, for example, 20 feet long and 8 feet in diameter--under solar radiation from the same direction, for a large class of situations.

In particular, if the 20-foot tank is insulated with 40 layers of the same foil, then the ratio n/D is the same as for the 10-foot tank. For similarity, α_o must be 0.1, since f_{\max} (solar flux) is the same in both cases; also, ϵ_o must be 0.45. In this situation, the heat input w will be in proportion to dimension--namely, 16 watts for the 20-foot tank.

(2) If n/D^2 is kept constant, then for similarity,

$$\alpha_o f_{\max} \text{ must vary as } D^{2/3}$$

and

$$\epsilon_o \text{ must vary as } 1/D^2$$

If these relationships are adhered to, Q_B will vary as $D^{8/3}$. If the 20-foot tank in the example above is insulated with 80 layers of the same foil, then the ratio n/D^2 is the same as for the 10-foot tank. For similarity, α_o must be $0.2 \times 2^{2/3} = 0.317$; ϵ_o must be $0.9/2^2 = 0.225$. In this situation the heat input will be $8 \times 2^{8/3} = 50.5$ watts.

b. Penetrations

Once the behavior of the blanket can be predicted, the contribution of penetrations must be considered.

If, as postulated above, a penetration affects the temperature distribution in the insulation blanket only locally, its contribution will be determined by inserting it (in a test or computation) at the correct location on the tank. The reason is that the temperature distribution in the undisturbed blanket in the neighborhood of the penetration is the environment that will determine the heat leak through the penetration. For example, a penetration located on the sunlit side of a tank (where the temperature gradients normal to the tank are high) will produce a greater heat leak than if located on the shaded side.

Penetrations constituting strong and absolute thermal shorts will in most cases have to be considered individually, as their effect cannot be predicted with linearized analysis. Note, however, that even a strong short may alter the temperature distribution in the insulation only locally; hence, its contribution can be superimposed, even though the (local) disturbance and the added heat flow be large.

The contribution of a weak thermal short to the total heat leak is more easily dealt with in most cases, as has been discussed in our previous reports. There are exceptions, such as when a reversal in temperature gradient occurs within the foils. In the latter situation the local gradient at the tank wall may be disturbed appreciably by the presence of even a weak short. Therefore, all penetrations must be carefully considered in order to determine the effect of each one on the total heat leak into a cryogenic tank.

IV. INSULATION SYSTEMS

The concept of an insulation composed of a series of radiation shields separated by non-conducting spacers, although relatively simple, hinges on the availability of suitable materials. The discovery of the high insulating effectiveness of multilayer insulations did not immediately result in their wide application, because practical problems were involved in obtaining either metallic or non-metallic radiation shields and spacers that were thin enough to permit the use of about 100 radiation shields per inch.

Because the phenomena governing heat transfer through these insulations have not been thoroughly treated in the literature, materials selection has proceeded primarily on an empirical basis. In making our selections of suitable materials to be used in the test program, we were guided by the following criteria:

1. Are the insulation materials now commercially available or will they shortly be made available?
2. Are the material properties constant and reproducible so that test results can have generalized applications?
3. Can the materials withstand some of the environmental factors which the thermal protection system may encounter during service?
4. Can the materials be applied to large liquid hydrogen tanks at a cost commensurate with their performance?
5. Are these materials available for test purposes without restrictive proprietary conditions?

On the basis of these criteria, the materials shown in Table II-IV-1 were used in assembling different multilayer insulations. The table indicates the nature of the radiation shield and spacer material, gives details of their construction, and indicates where they were obtained. In addition, some materials were supplied to us by manufacturers either assembled in multilayers or with instructions on how to do so. The variables studied with each insulation and the corresponding test numbers are also listed in the table. Figure II-IV-1 shows enlarged views of the different spacers.

In addition to multilayer insulations, samples of foam and foam-filled honeycomb were also tested because of the possibility of using a composite structure of foams and multilayer insulations.

We are fully aware that further optimization of the multilayer insulations, both as to the type of materials used and the specific properties, can be accomplished. However, we believe that the materials tested represent a broad cross section of the materials that are now commercially available.

TABLE II-VI-1

INSULATION SYSTEMS TESTED

A - Multilayer Insulation Samples					
Insulation System	Radiation Shield * Material	Spacer Material	Variable Investigated	Sample Number	Sample Submitted by Company **
A	(10) Aluminum 1145-H19 alloy bright on both sides, 0.002 in. thick (Company B)	(11) Vinyl-coated glass fiber screen 1/8 x 1/8 in. mesh. (Company C)	Temperature	1035, 1037, 1039	A
			Gas Pressure	3005	
B	(11) Fiberglass mat 0.008 in. thick and 50% perforated (Company D)	(11) Fiberglass mat 0.008 in. thick and 50% perforated (Company D)	Discontinuities	3002, 3003, 3004	
			Perforations	3007, 3009, 3015	
C	(20) Crinkled polyester film aluminized on one side 0.00025 in. thick (Company E)	None	Perforations	3012, 3013, 3016, 3017, 3018, 3024, 3025	
			Density	1010	
E	(40) "	None	Temperature	1036	E
			Discontinuities	2015, 2016, 2017	
E	(40) "	None	Perforations	1048, 1050, 1051	
			Density	1010	
E	(40) "	None	Miscellaneous	1008, 1009	

* Numbers in parentheses indicate the number of shields or spacers used.

** See Appendix A for explanation of symbols.

TABLE II-VI-1

INSULATION SYSTEMS TESTED (Continued)

<u>Insulation System</u>	<u>Radiation Shield Material</u>	<u>Spacer Material</u>	<u>Variable Investigated</u>	<u>Sample Number</u>	<u>Sample Submitted by Company</u>
C	(60) Crinkled polyester film aluminized on one side 0.00025 in. thick (Company E)	None	Mechanical Load	3001	E
D	(60) "	(61) Fiberglass cloth 0.001 in. thick (Company F)	Mechanical Load	2005	A
E	(10) "	(11) Fiberglass mat 0.008 in. thick and 50% perforated (Company D)	Mechanical Load	1033	A
F	(20) " (Arranged in groups of two with their polyester fiber sides touching)	(11) Vinyl-coated glass fiber screen 1/8 x 1/8 in. mesh (Company C)	Mechanical Load	1031	A
G	(20) Aluminum 1145-0 alloy bright on one side 0.0005 in. thick (Company B)	(21) Polyester fiber 0.003 in. thick (Company D)	Mechanical Load	2006	A
H	(10) Aluminum alloy 0.00025 in. thick, bright on one side (shields & spacers were glued together)	(11) Fibrous paper 0.001 in. thick (Company D)	Density	1040	G

TABLE II-IV-1

INSULATION SYSTEMS TESTED (Continued)

Insulation System	Radiation Shield Material	Spacer Material	Variable Investigated	Sample Number	Sample Submitted by Company
I	(10) Aluminum alloy 0.001 in. thick, bright on one side (bottom shield was in contact with the warm plate)	(10) Glass fiber paper 0.003 in. thick	Density Temperature Gas Pressure Mechanical Load	2013 2013 1043 1043	G
J	(10) Aluminum alloy	(11) Fiberglass mat 0.014 in. thick (Company H)	Density	2026	I
K	(10) Aluminum alloy	(11) Each spacer consisted of three layers of fiberglass cloth 0.004 in. thick (Company J)	Mechanical Load Density	2027 2027	I
L	(6) Aluminum 1145-1119 alloy, bright on both sides, 0.002 in. thick (Company B)	(7) CT-449 material 0.080 in. thick and 12.7 lb/ft ² when compressed to 0.048 in., 11% support area. See Figure II-VI-24 (Company K)	Mechanical Load	3027	A
M	(6) Smooth aluminumized polyester film 0.00025 in. thick (Company E)	(7) CT-449 material 0.080 in. thick and 12.7 lb/ft ² when compressed to 0.048 in., 11% support area. See Figure II-VI-24 (Company K)	Mechanical Load	3028	A

TABLE II-IV-1
INSULATION SYSTEMS TESTED (Continued)

B - Foam Insulation Samples

<u>Insulation System</u>	<u>Sample Description</u>	<u>Variable Investigated</u>	<u>Sample Number</u>	<u>Sample Submitted by Company</u>
N	Phenolic-glass honeycomb filled with polyurethane foam; bonded to one side of the honeycomb was a grooved aluminum plate and to the other side a three-ply phenolic-glass laminate covered with Tedlar. The groove in the aluminum plate and the edge were sealed with an epoxy resin. Two Tygon taps were provided for purging the sealed sample.	Gas Purge	1041	L
O	Same as N, except the foam was epoxy.	Gas Purge	2011	L
P	Sintered perlite 7-1/2 inch diameter and 1.15 in. thick, Density 15.7 lb/ft ³ .	Contact Resistance	None	A
Q	Phenolic-glass honeycomb, 3/4-in. cells and 1.0 in. thick, filled with polyurethane foam CO ₂ -blown. The faces of the sample were covered with an 0.008-in. thick nylon/phenolic laminate and Tedlar. Two lengths of 3/16-in. O.D. and 1/32-in. wall Tygon tubing were attached to the edges for introducing gas into the sample.	Gas Purge	1045	L
R	Octagonal-shape samples of Freon-blown polyurethane foam, 12 in. across corners and approximately 0.4 in. thick; faces covered by laminate of 0.00075-in. Mylar, 0.001-in. aluminum, and 0.00075-in. Mylar. (Samples fabricated by Company M)	Contact Resistance Cryopumping Joint Mechanical Load	2022, 2024 2021 2025 2021, 2023, 2022, 2024	N N

TABLE II-IV-1

INSULATION SYSTEMS TESTED (Continued)

<u>Insulation System</u>	<u>Sample Description</u>	<u>Variable Investigated</u>	<u>Sample Number</u>	<u>Sample Submitted by Company</u>
S	Polyurethane foam, 1/4 in. thick	Contact Resistance	1014	N
T	Polyurethane foam reinforced with glass fibers, 3/4 in. thick	Contact Resistance Temperature	1018 1018	A
U	Microfiber Glass Wool	Miscellaneous	1004	A
<u>C - Combination of Multilayer and Foam Insulation</u>				
V	Polyurethane foam reinforced with glass fibers, 3/4 in. thick and 10 radiation shields of 1145-H19 aluminum alloy, 0.002 in. thick with spacers of vinyl-coated glass fiber screen, 1/8 x 1/8 in. mesh	Miscellaneous	1025	A



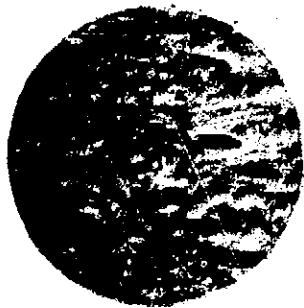
10 x Size

Polyester Fiber Mat
0.003 inch thick
contained in System G



10 x

Fiberglass Mat
0.014 inch thick
contained in System J



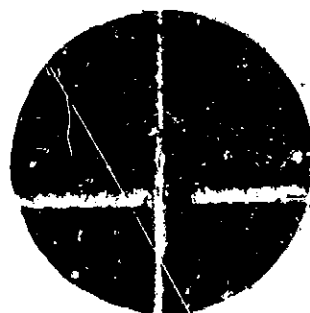
10 x

Glass Fiber Paper
0.003 inch thick
contained in System I

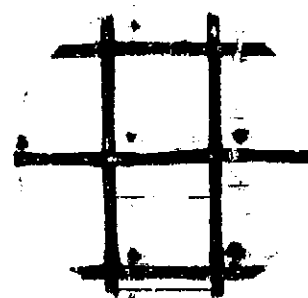


10 x

Fiberglass Cloth
0.001 inch thick
contained in System K



10 x



4 x

Vinyl-Coated Glass Fiber
Screen 1/8 x 1/8 mesh
contained in System A

FIGURE II-IV-1

ENLARGED VIEW OF TYPICAL SPACER MATERIALS

V. EXPERIMENTAL APPARATUS

A. Design Considerations

To measure the effects of different variables on the performance of multilayer insulations, we considered three basic designs of thermal conductivity apparatus: spherical, cylindrical, and flat plate. We found that no single type of apparatus described in the literature could meet all the required test conditions, namely, to permit the measurement of the effect of the following variables on thermal conductivity:

1. boundary temperature
2. gas pressure
3. gas type
4. mechanical load
5. gas purging
6. number of shields and thickness
7. thermal shorts and discontinuities.

After consultation with the National Bureau of Standards, Boulder, Colorado, we decided that a flat-plate thermal conductivity apparatus would be best suited for the experimental program because:

1. The test sample can be a small, easily assembled disc of varying diameter.
2. The sample can have a wide range of thickness which can be accurately measured while the sample is in contact with temperature-controlled boundaries.
3. A mechanical load can be applied to the sample under test.

4. The sample can be installed under closely controlled conditions.

Our experience with the single-guarded cold plate thermal conductivity apparatus, similar in design to the Wilkes calorimeter, helped us to establish the design criteria for the new apparatus. The latter incorporates the following features:

1. Thermal conductivities of multilayer insulations, powders, fibers, and cellular insulations of organic and inorganic materials, ranging from 0.0001 to 0.5 Btu-in./hr-ft²-°F can be measured.

2. The cold side of the sample can be exposed to a range of discrete temperatures from -452° to -22°F, depending upon the boiling point of the specific cryogenic fluid used. The warm side of the sample can be exposed to any temperature from -422° to 500°F. During the test, warm side temperatures can be changed or closely controlled by supplying a fluid from a constant-temperature bath.

3. The sample can be exposed to any desired gas at pressures from 10⁻⁶ torr up to 15 psia. The gas in the test chamber can be changed and the test chamber purged with an inert gas during a test.

4. Mechanical compression from 0 to 50 psi can be applied to the sample by a calibrated pressure unit while a test is in progress.

5. The distance between the cold and warm plates can be adjusted and measured to within 0.001 in. during a test so as to change the density of the sample without interrupting the test or changing the sample.

6. The edges of the sample can be exposed to temperatures ranging from -452° to 500°F during the test by means of a guard shield.

B. Description of the Apparatus

Figure II-V-1 shows the apparatus and Figure II-V-2 shows the design details. The major components, all of which are made of stainless steel (300 series), are as follows:

1. guarded cold plate
2. warm plate
3. sample chamber
4. nitrogen jacket
5. bell jar

1. Guarded Cold Plate

The guarded cold plate is the bottom of the measuring vessel which has a capacity of 2.5 liters and a diameter of 6 inches. The measuring vessel is completely enclosed by a guard vessel, 12 inch diameter and 27 liter capacity, except its lower surface which is on a plane with the lower surface of the guard vessel. Together these surfaces form the cold plate which is in contact with the sample during tests. The thickness of this surface on both vessels is 1/4 inch and the temperature drop across it is estimated not to exceed 1°F.

The measuring vessel is connected to the outside by three stainless steel tubes, each having a 3/8-inch diameter and a wall thickness of 0.016 inch. One tube is a fill and purge line; another is a vent; the third is a relief line. The mechanical load applied to the sample is transmitted from the measuring vessel to the guard vessel by these tubes. The heat transferred between the two vessels by conduction through the

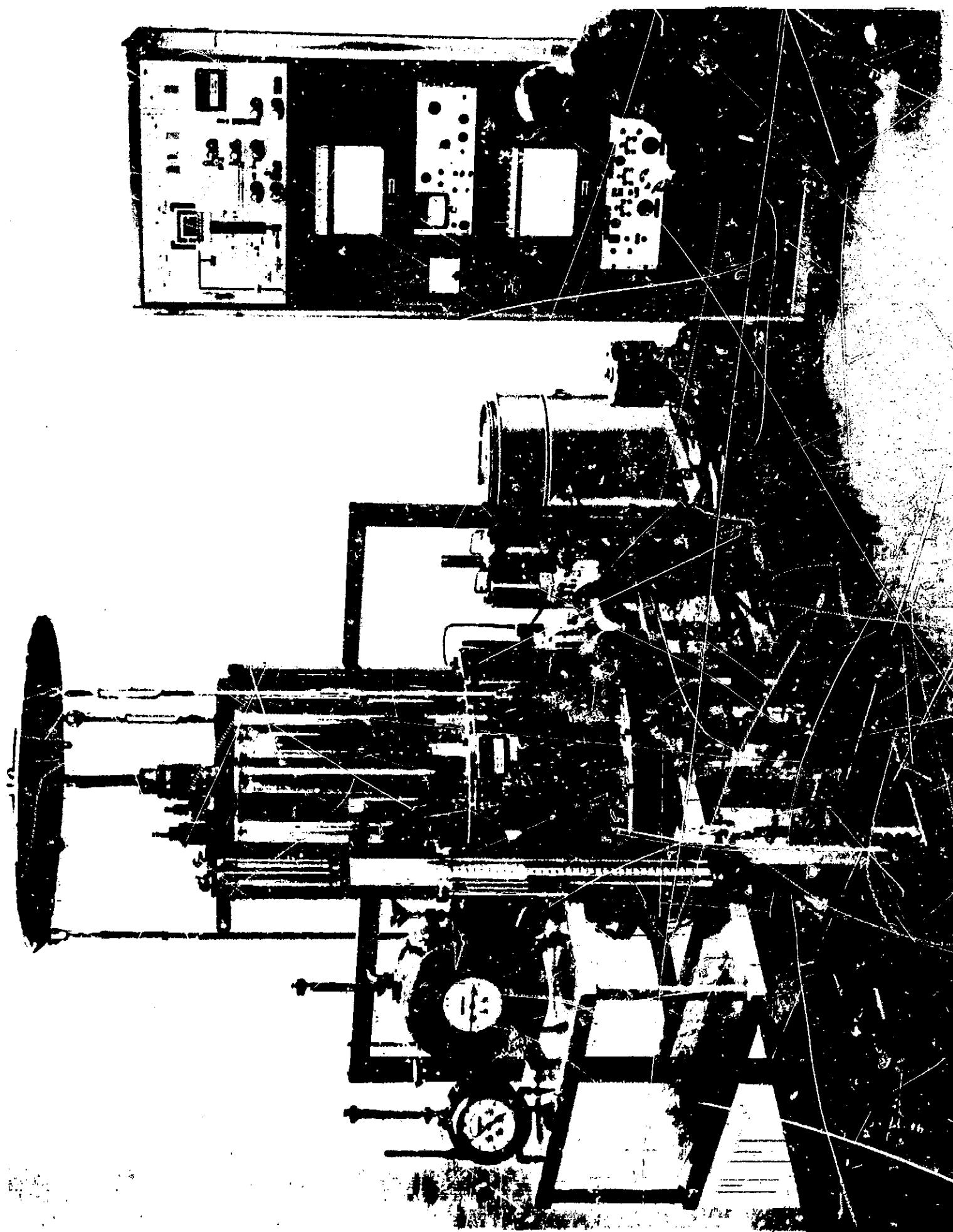


FIGURE II-V-1 DOUBLE-GUARDED COLD PLATE THERMAL CONDUCTIVITY APPARATUS

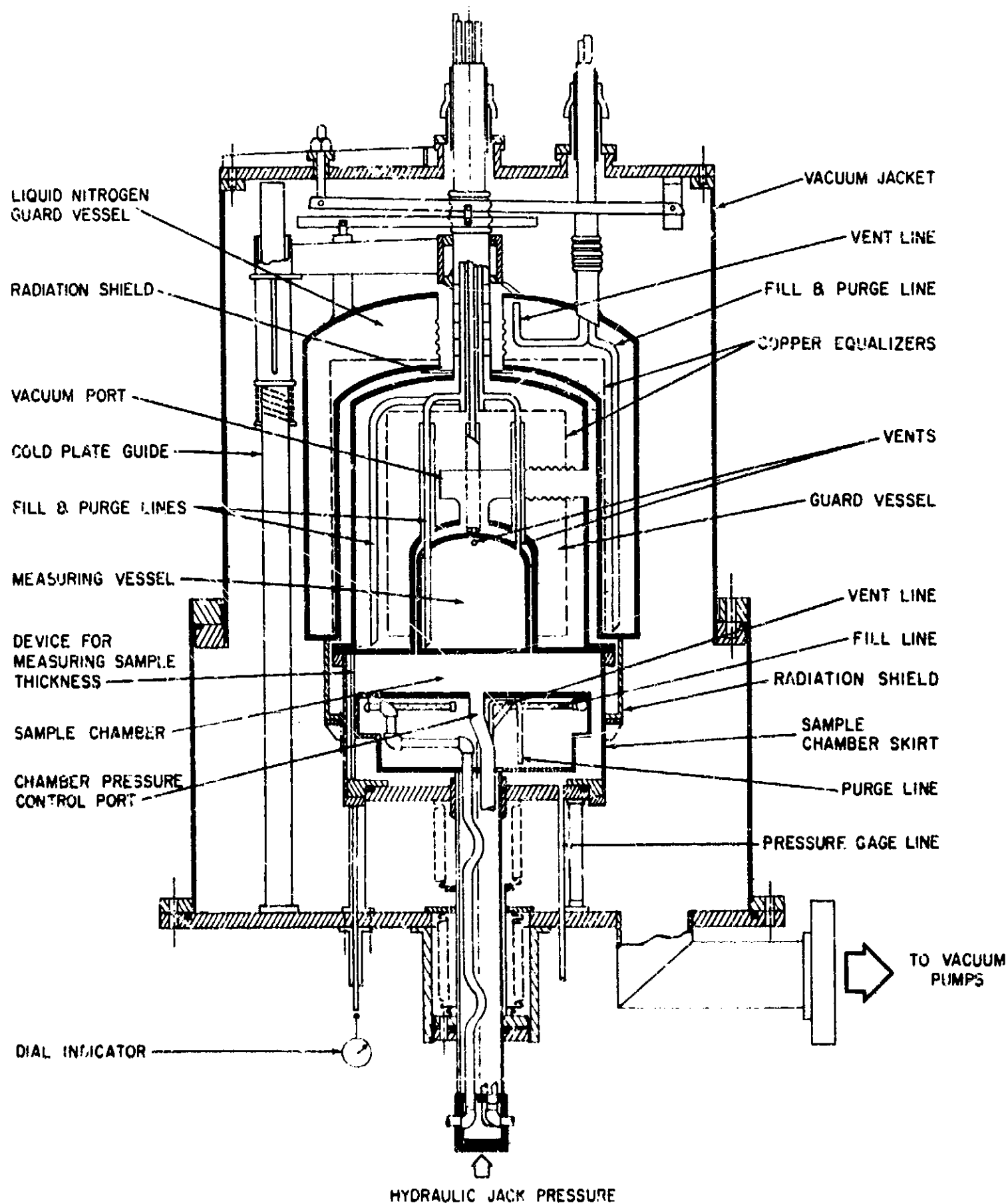


FIGURE II-V-2

CROSS-SECTION OF DOUBLE-GUARDED COLD PLATE THERMAL CONDUCTIVITY APPARATUS

three tubes, by radiation from the gold-plated walls of the vessels, and by residual gas conduction (if the vacuum between vessels is kept under 5×10^{-6} torr) is less than 3% of the heat transferred through a sample with a heat flux of 0.15 Btu/hr-ft^2 . Other features in the design of the guarded cold plate assembly include the following:

- a. Both guard and measuring vessels have inner shields of copper which serve as temperature equalizers to prevent thermal stratification of the liquid at low heat fluxes and as a radiation shield if the liquid level is low in the guard vessel.
- b. All lines to the measuring vessel have radiation traps in the form of a tee inside the guard vessel.
- c. During replacement of the sample, the cold plate assembly is guided accurately along the vertical axis on three rods.

2. Warm Plate

The height of the warm plate of the apparatus can be adjusted by means of a double-acting hydraulic cylinder (see Figure II-V-3). This not only permits the testing of samples with varying thicknesses of up to 2 inches but also makes it possible to apply up to 50 psi mechanical compression to the sample or to decrease its thickness during a test. A calibrated pressure gauge provides an indication of the pressure applied to the sample.

To keep the warm plate at a constant temperature, heated fluid or a cryogenic liquid can be channeled through a 7-liter reservoir attached to the underside of the warm plate. If temperatures between the boiling

points of the cryogenic liquids are required, cold or hot vapors can be sprayed through nozzles onto the plate. In this case, a constant temperature can be maintained by automatic control of the spraying rates. Eight thermocouples are embedded at various locations in the top surface of the warm plate to measure its temperature.

The warm plate has eight radial grooves 1/16-inch wide by 3/16-inch deep and a 3/4-inch opening in the center (the total open area is less than 10% of the sample surface) to assist in the evacuation of the sample.

Three rods with dial indicators spaced at 120° are used to measure the distance between the cold and warm plates and the parallel alignment of the plates to within 0.001 inch at all temperature conditions. Since the measurements are instantaneous, they are independent of thermal shrinkage of the rods.

3. Sample Chamber

The sample chamber is bounded by the cold plate assembly on top, by the warm plate on the bottom, and by a skirt which constitutes the guarded side wall. The upper part of the skirt is surrounded by a split copper ring which serves both as a radiation shield at liquid nitrogen temperature and as a thermal short to the lower part of the skirt. The copper ring intercepts the heat leak from room temperature surfaces to the guard vessel. The skirt itself can be removed and replaced with a heated shield if so desired. A horizontal copper ring between the warm plate and the sample chamber prevents radiation from warmer parts of the apparatus from reaching the sample. The sample chamber can be

hermetically sealed by placing a stainless sheet against the cold plate; it is then possible to evacuate the sample under test to any degree of vacuum or to introduce different gases into the chamber independently of the vacuum in the main vacuum jacket surrounding the cryogenic vessels.

4. Liquid Nitrogen Guard Vessel

The liquid nitrogen guard vessel has a 36-liter capacity. Its primary function is to decrease the boil-off rate of cryogenic fluid in the inner guard vessel, especially if liquid helium or hydrogen is used. Also, it keeps the top of the side wall of the sample chamber at a low temperature. It is provided with a copper equalizer radiation shield similar to the one in the inner guard vessel.*

5. Bell Jar

The cold and warm plates, sample chamber, and nitrogen jacket are placed inside a bell jar consisting of top and bottom plates and a cylindrical shell bolted in the middle. The shell is made in two parts to reduce the distance that the bell jar must be lifted when a sample is placed in the apparatus.

C. Instrumentation

1. Vacuum System

Figure II-V-3 shows the vacuum system and instrumentation used

* Unless "liquid nitrogen" is specified, the term "guard vessel" is subsequently used in this report to refer to the inner guard vessel.

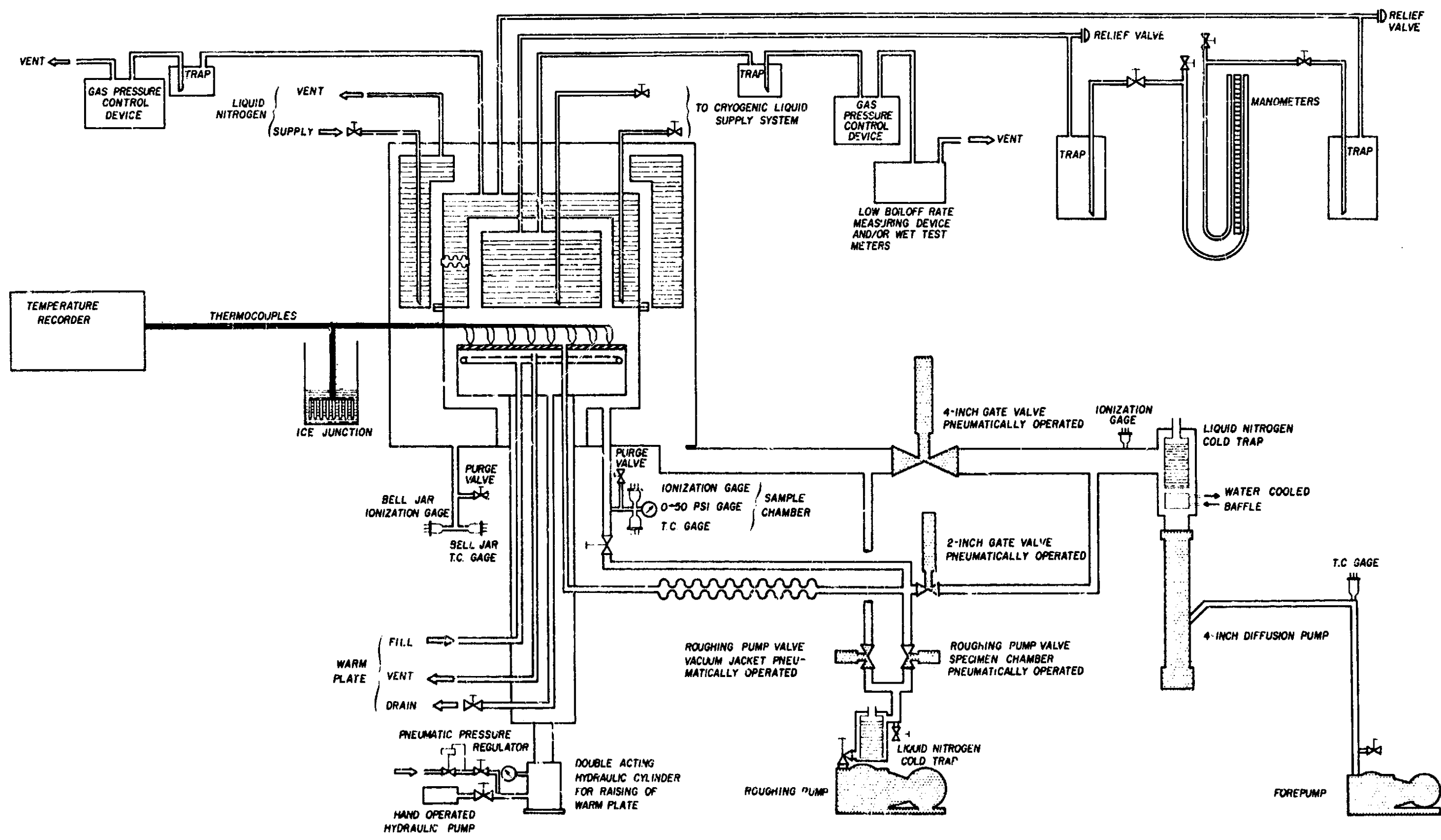


FIGURE II-V-3 INSTRUMENTATION FOR DOUBLE GUARDED COLD PLATE THERMAL CONDUCTIVITY APPARATUS

in conjunction with the thermal conductivity apparatus. Two mechanical pumps and one diffusion pump with a liquid nitrogen trap and a system of air-operated vacuum valves allow the bell jar and the sample chamber to be evacuated independently. An ionization gauge and a thermocouple gauge are used to measure the pressure in the bell jar; another set of identical gauges measures the sample chamber pressure. In addition, the sample chamber has a compound gauge which permits measurements to be made over a pressure range from 0 to 50 psia. A third ionization gauge is installed between the 4-inch air-operated valve and the liquid nitrogen cold trap.

2. Temperature Measurement

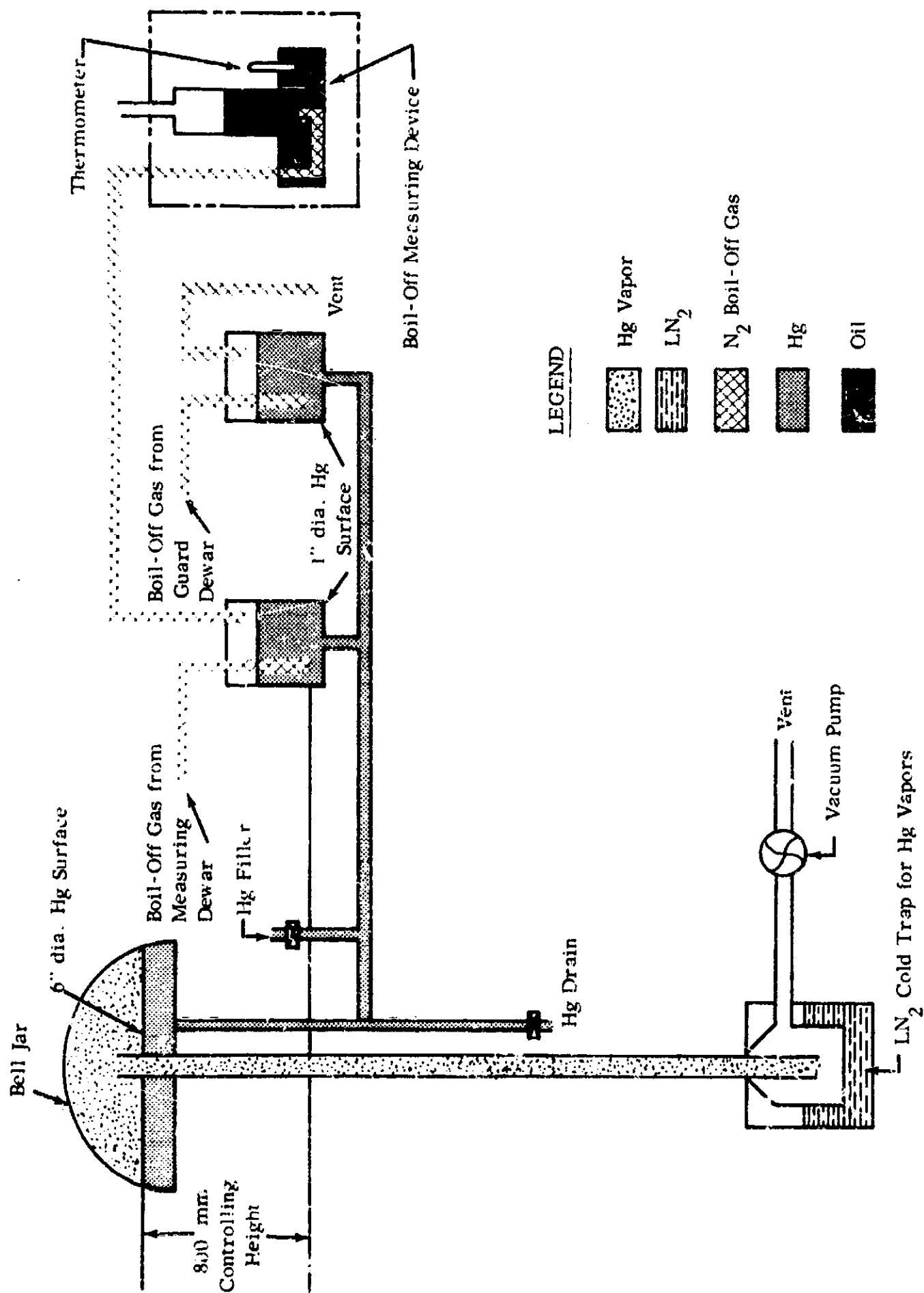
Sixteen thermocouples are available to measure temperatures of different parts of the apparatus and the sample. The temperature of the warm plate is measured with eight thermocouples embedded in its upper surface. Five thermocouples are available to measure temperatures of the sample or any part of the chamber. Three other thermocouples can be used to measure the temperature of the sample chamber radiation shield, the sample chamber skirt, or any of the walls of the three cryogenic vessels.

3. Gas Pressure Control Device

The gas pressure over the cryogenic liquid in the measuring vessel and guard vessel is subject to atmospheric pressure changes. These changes can lead directly to boff-off measurement errors. Calculations show that the pressure above the cryogenic liquid should be controlled within ± 0.1 torr; however, the atmospheric pressure variation may

extend over several torr during a testing period.

Figure II-V-4 is a schematic of the gas pressure control device. This device, which is basically two "L" shaped tubes filled with mercury, maintains a near-constant pressure level. Reduction of the atmospheric pressure variation is achieved by exposing a 6-inch-diameter surface of mercury in the longer leg of the "L" to a vacuum and submitting the gas in the measuring vessel and guard vessels to the pressure corresponding to the height difference of the two legs of the mercury column (approximately 800 mm). The exit of the line carrying away the boil-off gases is immersed in the mercury of the one-inch-diameter short leg of the "L" tube. This short leg is subjected to atmospheric pressure variations. Variations in the tube mercury level change the height of the mercury column between the level of the mercury surface in the bell jar and the exit of the boil-off gas line. The change in column height is proportional to the ratio of the areas of the tube and the bell jar. Thus, approximately 1/25 of the atmospheric pressure change is sensed by the gas in the measuring and guard vessels. Two low-vapor-pressure oil manometers indicate the pressure differences between the measuring and guard vessels. This pressure difference is arranged to be about 1 mm of oil, the guard vessel is maintained at the higher pressure to prevent recondensation of boil-off gases. Table II-V-1 shows typical performance data of the pressure control system.



II-79

4. Automatic Boil-Off Rate Recorders

a. Low Boil-Off Rates

Figure II-V-5 shows the device used for automatic recording of low boil-off rates up to $0.04 \text{ ft}^3\text{-hr}$ from the measuring vessel. The boil-off gases are allowed to collect in a graduate closed at the upper end by a solenoid valve. As the pressure builds up, the oil is displaced and collected in a reservoir whose surface area is large to minimize the effect of oil level changes until the lower photoswitch opens the solenoid and the gases are withdrawn from the graduate with an aspirator. As a result of the pressure reduction, the oil rises in the graduate until the solenoid valve is again closed by the upper photoswitch. By recording the number of times a fixed volume of gas is collected, one can determine the boil-off rate.

b. High Boil-Off Rates

Figure II-V-6 shows the device for automatic recording of high boil-off rates from the measuring vessel. This device utilizes a wet-test meter, a switching circuit, and a recorder. The wet-test meter is modified by adding a rotating face with attached magnets which actuate a switch that is fixed to the meter frame. This device provides an uninterrupted record of hydrogen boil-off rates and allows rapid completion of tests, because it clearly defines when thermal equilibrium is reached.

D. Test Procedure

A complete test can be run in two to three days, depending on the

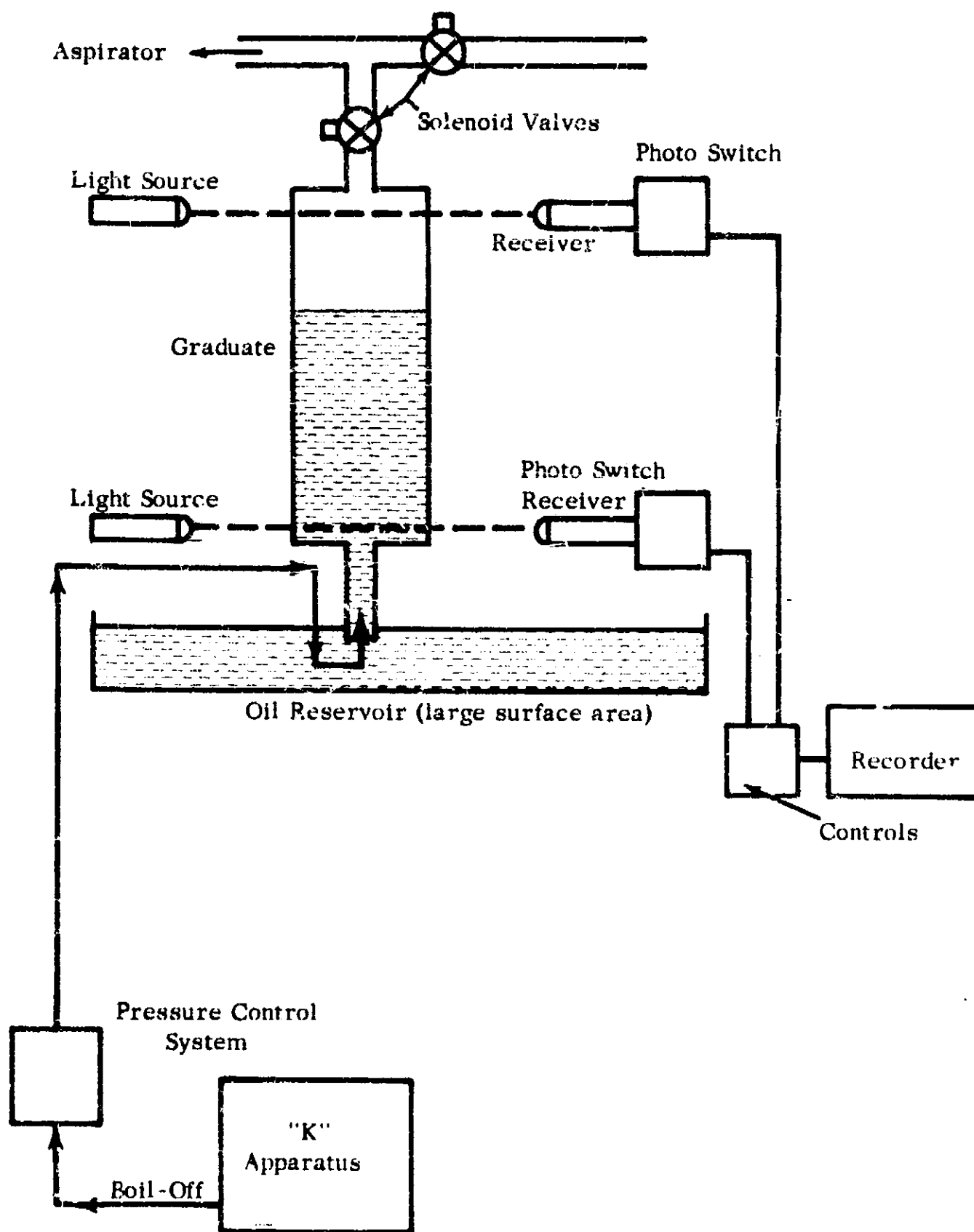


FIGURE II-V-5 APPARATUS FOR RECORDING LOW BOIL-OFF RATES

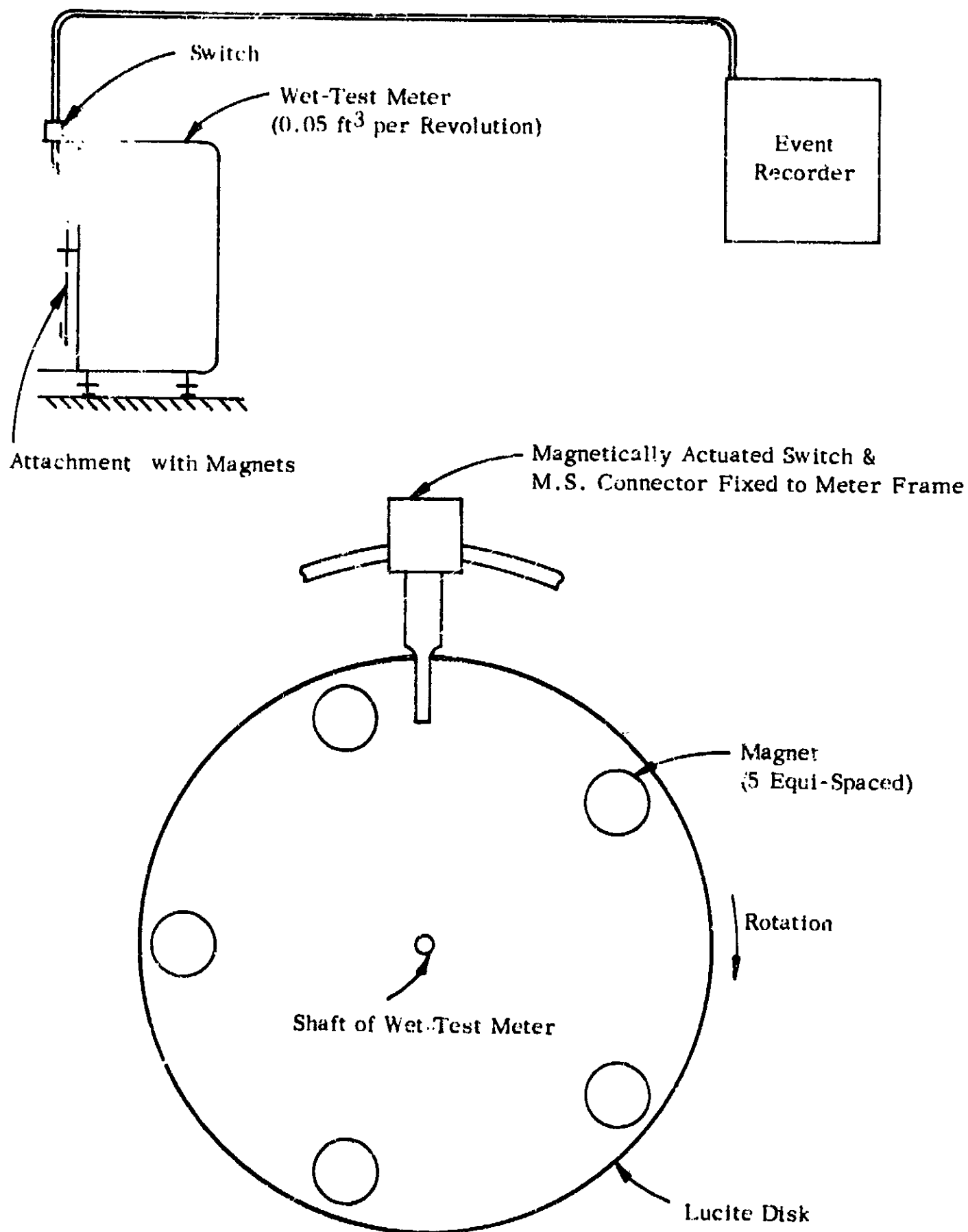


FIGURE II-V-6 ROTATING FACE ATTACHMENT TO WET-TEST METER FOR RECORDING

TABLE II-V-1

TYPICAL PERFORMANCE DATA OF THE PRESSURE CONTROL SYSTEM

January 3, 1963

<u>Time</u>	<u>Boil-off Rate (cc/hr)</u>	<u>Barometer (mm Hg)</u>
2:15		
2:45	220	768.9
3:00	240	
3:15	220	
3:30	220	
3:45	220	768.8
4:00	220	
4:30	240	
5:00	220	768.9
5:15	220	
5:45	220	769.0
6:00	220	
6:15	220	
6:45	230	769.1
7:15	230	
7:45	240	769.2
8:00	240	

January 5, 1963

<u>Time</u>	<u>Boil-off Rate (cc/hr)</u>	<u>Barometer (mm Hg)</u>
12:00		768.9
12:30	150	768.
1:00	150	768.4
1:30	140	768.3
2:00	140	768.1
3:00	150	768.1
3:30	140	768.2
4:00	140	768.2

January 8, 1963

<u>Time</u>	<u>Boil-off Rate (cc/hr)</u>	<u>Barometer (mm Hg)</u>
1:25		758.0
1:40	120	
2:40	115	757.5
3:10	120	757.5
3:40	120	757.4
4:40	125	757.7
4:55	120	
5:10	120	
5:25	120	757.7

insulating effectiveness of the sample used. It takes approximately one day to break down the unit, install a new sample, assemble the unit, evacuate the bell jar, and fill the vessels with cryogenic fluids. A part of the first night is needed for the unit to achieve thermal equilibrium; data can be automatically recorded during the remainder of the night. For most samples, the cryogenic liquid is blown out by the end of the second day, and the second night is used for warming up the unit. Samples with extremely low thermal conductivity, such as thick samples of multilayer radiation insulation, may require two days of running time to achieve thermal equilibrium.

The following steps have been, or should be, taken in the operation of the thermal conductivity apparatus to insure that accurate and reproducible data are obtained:

1. The measuring vessel should not be filled during a test, so that equilibrium conditions will not be disturbed. For a typical good insulator, the measuring vessel need not be filled for several days. For low conductivity samples, several hours may elapse before equilibrium conditions are achieved.

2. At very low boil-off rates, stratification of the liquid may occur. Copper wool has therefore been placed in the measuring vessel to provide better temperature equalization and reduce the probability of stratification.

3. Close control over the pressure difference in the measuring and guard vessels must be maintained to prevent heat exchange between

the two vessels. This pressure difference, as explained earlier, is measured by manometers connected to the measuring and guard vessels and is maintained at about one millimeter of oil. The guard vessel is kept at a slightly higher temperature than the measuring vessel, so that boil-off gases from the measuring vessel do not condense on its walls.

4. Changes in the ambient barometric pressure during a test period are not unusual and could lead to a corresponding change in the enthalpy of the cryogenic liquid. The gas pressure control system compensates for these changes by keeping a constant pressure within the measuring and guard vessels.

5. The design of the apparatus insures that the warm and cold plates are kept parallel throughout a test; this is necessary to prevent the samples from being subjected to unequal compression, which could result in a departure from the postulated one-dimensional heat flow conditions.

6. The diameter of the sample should not equal the diameter of the measuring vessel when a guard ring made out of the same sample material is used. Radiation from the warm plate could be transferred through the small opening between the sample and the guard ring and then be trapped in the space between the measuring and guard vessels, which would lead to an increase in boil-off rates.

7. Because the sample is not infinite in extent, the effect of edge losses must be considered. The design of the sample chamber permits control over the temperature gradient of the surfaces viewed by

the edges of the sample. In addition, the emittance of the side walls can be controlled by treatment of the surface to reduce reradiation or reflection from the warmer parts of the sample chamber. The exposed edges of multilayer insulations must be protected from radiant heat exchange. These edge effects are discussed in Section V-F.

8. Where feasible, the physical properties of the sample (emissivity, vapor pressure, internal structure, etc.) should be measured. Variations in any of these properties may produce a difference in thermal conductivity between nearly identical samples.

9. Although the gas pressures in the bell jar and sample chamber are measured, no direct measurements can be made of the pressure existing within the sample. Thus, some uncertainty exists regarding the contribution of gas conduction to the over-all heat transfer, particularly in those materials which are known to have a finite vapor pressure.

E. Calibration and Reproducibility

1. Electric Heater

Figure II-V-7 shows the results of a typical calibration test when a small electrical heater is attached to the bottom of the measuring vessel as the only heat source. The warm plate and the cold plate are kept at 77°K. The initial point on both curves establishes that the heat leak to the measuring vessel, when no power is supplied to the heater, is zero. The solid curve is based on the ideal performance. The dashed curve is based on experimental data and shows a 3% deviation from ideal conditions. The power loss in the heater leads is partially responsible for the 3% discrepancy.

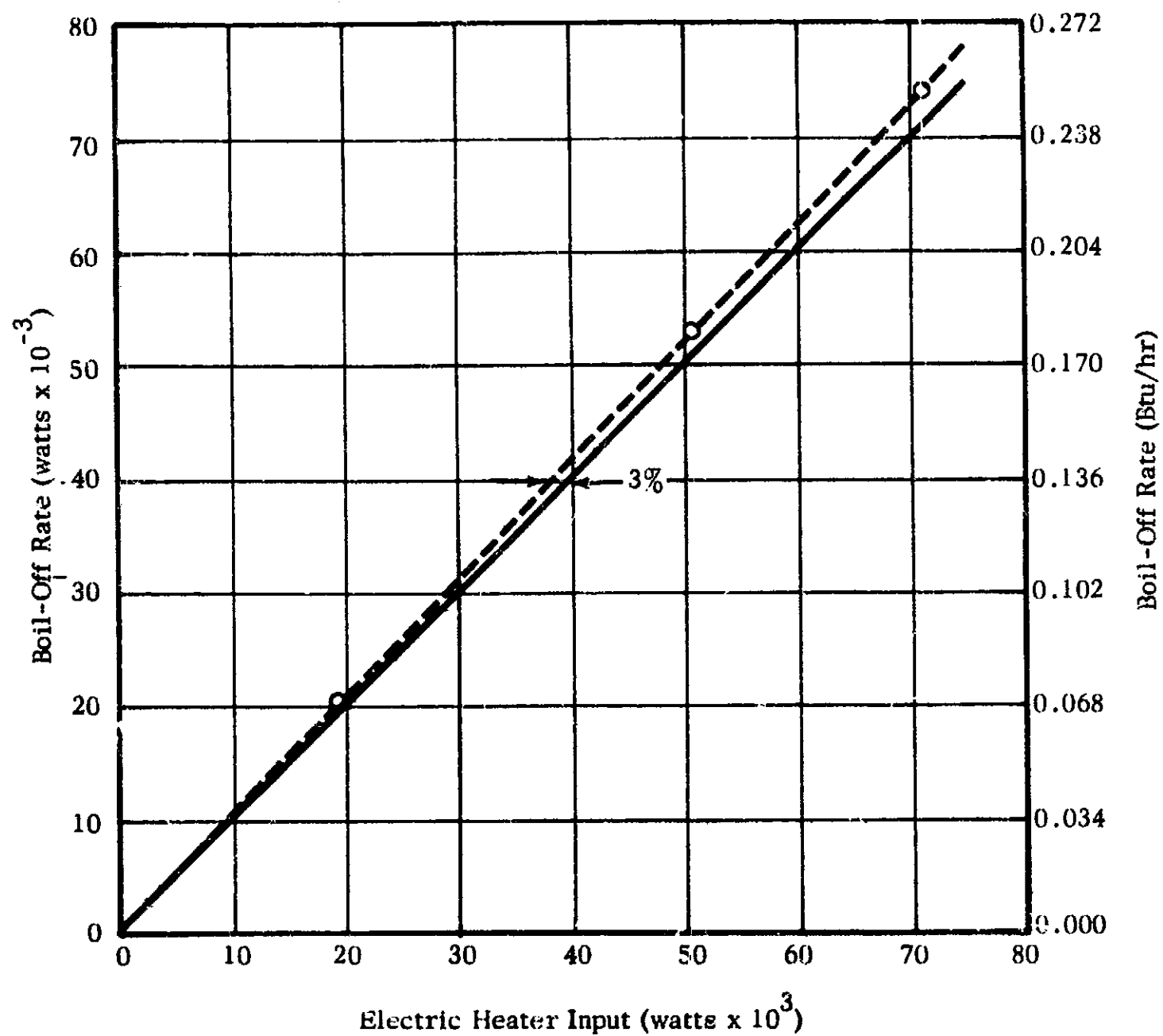


FIGURE II-V-7

VARIATION OF BOIL-OFF RATE WITH
ELECTRIC HEATER INPUT

The over-all accuracy of the thermal conductivity apparatus is estimated to be $\pm 10\%$. This estimate is based on the accuracy of measuring the volume of boil-off gases, controlling the gas pressures above the cryogenic liquids in the measuring and guard vessels, the effect of atmospheric pressure changes on boil-off rates, the difference in liquid level in the guard vessel, and the temperature measurement of the cold and warm surfaces. This estimate is conservative compared to the electrical heater calibration tests.

2. Standard Sample

The same sample of multilayer insulation was tested in three thermal conductivity apparatus (see Section VI) to compare their performance. In these tests the warm-plate temperature was not controlled and was subject to seasonal temperature changes in the tap water circulating through it. Table II-V-2 gives the test data. The test data were corrected to a common warm-plate temperature. This heat correction was found to be -0.02 for apparatus No. 2 and $-0.03 \text{ Btu/hr-ft}^2$ for apparatus No. 1, for a warm boundary temperature of 37°F . The corrected heat flux values for units Nos. 1, 2, and 3 were 0.21 , 0.18 , and 0.18 Btu/hr-ft^2 , respectively. These data indicated that tests of this sample on units Nos. 2 and 3 were reproducible, and that there was an apparent discrepancy in the results of the test on unit No. 1 of about 15% . However, such a discrepancy could have been the result of degradation of the reflective properties of the sample through handling or method of storage as well as the result of the performance of the apparatus.

The greatest uncertainty in the test results is associated with the sample itself, specifically, the reproducibility of the quality of the materials from one sample to the next for the same insulation system. Tempered aluminum foil and fiberglass mesh have provided the most reproducible samples. However, because the thickness of the fiberglass mesh spacer is not closely controlled, the change in spacer thickness may lead to a slight change in density of this multilayer insulation.

F. Effect of Discontinuity (Edge Effects)

The calculations of thermal conductivity of a sample tested in a flat-plate calorimeter assume one-dimensional heat flow through the portion of the sample below the measuring vessel. Any deviation from this will introduce measurement errors. The guard vessel is designed to minimize deviations from one-dimensional heat flow due to edge effects. Such effects are caused by radiation heat exchange with surfaces of the apparatus that are warmer or cooler than the sample, and they cause a distortion of the temperature gradient in the vicinity of the sample edges.

Because of the strongly nonisotropic behavior of multilayer insulations, these temperature distortions are rapidly propagated into the sample. In particular, when a certain sample thickness is exceeded, the guarded section of the sample may not be properly proportioned to assure the desired one-dimensional heat flow through the measuring section.

1. Analysis of Edge Effects

The following analysis demonstrates the magnitude of the error that would be incurred with the conventional guard ring arrangement and shows how to modify the guard ring to obtain accurate measurements.

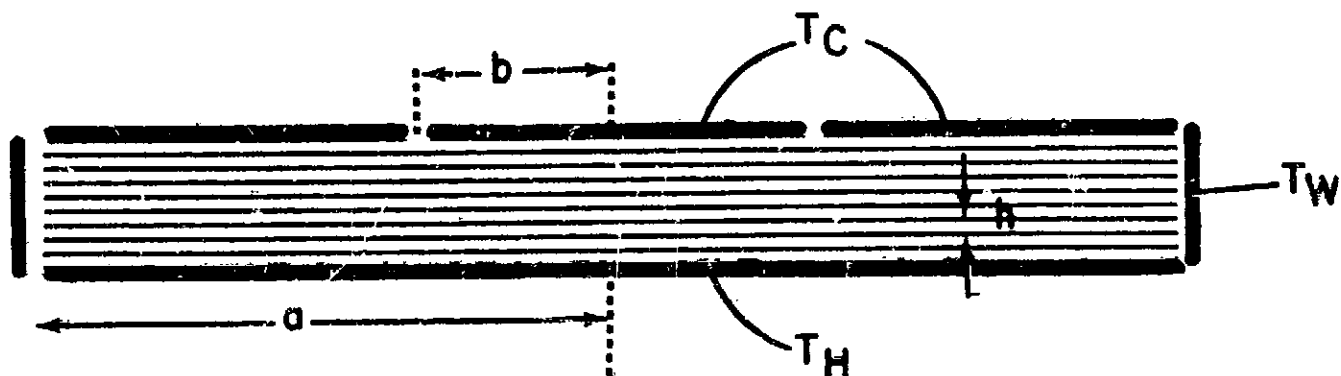


FIGURE II-V-8 SAMPLE BETWEEN CIRCULAR PLATES AND SURROUNDED BY VERTICAL PLATES

Consider the experimental arrangement shown in Figure II-V-8, in which a disk-shaped sample of multilayer insulation consisting of $N-1$ radiation shields with spacing h , is placed between two circular plates held at temperature T_C and T_H , respectively. The upper plate is divided into an inner measuring disc and an annular guard ring. The sample is surrounded by a vertical cylindrical wall at a temperature T_W .

The heat flux to the inner disc of the upper plate can be calculated in terms of T_H , T_C , and T_W . For simplicity we assume that the metal shields have infinite conductivity, and we ignore the effect of the spacers. Thus, each shield has a uniform temperature. The heat balance equation for the n th shield is

$$\frac{\pi a^2}{\frac{2}{\epsilon} - 1} (2\sigma T_n^4 - \sigma T_{n-1}^4 - \sigma T_{n+1}^4) = 2\pi ah(\sigma T_W^4 - \sigma T_n^4) \quad (\text{II-V-1})$$

where a is the radius of the sample, ϵ is the emissivity of the foils and σ is the Stefan-Boltzmann radiation constant. The term on the right of the equation is the net radiation received from the cylindrical wall, which we assume to be black. The spacers between the shields are also assumed to act like black bodies.

The general solution of the set of difference equations represented by (II-V-1) is

$$\sigma T_n^4 = \sigma T_W^4 + A\beta_1^n + B\beta_2^n \quad (\text{II-V-2})$$

where A and B are arbitrary constants and β_1 and β_2 are the two roots of the quadratic equation

$$\beta^2 - 2 \left[1 + \frac{h}{a} \left(\frac{2}{\epsilon} - 1 \right) \right] \beta + 1 = 0 \quad (\text{II-V-3})$$

For a typical case studied in the thermal conductivity apparatus, $h = .018$ inch, $a = 3$ inches, and $\epsilon = 0.05$; thus,

$$\beta_1 = 0.51, \beta_2 = 1.95 \quad (\text{II-V-4})$$

The constants A and B are determined by the boundary conditions at the top and bottom, which have the form

$$\sigma T_C^4 = \sigma T_W^4 + A + B \quad (\text{II-V-5})$$

and

$$\sigma T_H^4 = \sigma T_W^4 + A \beta_1^N + B \beta_2^N \quad (II-V-6)$$

Thus

$$A = \frac{-(\sigma T_H^4 - \sigma T_W^4) - \beta_2^N (\sigma T_W^4 - \sigma T_C^4)}{\beta_2^N - \beta_1^N} \quad (II-V-7)$$

and

$$B = \frac{(\sigma T_H^4 - \sigma T_W^4) + \beta_1^N (\sigma T_W^4 - \sigma T_C^4)}{\beta_2^N - \beta_1^N} \quad (II-V-8)$$

The flux to the upper disk is

$$\begin{aligned} Q &= \frac{\pi b^2}{\frac{2}{\epsilon} - 1} (\sigma T_H^4 - \sigma T_C^4) \\ &= \frac{\pi b^2}{\frac{2}{\epsilon} - 1} (\sigma T_W^4 + A \beta_1 + B \beta_2 - \sigma T_C^4) \\ &= \frac{\pi b^2}{\frac{2}{\epsilon} - 1} \left[(\sigma T_W^4 - \sigma T_C^4) + \frac{(\beta_2 - \beta_1)(\sigma T_H^4 - \sigma T_W^4) - (\beta_1 \beta_2^N - \beta_2 \beta_1^N)(\sigma T_W^4 - \sigma T_C^4)}{\beta_2^N - \beta_1^N} \right] \end{aligned} \quad (II-V-9)$$

If N is reasonably large, $\beta_2^N \gg \beta_1^N$, and (II-V-9) simplifies to

$$Q = \frac{\pi b^2}{\frac{2}{\epsilon} - 1} \left[(1 - \beta_1 - \frac{\beta_2 - \beta_1}{\beta_2^N})(\sigma T_W^4 - \sigma T_C^4) + (\frac{\beta_2 - \beta_1}{\beta_2^N})(\sigma T_H^4 - \sigma T_C^4) \right] \quad (II-V-10)$$

For the case $N = 10$ and with the values of β_1 and β_2 given by (II-V-4), the flux becomes

$$Q = \frac{\pi b^2}{\frac{2}{\epsilon} - 1} \left[0.49 (\sigma T_W^4 - \sigma T_C^4) + 0.0018 (\sigma T_H^4 - \sigma T_C^4) \right] \quad (\text{II-V-11})$$

Thus, the effect of the side wall temperature T_W is 270 times larger than that of the hot plate temperature T_H . Clearly, no meaningful measurements can be obtained with this experimental arrangement unless the sample is suitably guarded.

2. Insertion of a Buffer Zone

The difficulty with the arrangement of Figure II-V-8 is that the cylindrical wall at temperature T_W couples much too strongly with the flux-collection disk at temperature T_C because of the excellent tangential conductance of the metal shields. The remedy is to insert an annular buffer zone between the side wall and the shields, as shown in Figure II-V-9.

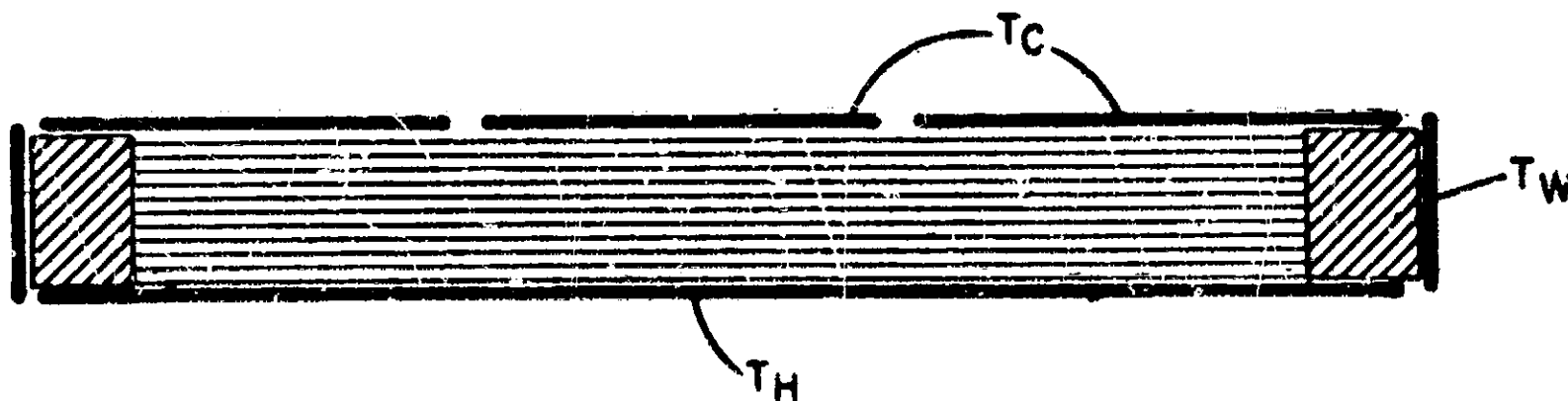


FIGURE II-V-9 SAMPLE WITH ANNULAR BUFFER ZONE

a. Required Width of Buffer Zone

Figure II-V-10 shows the heat flow pattern in the buffer zone. Near the side wall the lines of flow are considerably distorted, but they rapidly straighten out at a short distance from the side wall.

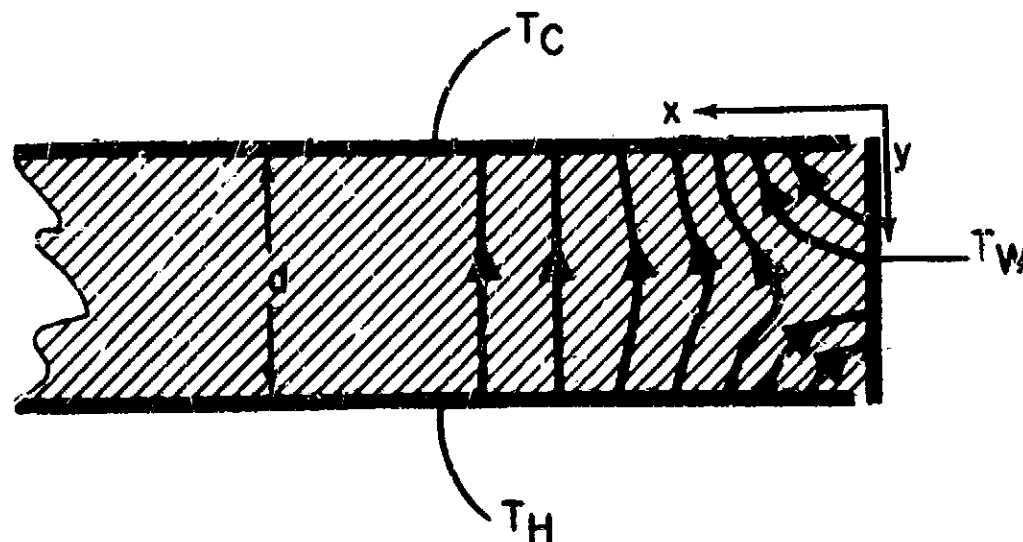


FIGURE II-V-10 HEAT FLOW PATTERN IN BUFFER ZONE

The width of buffer ring needed to make the flow pattern uniform can be calculated as follows:

In the case of a buffer material of uniform conductivity, the temperature distribution must satisfy Laplace's equation

$$\frac{\partial^2 T}{\partial x^2} + \frac{\partial^2 T}{\partial y^2} = 0 \quad (\text{II-V-12})$$

where, for simplicity, the curvature of the side wall has been neglected.

$$T = T_C + (T_H - T_C) \frac{y}{d} + \sum_{n=1}^{\infty} \frac{2}{n\pi} \left[\{1 - (-1)^n\} (T_W - T_C) + (-1)^n (T_H - T_C) \right] e^{-\frac{n\pi x}{d}} \sin \frac{n\pi y}{d}$$

(II-V-13)

where d is the thickness of the buffer zone.

The heat flux density received by the upper plate is

$$q = K \left(\frac{\partial T}{\partial y} \right)_{y=0} = \frac{K}{d} (T_H - T_C) + \frac{2K}{d} \sum_{n=1}^{\infty} \left[\{1 - (-1)^n\} (T_W - T_C) + (-1)^n (T_H - T_C) \right] e^{-\frac{n\pi x}{d}}$$

(II-V-14)

For sufficiently large values of x , only the first term of the series in (II-V-14) is important. Then

$$q = \frac{K}{d} (T_H - T_C) + \frac{2K}{d} 2(T_W - T_C) - (T_H - T_C) e^{-\frac{\pi x}{d}}$$

(II-V-15)

The flux becomes constant to 1%, and therefore the lines of flow become essentially straight, when

$$x \geq 2d$$

(II-V-16)

Thus, a buffer ring of width only twice its thickness serves to decouple the sample almost completely from the side wall, even in the extreme case where the buffer material touches the side wall. With only radiative interchange between buffer and side wall, the decoupling is even better.

The same result is obtained if the buffer material transports heat by radiation rather than conduction. For example, the porous spacers between the metal foils of the sample form an excellent buffer if allowed to extend beyond the edges of the foils by twice the sample thickness.

b. Interaction of Buffer Zone with Sample

The interaction of the buffer zone with the sample can be estimated. For this purpose it is sufficient to consider the situation shown in Figure II-V-11, in which the sample and buffer are taken to be rectangular conducting slabs in contact at $x = b$ and contained between parallel plates at temperatures T_H and T_C . The end walls are no-flux surfaces.

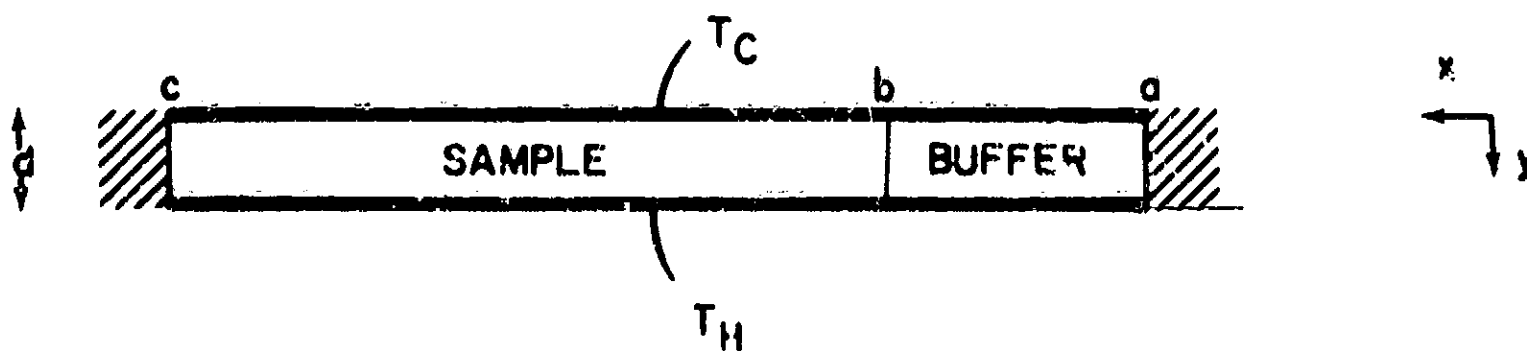


FIGURE II-V-11 INTERACTION BETWEEN BUFFER AND SAMPLE WITH NO-FLUX END WALLS

We can show that the total heat flux from the hot to the cold plate is the same as it would be if the interface between the two solids were also a no-flux surface.

The total flux across any horizontal plane, defined by some fixed value of y , is

$$Q = \int_a^b K_B \frac{\partial T}{\partial y} dx + \int_b^c K_S \frac{\partial T}{\partial y} dx \quad (\text{II-V-17})$$

where K_B and K_S are the thermal conductivities in the vertical direction for the buffer and sample, respectively. K_B and K_S are, in general, functions of T . Equation (II-V-17) can now be integrated with respect to y from one plate to the other, to give

$$Q = \frac{(b-a)}{d} \int_{T_C}^{T_H} K_B(T) dT + \frac{(c-b)}{d} \int_{T_C}^{T_H} K_S(T) dT \quad (\text{II-V-18})$$

Now the two terms on the right-hand side of (II-V-18) are simply the fluxes through the sample and buffer, respectively, when a no-flux barrier is placed between the two solids at $x = b$. Thus, the total flux, Q , is not changed when this barrier is removed. However, the individual fluxes Q_S and Q_B through the sample and barrier do change. An upper limit to the change in flux through the sample is obtained by assuming that all the flux through the buffer in the case of a no-flux barrier is transferred to the sample when the barrier is removed. Thus, from (II-V-18), the maximum fractional error in sample flux is

$$\frac{\Delta Q}{Q_3} = \frac{(b - a) \int_{T_C}^{T_H} K_B dT}{(c - b) \int_{T_C}^{T_H} K_S dT}$$

$$\frac{(b - a) \bar{K}_B}{(c - b) \bar{K}_S} \quad (II-V-19)$$

where \bar{K}_B and \bar{K}_S are the average conductivities of buffer and sample in the y-direction over the temperature range T_C to T_H .

Since, as stated earlier, $2d$, the width $(b - a)$ of the buffer zone can be equated to $2d$. Also $(c - b)$ can be taken as the radius, r , of the sample.

$$\frac{\Delta Q}{Q_S} = \frac{2d \bar{K}_B}{r \bar{K}_S} \quad (II-V-20)$$

Equation (II-V-20) gives an estimate of the maximum error in flux measurement. In practice the error can be made very much smaller by choosing a buffer material that gives the same vertical temperature distribution as in the sample. For example, if the sample transports heat mainly by radiation, as in the case of multilayer insulation, the buffer should be chosen to do likewise.

Equation (II-V-20) indicates that the error is minimized if the sample is very thin compared with its diameter and if the conductivity of the buffer is as small as possible compared with that of the sample.

We have, therefore, prepared our test samples with the spacer

diameter always larger than the shield diameter whenever this was feasible. In this manner, we also prevented accidental thermal shorts between adjacent metal radiation shields.

VI. EXPERIMENTAL RESULTS

During this program, three double-guarded cold plate apparatus were used to measure the thermal conductivity of various thermal insulators at liquid hydrogen and liquid nitrogen temperatures. Two units, No. 1 and No. 2, are located at the Lewis Research Center in Cleveland, and unit No. 3 is located at the Arthur D. Little laboratory in Cambridge. Units 1 and 2 have been in operation since November 1961 and August 1962, respectively, while the unit in Cambridge has been operating since September 1962. The paragraphs below describe the data that have been obtained on the variables affecting thermal conductivity.

A. Density

The density to which a multilayer insulation system is packed has a definite effect on the solid conduction contribution to thermal conductivity. Figure II-VI-1 shows that the radiation contribution of heat transport across the insulation decreases with increasing number of layers per unit thickness while the solid contribution increases at a greater rate. Therefore, it is possible to find an optimum number of radiation shields per unit thickness and, hence, density for a specific material combination.

Figure II-VI-2 shows experimentally obtained data on the effect of density on thermal conductivity for four multilayer insulation systems. Data for insulation at less than the optimum number of shields indicates an inefficient use of available space. When a sample is installed in the test apparatus, its optimum density is first determined, and the investigation of other variables is then carried out at that density. From

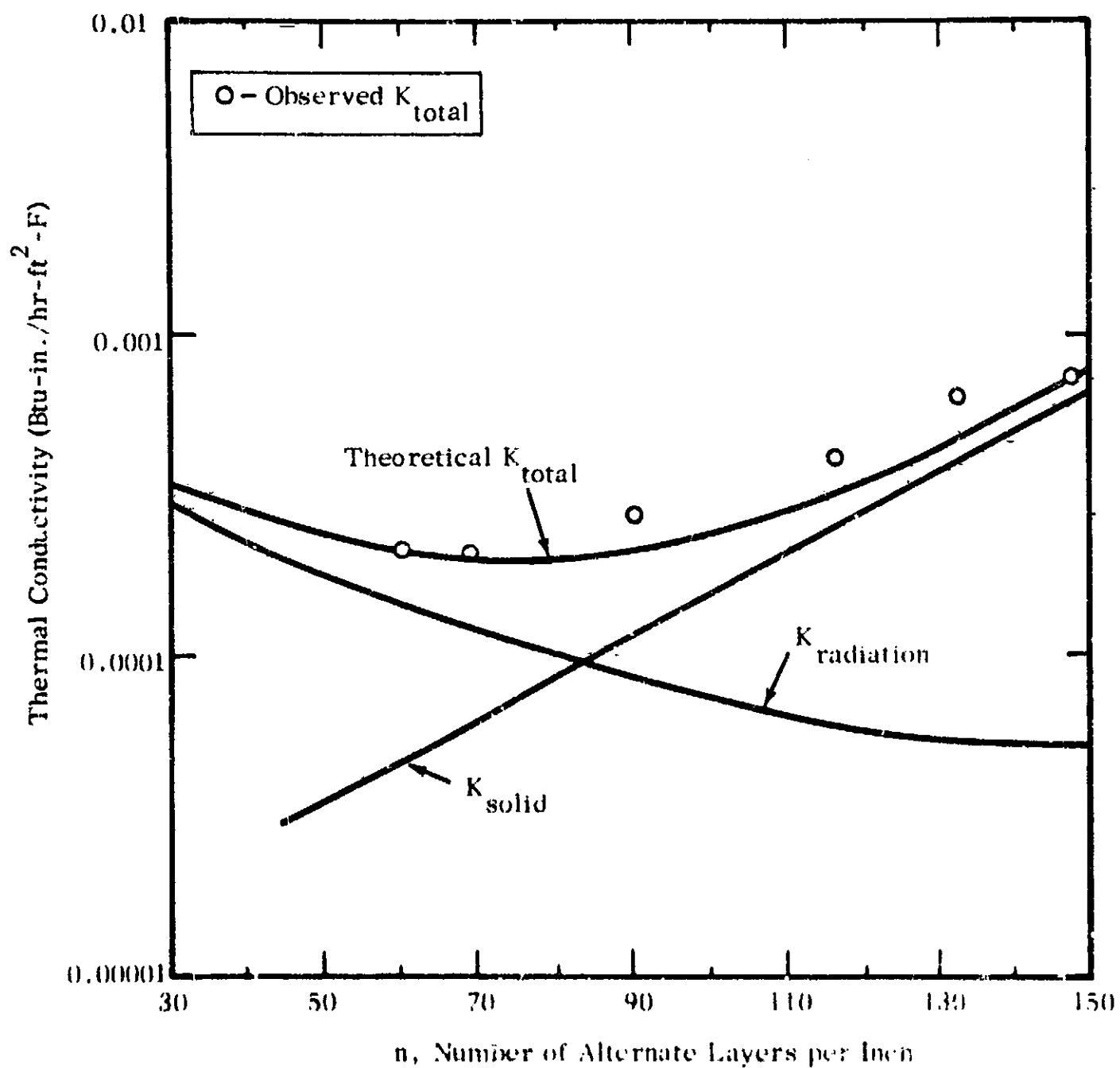


FIGURE II-VI-1 THE CONTRIBUTION OF SOLID CONDUCTION AND RADIANT HEAT TRANSFER TO THE THERMAL CONDUCTIVITY OF MULTILAYER INSULATIONS

Source: D.I. -J. Wang, "Multiple Layer Insulations in Aerodynamically Heated Structures", P.E. Glaser, ed., Prentice-Hall, Inc., 1962, p. 45.

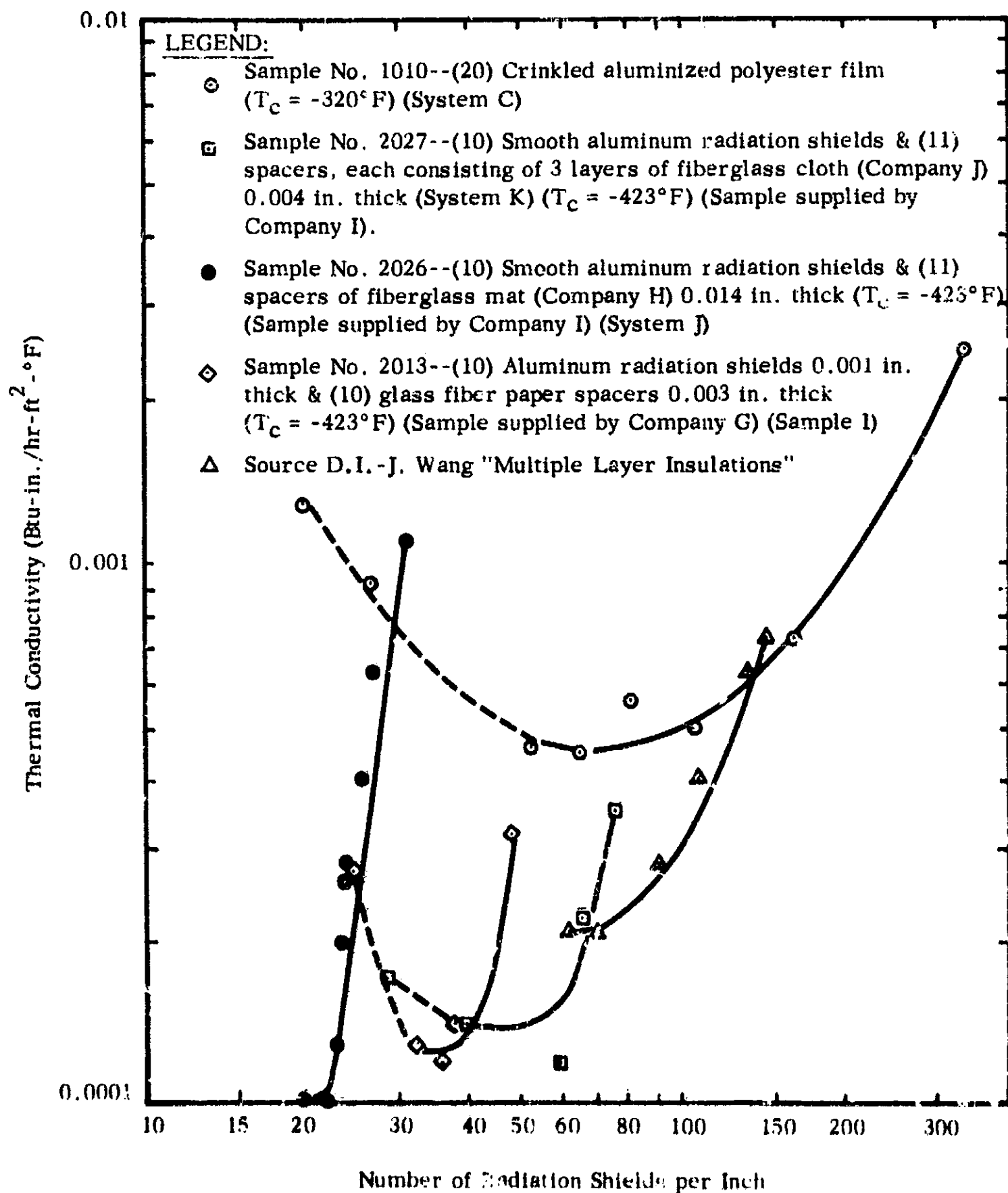


FIGURE II-VI-2 EFFECT OF DENSITY ON THERMAL CONDUCTIVITY

three to five data points are generally required to determine the optimum density of a sample of a multilayer insulation system.

From the design standpoint, the comparison parameters $K\rho$ and $\sqrt{K\rho}$ (weight penalty for vented tank) can be used to determine the insulating effectiveness of a multilayer insulation. If weight calculations are to be realistic, however, they must take into consideration various means of attachment of the insulation, outer heat shields, and insulations around penetrations.

B. Mechanical Load

The effect of mechanical load on the density and thereby on the heat flux through a sample of a multilayer insulation is of considerable practical significance. An increase in mechanical load will cause the radiation shields and spacers to be compressed into a thinner sandwich of higher density. A subsequent decrease in mechanical load will allow the radiation shield and spacers to return to their original density, provided that no permanent deformation has taken place.

We examined the capability of several insulation systems to withstand compressive mechanical loading. The procedure followed in most of these tests was: (a) find the optimum density of the sample, and (b) apply a hydraulically controlled force to the movable warm plate to produce compressive loadings up to 15 psi on the sample. The point of optimum density was taken as zero loading, under the assumption that only slight or no compression of the insulation occurs at that density. To minimize the influence of friction losses between the moving parts of the warm plate support, the warm plate was returned to the zero load position after each point and before the new force desired was applied.

The results of these tests, which appear in Figure II-VI-3, illustrate the following:

1. As the mechanical load increases, the solid conduction contribution to heat transfer becomes dominant.

2. The differences in thermal conductivity at zero load are the result of differences in the spacer materials. Spacers consisting of oriented fibers have a high contact resistance, which impedes solid conduction. With no external load on the insulation, the closeness of the packing of these fibers (and hence the contact resistance) depends upon the previous history, such as number of load applications, method of manufacture, and storage conditions.

Crinkled polyester film is subject to a more rapid increase in heat flux under compressive loading than other multilayer insulations. The thin film has little mechanical strength, and solid conduction increases rapidly as the crinkles flatten. The thermal conductivities of multilayer insulations with fiber spacers exhibit similar thermal conductivities for loads exceeding 3 psi under identical temperature boundary conditions.

3. Once the heat flux has completed its initial sharp rise, it varies as the two-thirds power of the mechanical load. This relationship corresponds to the deformation of a sphere resting on a plane and appears to approximate the deformation of the contact areas between the spacers and the radiation shields. The trend of the effects of mechanical load on thermal conductivity indicates that the insulating effectiveness of most multilayer insulations is greatly reduced when compressive loads are applied.

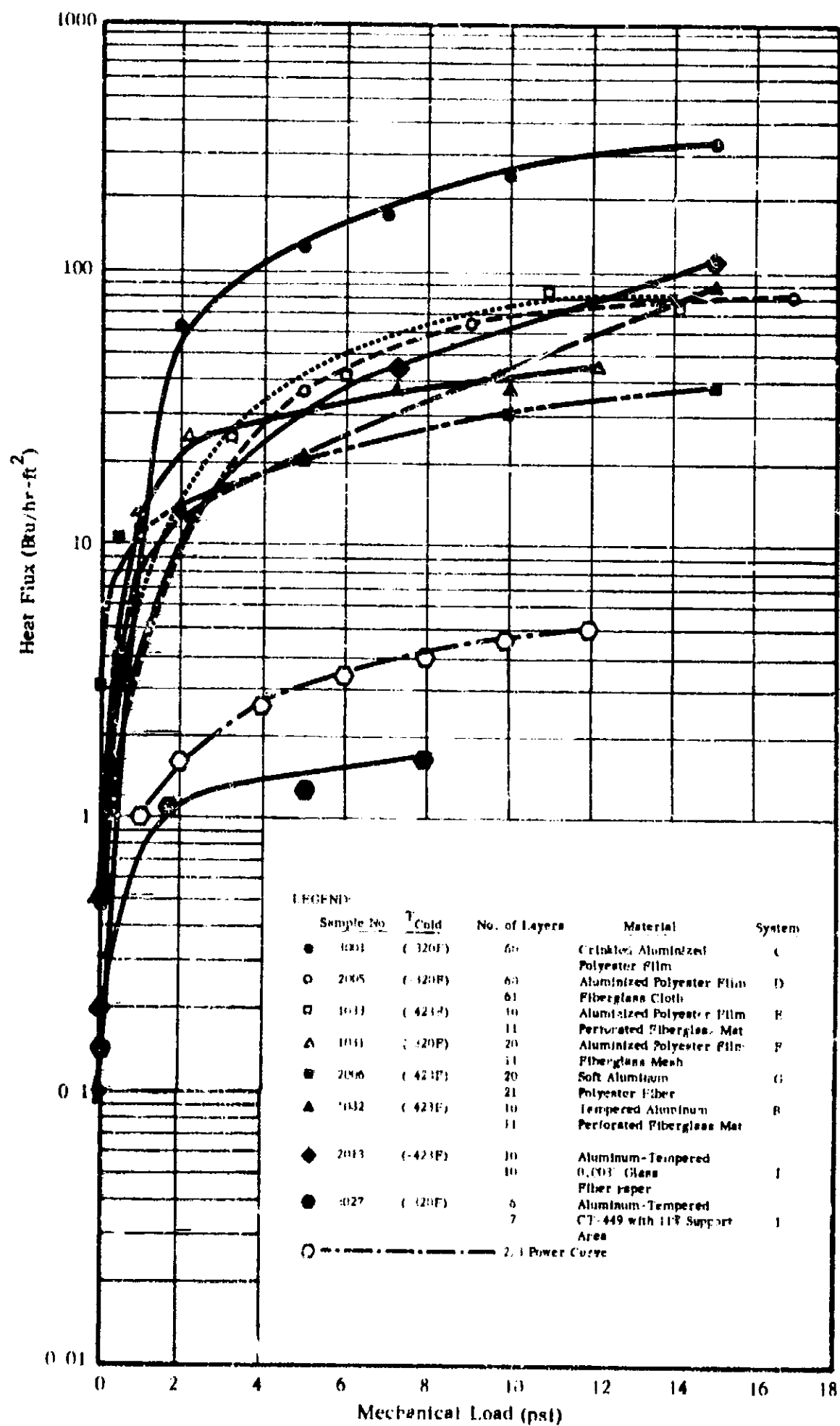


FIGURE II-VI-3 EFFECT OF MECHANICAL LOADING ON HEAT FLUX OF MULTILAYER INSULATIONS

tion systems on the parameter $K\rho$ (product of thermal conductivity and density). Because a considerable choice exists in the thickness of radiation shields and spacers, the insulation density can be adjusted to meet a particular set of conditions. The selection of a combination of materials may be influenced by specific design requirements, including the effects of lateral heat conduction through the radiation shield, structural integrity, high-temperature stability, and production considerations.

The density of the crinkled polyester film is strongly dependent on repeated mechanical load application. Table II-VI-1 presents the results of compression on a sample consisting of 20 shields and indicates the permanent deformation obtained by repeated compressions, which cause a flattening of the crinkles. The density of the sample was calculated from the thickness, which was measured during the test in a fixture constructed for this purpose.

C. Temperature

Tests were performed to determine the effect of warm and cold boundary temperature variation on the thermal conductivity of several multilayer insulation systems. The cold side was maintained at either -423°F (liquid hydrogen), -320°F (liquid nitrogen), or -22°F (liquid Freon 12), and the temperature was taken as the normal boiling temperature of these fluids at atmospheric pressure. The warm boundary temperature was measured by thermocouples embedded in the warm plate and was maintained at desired levels by circulating liquid nitrogen at various rates (-209 to -300°F), alcohol precooled by carbon dioxide (-99°F),

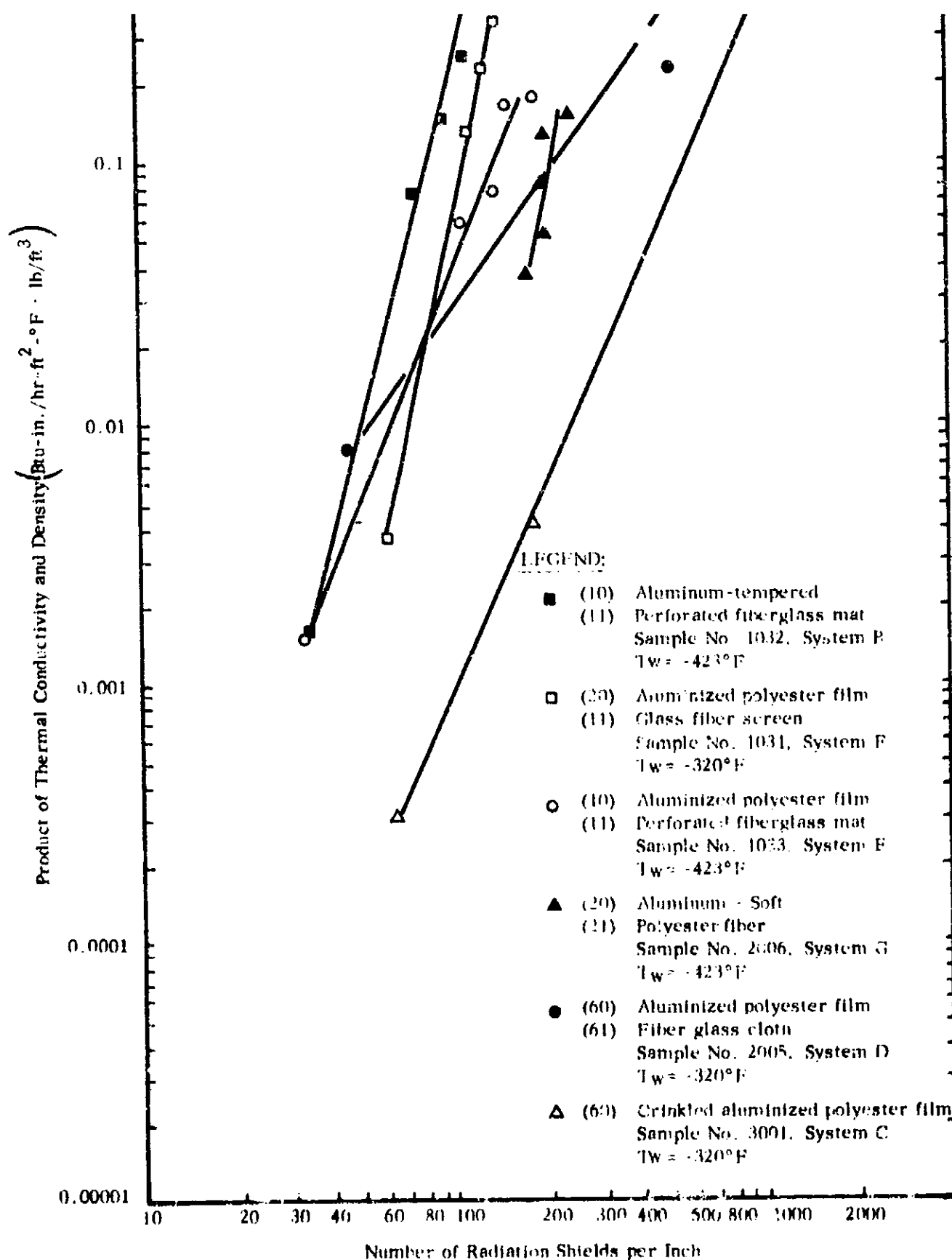


FIGURE II-VI-4

EFFECT OF COMPRESSIVE LOADING ON
PRODUCT OF THERMAL CONDUCTIVITY
AND DENSITY

plate of the apparatus.

TABLE II-VI-1
EFFECT OF COMPRESSION ON POLYESTER FILM

	<u>Compressive</u> <u>Load</u> (lb/in. ²)	<u>Sample</u> <u>Thickness</u> (in.)	<u>Density</u> (lb/ft ³)
A. 0.00025-inch Crinkled Polyester Film, Uncompressed	0.000	1.000	0.44
	0.006	0.500	0.87
	0.018	0.310	1.39
	0.054	0.180	2.31
	0.117	0.125	3.46
B. Repeat Tests	0.017	0.142	3.05
	0.054	0.080	5.42
	0.164	0.055	7.90
	0.185	0.044	9.87
C. Repeat Tests	0.018	0.059	7.36
	0.054	0.051	8.50
	0.164	0.047	9.22
D. Repeat Tests	0.185	0.042	10.31

Table II-VI-2 and Figures II-VI-5, -6, and -7 show the effect of temperature on the thermal conductivity of three multilayer insulation systems. Table II-VI-2 presents data for various insulations which were tested at cold plate temperatures of -320°F (liquid nitrogen) and -423°F

(liquid hydrogen). The heat flux through these insulation samples was approximately the same (within reasonable experimental error) for both temperature levels. Figure II-VI-5 shows the results of tests in which both the warm and cold boundary temperatures were varied. The data indicate that the heat flux is primarily a function of the fourth power of the warm plate temperature; over the range considered, the flux is independent of cold boundary temperature, even for T_{cold} as high as -22°F . This result is in accord with theoretical predictions. Figures II-VI-6 and -7 show that the dependence of thermal conductivity on the warm boundary temperature follows an approximate third power relationship, as had been predicted by analysis, which assumed that changes in solid and gaseous conduction could be neglected.

TABLE II-VI-2

EFFECT OF COLD BOUNDARY TEMPERATURE ON THERMAL CONDUCTIVITY

Sample Chamber Pressure: Below 5×10^{-5} torr

Warm Plate Emissivity: 0.3

Cold Plate Emissivity: 0.1

Temp. Cold plate (F)	Heat Flux $\left(\frac{\text{Btu}}{\text{hr-ft}^2}\right)$	Thermal Conductivity $\left(\frac{\text{Btu-in.}}{\text{hr-ft}^2-\text{F}}\right)$	Temp. Warm Plate (F)	Sample	Sample Thickness (in.)	Density (lb/ft ³)	Test #
-320	0.23	0.00018	63	(10) Tempered aluminum and (11) fiberglass mat, perforated (50% open area)	0.301	12.9	1032a
-423	0.20	0.00012	61				1032b
-320	0.90	0.00097	40	(20) Aluminized polyester film, crinkled	0.385	0.9	1036b
-423	0.84	0.00069	45				1036c
-320	0.62	0.00043	38	(10) Shields and (11) spacers-sample {edges glued}	0.250	--	1040h
-423	0.72	0.00040	38	submitted by Company G			1040i
-320	0.42	0.00088	58	(95) Smooth aluminized Mylar 0.0005 in. thick and	0.800	19.2	2007a
-423	0.43	0.00072	54	(96) fabric (AGC)			2007b

II-110

TABLE II-VI-2
(continued)

EFFECT OF COLD BOUNDARY TEMPERATURE ON THERMAL CONDUCTIVITY

Temp. Cold Plate (F)	Heat Flux $\left(\frac{\text{Btu}}{\text{hr-ft}^2}\right)$	Thermal Conductivity $\left(\frac{\text{Btu-in.}}{\text{hr-ft}^2\text{-F}}\right)$	Temp. Warm Plate (F)	Sample	Sample Thickness (in.)	Density (lb/ft ³)	Test #	Date
-320	0.18	0.00017	53	(10) Tempered aluminum and (11) 1/8 x 1/8 in. vinyl-coated glass fiber screen	0.355	10.9	2014b	5/
-423	0.15	0.00012	49		0.353	11.0		
-320	2.5	--	69	(10) Tempered aluminum and (11) 1/8 x 1/8 in. vinyl-coated glass fiber screen (6 x 1/4-in. slot cut in radiation shields)	0.350	--	2020f	7/1
-423	2.5	--	68				2020e	7/1
-320	0.24	0.00021	67	(10) Tempered aluminum and (11) 1/8 x 1/8 in. vinyl-coated glass fiber screen	0.332	11.7	1049c	9/1
-423	0.21	0.00014	68				1049d	9/1

II-111

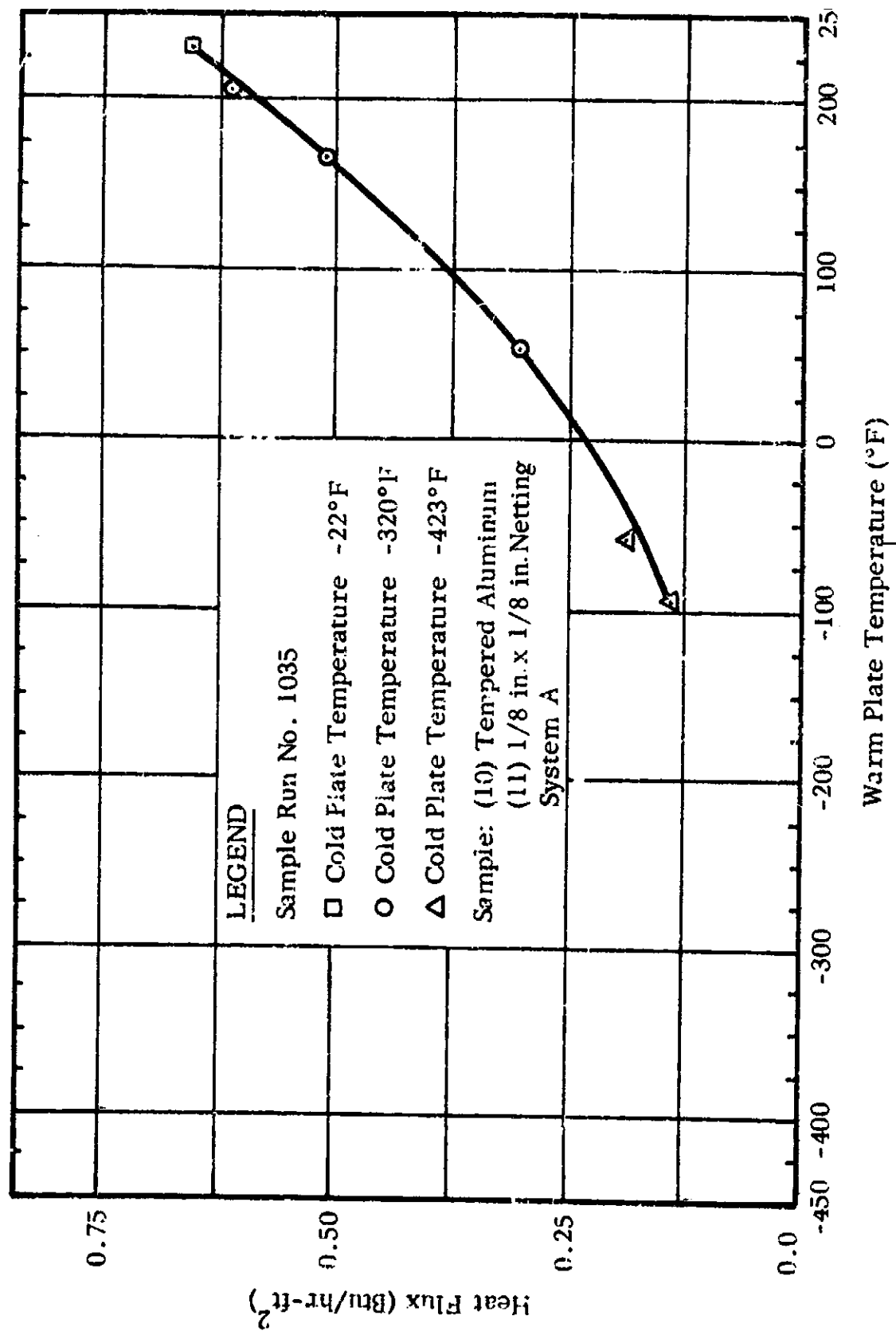


FIGURE II-VI-5 EFFECT OF WARM PLATE TEMPERATURE ON HEAT FLUX

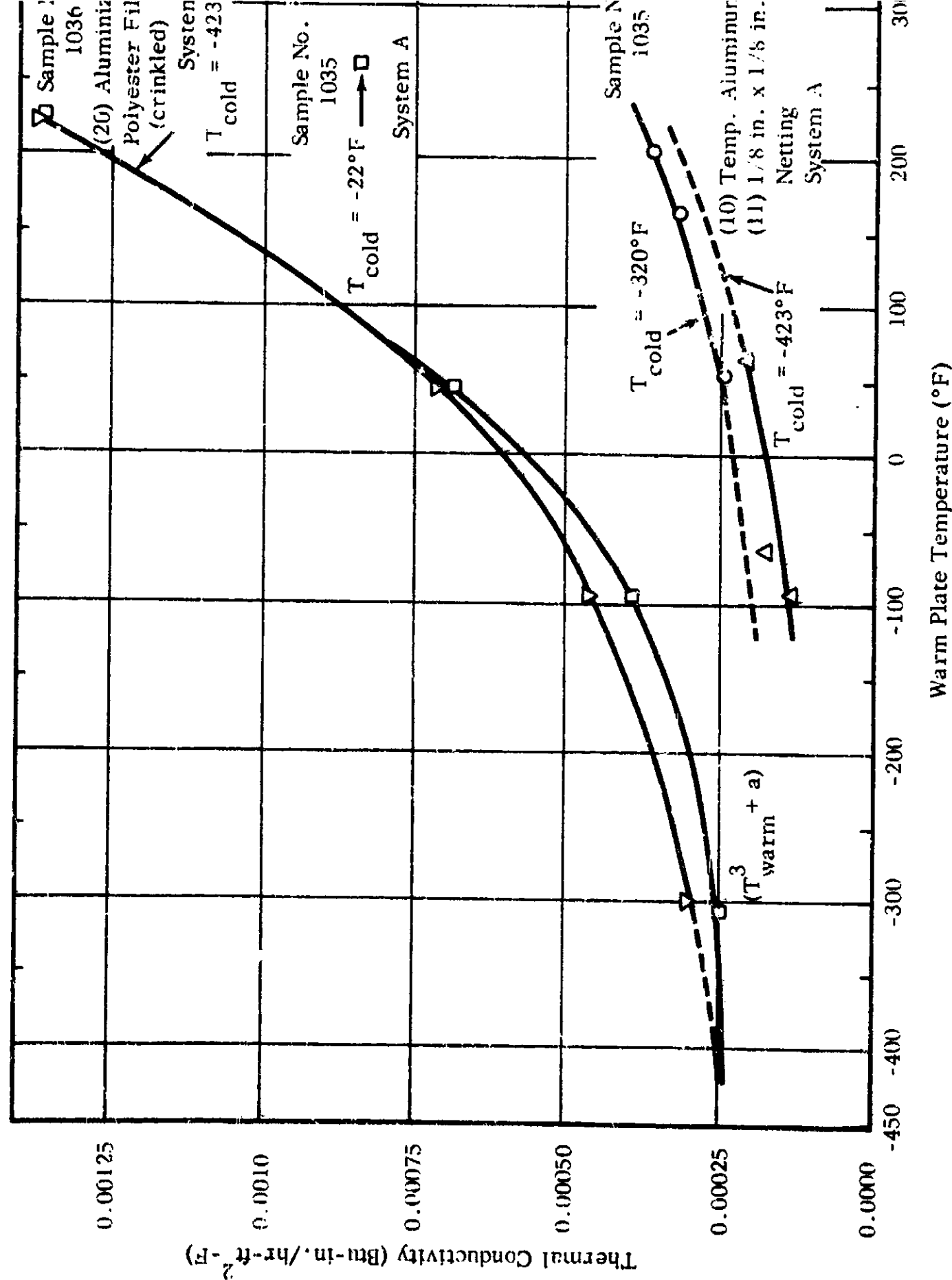


FIGURE II-VI-6

EFFECT OF BOUNDARY TEMPERATURE ON THE MEAN APPARENT THERMAL CONDUCTIVITY AND ON HEAT FLUX OF MULTIPLE-LAYER INSULATIONS

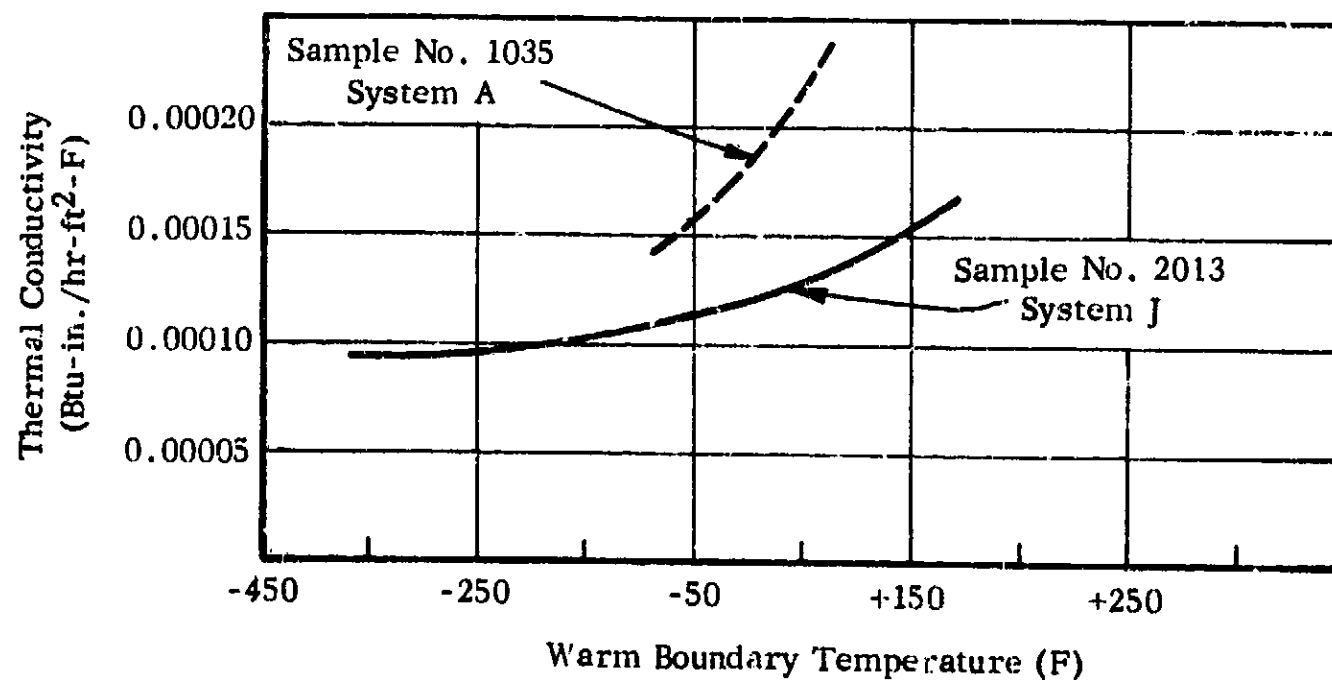
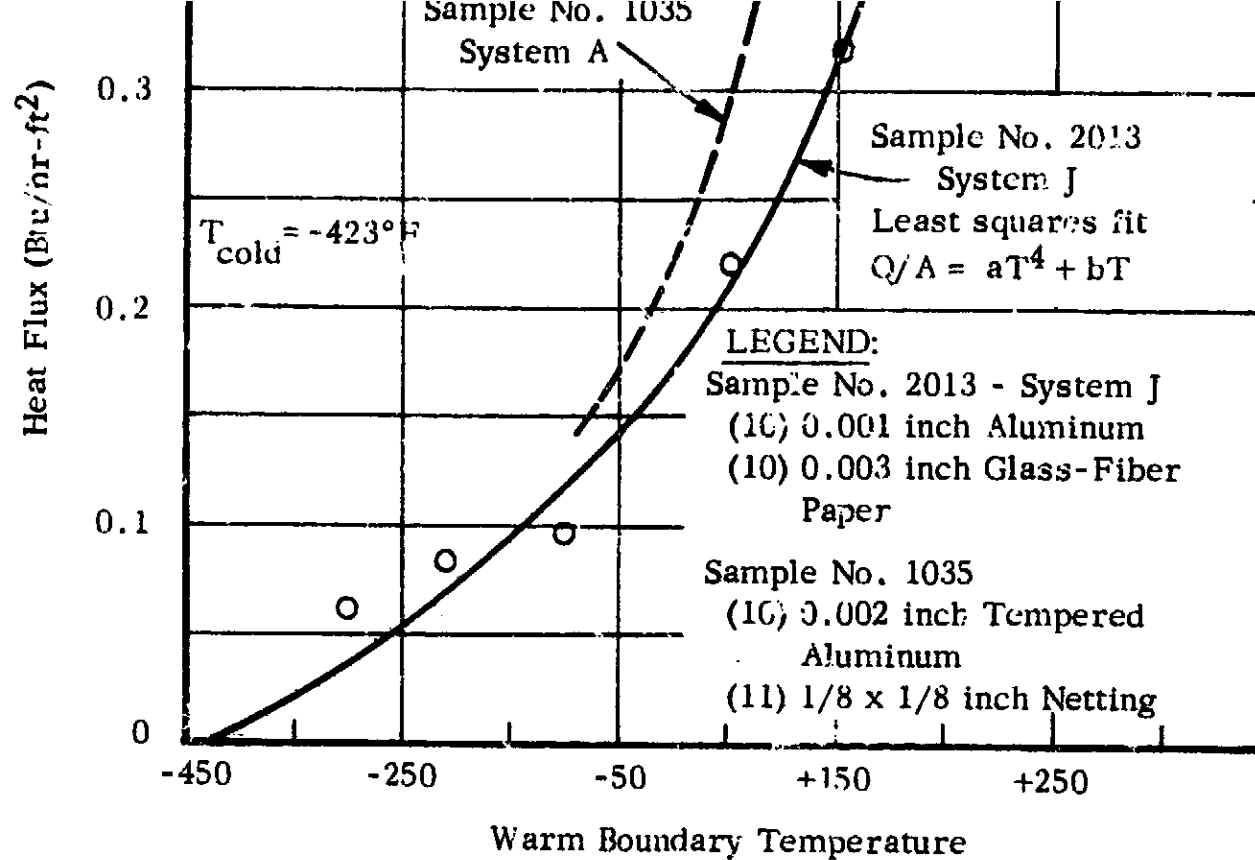


FIGURE II-VI-7

EFFECT OF WARM BOUNDARY
TEMPERATURE ON HEAT FLUX
AND THERMAL CONDUCTIVITY

D. Residual Gas Pressure

The effect of helium gas pressure on thermal conductivity was tested on samples of two multilayer insulation systems. (Systems A and 1 of Table II-IV-1). The test procedure consisted of pumping the sample chamber to a high vacuum and then bleeding in helium gas to obtain the desired pressure, which was held constant for each test. The series of pressures examined cover the range 10^{-6} to 750 torr.

The experimental results of these tests are given in Figure II-VI-8. The thermal conductivity increases rapidly between pressures of about 5×10^{-4} and 5 torr; it is in this pressure range that the mean free path of the gas molecules approaches the distance between individual particles of the insulation system.

The practical significance of these results is that multilayer insulations reach a lower thermal conductivity than opacified evacuated powders only at pressures less than about 10^{-4} torr. Figure II-VI-9 compares the thermal conductivity of a multilayer insulation with that of powder and fiber insulations as a function of gas pressure.

The dependence of thermal conductivity on residual gas conduction indicates that every effort must be made to obtain a low pressure within the multilayer insulation. If the low pressure existing in space is to be relied upon to assist in evacuating the insulation, steps must be taken so that the outgassing rate from the insulation surfaces, as well as gas diffusion from the tank due to very small leaks, can be accommodated.

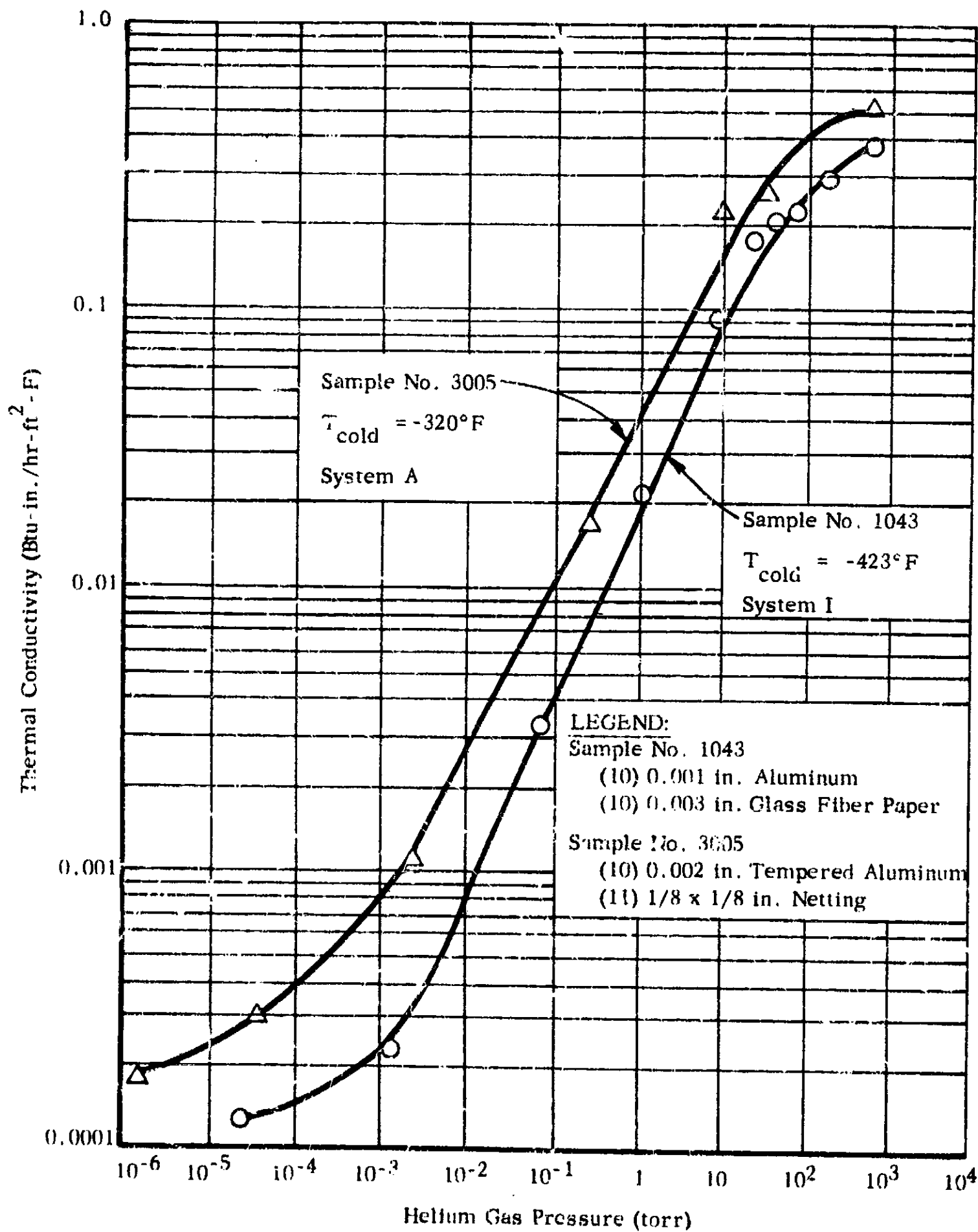


FIGURE II-VI-8

EFFECT OF HELIUM GAS PRESSURE ON THERMAL CONDUCTIVITY

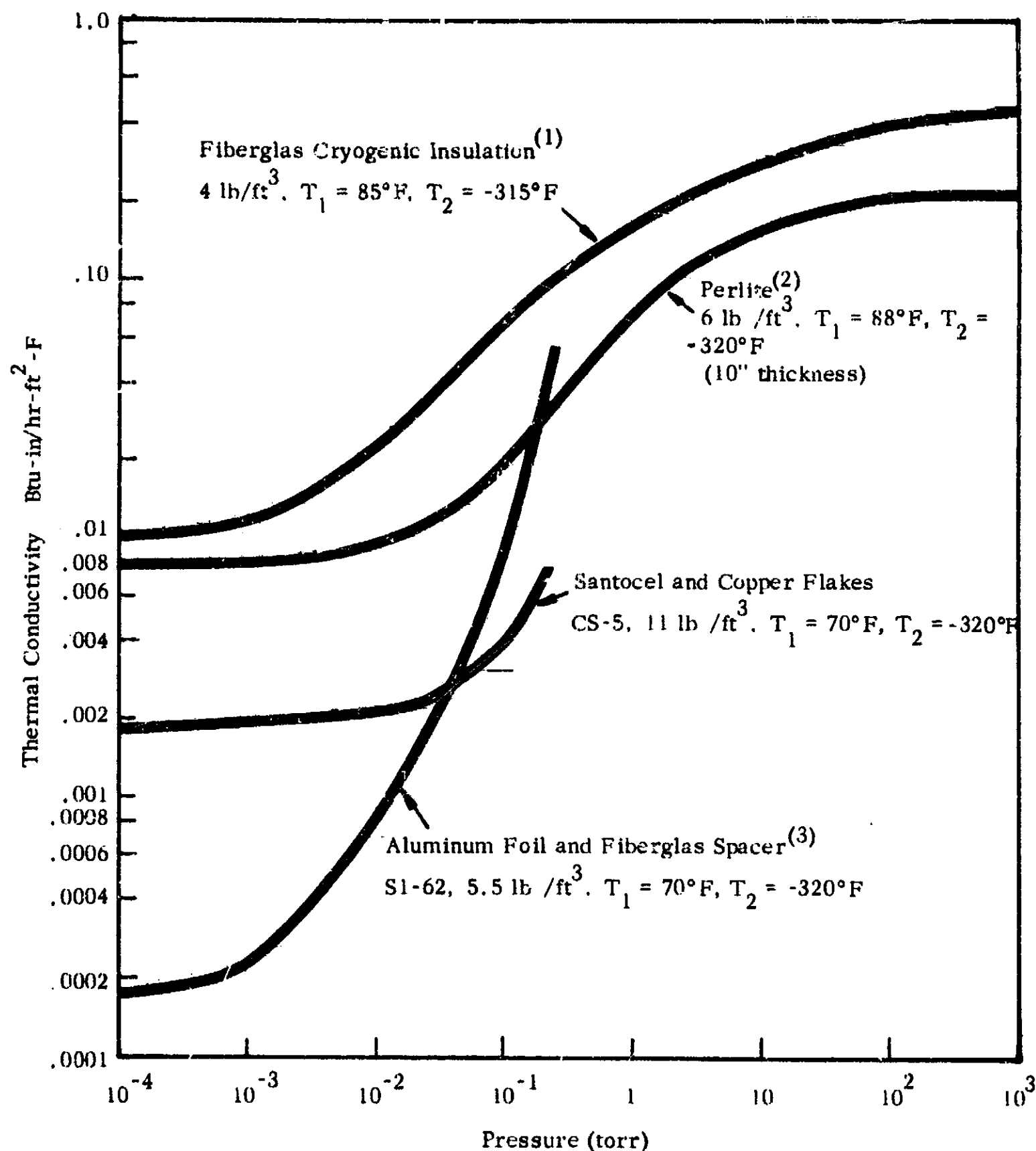


FIGURE II-VI-9 THE DEPENDENCE OF THERMAL CONDUCTIVITY ON GAS PRESSURE OF TYPICAL POWDERS, FIBERS, AND MULTI-LAYER INSULATIONS

- Sources: (1) R.M. Christiansen, M. Hollingsworth, Jr., and H.N. Marsh, Jr., "Low Temperature Insulating Systems," Adv. in Cryogenic Engineering, K.D. Timmerhaus (ed.), Vol. 5, Plenum Press, Inc., New York (1960), p. 171.
- (2) D.B. Chelton and D.B. Mann, Cryogenic Data Book.
- (3) M.A. Duba and L.I. Dana, "Superinsulation for the Large Scale Storage and Transport of Liquefied Gases," Bull. Inst. Int. du Froid, Annexe 1961-5, Paris, p. 75.

E. Perforations

The effect on thermal conductivity caused by perforating the radiation shields was tested on samples of two multilayer insulations. In these samples the radiation shields had uniform patterns of perforations of 1/16-, 1/8-, and 1/4-inch diameter and an amount of open area as high as 12.6%. Smaller perforations, although desired, could not be made readily. The shields were oriented so that the holes in each shield did not align with the holes in adjacent shields.

The results of these tests appear in Figures II-VI-10 and -11. The data show that: (1) heat flux through the insulation increases directly with the amount of open area in the radiation shields for perforations of a given diameter, (2) heat flux decreases as the diameter of perforations increases for a given amount of open area.

The experimental results may be compared with the two extreme theoretical values given by the formulas for very small and very large perforations. For large perforations which do not overlap, the flux is

$$q = \frac{\sigma(T_a^4 - T_1^4)}{n \left(\frac{2}{\epsilon} - 1 \right) \left(\frac{1}{1 + 2\tau} \right) + 1} \quad (\text{II-VI-1})$$

When ϵ is small, this can be approximated by

$$q = q_0 (1 + 2\tau) \quad (\text{II-VI-2})$$

where q_0 is the flux in the absence of perforations. This curve is plotted as the lower theoretical line in Figure II-VI-10.

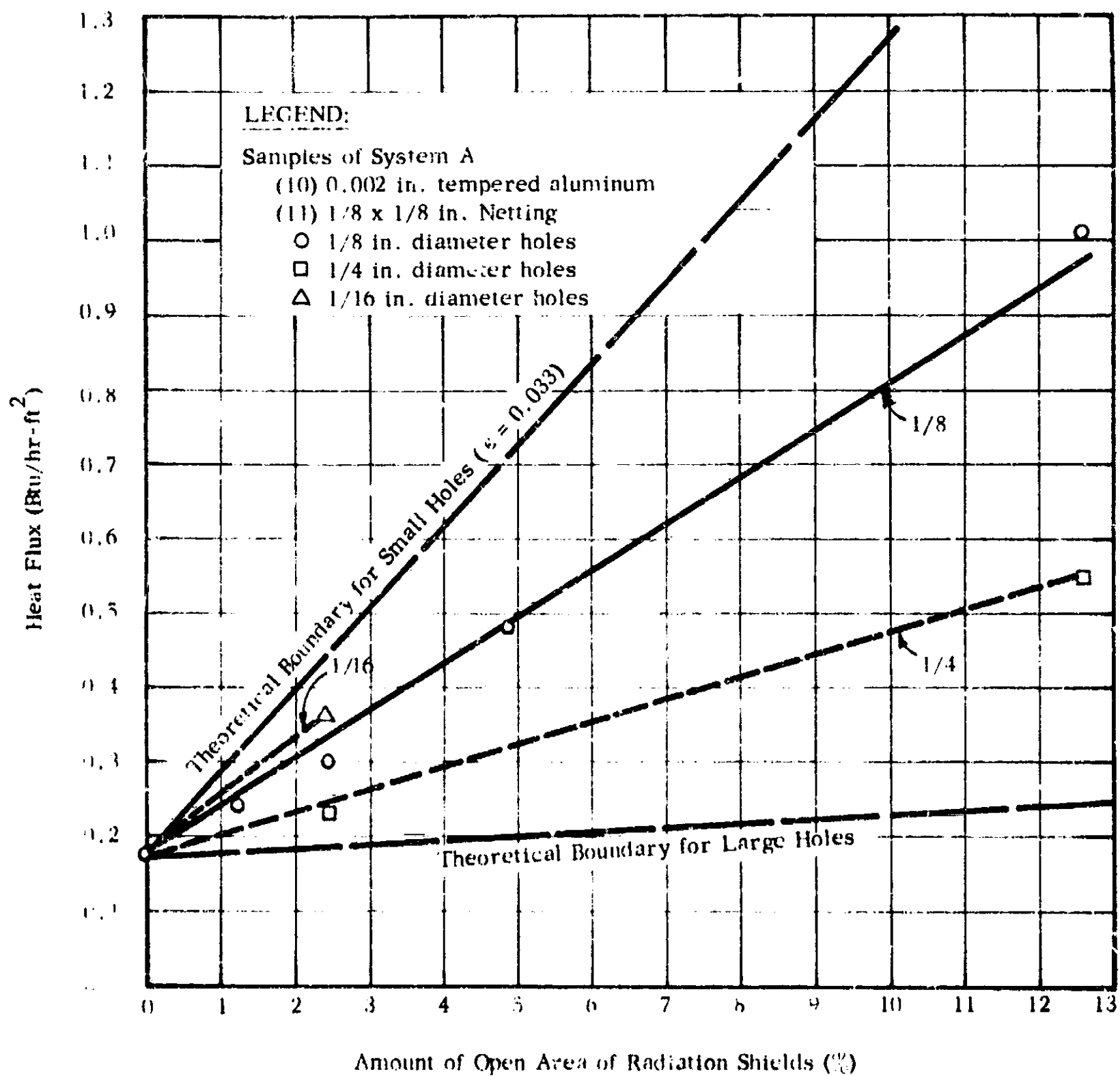


FIGURE II-VI-10 EFFECT OF PERFORATIONS ON HEAT FLUX

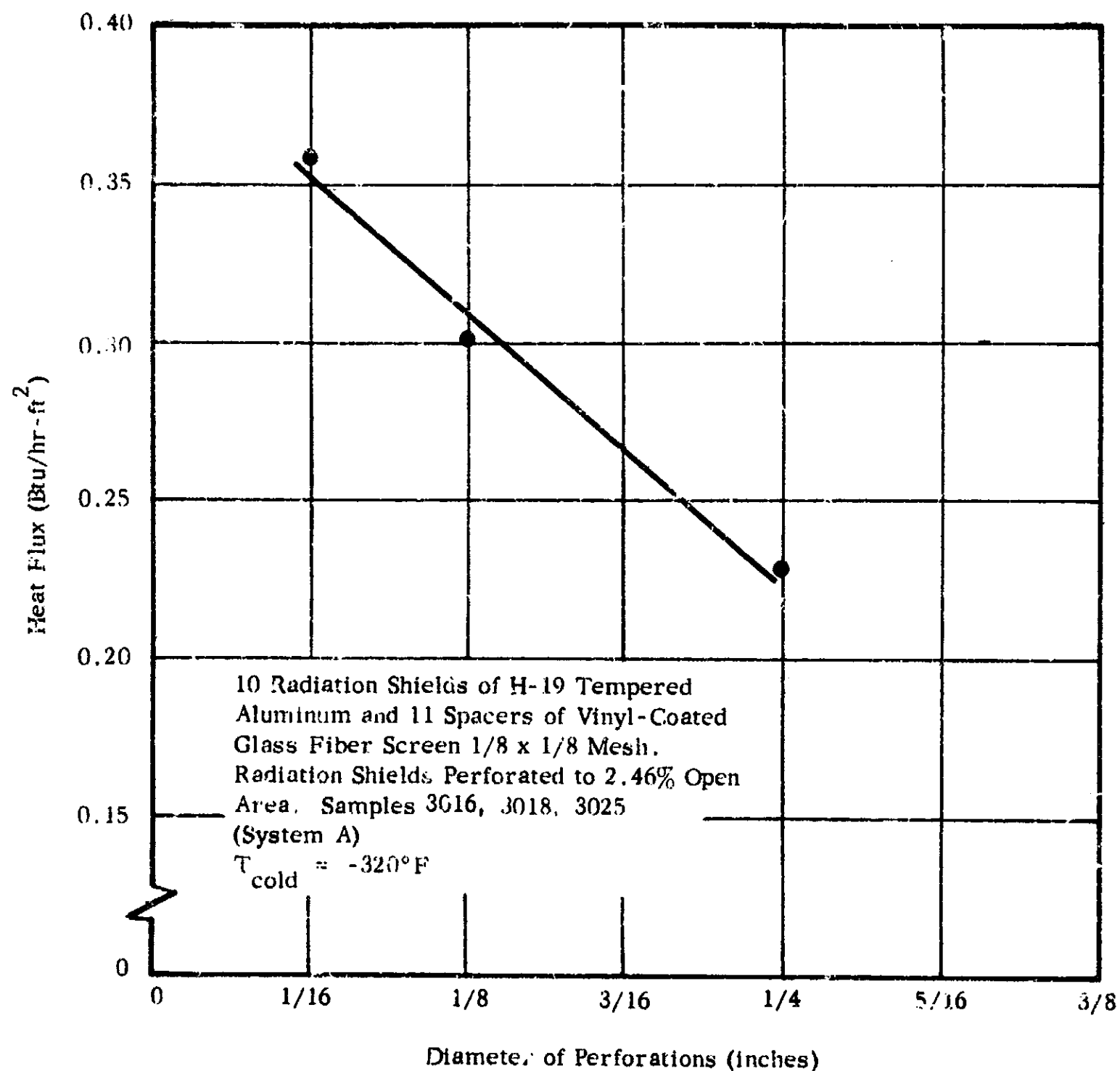


FIGURE II-VI-11

EFFECT OF DIAMETER OF PERFORATIONS ON HEAT FLUX

For small perforations, the flux is

$$q = \frac{\sigma (T_s^4 - T_i^4)}{n \left[\frac{2}{\epsilon + (2 - \epsilon) \tau} - 1 \right] + 1} \quad (\text{II-VI-3})$$

When ϵ is small, this reduces to the approximate form

$$q = q_0 \left(1 + \frac{2}{\epsilon} \tau \right) \quad (\text{II-VI-4})$$

This expression explicitly involves the emissivity ϵ , whereas Equation II-VI-2 does not. In plotting this curve as the upper theoretical boundary in Figure II-VI-10, we have assumed that $\epsilon = .033$, so that

$$q = q_0 (1 + 60 \tau) \quad (\text{II-VI-5})$$

The experimental points are bracketed by these theoretical bounds. To develop a formula to predict the effects of intermediate-size perforations, such as those used in the experimental program, a substantially more complicated analysis would be required.

These results (which include only radiation inleakage) indicate that the amount of open area should be kept small and that the diameter of the holes should be large. However, the purpose of perforating is to enhance pumping of the gas from within the multilayer insulation, and the theoretical analysis presented in Part II-III-C-1 indicates that pumping efficiency, relative to radiation inleakage, is much less for large holes than for smaller holes totaling the same amount of open area.

F. Discontinuities

Two series of tests have been performed to demonstrate the effect of discontinuities in multilayer insulation systems. In one series rectangu-

lar gaps of various widths were cut in samples of multilayer insulations; in the other series, the area of the sample edge was varied as well as the thermal environment to which the sample edge was exposed.

Rectangular gaps of 6-inch length and variable widths were cut through all the radiation shields of the sample except the bottom one, next to the warm plate. The gap in each radiation shield was aligned with that of adjacent shields and was positioned directly under the measuring portion of the cold plate. The configuration of the sample is shown in Figure II-VI-12. Samples of insulation systems A and C were tested, each with gap widths of 1/16-, 1/8-, and 1/4-inch.

The results of these tests (Figure II-VI-13) show that for both insulations the heat flux and, hence, thermal conductivity increased in direct proportion to the width of the gap. The insulation sample containing crinkled aluminized polyester film was less affected than the sample containing aluminum radiation shields.

Samples of 6-1/2 and 9-inch diameter were tested under three types of edge treatments. The edge treatments, as sketched in Figure II-VI-14, consisted of (a) a ring of multilayer insulation of the same material as the sample, (b) a ring of microfiber glass wool, and (c) no insulating material beyond the edge of the sample. For treatments (a) and (b), a 1/16-inch gap was maintained between the sample and the ring. Additionally, samples of 11, 12, and 12-5/8 inch diameter were tested with no insulation beyond their edges.

The results of these tests are given in Figure II-VI-15, which is a plot of heat flux into the measuring vessel as a function of sample diameter. The curve applies to tests for edge treatment (c), that is,

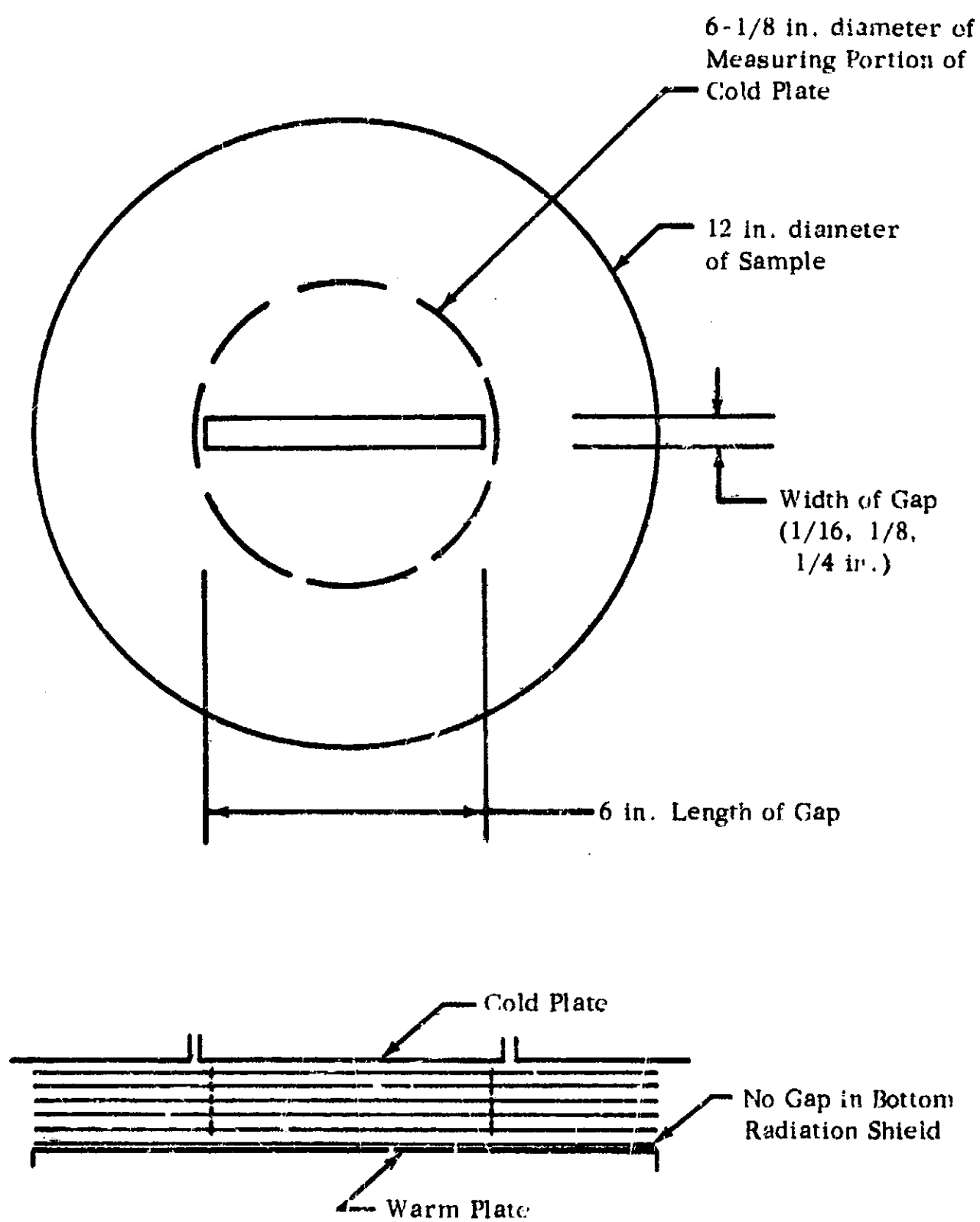


FIGURE II-VI-12

CONFIGURATION OF MULTILAYER SAMPLE TESTED FOR THE EFFECT OF A DISCONTINUITY ON THERMAL CONDUCTIVITY

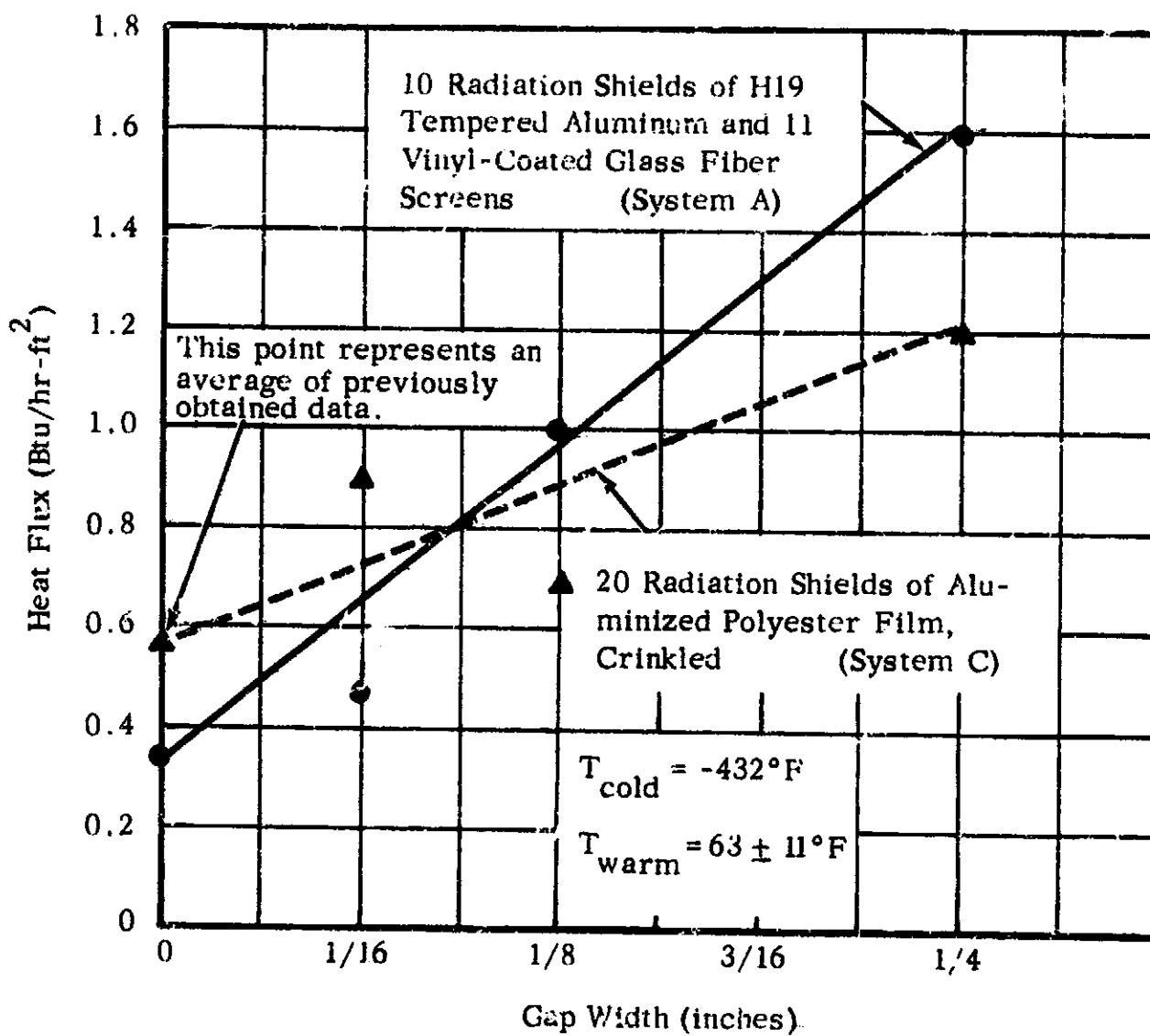


FIGURE II-VI-13

EFFECT OF DISCONTINUITY ON THERMAL CONDUCTIVITY OF A MULTILAYER INSULATION

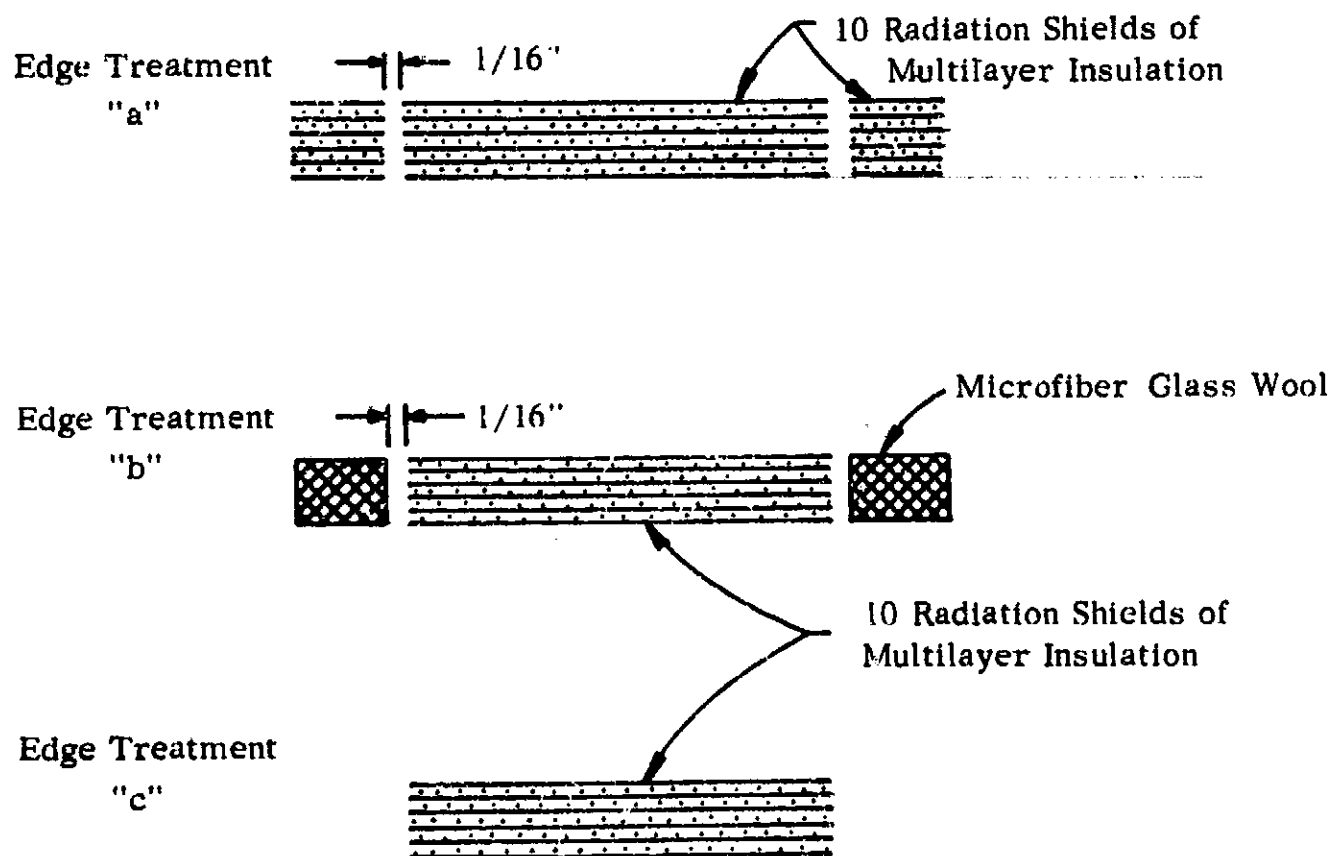
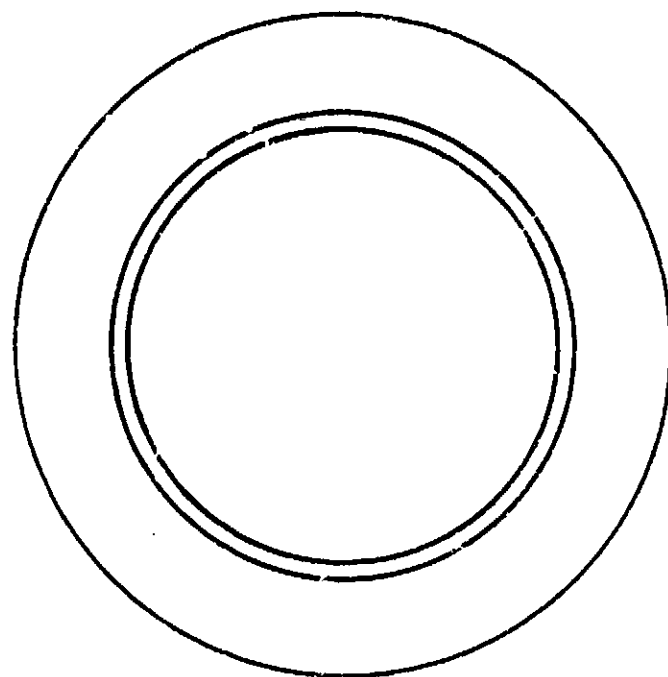


FIGURE II-VI-14

SKETCH OF EDGE TREATMENTS FOR SAMPLES USED
IN DISCONTINUITY TESTS

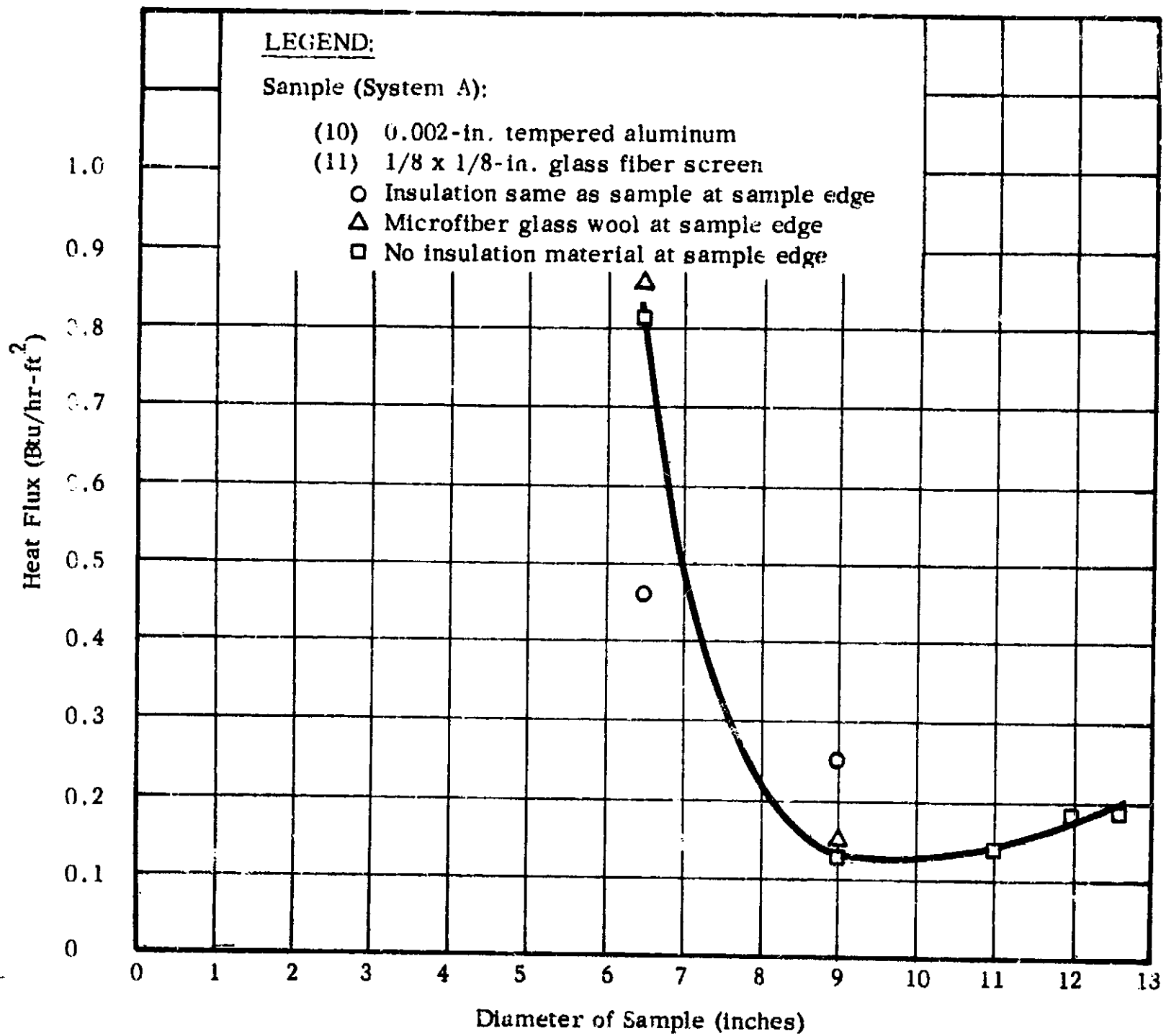


FIGURE II-VI-15 EFFECT OF DISCONTINUITIES IN THE RADIATION SHIELDS OF MULTILAYER INSULATION

with no insulating material beyond the sample edge. Data points are plotted for the remaining tests, but no curve has been drawn connecting them. The decreasing heat flux with increasing sample diameter shown in the figure for sample diameters up to 9 inches is as expected, because more of the guard ring is being utilized with increasing diameter. The apparent minimum point and subsequent increase in heat flux as the sample diameter exceeds 9 inches appears to be due to the complex interaction of the sample edges with radiation emanating from surfaces at different temperatures.

G. Emissivity

The effect of emissivity on the thermal conductivity of a multi-layer sample can be illustrated by tests made on an assembly of aluminized polyester film (System C). In one sample the thermal conductivity was $0.001 \text{ Btu-in/hr-ft}^2\text{-F}$. After a sample was made up from a new shipment from the supplier, a thermal conductivity of $0.0004 \text{ Btu-in/hr-ft}^2\text{-F}$ was measured. It was subsequently we learned that the aluminized coating in the earlier sample was near the borderline of acceptable quality (electrical resistance of 7 ohms/cm^2).

In another test, aluminum foils in a sample were replaced by foils just received from the supplier. An 80% decrease in thermal conductivity was obtained, indicating that either oxidation or a different treatment of the foil had resulted in a reduced emissivity and thereby a lower thermal conductivity. Since the contribution of radiation heat transfer is proportional to the emissivity, stringent quality control is required to assure that reproducible emissivities are obtained.

It is possible that the placing of radiation shields very close to each other may cause a substantial increase in the radiation heat transfer rate through the phenomenon of constructive interference, as the wave emitted by a foil is reflected back and forth in the small gap between two foils. This can be of importance in the transmission of energy across the gap when the spacing is very small compared to the wavelength of the radiation, which may be the case at cryogenic temperatures.

H. Contact Resistance

Table II-VI-3 shows the results of tests of the influence of contact resistance between a surface and a foam sample. When the space around the sample was evacuated, the contact resistance between the sample and the surface increased to the extent that the heat flux decreased by a factor of four. Since the foam sample had approximately a 90% closed cell structure, the conductivity of the bulk of the foam appeared to be unaffected by the evacuation of the gas on the outside. Thus, the increase in the resistance was apparently due to a removal of gas from broken cells near the surface. A similar increase in contact resistance was observed on a second sample of foam when a thin evacuated gap was formed between the cold plate and the sample.

TABLE II-VI-3

THE INFLUENCE OF CONTACT RESISTANCE BETWEEN PLATES AND SAMPLE
ON THERMAL CONDUCTIVITY

	Pressure in Specimen Chamber (torr)	Heat Flux ($\frac{\text{Btu}}{\text{hr} - \text{ft}^2}$)	Thermal Conductivity ($\frac{\text{Btu} - \text{in.}}{\text{hr} - \text{ft}^2 - \text{F}}$)	Density (lb/ft ³)	Thick- ness (in.)	Test #
Polyurethane Foam System S	760*	224	0.141	3.85	0.246	1014c
Polyurethane Foam System S	10 ⁻⁵	63.8	0.040	3.85	0.246	1014b
Polyurethane Foam System S	10 ⁻⁵ **	23.3	0.0176	3.85	0.280	1014a
Glass Fiber Re- inforced Foam System T	10 ⁻⁵	41.2	0.0808	5.0	0.758	1018b
Glass Fiber Re- inforced Foam System T	10 ⁻⁵ **	22.6	0.0458	5.0	0.782	1018a

*Nitrogen

**Evacuated gap

I. Foam-Filled Honeycomb Insulation

Tests were carried out on samples of three insulation systems that were submitted to NASA by Company L. The insulation samples are identified in Table II-IV-1 as Systems N, O, and Q and described therein per Company L letters 63MA1429 and 63MA7233.

The test conditions desired for the samples of Systems N and O are as follows:

It is desired that the cold side (the aluminum side on the foam-filled samples) be at boiling liquid hydrogen temperature (-423°F) for all measurements. Other desired conditions are:

<u>Test</u>	<u>System</u>	<u>Hot Side Temp. ($^{\circ}\text{F}$)</u>	<u>Atmosphere in Sample</u>
1	N	-92	Air (sealed)
2	N	32	Air (sealed)
3	N	-92	Air (leakage of air)
4	N	32	Air (leakage of air)
5	N	-92	Helium purge, 2 psia - 5 cc/min
6	N	32	Helium purge, 2 psia - 5 cc/min
7	O	-92	Air (sealed)
8	O	32	Air (sealed)
9	O	-100	Helium (1 atm)
10	O	-320	Helium (1 atm)

The conditions for the helium atmosphere tests will require evacuation of the samples for twelve (12) hours and subsequent purging with helium.

Table II-VI-4 shows the test results obtained on the samples of Systems N and O. In these tests, the desired conditions could not be obtained because the sample edges were not adequately sealed, and purge gas could leak out into the low pressure surroundings. In addition, gas purge flow at the specified 5cc/hr would stop as the sample cooled to

TABLE II-VI-4

EFFECT OF PURGE GAS ON A FOAM

SAMPLE: Glass-phenolic honeycomb, 3/8-inch cell, filled with foam, CO₂ blown

COLD PLATE EMISSIVITY: 0.1

WARM PLATE EMISSIVITY: 0.3 at 43 F; 0.1 at -320 F

ATMOSPHERE IN SAMPLE	HEAT FLUX ($\frac{\text{Btu}}{\text{hr-ft}^2}$)	THERMAL CONDUCTIVITY ($\frac{\text{Btu-in}}{\text{hr-ft}^2\text{-F}}$)	TEMP. WARM PLATE (F)	THICKNESS (in)	TEMP. COLD PLATE (F)	SAMPLE CHAMBER PRESSURE (torr)	NAA SAMPLE DESIGNATION NUMBER	SYSTEM	CONFORMS TO TEST NO. OF LETTER NO. 63MA 1429	TEST NO.	DATE
Evacuated*	22	0.025	-98	3/8	-423	2×10^{-4}	II	0	7	2011a	2/16/63
Evacuated*	102	0.082	43	3/8	-423	2.5×10^{-4}	II	0	8	2011b	3/17, 20/63
Nitrogen**	57	0.09	-94	3/8	-320	$3 \times 10^{-4}(\text{N}_2)$	I	N	none	1041a	3/25/63
Helium**	139	0.24	-100	3/8	-320	1 (He)	I	N	none	1041b	3/26/63
Helium**	227	0.27	-102	3/8	-423	2 (He)	I	N	5	1041c	2/27/63
Helium**	633	0.52	34	3/3	-423	2 (He)	I	N	6	1041d	3/28/63
Nitrogen**	287	0.24	33	3/8	-423	1 (N ₂)	I	N	2	1041e	3/28/63

* We believe that the sample is gas-permeable and allows air to be evacuated from the foam-filled honeycomb. Data obtained would, therefore, be more representative of an evacuated sample rather than a sample with a sealed-in atmosphere of air.

** Gas flow through the sample stopped as the cold side of the sample cooled to -320F. A positive pressure was maintained on the inlet part, but the gas flow through the sample was too small to be detected.

the liquid nitrogen boiling point. This may have been the result of a failure that occurred while setting up the test. At that time, oil backed up from the low-gas-flow measuring graduate into the exhaust side of the sample. Subsequent tests showed traces of oil near the exhaust ports which were located in the guard area of the sample. The oil may have solidified at the purge line exit at the cold temperatures and reduced the flow of purge gas through the sample. Good thermal contact with the cold plate could not be achieved, because the sample was not perfectly flat.

The test results indicate the controlling effect of helium on thermal conductivity at the various temperature differences used for the test.

Table II-VI-5 shows the test results obtained on the samples of System Q. In the first tests (1045a, d, and e) the sample was purged with gaseous nitrogen for two to five hours, the tubes attached at the edges were sealed, and the sample was chilled to -423F; cryopumping of the gas then took place at the cold side of the sample. The tubes were sealed to prevent additional nitrogen gas from entering the sample as the pressure of the contained gas decreased. The heat flux through the sample under these conditions was measured at three warm plate temperatures: -97, +37, and +97.

In a second test on the sample of System Q, nitrogen gas was introduced into the sample for two hours before cooling, and the tubes leading into the sample were not closed off during the test. Nitrogen gas was continuously metered into the sample at a pressure of 1/2psig during the test. The results of three trials under these test conditions were erratic, indicating a high degree of thermal instability in the sample,

TABLE II-VI-5

EFFECT OF PURGE GAS ON A FOAM INSULATION

SAMPLE: Glass-phenolic honeycomb, 3/4-inch cells, filled with polyurethane foam, CO₂ blown (System Q)

WARM PLATE EMISSIVITY: 0.3

COLD PLATE EMISSIVITY: 0.1

TEMP. WARM PLATE (F)	HEAT FLUX ($\frac{\text{Btu}}{\text{hr-ft}^2}$)	THERMAL CONDUCTIVITY ($\frac{\text{Btu-in}}{\text{hr-ft}^2-\text{F}}$)	SAMPLE THICKNESS (in)	MECH. LOAD ON SAMPLE (psi)	TEMP. COLD PLATE (F)	ATMOSPHERE IN SAMPLE CHAMBER*	TEST NO.	DATE
37	62	0.14	1.030	15	-423	N ₂	1045a	6/19/63
-97	20	0.063	1.026	15	-423	N ₂	1045d	6/21/63
+97	68	0.14	1.028	15	-423	N ₂	1045e	6/24/63
40	**		0.818	15	-423	Argon	1046	7/12/63

Tests 1045a, d, e: Atmosphere of nitrogen at 760 torr sealed in the sample and cryopumped.

Test 1046: Argon 1/2 psig at the sample ports

* Cryopumped from 760 to 1 torr.

** See Figure II-VI-16.

and are not included in the table.

In a third test of System Q (test No. 1046) argon instead of nitrogen was used as the purge gas. Six trials were conducted, three each on two successive days. The duration of each trial was approximately one hour. The apparatus was refilled with liquid hydrogen immediately after each trial and then warmed up to approximately -100F during the intervening night.

Approximately two cubic feet of argon flowed into the sample during both days. Because the sample leaked at the edges, the amount of gas actually introduced into the sample could not be measured. The results of this test are given in Figure II-VI-16. The sample appeared to be approaching thermal equilibrium when the tests were terminated. The lower heat flux through the sample on the beginning of the second day compared to that at the end of the first day may be due to the fact that the apparatus was relatively cold at the beginning of the day, so that the sample reached thermal equilibrium in a shorter time.

Because the sample was leaking badly, it was removed from the apparatus. Subsequent examination showed that the laminate covering the cold face of the sample had become completely separated from the honeycomb and foam insulation. This separation presumably occurred as the sample warmed up after the second day of testing and the pressure increase associated with the phase change from liquid to gas inside the sample became excessive.

The test results indicate the dominating effect of the purge gas or the thermal conductivity and particularly the substantial increase obtained when the sample is allowed to cryopump. If it could be arranged

to have the insulation cryopumped during the time maximum insulating effectiveness is required, it would appear that a good thermal protection system would result.

Considerable difficulty was experienced with the present method of edge-sealing and connection of purge lines at the sample edges. In future samples it would be advantageous to arrange the purge line as shown in Figure II-VI-17.

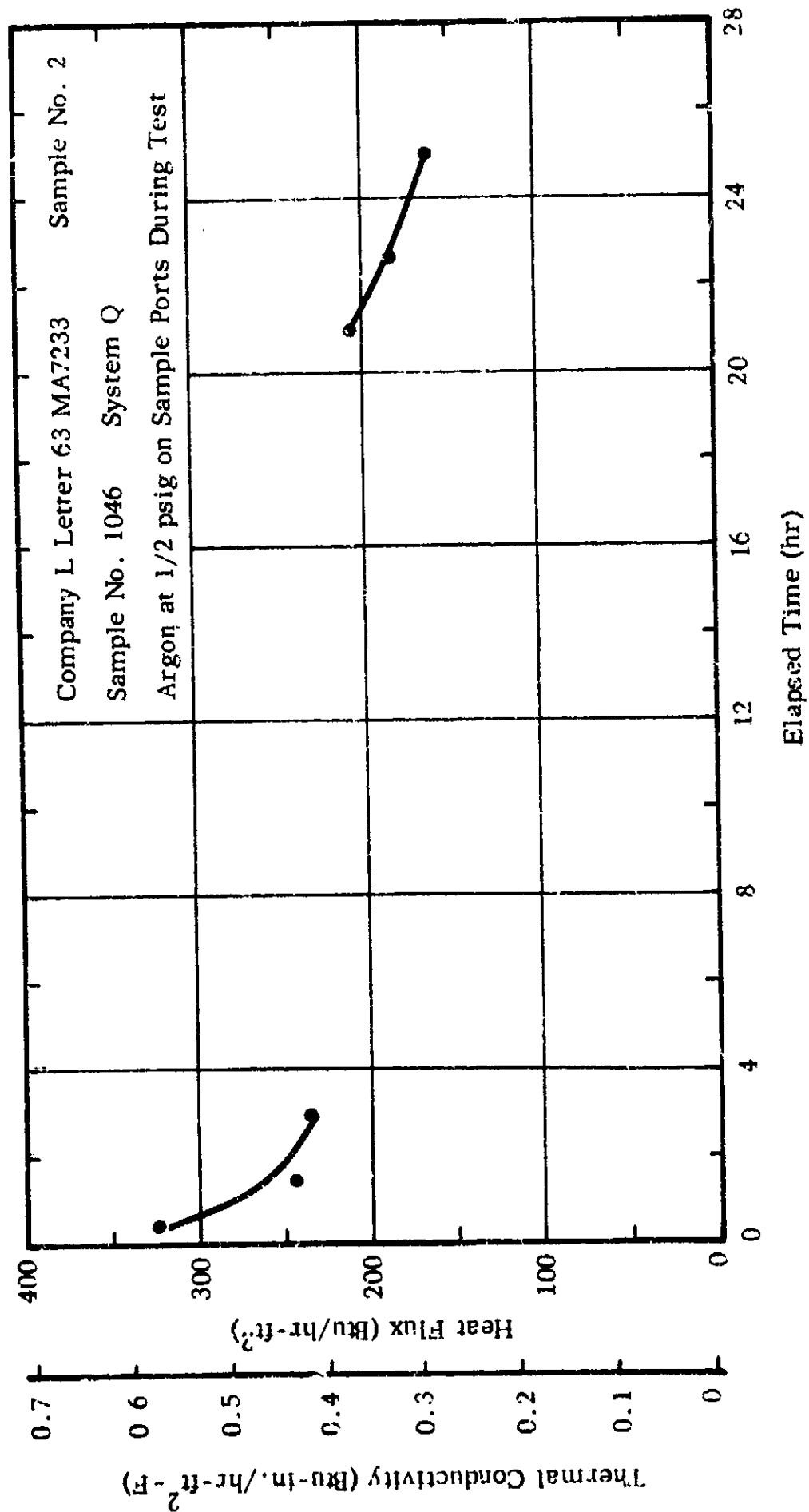


FIGURE II-VI-16 EFFECT OF PURGE GAS ON THERMAL CONDUCTIVITY OF A FOAM INSULATION

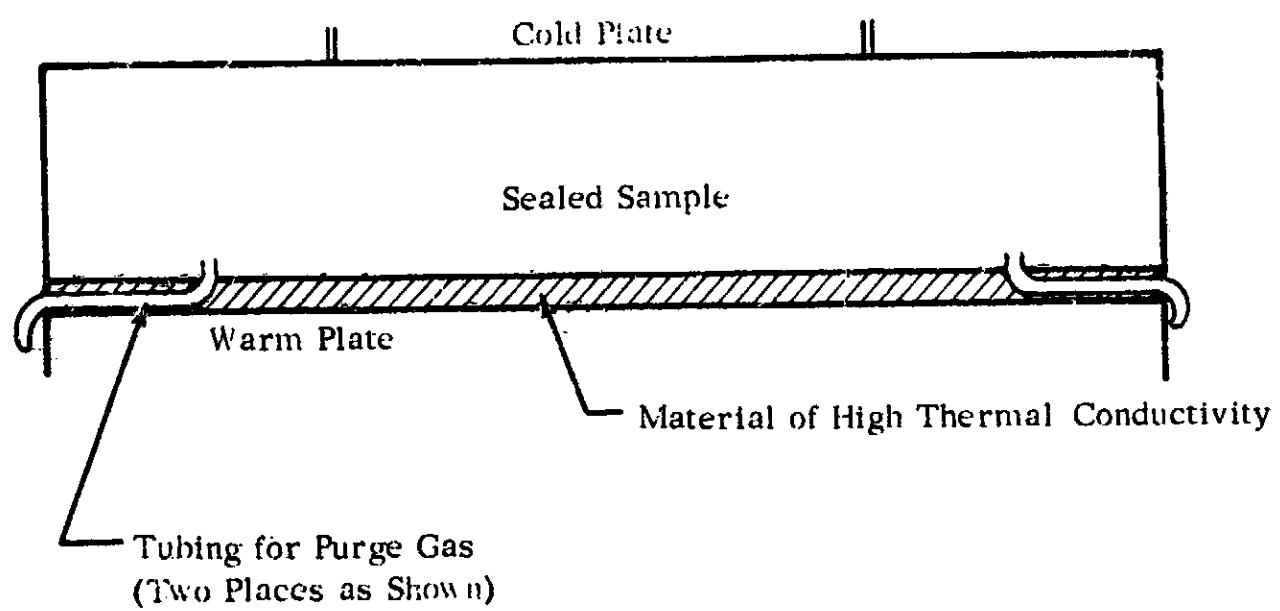


FIGURE II-VI-17 SUGGESTED FUDGE LINE ARRANGEMENT

J. Polyurethane Foam Insulation

Thermal conductivity measurements were made on a polyurethane foam insulation system. (See R, Table II-IV-1.)

The heat flux through this insulation was measured using several arrangements of the laminate at the sample edge, at different compressive loads, and with different thermal resistances interposed at the cold side of the sample. The condition of the sample for each test was as follows:

Sample Number 2021: The edges of the sample were sealed with a laminate of Mylar, aluminum and Mylar (see configuration "a" in Figure II-VI-18) and the sample was subjected to compressive loads of 15 and 2 psi, respectively.

Sample Number 2021-I: The seal at the edges of the sample was removed so that the polyurethane foam was directly exposed to the low pressure (see configuration "b" in Figure II-VI-18). The sample was subjected to a compressive load of 15 psi.

Sample Number 2023: The edges of the sample were sealed with a 0.002 inch thick Mylar strip (see configuration "a" in Figure II-VI-18). The sample was subjected to 2, 15, and 2 psi compressive loads.

Sample Number 2022: The edges of the sample were sealed with a 0.002 inch thick Mylar strip. A glass fiber screen, 1/10 x 1/10 inch mesh and 0.003 inch thick was placed between the sample and the cold plate of the test apparatus to provide thermal resistance. (See configuration "c" in Figure II-VI-18.)

Sample Number 2024: The edges of the sample were sealed with a 0.002 inch thick Mylar strip. A glass fiber screen, 1/8 x 1/8 inch mesh

and 0.020 inch thick was placed between the sample and the cold plate of the test apparatus to provide thermal resistance. (See configuration "c" in Figure II-VI-18.) The sample was subjected to 2 and 15 psi compressive loads. Tests were also run with gaps of approximately 0.04 and 0.01 inch thickness between the sample and the cold plate.

The results of these tests appear in Table II-VI-6 and indicate the following:

1. There was little, if any, difference in edge heat leakage between the Mylar edge seal (2023) and the Mylar-aluminum-Mylar laminate (2021).
2. Opening of the sealed edges of the insulation sample (2021-I) to the evacuated surroundings had little effect on the thermal conductivity because of the low gas diffusion rate of closed-cell foams. The amount of gas contained in the sealed and unsealed samples was probably of the same order of magnitude.
3. Mechanically loading the insulation samples to 15 psi had a very small effect on the thermal conductivity, because this insulation possesses good strength and resists change in density.
4. Introducing a spacer between the sample and the cold plate (2022, 2024) decreased the thermal conductivity of the system by increasing the contact resistance at that boundary.

An evacuated 0.04-inch gap between the insulation sample and the cold plate decreased the thermal conductivity of the system by eliminating solid conduction completely at that boundary. The smaller gap (0.01) was also effective, but apparently there was some solid conduction through irregularities in the spacer.

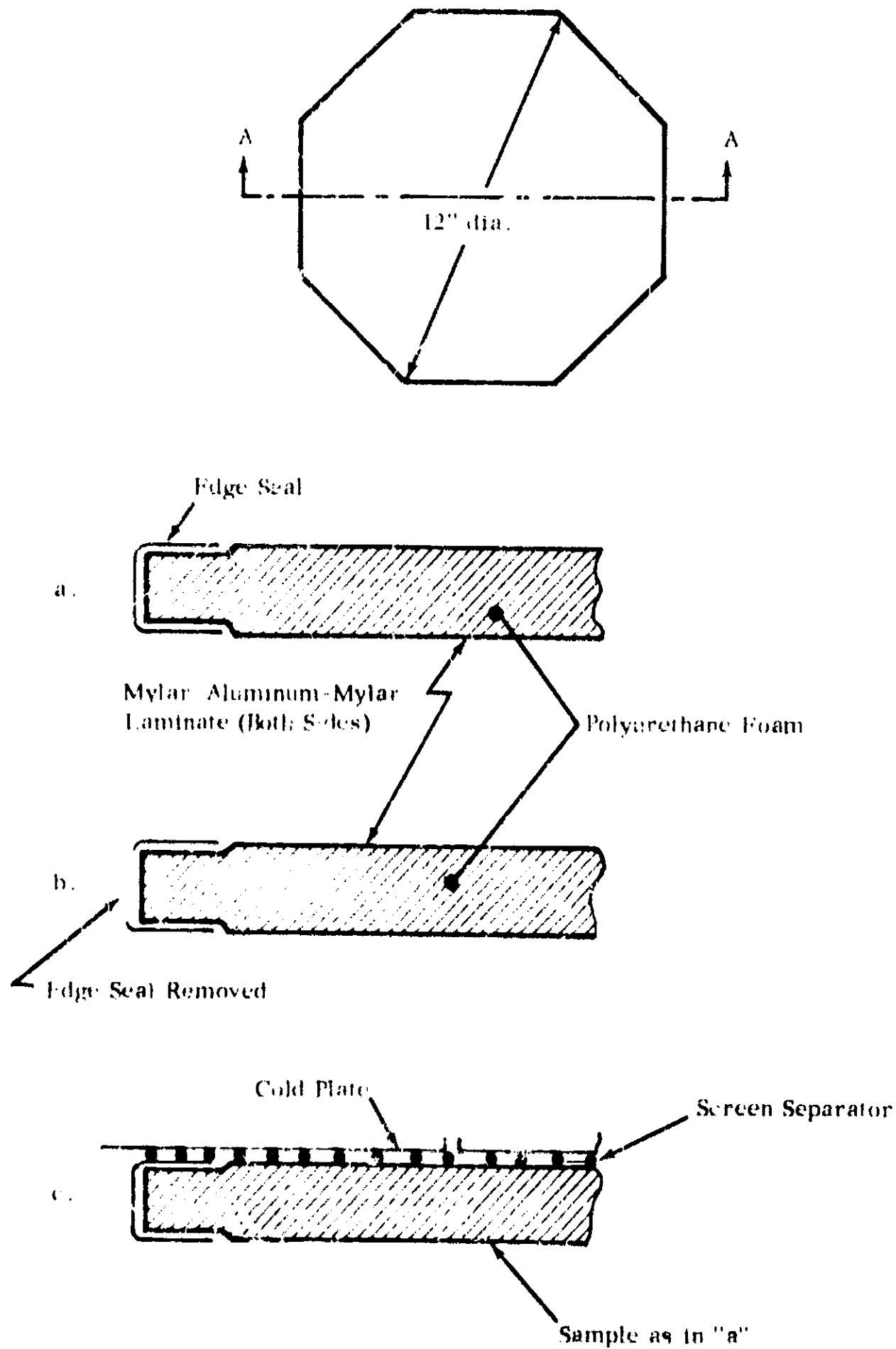


FIGURE II-VI-18 DIAGRAM OF POLYURETHANE FOAM SAMPLES

TABLE II-VI-6

RESULTS OF THERMAL CONDUCTIVITY TESTS ON A SAMPLE OF POLYURETHANE FOAM

Sample Description: The samples were octagonal panels of polyurethane foam, 12 inches across points, Freon blown, and approximately 0.4 inch thick. A laminate of 0.00075-inch Mylar, 0.001-inch aluminum and 0.00075-inch Mylar covered the surfaces of the sample.

Sample Density: Approximately 2 lb/ft³

Cold Plate Temperature: -423°F

Cold Plate Emissivity: 0.1

Warm Plate Emissivity: 0.3

Mechanical Load on Sample (psi)	Heat Flux Btu hr-ft ²	Thermal Conductivity Btu-in. hr-ft ² -F	Distance Between Plates (in.)	Warm Plate Temperature (F)	Sample Chamber Pressure	Test Number	Test Date
15	187	0.15 (1)	0.389	68	1 x 10 ⁻⁵	2021 d	7/30/63
2	175	0.14 (1)	0.396	68	1 x 10 ⁻⁵	2021 e	7/30/63
15	179	0.14 (2)	0.392	67	6 x 10 ⁻⁶	2021-1a	8/2/63
2	115	0.10 (3)	0.434	71	1 x 10 ⁻⁵	2022 a	8/7/63
15	160	0.14 (3)	0.422	72	1 x 10 ⁻⁵	2022 b	8/7, 8/63
2	134	0.12 (3)	0.435	72	1 x 10 ⁻⁵	2022 a	8/8/63
2	173	0.15 (4)	0.425	70	8 x 10 ⁻⁶	2023 a	8/10/63
15	170	0.14 (4)	0.416	71	8 x 10 ⁻⁶	2023 b	8/10/63
2	162	0.14 (4)	0.430	72	8 x 10 ⁻⁶	2023 c	8/11/63
2	118	0.11 (5)	0.440	70	1 x 10 ⁻⁵	2024 a	8/13/63
15	148	0.13 (5)	0.432	70	1 x 10 ⁻⁵	2024 b	8/13/63

TABLE II-VI-6 (Continued)

Mechanical Load on Sample (psi)	Heat Flux $\frac{\text{Btu}}{\text{hr-ft}^2}$	Thermal Con- ductivity $\frac{\text{Btu-in.}}{\text{hr-ft}^2-\text{F}}$	Distance Between Plates (in.)	Warm Plate Temperature (F)	Sample Chamber Pressure	Test Number	Test Date
0	15	0.015 (5)	0.484 (approx. 0.04 gap)	71	8×10^{-6}	2024 c	8/13/63
0	42	0.039 (5)	0.456 (approx. 0.01 gap)	72	7×10^{-6}	2024 d	8/13/63

Notes:

- 1) Edge of sample sealed with Mylar-aluminum-Mylar laminate (see Figure II-VI-18).
- 2) Edge of sample not sealed (see Figure II-VI-18).
- 3) Edge of sample sealed with Mylar only. Glass fiber screen separator, 1/10 x 1/10-inch mesh, inserted between sample and cold plate (see Figure II-VI-18).
- 4) Edge of sample sealed with Mylar only (see Figure II-VI-18).
- 5) Edge of sample sealed with Mylar only. Resin-coated glass fiber screen separator, 1/8 x 1/8-inch mesh, inserted between sample and cold plate (see Figure II-VI-18).

K. Microfiber Glass Wool

Tests were performed on a two-inch-thick microfiber glass wool insulation (sample U, Table II-IV-1). The purpose of this test was to determine the following:

1. The effectiveness of a Mylar disc seal at low temperature (see Figure II-VI-19).
2. A comparison of the observed thermal conductivities with those reported in the literature.
3. The temperature of the Mylar disc and temperatures within the sample at distances of 1/2 inch and 1 inch from the cold plate.

When we assembled the apparatus the Mylar disc appeared to be leaking slightly (detectable only with helium leak detector). We were able to keep a pressure of 1.5×10^{-4} torr in the vacuum jacket, while helium at one atmosphere was in the sample chamber. The leak was found to be due to helium diffusion through the Mylar. When we introduced liquid nitrogen into the guard vessel the pressure rose sharply in the vacuum jacket. Examination after completion of the test showed that the Mylar disc was ripped. Both thermocouples attached to the Mylar indicated a temperature 65°F above the boiling point of liquid nitrogen.

The Mylar disc was removed and the experiment repeated. The readings of thermocouples which were placed on top of the sample, 1/2 inch and 1 inch from the cold plate, were recorded. The thermocouple on top of the specimen indicated liquid nitrogen temperature. Figure II-VI-20 shows the mean apparent thermal conductivity plotted against the mean temperature, calculated from reading of the thermocouples;

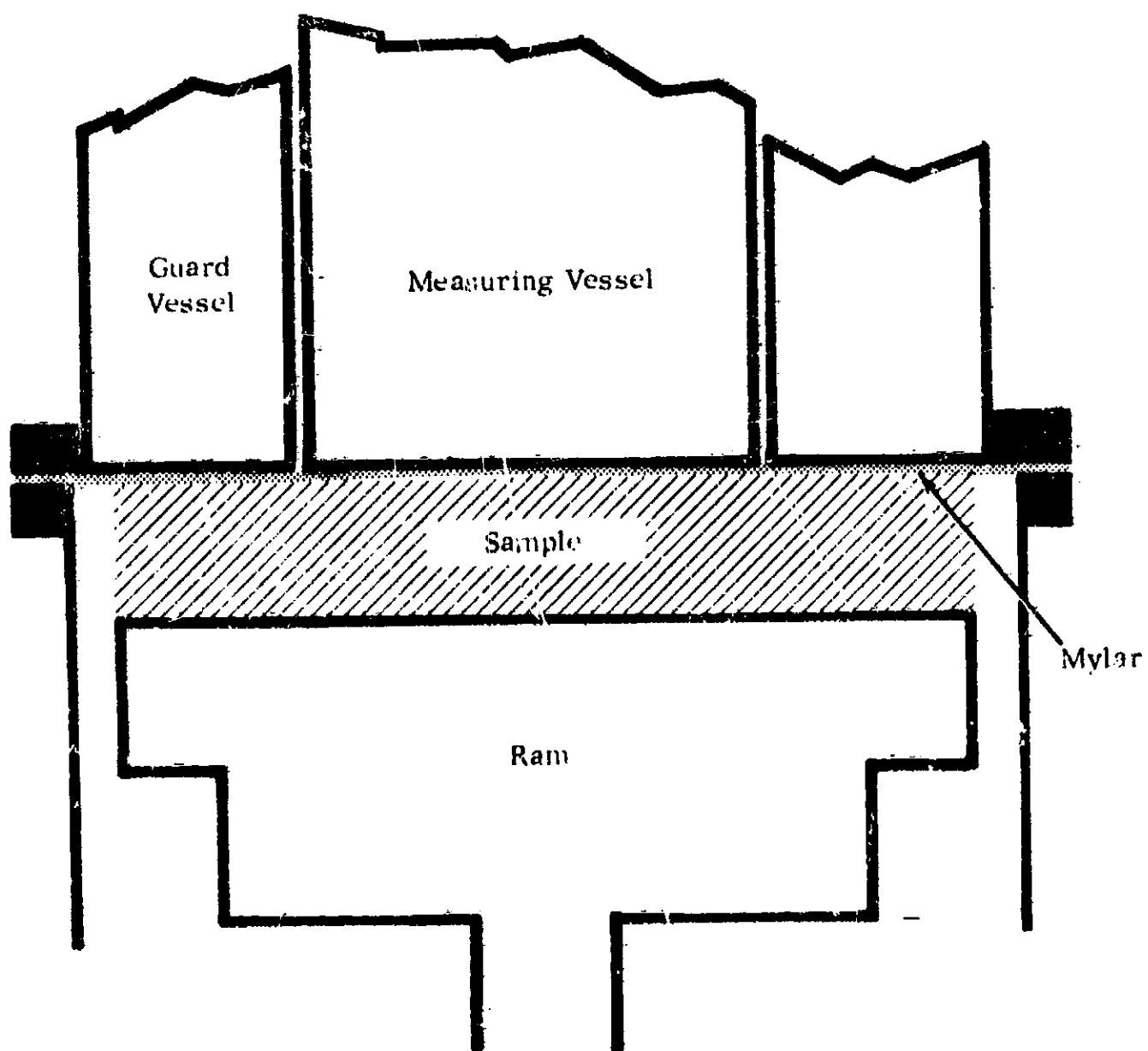


FIGURE II-VI-19 LOCATION OF MYLAR DISC

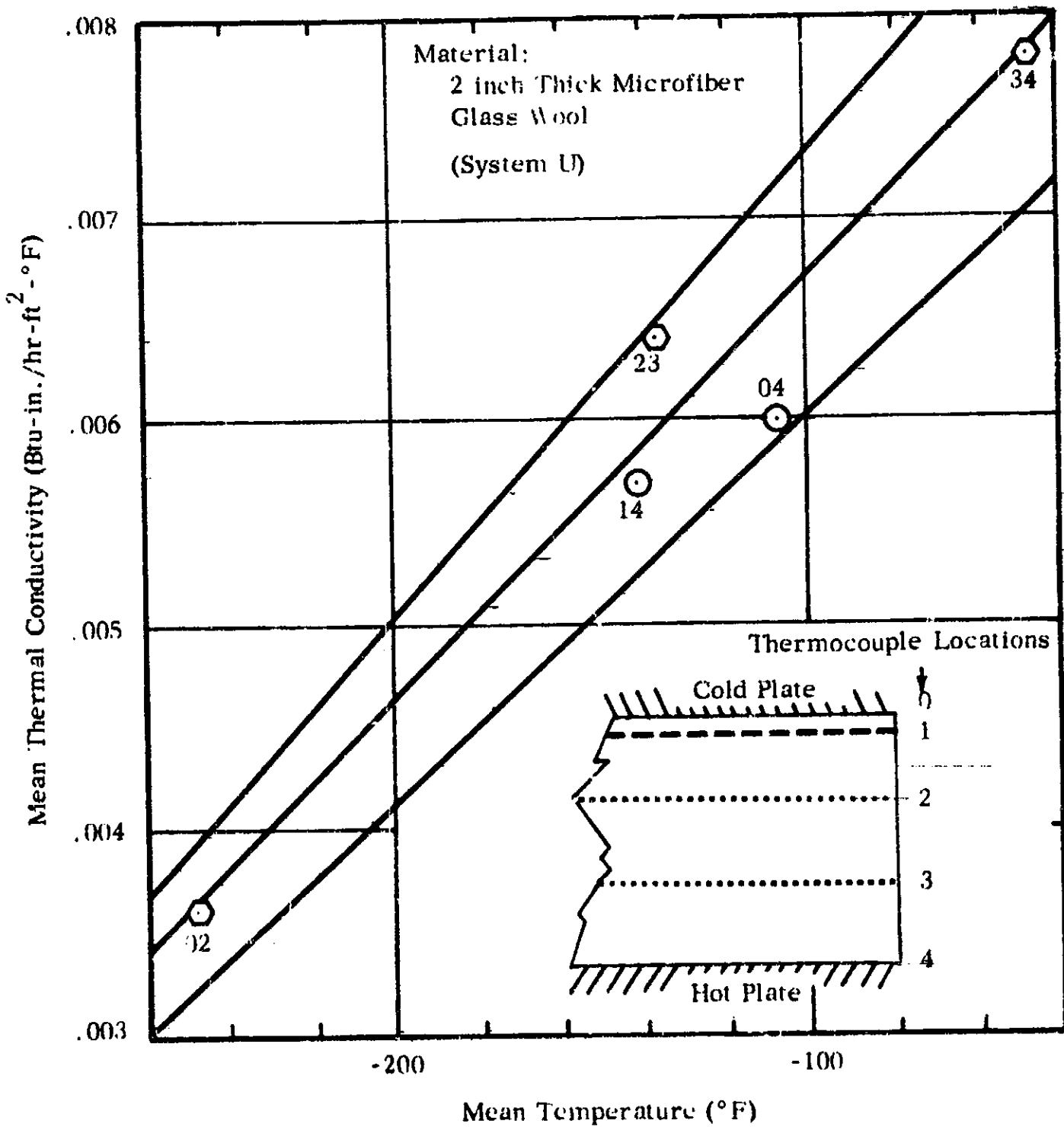


FIGURE II-VI-20

INFLUENCE OF T_{mean} OF SAMPLE ON MEAN
THERMAL CONDUCTIVITY

the points 14 and 04, which denote thermocouple locations, show values obtained from the two tests with and without the Mylar disc as calculated for the total temperature difference. The points scatter within 10% of the best straight line drawn through them. In Table II-VI-7 our results are compared with those published by Company C and show very good agreement. The difference in pressure during our tests and those reported by Company C should not be of particular concern, because at 11 microns (the pressure used in the Company C experiments) the air conduction is already negligible.

TABLE II-VI-7
THERMAL CONDUCTIVITY OF GLASS WOOL INSULATION
(SYSTEM U)

	Thermal Conductivity ($\frac{\text{Btu-in.}}{\text{hr-ft}^2\text{-F}}$)	Density (lb/ft ³)	Temperature - °F			Pressure (10 ⁻⁶ mm Hg)
			Warm Plate	Cold Plate	Avg.	
With Mylar Disc	6.0x10 ⁻⁵	2.2	42	-255	-107	20
Without Mylar Disc	5.7x10 ⁻³	2.2	41	-320	-140	7
Interpolated from Fig. II-VI-20	6.3x10 ⁻³	2.2	--	----	-122	--
Company C	6.1x10 ⁻³	4.0	75	-320	-122	11,000

L. Edge Effects

Tests were performed to measure the effects on the heat flux through multilayer insulations caused by changing 1) the edge configuration of the samples and 2) the conditions of the walls to which the sample edges were exposed.

1. Turned-Up Edges

Figure II-VI-21a shows the configuration of a sample of multilayer insulation (system C, Table II-VI-1) as it was installed and tested in the apparatus. All of the radiation shields were turned up and back over the sample and, consequently, the number of layers of material contained between the cold and warm plates at that location was doubled. The heat flux measured for this configuration was 0.62 Btu/hr-ft^2 . Another test was performed on a sample of the same insulation (system C), this time in the configuration shown in Figure II-VI-21b. Only the lowermost radiation shield was extended to cover the sample edge. The heat flux measured in this test was 0.40 Btu/hr-ft^2 , indicating that this method of edge shielding is more effective than the previous method for this insulation system in the thickness tested (0.74 inch). The high heat flux observed for the first method was apparently the result of compressing the sample at its edges.

2. Emissivity of Edge Boundaries

Tests were performed on samples of two multilayer insulation systems (A and C, Table II-IV-1) to determine the effects of changes in the emissivity of the surfaces at the edge boundaries of the sample on the heat flux through the system. The temperature of the surface to

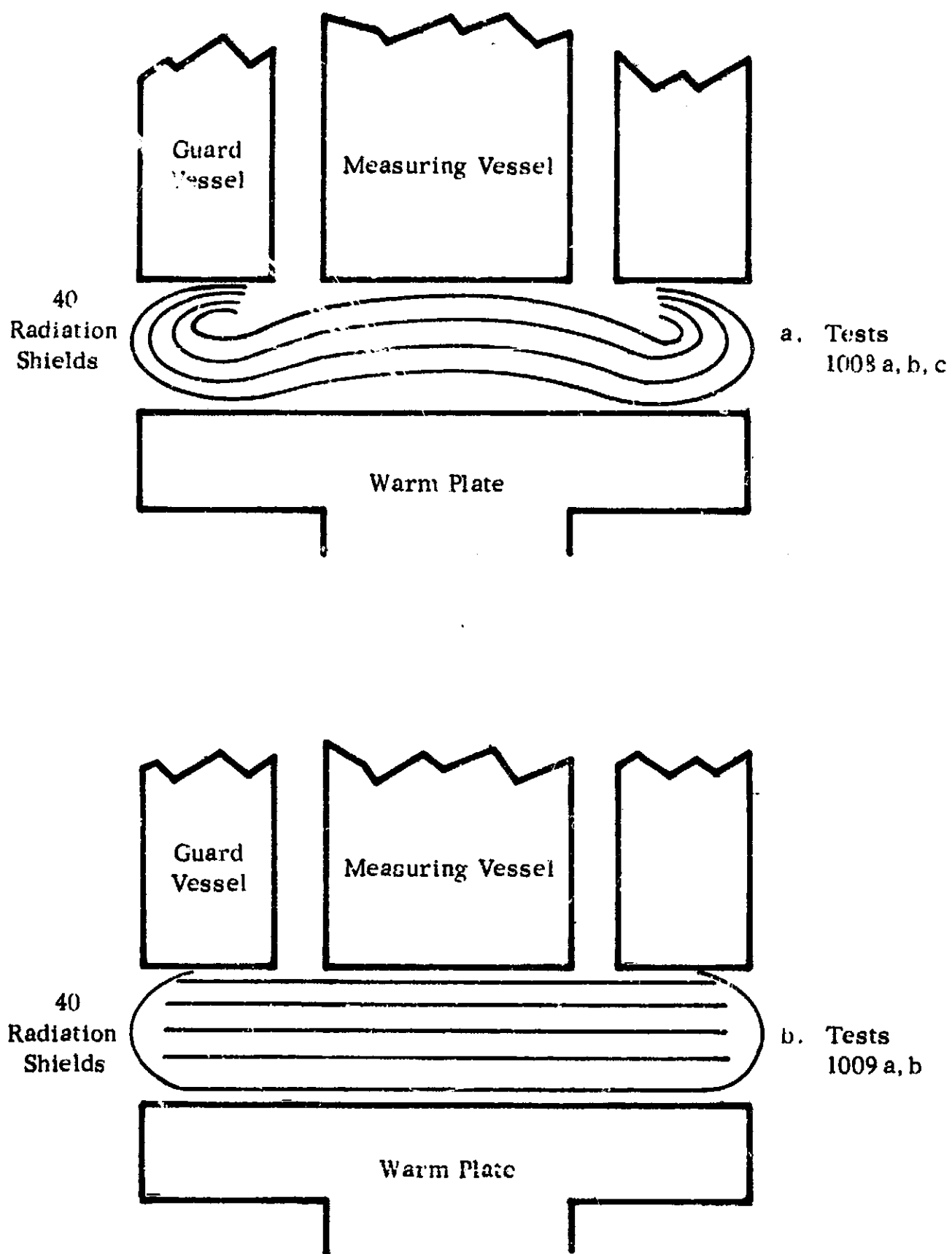


FIGURE II-VI-21 CONFIGURATION OF INSULATION
SAMPLE USING CRINKLED ALU-
MINIZED POLYESTER FILM,
SYSTEM C

which the edge of the sample was exposed was kept at -320°F while the emissivity of that surface was changed from bright stainless steel to black, obtained with an optical black paint. The results of these tests are given in Table II-VI-8.

The sample of system C, which contains aluminized crinkled polyester film, was very sensitive to these boundary emissivity changes when loosely packed (the heat flux differed by a factor of 2.8), but the sensitivity decreased as the packing became more dense. The sample of system A, which contains spacers $1/8$ inch larger in diameter than the radiation shields, was less sensitive to the edge boundary emissivity changes; the heat flux differed by a factor of only 1.3. The larger size of the spacers provided a buffer zone $1/16$ inch wide, similar to that described and treated theoretically in Section III.

The difference in the behavior of systems A and C tends to confirm that the overlapping of spacers provides an effective buffer zone around the insulation sample.

3. Effect of Edge Wall Temperature Variation

In another test of system A insulation, the sample was first tested at several plate separations until the minimum heat flux was determined. The side walls were bright stainless steel at -320°F during these tests. When the optimum thickness was determined, the test chamber was modified to present a 41°F black wall to the sample edges. This warm wall was a copper cylindrical shield which surrounded the sample and was attached to the warm plate. The temperature of the copper shield was measured

TABLE II-VI-8

EFFECTS OF EMISSIVITY OF EDGE BOUNDARIES

Hot Plate Temperature:	55°F	Cold Plate Temperature:	-320°F	
Hot Plate Emissivity:	0.2	Cold Plate Emissivity:	0.1	
Chamber Pressure:	Below 1 x 10 ⁻⁵ torr (air)			
Edge Wall Temperature:	-320°F			
Black Surface Emissivity:	0.95 Optical Black Paint			
Bright Surface Emissivity:	Bright Stainless Steel			
Sample	Thickness (in.)	Heat Flux ($\frac{\text{Btu}}{\text{hr-ft}^2}$)	Thermal Conductivity ($\frac{\text{Btu-in.}}{\text{hr-ft}^2-\text{°F}}$)	Edge
No. 3001 - 60 sheets of crinkled aluminized polyester film (compressed at different loads) System C	0.450 0.450 0.070 0.070	0.19 0.53 63.2 63.2	0.00023 0.00065 0.012 0.012	Black Bright Black Bright
No. 3002 - 10 sheets of H-19 tempered aluminum and 11 spacers of fiberglass mesh. System A	0.312 0.312	0.12 0.17	0.00010 0.00015	Black Bright

by a thermocouple installed at its upper edge (nearest to the cold plate). The inside surface of the shield was painted with optical black paint. When measured at these edge wall temperature extremes, the heat flux through the sample showed a difference of 6.3%. Table II-VI-9 gives the test results. The data indicate that, for the thickness tested, the effect of stray radiation at the sample edge was small and that the buffer zone provided an efficient shield.

4. Effects of Plate Separation

Tests were conducted to determine if the heat flux between warm and cold plates changes when the distance between the plates is varied. With no insulation in the sample chamber, heat flux measurements were made at six plate separations between 0.135 and 1.0 inch. The data did not show any definite tendency toward increasing or decreasing heat flux but showed a random scatter of $\pm 20\%$. This scatter appears to be the result of saturation temperature changes of the liquid caused by atmospheric pressure changes. The pressure control device described in Section II-V-B-3 was not designed at the time of these tests, and without that device errors of this magnitude were commonly observed. The results of the tests appear in Table II-VI-10. (Note: The heat flux measured was nearly one hundred times greater than that normally measured through a sample of multilayer insulation.)

5. Effects of Sample Edge Treatments

Tests were performed on a sample of multilayer insulation (system A, Table II-IV-1) to examine the influence of different edge treatments on the heat flux through the sample.

TABLE II-VI-9
EFFECT OF WALL TEMPERATURE

Sample Description:	(10) Tempered Aluminum (11) 1/8 x 1/8 Mesh Spacers
Cold Plate Temperature:	-320°F
Warm Plate Temperature:	+1°F
Sample Chamber Pressure:	$< 5 \times 10^{-5}$ torr
Sample Thickness:	0.273 inch

Edge Wall Temperature (°F)	Heat Flux ($\frac{\text{Btu}}{\text{hr-ft}^2}$)	Wall Emissivity
-320	0.32	Bright stainless steel
+41	0.34	Optical black paint

TABLE II-VI-10
EFFECT OF PLATE SEPARATION ON HEAT FLUX

Test Number: 1029
Date of Test: September 1962
Sample: None
Warm Plate Temperature: 69°F
Cold Plate Temperature: -320°F

Plate Separation (in)	Heat Flux ($\frac{\text{Btu}}{\text{hr-ft}^2}$)
0.135	17.0
0.200	16.8
0.250	21.1
0.370	21.5
0.850	23.6
1.000	14.9

Two strips of 0.00025-inch aluminized polyester film and a stiffening member of 0.003-inch polyester film were wrapped about the edge of the sample. The sample was tested first with the polyester film edge shield in contact with the warm surface only and secondly with the edge shield in contact with both the warm and the cold surfaces. For each condition, the sample was tested at two thicknesses to determine that optimum thickness was achieved. The samples tested contained a buffer zone 1/16-inch thick made of spacers extending beyond the radiation shields.

The results of these tests, which are given in Table II-VI-11, indicate that the precise location of the film has a critical influence on the heat flux and that an installation technique using this type of edge treatment gives unpredictable results; alternative edge treatments should be used or, preferably, construction with interleaved radiation shields which circumvent formation of an edge discontinuity.

Similar tests were performed on another sample of system A using the edge treatments shown in Figure II-VI-22. All of the samples shown therein contained a 1/16-inch wide buffer zone made by extending the spacers beyond the radiation shields.

In Figure II-VI-22b a black plate in good thermal contact with the -320°F guard vessel is placed around the edges, and an aluminized polyester film is wrapped around the sample.

In Figure II-VI-22c the same sample is wrapped with aluminized polyester film, and a horizontal copper ring is placed between the

TABLE II-VI-11 EFFECT OF SAMPLE EDGE TREATMENT

Sample Description: System A - 10 radiation shields of 0.002-in. H-19 tempered aluminum (Company B Alloy 9945) bright on two sides, and 11 spacers of 0.020-in. vinyl-coated glass fiber screen, grid dimensions 1.8 x 1.8 in. (Company C)

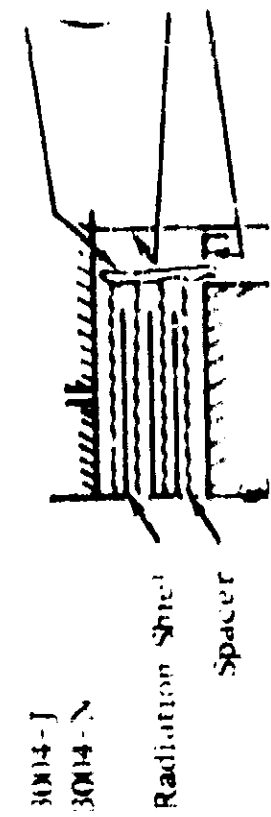
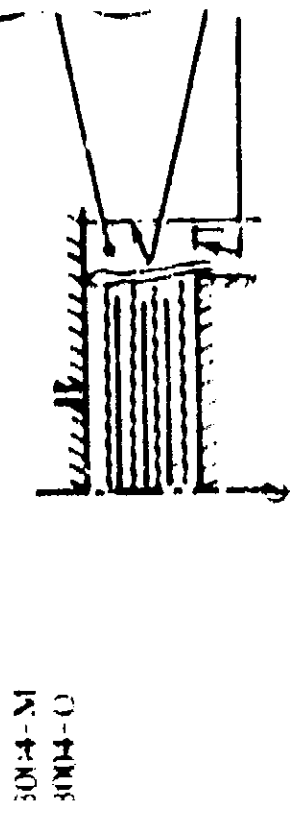
Warm Plate Temperature: 44°F

Warm Plate Emissivity: 0.1

Cold Plate Temperature: -120°F

Cold Plate Emissivity: 0.9

Sample Chamber Pressure: Below 1×10^{-5} torr

Test Number	Sample Edge	Heat Flux ($\text{Btu hr}^{-1} \text{ft}^{-2}$)	Thickness (in.)
3004-J		0.15	0.372
3004-N		0.17	0.422
3004-M		0.05	0.582
3004-O		0.13	0.402

LEGEND:

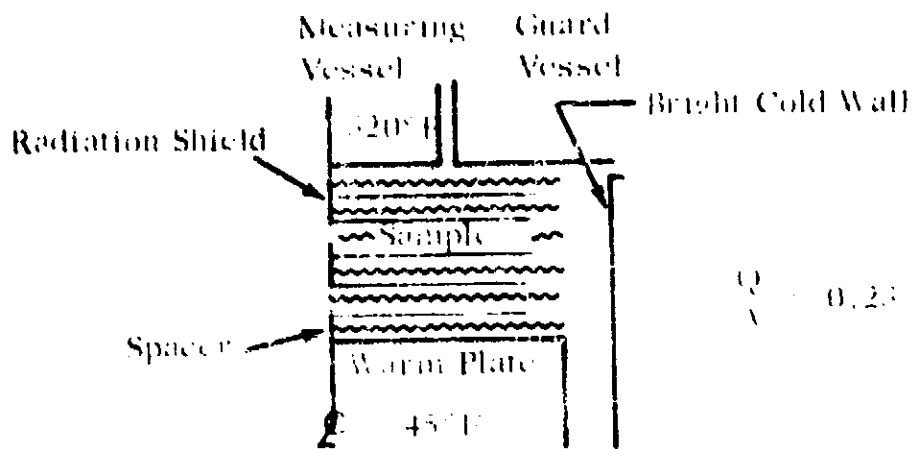
Sample Nos. 3007 & 3004

(10) Aluminum

(11) Glass Fiber Screen

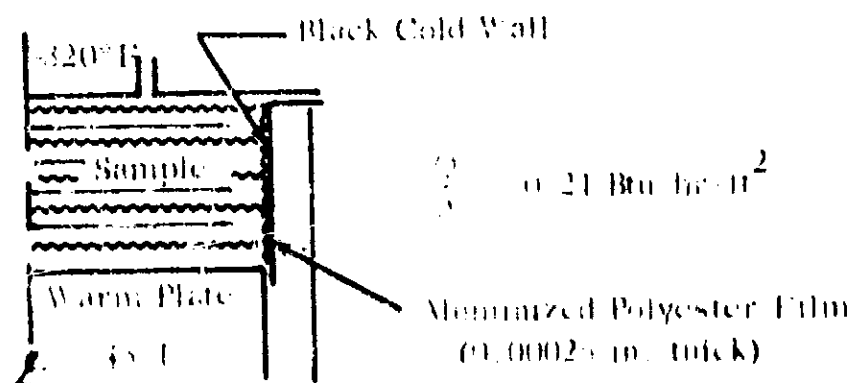
System A

Note: Applies to a, b, c, d



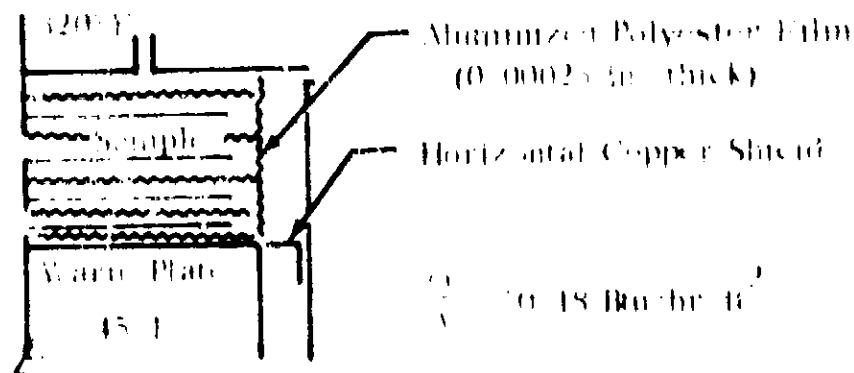
$$\frac{Q}{A} = 0.23 \text{ Btu/hr ft}^2$$

(a)



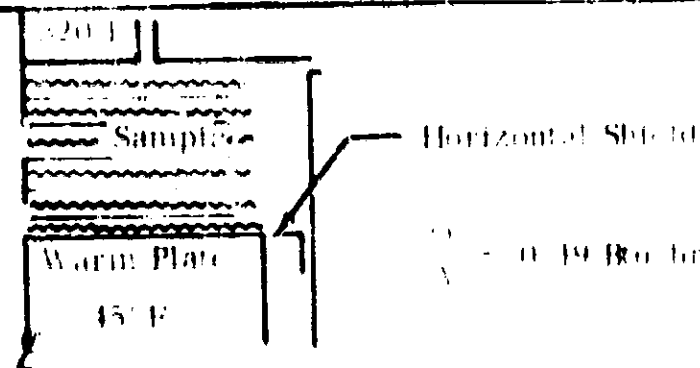
$$\frac{Q}{A} = 0.21 \text{ Btu/hr ft}^2$$

(b)



$$\frac{Q}{A} = 0.18 \text{ Btu/hr ft}^2$$

(c)



$$\frac{Q}{A} = 0.19 \text{ Btu/hr ft}^2$$

(d)

FIGURE II VI 22 EDGE TREATMENTS

warm plate and the sample chamber enclosure. The copper ring is fastened to the enclosure (which is at a temperature of about -320°F) in such a way that it does not touch the warm plate. The arrangement of Figure II-VI-22d is the same, except that the polyester film wrapping is removed.

The results of these edge treatments show: 1) that the presence of a buffer zone (see Section V-E) tends to reduce edge effects, 2) as in the previous tests, wrapping of aluminized polyester film gives unpredictable results, and 3) the horizontal copper ring is useful in preventing stray radiation from the warm parts of the apparatus from reaching the sample edges.

6. Effectiveness of Buffer Zone

The effectiveness of the buffer zone can be demonstrated using results obtained from tests on the effect of gaps in a multilayer insulation sample (see Section VI-F). The theoretical derivation of the effect of a gap of unit length on heat flux was derived in Equation II-III-38. For a slot of finite length, the additional heat input to a multilayer insulation can be written as:

$$\Delta Q = l d \sigma (T_1^4 - T_0^4) f\left(\frac{l}{d}\right) \quad (11-VI-6)$$

where l = length of the slot

The total heat flux passing through a sample is

$$Q = \frac{A \sigma (T_1^4 - T_0^4)}{\left(\frac{2}{\epsilon} - 1\right)u} + \frac{l}{4} d \sigma (T_1^4 - T_0^4) f\left(\frac{l}{d}\right)$$

where A = area of central guarded area

ϵ = emissivity of the foils

n = number of foils

The first term is the flux passing through a sample with no slot. The factor of $1/4$ in the second term allows for the fact that the flux ΔQ , due to the slot, is distributed over the whole 12-inch-diameter area of the sample, which is four times that of the 6-inch-diameter measuring area.

The flux per unit area is

$$q = q_0 \left[1 + \frac{1}{4} \left(\frac{\ell d}{A} \right) \left(\frac{2}{\epsilon} - 1 \right) n f \left(\frac{\delta}{d} \right) \right]$$

where q_0 is the flux density when $\delta = 0$, i.e., with no slot.

To compare this theoretical expression with experimental results, we use the heat flux of 0.27 Btu/hr-ft^2 for q_0 (see Figure 11-VI-15) rather than a computed value, to allow for the effect of thermal conduction through the spacers. The other constants are:

$\ell = 6 \text{ in.}$

$d = 0.35 \text{ in.}$

$A = 28 \text{ in.}^2$

$n = 10$

$\epsilon = 0.033$ (assumed)

Figure 11-VI-23 shows that the theoretical curve for q/a versus the slot width δ agrees very well with the experimental data. The

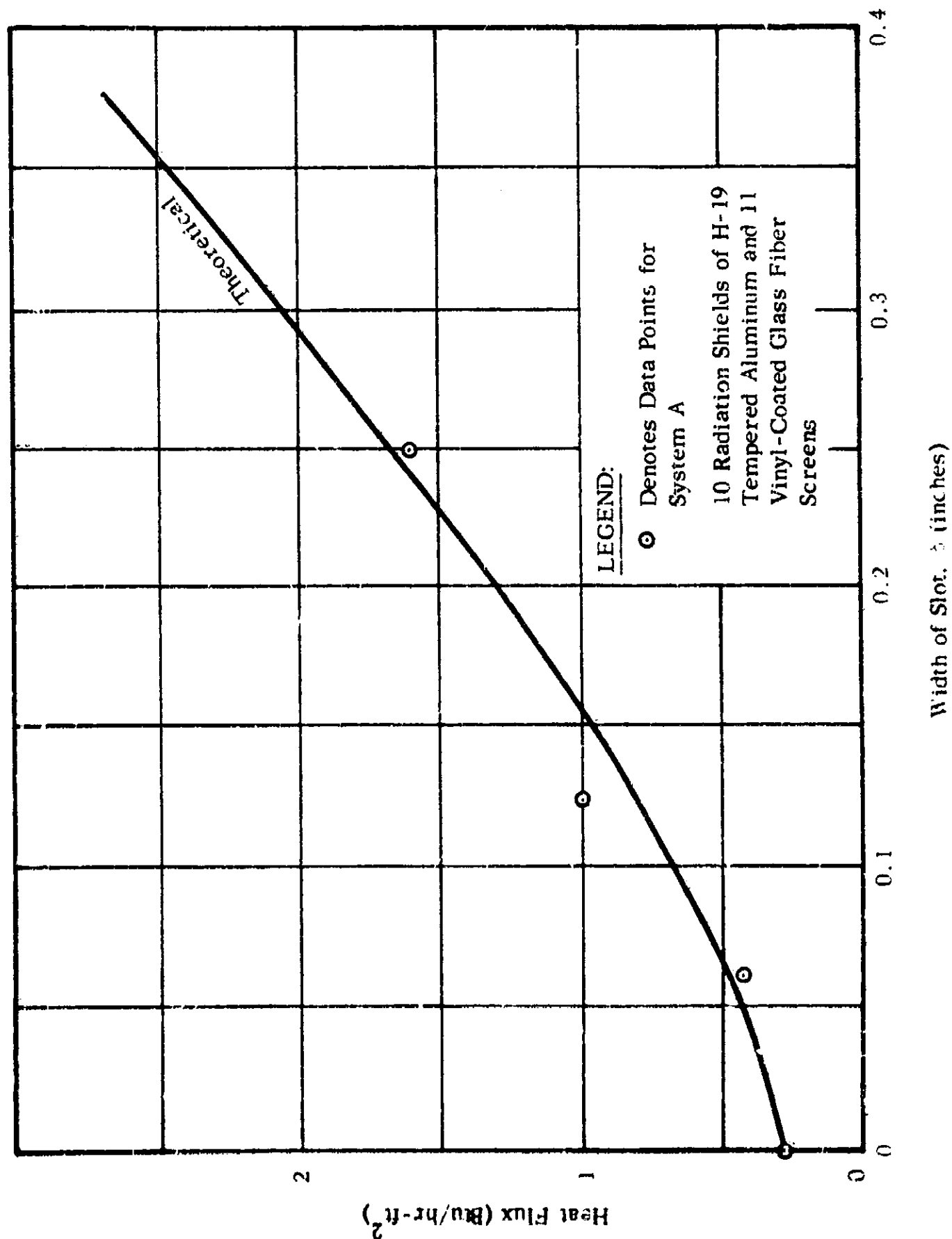


FIGURE II-VI-23 EFFECT OF SLOT WIDTH ON HEAT FLUX THROUGH A MULTILAYER INSULATION

agreement not only confirms the theory of the effect of the slot but also shows that the exposed edge of the 12-inch sample is well enough buffered to act as a no-flux surface. Otherwise, the factor of $1/4$ used in the theory to calculate the fraction of the heat flux, due to the slot, that enters the 6-inch central guarded area would not be correct.

7. Conclusions

The tests conducted for the purpose of measuring the effect of edge conditions on the heat flux through multilayer insulations, as described in the six previous portions of this section, indicate the following:

a. Shielding the exposed edges of a multilayer insulation by rolling the edges of the radiation shields toward the cold wall (Figure II-VI-21a) degraded the insulating effectiveness, possibly because the system became compressed in that region. Rolling only the bottom (warm) shield toward the cold wall appeared to produce better shielding of the edges of a loosely packed sample of insulation system C.

b. Shielding the exposed edges of a multilayer insulation by wrapping the edges with aluminized polyester film (Table II-VI-11 and Figure II-VI-22) gave unpredictable results and thereby indicated that an alternate method of edge treatment should be used.

c. The distance between the warm and cold plates of the apparatus apparently had no effect on the heat flux between the plates.

d. A horizontal copper ring placed approximately level with the warm plate (Figure II-VI-22) reduced the amount of stray radiation that reached the sample edges from the warm parts of the apparatus.

e. When the spacers were extended 1/16 inch beyond the edges of the radiation shields in samples of system A (Table II-IV-1), an effective buffer zone was formed. This reduced the influence of temperature and emissivity variation at the edges of 12-inch diameter samples on the heat flux through the insulation.

f. The buffer zone formed by the 1/16-inch-wide ring of spacer material at the edge of the samples acted as a no-flux surface for the thickness tested. This conclusion is indicated by the agreement between experimental data and theoretical predictions for tests of slotted samples of such insulation systems.

M. Spacer Material with 11% Support Area

Thermal conductivity measurements were made on two insulation systems which consisted of spacers arranged so as to produce only 11% support area. The samples (systems L and M, Table II-IV-1) contained slotted spacers of the configuration shown in Figure II-VI-24. Each spacer was arranged so that its slots were displaced 90 degrees from those of its neighboring spacer; this formed a pattern of 1/2-inch-square areas of continuous contacts across the insulation systems corresponding to 11% of the total sample area.

Several measurements were made in an attempt to determine the optimum density of these samples; however, the point was not found for

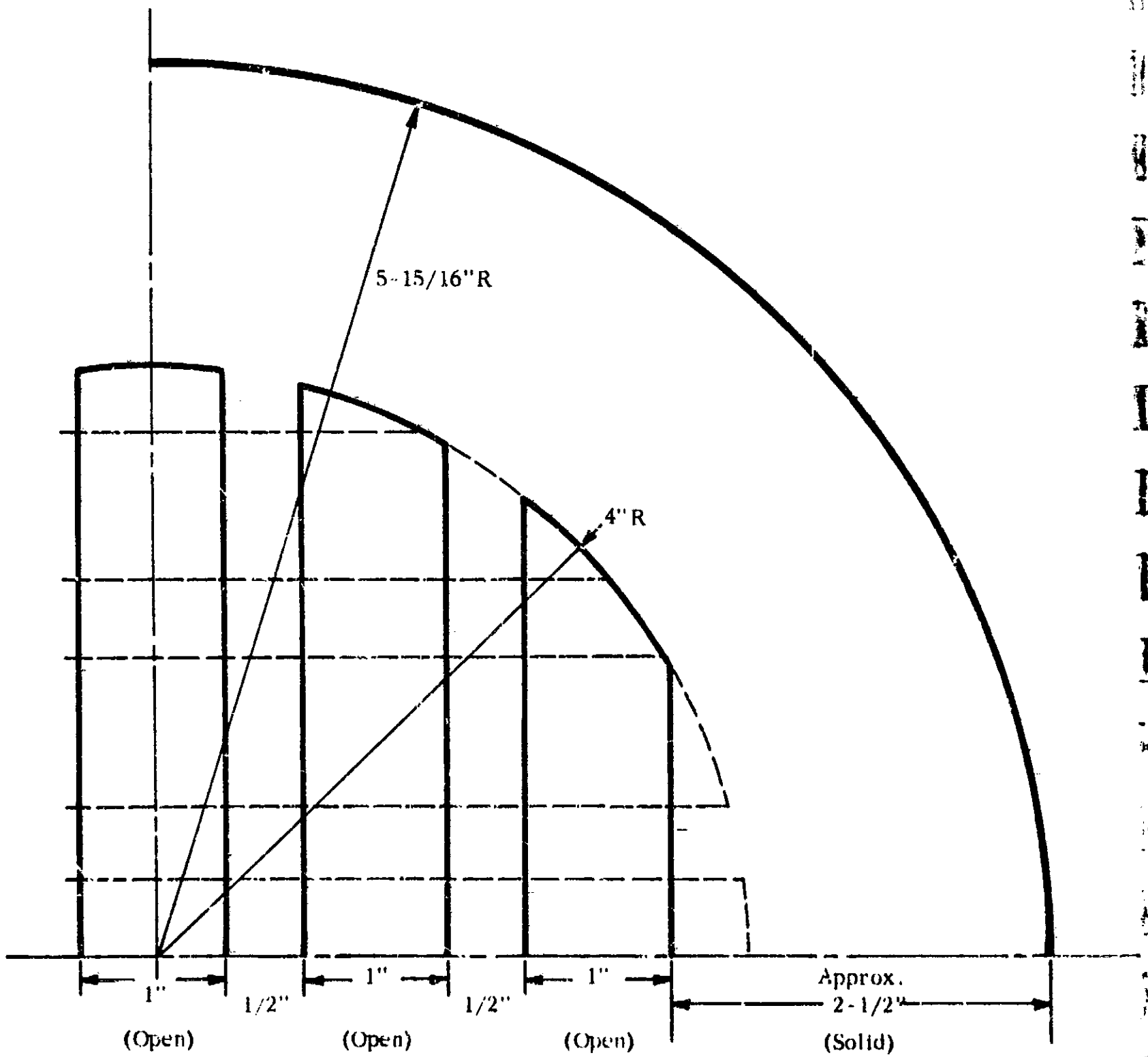


FIGURE II-VI-24

CONFIGURATION OF SPACER USED IN SAMPLE OF 11% SUPPORT
AREA SYSTEMS L & M

either sample, possibly because of distortion of the spacers or because of radiation losses at the large area of exposure at the sample edge to the cold side wall of the test chamber.

These samples were also tested under compressive loads of up to 8 psi. Their thermal conductivity appears to be less sensitive to loading than any of the other insulation system that we have tested. The data obtained from these tests is given in Table II-VI-12.

N. Comparison of Two Radiation Shield Materials

Samples of two multilayer insulation systems were tested to determine the effect of emissivity of the radiation shields on thermal conductivity. The number of radiation shields and spacers was the same for both samples. The shield material was in one case polyester film, aluminized on one side (system C, Table II-IV-1) and in the other aluminum foil (system A). The spacers in both cases were vinyl-coated fiberglass mesh. The heat flux through the sample containing aluminized polyester film was approximately 2.5 times greater than that through the sample containing aluminum foil. This difference may be due to the fact that the polyester film is bright on one side only and has greater solid conduction at the spacer contact areas. The results of these tests appear in Table II-VI-13.

O. Combination of Multilayer and Foam

A sample consisting of 3/4-inch thick fiberglass-reinforced polyurethane foam and a multilayer insulation (system V in Table II-IV-1) was tested. The foam rested on the multilayer insulation. The heat

TABLE II-VI-12

RESULTS OF TESTS ON A SPACER MATERIAL SUPPLIED BY CTL

Sample Description: Six radiation shields (of 0.00025-inch smooth polyester film for sample no. 3027 and of 0.002-inch aluminum alloy 9945-H19 for sample no. 3028) and seven spacers of material with 112 support area. (System 30)

Cold Plate Temperature: -320°F

Cold Plate Emissivity: 0.9

Warm Plate Emissivity: 0.9

Sample Chamber Pressure: Less than 5×10^{-5} torr

Sample Thickness (in.)	Heat Flux ($\frac{\text{Btu}}{\text{hr-ft}^2}$)	Thermal Conductivity ($\frac{\text{Btu-in}}{\text{hr-ft}^2-\text{F}}$)	Mechanical Load Supported by Spacer Material (psi)	Warm Plate Temperature ($^{\circ}\text{F}$)	Test Number	Test Date
0.800	0.50	0.0019	*	71	3027 a	9/5/63
0.746	0.58	0.0013	*	69	3027 b	9/10/63
0.775	0.59	0.0012	*	69	3027 c	9/12/63
0.543	1.12	0.0016	1.5	69	3027 d	9/13/63
0.443	1.30	0.0015	5	69	3027 e	9/14/63
0.400	1.64	0.0017	8	69	3027 f	9/16/63
0.798	0.34	0.00075	*	66	3028 g	9/17/63
0.851	0.31	0.00068	*	66	3028 h	9/18/63
0.750	0.81	0.0015	*	56	3028 a	9/20/63
0.800	0.38	0.00080	*	66	3028 b	9/23/63
0.854	0.14	0.00053	*	65	3028 c	9/24/63
0.402	1.6	0.0017	8	64	3028 d	9/25/63

* Not measurable.

TABLE II-VI-13
COMPARISON OF TWO RADIATION SHIELD MATERIALS

Boundary Temperatures: $68 \pm 2^\circ \text{F}$ and -320°F
Test Chamber Pressure: Less than 1×10^{-5} torr

Plate Separation (in.)	Heat Flux ($\frac{\text{Btu}}{\text{hr-ft}^2}$)	Thermal Conductivity ($\frac{\text{Btu-in.}}{\text{hr-ft}^2-\text{F}}$)	Sample Description	Sample Density (lb/ft ³)	Thermal Conductivity Times Density ($\frac{\text{Btu-in.}}{\text{hr-ft}^2-\text{F}} \times \frac{\text{lb}}{\text{ft}^3}$)	Sample Number
0.383	0.36	0.00035	(a)	13.8	0.0050	1022 a
0.293	0.38	0.00028	(a)	18.0 (c)	0.0050	1022 b
0.530	0.71	0.00097	(b)	4.7	0.0046	1023 a
0.27 ^a	1.26	0.00091	(b)	9.1	0.0083	1023 b
0.300	0.93	0.00072	(b)	8.4	0.0061	1023 c
0.527	0.62	0.00085	(b)	4.8 (c)	0.0041	1023 d

(a) Ten radiation shields of 0.002-inch H-19 tempered aluminum and eleven spacers of 0.020-inch vinyl-coated fiberglass mesh, size 1/8 x 1/8 inch.

(b) Ten radiation shields of 0.00025-inch crinkled polyester film aluminized on one side and eleven spacers of 0.020-inch vinyl-coated fiberglass mesh, size 1/8 x 1/8 inch.

(c) Optimum density.

flux through this insulation system was twice that previously measured for the multilayer insulation alone. The test was repeated, this time with the foam suspended from the cold plate so as to prevent compression of the multilayer. The resulting heat flux, although less than in the first test, was still higher than for the multilayer insulation alone. This behavior may have been caused by outgassing of the foam or increased edge effects on the composite system caused by the position of the multilayer insulation.

P. Penetrations

Tests were performed to measure the effects of penetrations in a multilayer insulation on thermal conductivity. The sample tested was system A (Table II-IV-1). A hole was punched in the center of each radiation shield and a pin whose diameter was within ± 0.003 inch of the hole size was inserted through the holes. The pin was threaded so that it could be screwed into a mating hole in the center of the cold plate. The pin was not in contact with the warm plate but was exposed to radiation from the warm plate. A diagram of the arrangement of the sample and pin is shown in Figure II-VI-25. Three pins were tested--1/16 and 1/8-inch diameter made of 300 series stainless steel, and 1/8-inch diameter made of nylon. The results of these tests appear in Table II-VI-14. The sample thickness shown in that table is the optimum thickness found for each sample. There is a greater than normal variation in this thickness between each sample, which may have been caused by inserting the pins and pushing the radiation shields together. This test series is still in progress and no conclusions can be reached at this time.

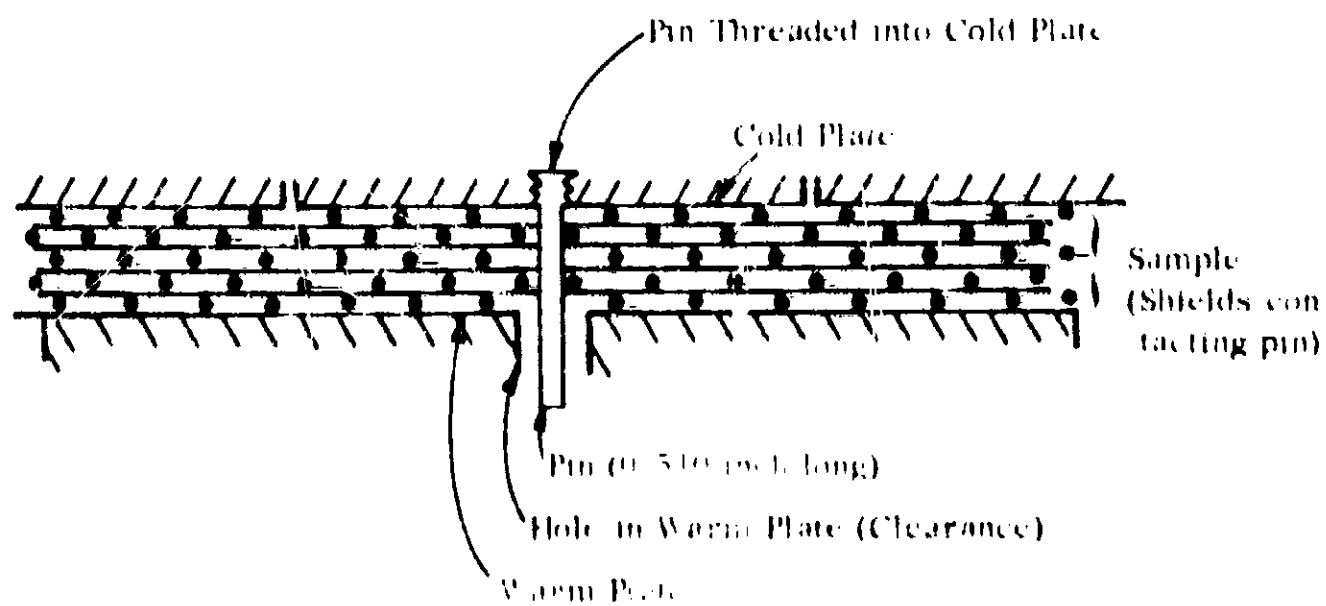


FIGURE II VI 25 SCHEMATIC DIAGRAM OF ARRANGEMENT OF SAMPLE AND PIN FOR PENETRATION TEST

TABLE II-VI-14

EFFECT OF A PENETRATION IN A SAMPLE OF MULTILAYER INSULATION

Sample Description: Ten H-13 tempered aluminum radiation shields 0.002 inch thick and eleven vinyl-coated glass fiber screens 1/8 x 1/8 inch mesh and 0.020 inch thick.

Sample Chamber Pressure: Less than 2×10^{-5} torr.

Warm Plate Emissivity: 0.3

Cold Plate Temperature: -320°F

Cold Plate Emissivity: 0.9

Diameter of Pin (in.)	Material of Pin	Heat Flux ($\frac{\text{Btu}}{\text{hr-ft}^2}$)	Sample Thickness (in.)	Warm Plate Temperature	Test Number	Test Date
1/16	Stainless Steel	1.3	0.326	72	3019	7/11/63
1/8	Stainless Steel	1.9	0.375	72	3026	8/21/63
1/8	Nylon	0.84	0.351	72	3026 I	8/27/63
no pin	no pin	0.20	0.348	54	2014	5/15/63

II-16A

VII. ABSTRACTS OF PREVIOUSLY ISSUED REPORTS

The major portion of our analytical studies on thermal protection systems were accomplished in the early phases of the program and are reported as abstracts as well as reviewed herein.

ADL Report #63270-04-01

ASTIA No. AD 256-894

Date: April 1961

OTS \$1.10

Title: Gas Conduction Problem with Multilayered Radiation Shields

Author: A. G. Emalie

Abstract:

On a long mission in space, a cryogenic fuel tank may require radiation shielding consisting of 100 sheets of low-emissivity metal foil if heat is transferred through the shielding only by radiation. If gas conduction also occurs, more foils will be needed for the same rate of fuel boil-off. For a gas pressure of 1.4×10^{-4} mm Hg, 200 foils are required. Consequently, an adequate sealed-off, evacuated shield is difficult to construct. If outgassing of the foils and gas diffusion from the fuel tank are appreciable, it is also difficult to arrange the geometry of the shields to use the external space vacuum for pumping. In the case of pumping through the edges of a 100-cm wide shield panel, the outgassing rate should not exceed about 10^9 molecules sec^{-1} from each cm^2 of foil surface, if the number of foils is to remain about 100. The allowable outgassing rate for broadside pumping of optimally perforated foils is around 10^{10} molecules $\text{sec}^{-1} \text{cm}^{-2}$. The allowable diffusion rate from the fuel tank is 10^{12} molecules $\text{sec}^{-1} \text{cm}^{-2}$ of tank surface. A basic consideration is that any geometrical arrangement of the foils that enhances pumping of the gas also reduces the effectiveness of the foils as

a radiation shield, since radiation can enter by the same path by which molecules leave. As a result, only a limited number of layers of foil is useful. Beyond this number, no further improvement in shielding is gained.

ADL Report #6327C-04-02

ASTIA No. AD 257-466

Date: May 1961

OTS \$2.60

Title: Radiation Transfer by Closely Spaced Shields

Author: A. G. Emslie

Abstract:

The usual formula for radiation transfer through a stack of radiation shields breaks down when the spacing of the shields is less than the wavelength of the peak of the blackbody spectral distribution corresponding to the temperature of the shields. Two effects set in at these close spacings--wave interference and radiation tunneling. Wave interference of the emitted radiation occurs in the narrow gaps between the shields and may increase or decrease the energy transfer, depending on the spacing. Radiation tunneling allows transfer of radiation that ordinarily suffers total internal reflection inside the shield material. This effect gives an energy transfer that increases exponentially as the spacing decreases. The two effects together give an energy transfer rate per unit area which becomes, in the limit of zero spacing,

$$q = \frac{n^4}{n^2 + k^2} (\sigma T_2^4 - T_1^4)$$

where n and k are the real and imaginary parts of the complex refractive index, σ is the Stefan-Boltzmann constant, and T_2 and T_1 are the

temperatures on the two sides of a gap.

The formula implies that the radiation density e' and velocity of propagation c' in the shield material are:

$$e' = \frac{n^2 \sigma T^4}{c}$$

$$c' = \frac{n^2 c}{n^2 + k^2}$$

For moderate values of the absorption index k , the flux formula predicts a transfer rate between two close shields greater than that between two black surfaces.

In the case of metal shields, when the spacing between the two shields is increased from zero, the radiation transfer rate at first rises sharply to a high maximum and then falls below the usual value for widely spaced shields. The flux returns to the normal level when the spacing exceeds about one half of the wavelength of the blackbody peak.

ADL Report #63270-04-03

ASTIA No. AD 270-973

Date: December 1961

OTS \$6.60

Title: An Analysis of Thermal Protection Systems for Propellant
Storage During Space Missions

Authors: John Ehrenfeld and Peter Strong

Abstract:

This report presents an analytic study of thermal protection systems for propellant storage during space missions. The effects of various models for insulation behavior are investigated. Approximate methods for calculating burn-off and their limitations are developed, as well as

optimum design parameters based on these techniques. A number of general practices leading to good design are discussed.

ADL Report #63270-04-04

Office of Scientific and Technical
Information

Date: April 1962

NASA

Title: Radiative Heat Transfer Through Seams and Penetrations in
Panels of Multilayer Metal-Foil Insulation

Author: A. G. Emslie

Abstract:

The report is a theoretical analysis of some aspects of the feasibility of insulating a storage tank containing cryogenic fuel by means of prefabricated panels of multilayer metal-foil insulation, in view of the extra heat leakage into the tank at seams and penetrations. The difficulty arises because the very high thermal conductivity in the plane of the panels prevents overlapping or caulking of the joints. Thus, gaps must be left between adjacent panels and around penetrating pipes and struts. The extra heat input due to the gaps is calculated. In order that this heat input be no larger than 10% of the total input to a 10 ft x 10 ft cylindrical tank, the gap at the seam would have to be less than 0.02 inch. Since this is impractically small, we conclude that multilayer metal foils cannot be applied to a tank in the form of prefabricated panels. Other methods, such as filament-winding or layer-by-layer application of the foil, must be used instead.

The calculated effect of a penetration is not so serious. For example, a venting tube of diameter 1 inch causes a 5% increase in radiative heat input to the 10 ft x 10 ft tank.

ADL Report #63270-11-01

Office of Scientific and Technical
Information

Date: May 1962

NASA

Title: Estimation of Weight Penalties Associated with Alternate
Methods for Storing Cryogenic Propellants in Space

Author: Arthur A. Fowle

Abstract:

This report presents an evaluation and a comparison of the weight penalties associated with alternate methods for preserving cryogenic propellants stored in space. Storage in a vented vessel, storage in a nonvented vessel, and the use of close-cycle refrigerators are considered. Approximate methods are presented whereby the storage system giving the least weight penalty can be identified for any mission in which the stored amount and stay time in space is specified. Illustrative examples involving the space storage of liquid hydrogen are carried out.

ADL Report #63270-11-02

Office of Scientific and Technical
Information

Date: May 1962

NASA

Title: Conceptual Design Study of Space-Borne Liquid Hydrogen Re-
condensers for 10 and 100 Watts Capacity

Author: Raymond W. Moore, Jr.

Abstract:

Conceptual designs of refrigerators for recondensing hydrogen at 20°K , with capacities of 10 and 100 watts, have been evolved to assess the feasibility of making such units and to provide a basis for specific weight estimates. The designs are based on the use of a helium gas refrigerator cycle. The heart of both systems is a combined rotary unit

(CRU) consisting of a compressor, turboexpander, and electric-motor drive operating at a high shaft rotational speed on gas bearings. The feasibility of using such a system depends on the successful developments of the CRU. The designs projected show specific weights of 20.5 and 10.0 pounds/watt at 20°K for the 10-watt and 100-watt units, respectively.

ADL Report #63270-04-05

Office of Scientific and Technical
Information

Date: June 1962

NASA

Title: Techniques for Computing the Thermal Radiation Incident on
Vehicles in Space

Author: Jacques M. Bonneville

Abstract:

This report presents techniques for calculating the thermal radiation incident on vehicles in space. The surface of a vehicle is subdivided into a finite number of parts of sufficient flatness to ensure the accuracy of the ensuing thermal calculation. Then, methods are presented for computing radiation arriving at each vehicle part from the sun, planet, and moon for various vehicle orbits and for various modes of vehicle orientation stabilization. A method is presented to account for the shadowing of one vehicle part by another.

ADL Report #63270-13-01

Office of Scientific and Technical
Information

Date: September 1962

NASA

Title: A Guide to the Computation of Heat Flow in Insulated Cryogenic
Storage Vessels in the Space Environment

Authors: Jacques Bonneville and Frank Gabron

Abstract:

A guide for analyzing and computing heat flows in insulated cryogenic storage vessels in the space environment is presented. Means for calculating the incident heat fluxes from environmental sources are described qualitatively and detailed procedures are included by references. A finite difference technique for obtaining temperature distributions and heat fluxes in an insulated system having thermal properties which are anisotropic but independent of temperature is given. The results of machine computations of the temperature distributions and heat flows in model insulated liquid hydrogen storage vessels illustrate the application of this technique.

ADL Report #65008-03-01

Office of Scientific and Technical
Information

Date: April 1963

NASA

Title: Design of Thermal Protection Systems for Liquid Hydrogen Tanks

Prepared under Contract Number NAS5-664, NASw-615

Abstract:

An account of the progress achieved in the design, experimental measurement and analysis of thermal protection systems for liquid hydrogen tanks is given in this report. The objectives of the work are: (1) to provide data to guide the design of efficient thermal protection systems for cryogenic fuel tanks for use in extended space missions with primary emphasis placed on multilayer insulations for liquid hydrogen tanks; (2) to establish design parameters adequate to meet production requirements, preflight check-out, and mission objectives to assure highest insulating effectiveness; and (3) to measure the thermal

within the present state of the art.

II-176

Arthur D. Little, Inc.

PART III

THE INSULATED-TANK PROGRAM

TABLE OF CONTENTS

	<u>Page</u>
List of Figures	III-1
List of Tables	III-11
I. Summary	III-1
II. Approach	III-4
III. Experimental Equipment	III-5
IV. Experimental Results	III-30
V. Conclusions	III-55

LIST OF FIGURES

<u>Figure No.</u>	<u>Subtitle</u>	<u>Page</u>
1	Calorimeter Tank	III-7
2	Calorimeter Copper Tank Details	III-8
3	Chamber and Calorimeter Assembly	III-9
4	Aluminum Foil Insulation - Details	III-14
5a & b	Aluminum Foil System - Spacer Netting	III-16
6a & b	Aluminum Foil System - No. 4 Al. Foil and No. 5 Spacer Netting	III-17
7a & b	Aluminized Polyester Film - No. 5 Foil and No. 6 Spacer Netting	III-19
8	Test Insulation Edge Guard	III-21
9	Insulation System, Thermocouple Locations	III-22
10	Thermocouple Lead Wires - Exit of Insulation System	III-24
11	Flow Schematic	III-27
12	Dummy Tank and Mounting Fixture	III-31
13	Shipping Container	III-32
14	Heat Flux vs. Guard Temperature Test 1 Data	III-40
15	Al-System, Radiation Shield Time - Temperature Distribution	III-47
16	Al-Mylar System Radiation Shield Time - Temperature Distribution	III-48
17	Al-System, Temperature Distribution	III-50
18	Al-Mylar System, Temperature Distribution	III-51
19	Residual Gas Heat Transfer	III-54

LIST OF TABLES

<u>Table No.</u>	<u>Title</u>	<u>Page</u>
I	Aluminum Foil Insulation System	III-13
II	Equipment and Instrument List	III-26
III	Tank Insulation Program - Test No. 1, Al Foil System	III-36
IV	Tank Insulation Program - Test No. 2, Aluminized Polyester Film System	III-37
V	Normalized Thermal Conductivity Apparatus Data	III-42

III. THE INSULATED-TANK PROGRAM

I. Summary

The performance of multilayer insulation is measured calorimetrically, usually with a flat-plate or cylinder-type calorimeter. We have made extensive measurements with flat-plate calorimeters (thermal conductivity apparatus) in this contract for a large variety of variables that are discussed elsewhere in this report. The applicability of these data for use in the design of insulation systems for a space-vehicle tank may be configuration-dependent, because of the extent and curvature of the surfaces to be insulated and because of support and other penetrations in the insulation. In order to investigate this dependence, a program to apply multilayer insulations to small tanks was initiated. The objectives of this program are as follows:

1. To develop techniques for mounting and conforming multilayer insulations to cylindrical and spherical surface segments.
2. To measure the heat transfer from 300°K and 77°K surfaces through multilayer insulations to a liquid-hydrogen reservoir, for both insulation systems that contain and insulation systems that are free from simulated structural penetrations and gaps in the foil system.
3. To correlate the heat-transfer results obtained from the tests with those predicted from the thermal conductivity apparatus and our analytical studies for comparable insulations and boundary-temperature conditions.

4. To initiate the development of a practical insulation system that will meet the ground-hold, boost and space requirements of cryogenic containers of the type under consideration for various space missions.

To achieve these objectives we fabricated two special tanks and applied multifoil insulation onto them. These test articles were to be shipped to the NASA Plum Brook Station in Ohio, where tests at liquid-hydrogen temperatures could be performed. Seven tests had been scheduled but could not be performed, because the test facilities were unavailable. Two tests of a limited nature were performed in a modified, Arthur D. Little, Inc., facility at Cambridge.

We measured the heat transfer performance of two multilayer insulation systems. One of these consisted of five aluminum shields, and the second consisted of five aluminized polyester film shields. These multilayer insulation systems were applied and conformed to the outer surface of separate cylindrical tanks, 48 inches in diameter and 26 inches deep, having torispherical ends. The shields in each system were spaced with layers of 1/8-mesh, vinyl-coated, fiberglass netting. The insulated tanks were successively placed in a chamber at less than 10^{-5} mm Hg. A liquid nitrogen bath in the tank provided a cold boundary temperature of -320°F , and the chamber walls formed the warm boundary of the insulation system. The heat flow through the insulation was determined from the boil-off of liquid nitrogen within the tank.

The measured heat flux for the two insulation systems tested in both the tank calorimeter and thermal conductivity apparatus is a function of the boundary temperatures and the boundary surface emissivities, which have been often different for one test as compared to another. In order to compare the heat transfer performance obtained in several tests for a given system, we have found it advisable to adjust the measured heat flux to a set of standard boundary conditions, i.e., 80°F warm boundary and -320°F cold boundary temperatures and 1.0 for the boundary surface emissivities. This adjustment to the measured values is based on the relations for radiant heat transfer, assuming that this is the predominant mode by which the heat energy is transmitted.

The average measured heat flux rate on the aluminum shield system was 0.40 BTU/hr ft². This compares with adjusted heat flux values that range from 0.46 to 0.89 BTU/hr ft², as measured with the thermal conductivity apparatus for a comparable shield and spacer system.

The aluminized polyester shield system gave results of 1.01 BTU/hr ft². This compares with adjusted heat flux value of 1.38 BTU/hr ft² obtained with the thermal conductivity apparatus in Test 1032 for 20 crinkled aluminized polyester films with two layers placed back to back and separated by eleven, 1/8-mesh, vinyl-coated, glass fiber screen. Test 1033, performed with the thermal conductivity apparatus for a 10-foil, aluminized polyester film system spaced with eleven glass fiber mats, 0.008-inch thick and 50% perforations, gave a lowest result of 0.75 BTU/hr ft².

Only preliminary conclusions can be drawn from the limited data obtained in the current period of this program with the aluminum and the aluminized polyester film systems. These are:

1. Through the use of gores and/or pressure forming of the shields and spacers, multilayer insulations can be applied and conformed to tanks whose geometry is made up of spherical and cylindrical segments.

2. By careful application of the foils and spacers, heat transfer results comparable with those measured with the thermal conductivity apparatus are obtainable.

The results obtained thus far give promise that significant information applicable to future space-vehicle programs can be obtained with our current approach. We recommend that the objectives of this program be implemented in a continuing effort.

II. Approach

Multilayer insulation was applied onto a vessel to cover its surface completely. The vessel was then placed in a chamber so that the pressure in and around the insulation system could be reduced to less than 10^{-5} mm Hg. The vacuum chamber wall served as the warm boundary of the insulation. Through the use of a baffle located in the vacuum space between the insulated tank and chamber wall the warm boundary temperature could be controlled at levels below the local ambient. The cold boundary was formed by the tank wall, which was maintained at the desired temperature level by filling the tank with liquid nitrogen or hydrogen. The tank support was refrigerated from a separate

2

source in order to isolate the tank from all conductive heat resulting from the support. The heat transfer performance of the insulation system was determined from the measured quantities of liquid evaporated from the insulated tank.

The insulation systems used in the initial tests consisted of shields and spacers identical with or very similar to those from which considerable heat flux data had been obtained in the thermal conductivity apparatus. Great care was used in applying the insulation systems to the tanks, in order that heat transfer performance levels as close as possible to those measured on the thermal conductivity apparatus might be achieved. The insulation systems chosen and the manner and techniques of their application to the tanks were not intended to represent development of optimized systems meeting specific vehicle requirements.

III. Experimental Equipment

A. Calorimeter

The calorimeter was a vertical, cylindrical vessel, 48-inches in diameter and 26-inches deep, having torispherical heads. These dimensions were dictated essentially by the dimensions of the J-3 vacuum chamber into which it had to fit eventually. The vessel was fabricated from 1/4-inch thick, oxygen-free, annealed copper. Annealed copper was used because its high thermal conductivity promotes isothermal-temperature conditions in the cold boundary over wide ranges of liquid bath level and insulation heat flux levels. The vessel had a maximum internal working pressure 30 psi above the external pressure and a maximum external working

pressure 15 psi above the internal pressure. The tank was supported from a support flange by a 5-inch, schedule 5, type 304 stainless steel pipe that also acted as the tank vent. The 24-inch diameter support flange was mounted into the top of the J-3 chamber with bolts and was sealed with O-rings.

The calorimeter vessel is shown in Figure III-1, and dimensions and details are given in Figure III-2. In Figure III-3, a sectionalized view of the calorimeter mounted into the Arthur D. Little, Inc., test chamber is shown.

The calorimeter vent support line extended into the copper vessel, where it connected to the bottom head through a simple sliding support, as shown in Figure III-2. This section of the vent served several purposes, one of which was to provide the heads with additional stiffening under external pressure conditions. Further, this extension served to eliminate severe bending movements that were present in the top head in certain handling situations. The extension into the vessel was perforated to allow the vaporized liquid to pass out through the vent. It also contained a capacitance-type liquid level gauge supplied by NASA/Lewis and served as a liquid-stilling tube for the gauge.

As mentioned previously, the vent support pipe was to be mounted in the J-3 chamber by means of a bolting flange. This flange was used also to support the calorimeter during shipment and at the time the insulation was being applied. The fill and vent lines for the cold guard and baffle lines penetrated through the flange with appropriate isolating

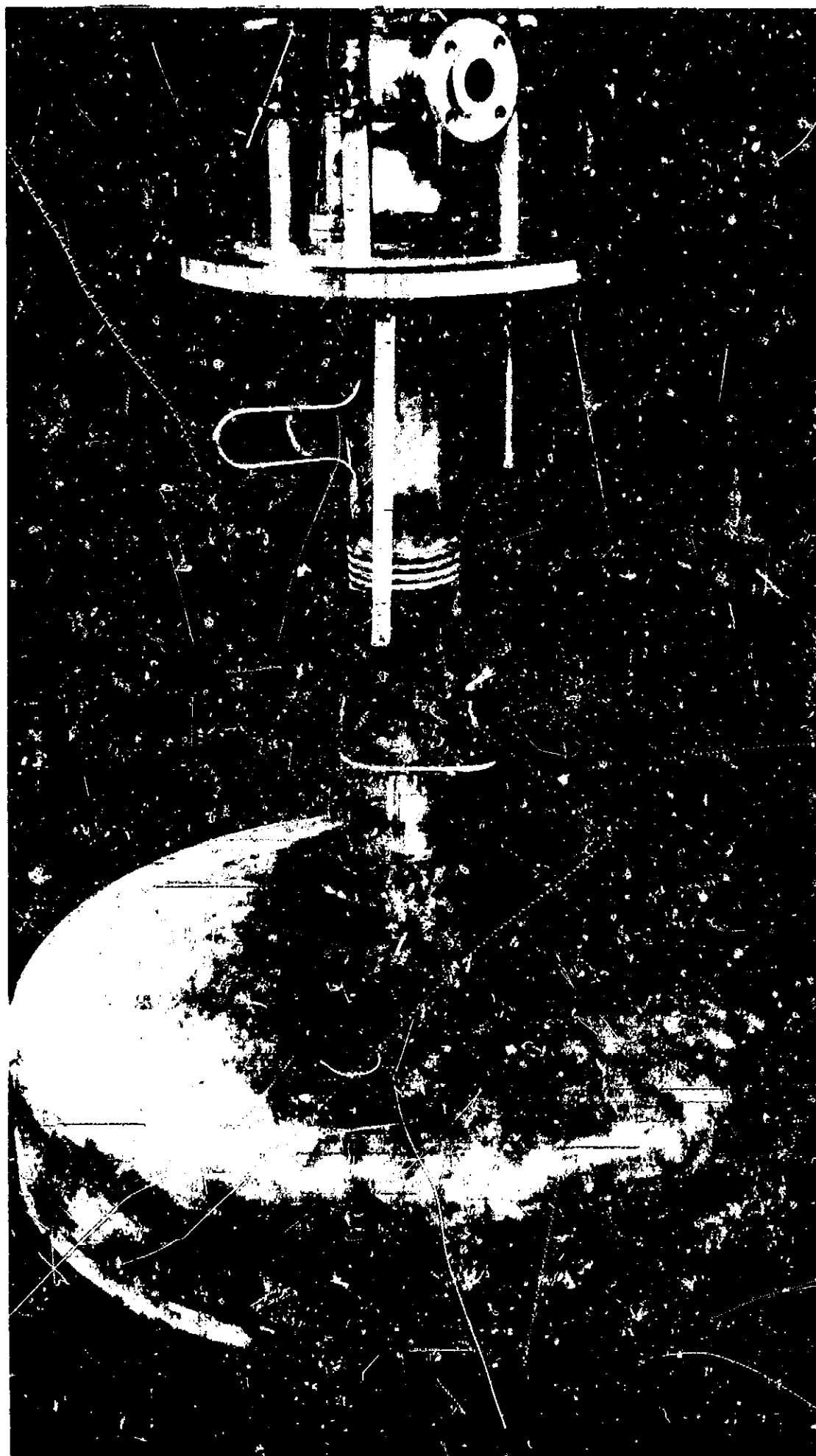
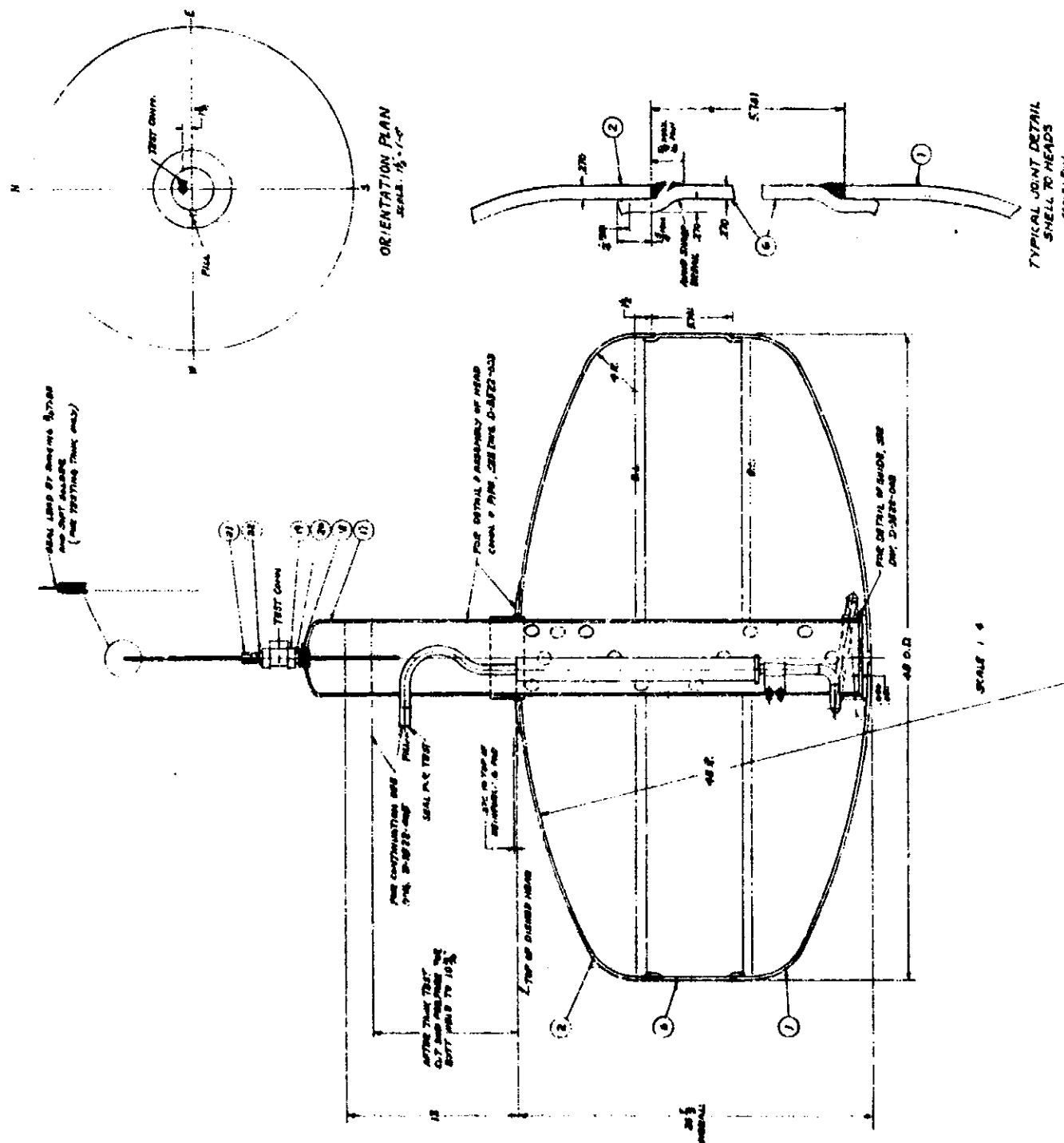


FIGURE III-1 TANK CALORIMETER

III-7



CALORIMETER TANK NOTES

1. ALL WELDS ARE TO BE DESIGNED FOR A VESSEL WORKING PRESSURE OF 50 PSIG, IN ACCORDANCE WITH ASME BOILER AND PRESSURE VESSEL CODE, SECTION VIII, FOR UNFURRED PRESSURE VESSELS.
2. THE VESSEL MATERIALS ARE TO BE OF CUPRUM (HAVING A MINIMUM YIELD POINT STRESS OF 10,000 PSI). THE VENT-PIPING LINE AND OTHER ACCESSORIES ARE TO BE OF 304 STAINLESS STEEL AS NOTED IN THE BILL OF MATERIALS.
3. ALL WELDS ARE TO BE RADIOGRAPHED IN ACCORDANCE WITH PARAGRAPH M-57 OF THE ASME BOILER AND PRESSURE VESSEL CODE, SECTION VIII, FOR UNFURRED PRESSURE VESSELS.
4. THE VESSEL IS TO BE HYDROSTATICALLY TESTED TO A MINIMUM PRESSURE OF 45 PSIG, AFTER THE TANK HAS BEEN FILLED WITH HELIUM. THE TEST PRESSURE IS TO BE MAINTAINED FOR 10 MINUTES. THE LEAKAGE THROUGH THE VESSEL IS NOT TO EXCEED 10-7 SEC/SEC AT THE LOCAL TEST PRESSURE. THE LEAKAGE AT THE CAP ON THE STRAP-ON TEST CHAMBER IS NOT TO EXCEED 10-7 SEC/SEC. THIS LEAKAGE REQUIREMENT IS NOT INCLUDED AS PART OF THIS LEAKAGE REQUIREMENT.
5. THE CALORIMETER VESSEL IS TO BE LEAK TESTED WITH THE HELIUM MASS SPECTROMETER. THE LEAKAGE THROUGH THE VESSEL IS NOT TO EXCEED 10-7 SEC/SEC AT THE LOCAL TEST PRESSURE. THE LEAKAGE AT THE CAP ON THE STRAP-ON TEST CHAMBER IS NOT TO EXCEED 10-7 SEC/SEC. THIS LEAKAGE REQUIREMENT IS NOT INCLUDED AS PART OF THIS LEAKAGE REQUIREMENT.

SUGGESTED PROCEDURE FOR ASSEMBLING TANK

1. WELD COPPER COLLAR TO TOP HEAD.
2. WELD PAD TO TANK AND COLLAR.
3. WELD 5" PIPE TO COLLAR.
4. WELD 48 O.D. CYLINDER TO TOP HEAD. IT MAY BE DESIRABLE TO WELD THIS CYLINDER AFTER OR BEFORE STEP NO. 1.
5. LOCATE LOWER FLANGE IN POSITION AND CHECK FOR PROPER CLEARANCE BETWEEN BOTTOM OF 5" PIPE AND STAINLESS STEEL PAD PLATE. WELD INTO BOTTOM HEAD.
6. INSTALL LIQUID LEVEL GAGE INSIDE THE 5" PIPE.
7. WELD BOTTOM HEAD TO TANK.

FIGURE III-2 CALORIMETER COPPER TANK DETAILS

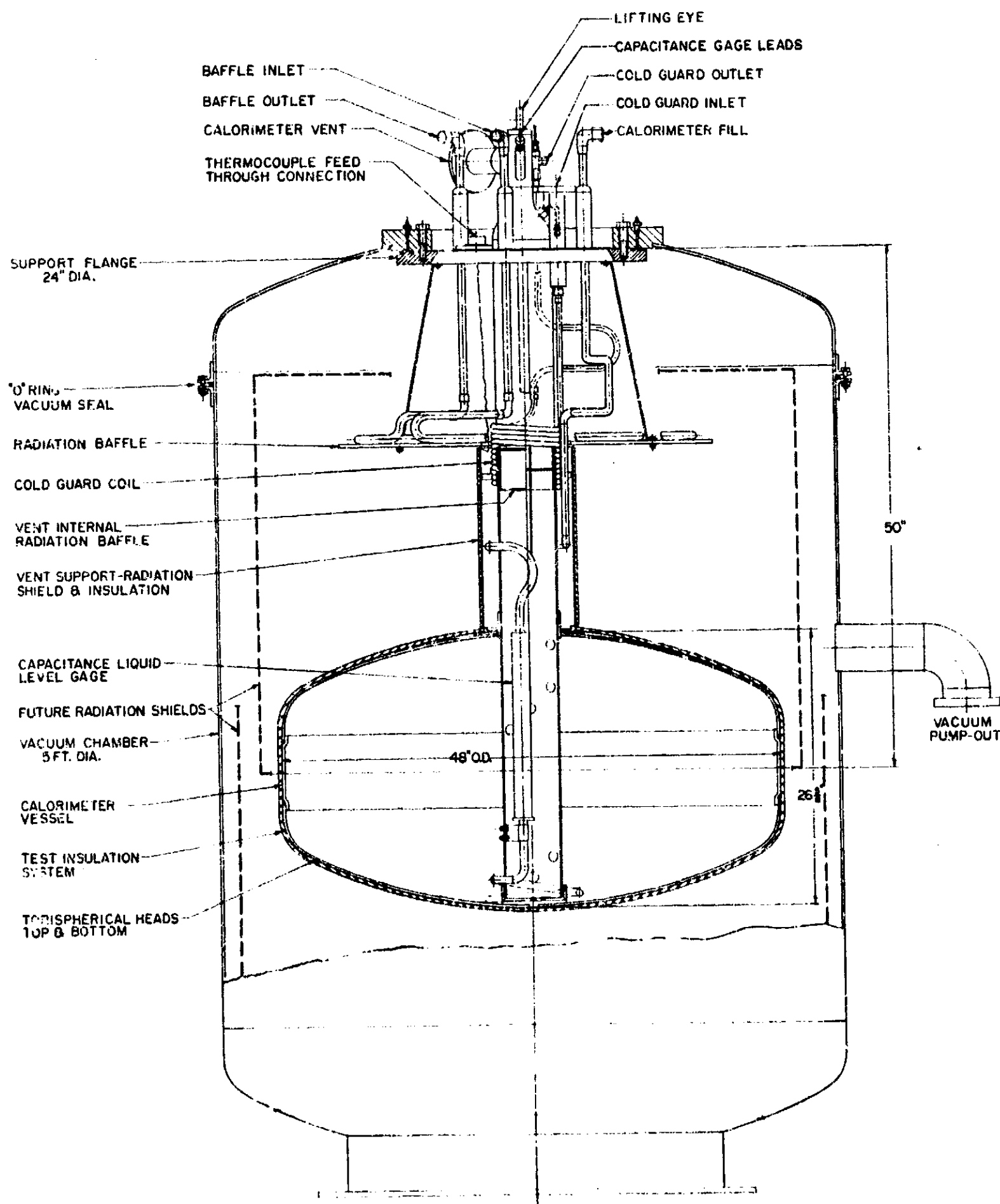


FIGURE III-3 CHAMBER AND CALORIMETER ASSEMBLY

columns. Thermocouple lead wires associated with the calorimeter and insulation temperature measuring sensors were also fed through the support flange. As shown in Figure III-1, the flange also served to support the calorimeter mounted radiation baffle.

The calorimeter tank was thermally insulated from the mounting flange by a guard coil that limited the heat leak during operation to approximately 0.1 BTU/hr. The guard coil, shown in Figure III-3, could be supplied with either nitrogen or hydrogen. The guard coolant was saturated at 2 to 5°F above the calorimeter tank liquid in order to limit the conductive heat leak. The internal radiation from the warm end of the vent was trapped in a copper baffle that was coated with high emissivity paint; this heat was thermally shorted to the guard coil. Since the cold guard was soldered to the vent, the heat conducted down the vent from the support flange was also shorted to the cold guard. The section of vent pipe between the coil and the tank was shielded from the warm boundary heat flux by a copper shield that was shorted to the cold guard and was able to conduct the radiated heat to the coil. The calorimeter fill tube and the capacitance gauge lead wires were also thermally bonded to this coil to preclude heat leaks by these conductors from the outside. The heat absorbed by the coil resulted in boil-off of the continually flowing refrigerant stream.

Arthur D. Little, Inc., has permanently mounted a baffle on the vent support to thermally decouple the insulated tank from the warm chamber surfaces when baffles are used in the chamber as the source boundary. This baffle is to be positioned with respect to any chamber baffles to offer low pumping impedance between the enclosed volume and the chamber vacuum systems. In the tests reported here, this baffle was not used.

In order to assure reliable and hazard-free operation of the calorimeter vessel, we designed, fabricated, and tested the vessel in accordance with the ASME Code for Unfired Pressure Vessels and in accordance with procedures and practices widely accepted for cryogenic vessels. In addition to Code design calculations, a computer analysis was performed to further identify the operating limitations of the vessel. The vessel welds were radiographed in accordance with Code procedure. Hydrostatic tests were performed at 1.5 times the working pressure (45 psi), and strain gauge measurements at critical areas were taken. Leakage tests with a helium mass spectrometer were performed at room and liquid nitrogen temperatures. Thus, we achieved reliable and trouble-free operation of the calorimeter and were able to concentrate our efforts on measuring and evaluating the performance of the insulation system.

B. Aluminum-Foil Insulation System

The first insulation system to be applied to the completed tank calorimeter consisted of five aluminum foils, 0.002 inch thick, spaced from each other with glass fiber netting. This foil system had been tested extensively in the thermal conductivity apparatus, and consistent results had been reported. Its application to the tank calorimeter served to bridge the drastic geometry differences between the two calorimeters. At a later date this system will be used to study also the temperature distribution in the shields resulting from gaps and penetrations introduced into the insulation system.

Details of the aluminum foil system applied to the tank calorimeter are presented in Table III-I. The system consisted of five foil layers and six spacer layers contoured to the cylindrical and spherical curvature of the calorimeter vessel.

The aluminum foils for the top and bottom of the vessel were formed from 1145-0 grade aluminum. The sheet stock was cut into discs and stretch-formed in a vacuum jig to a spherical curvature with radii corresponding to the top and bottom vessel curvatures. The 1145-H19 grade aluminum was not used, because it would have ruptured in the stretch-forming operation, due to its low elongation when stressed. —

The cylindrical and knuckle sections of the shields were formed from 1145-H19 sheet aluminum, 0.002 inch thick. Gore sections were cut into the upper and lower portions of the side sheet in order to conform the sheet at the knuckles when the elements were folded. The maximum gore width was 3 inches at the base. To prevent tearing at the base of the gore elements, the sheets were perforated with 1/8-inch diameter holes to redistribute the local stresses. The butt seams between gores were staggered in each foil layer relative to the adjacent layers to prevent direct viewing between warm and cold boundary surfaces.

The side sheets were positioned relative to the vessel through the use of five 0.030-inch diameter stainless steel pins that had been stud-welded to the copper vessel. These pins were sheathed with teflon to prevent the occurrence of localized heat "shorts" between the different foil layers. The orientation of the three sections of sheet aluminum forming each shield layer and the location and type of seam used are illustrated in Figure III-4.

TABLE III-I

ALUMINUM FOIL AND ALUMINIZED POLYESTER FILM INSULATION SYSTEMS

TANK CALORIMETER TEST INFORMATION
FOR TESTS CONDUCTED AT LIQUID NITROGEN TEMPERATURES

<u>Insulation System Data</u>		<u>Aluminum Foil System</u>	<u>Aluminized Polyester Film System</u>
No. of foils	5		5
Foil material Side sheet		Alcoa 1145-H19, 0.002 inch thick, bright on both sides.	Polyester film, .00025 inch thick, aluminized on one side (NRC). Aluminized surface facing warm boundary.
Heads		Alcoa 1145-0, 0.002 inch thick, stretch- formed into spherical segment.	Same as above.
Separator		1/8 x 1/8 inch resin-coated fiberglass netting, 0.020 inch thick.	Same as for aluminum foil system
Attachment pins		5 pins, 0.030 inch diameter covered with teflon sheath 0.012 inch thick; pins located on the cylindrical portion of the tank.	5 pins, .045 inch diameter, covered with teflon sheath .012 inch thick; pins located on the cylindrical portion of the tank.
Perforations		Slits in the foil system formed by the gore sections at the knuckle radius on the tank heads.	Same as for aluminum foil system
Foil joint design			Same as for aluminum foil system
1. Gore sections		Butt joint.	
2. Circumferential seams		Overlapped foils in contact.	
3. Longitudinal seams		Overlapped foils in contact.	
Surface emissivities			
1. Vacuum chamber		0.97; obtained with 3M optical black	0.97
2. Calorimeter tank		0.97; obtained with 3M optical black	0.97
3. Aluminum foils		0.03 (estimated)	0.05 (estimated)
Surface area		38.14 ft ²	39.5 ft ²
Insulation weight		0.225 lbs/ft ²	0.104 lbs/ft ²
Theoretical Insulation thickness		0.130 inches	0.121 inches

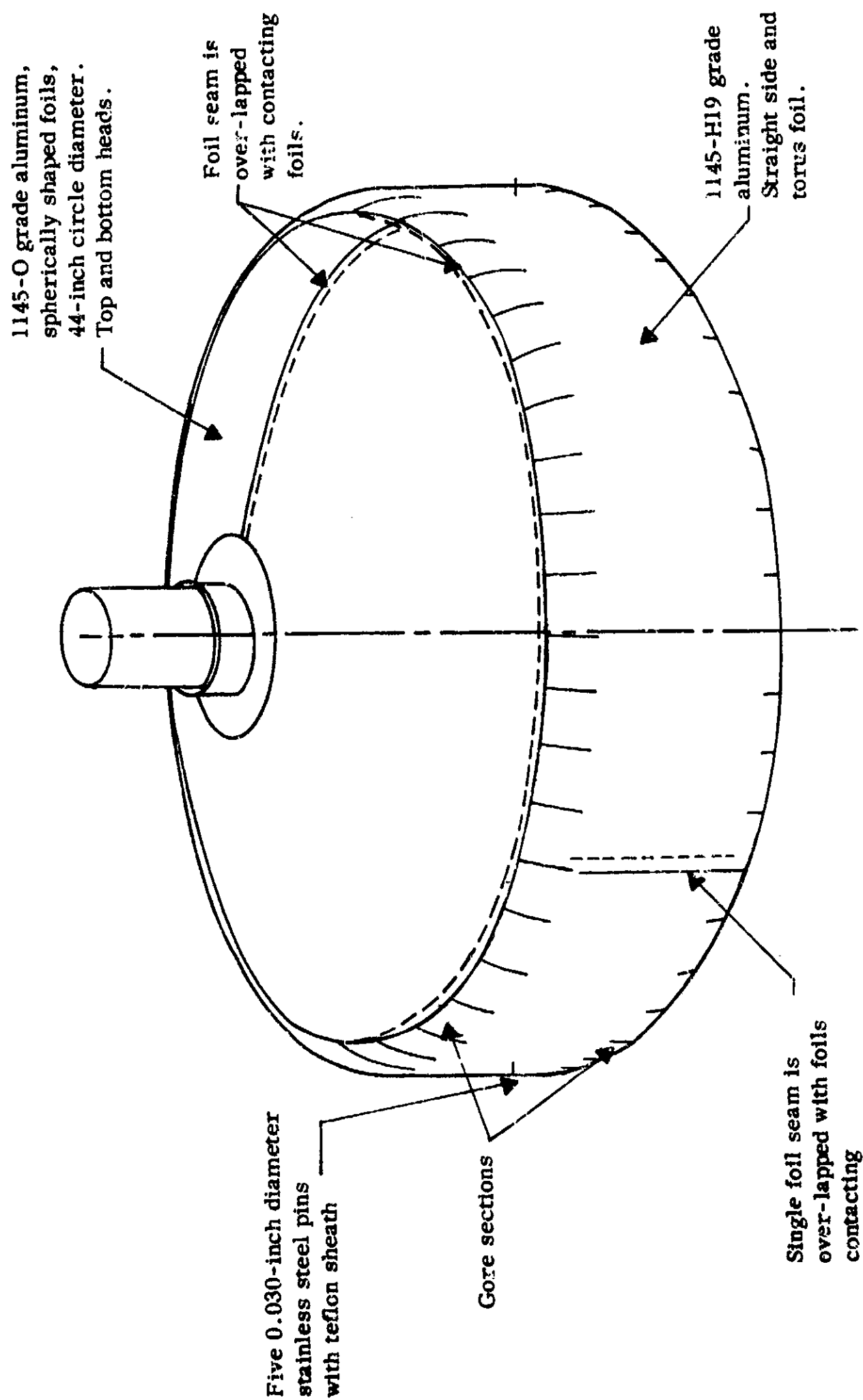


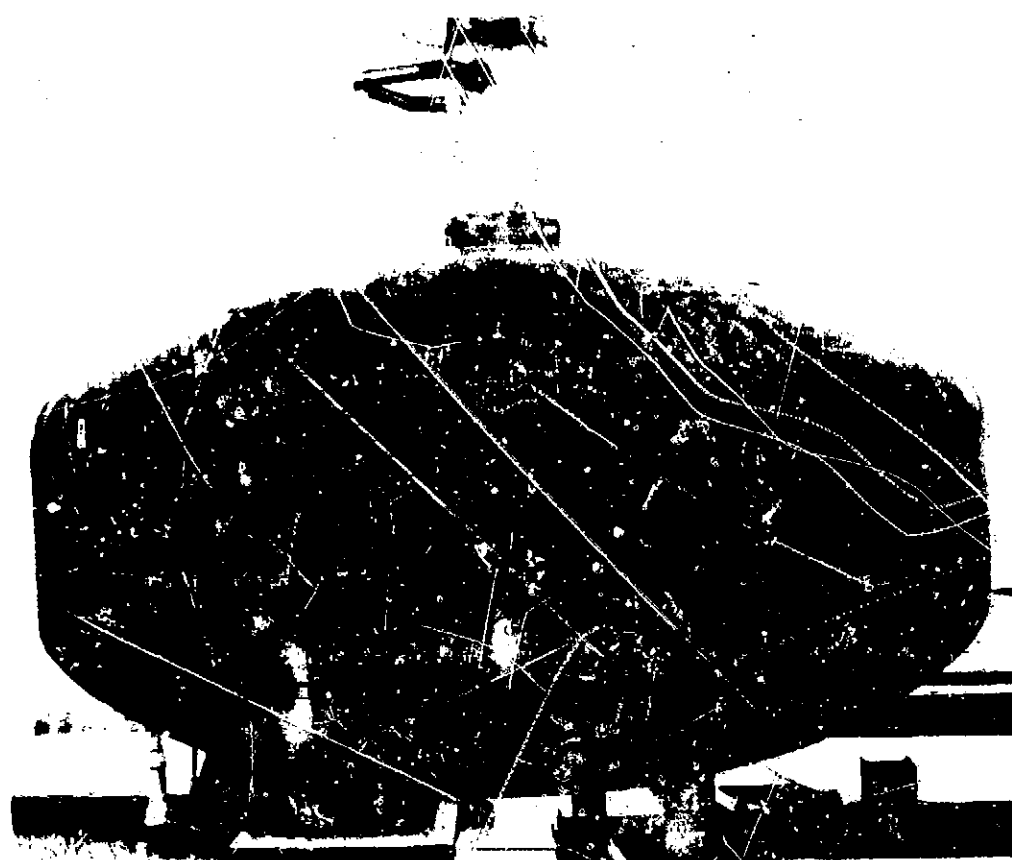
FIGURE III-4 ALUMINUM FOIL INSULATION DETAILS

The spacer netting was conformed to the vessel surface in much the same manner that the aluminum was conformed. The spherical portions were formed by stretching the netting while it was held in a circular frame over a male die of appropriate curvature (dummy tank) and simultaneously heated to 200°F with a natural gas, infrared, space heater. When cooled the netting retained its heat-formed shape.

The cylindrical and knuckle sections were formed from a single sheet of netting. Gore sections were cut into the upper and lower ends of this netting so that the folded elements would conform to the knuckles and a portion of the spherical tank ends. The netting gores were made longer than the aluminum in order to displace the girth seams relative to one another. Further, the netting-gore seams were displaced relative to the aluminum-gore seams. The three sections comprising each layer of netting were sewn together along the principal seams.

Prior to the application of the netting, the vessel was coated with "3M" Brand Velvet Coating No. 9564, optical black, manufactured by Minnesota Mining and Manufacturing Company. This coating produces a known surface emissivity of about 0.97, which has been experimentally verified in work conducted under contract AF 04(641)-787.

The bottom and side views of the first netting spacer applied to the calorimeter vessel are shown in Figure III-5. Figure III-6 shows similar views of the fourth aluminum layer and the fifth netting spacer.



(a) Calorimeter Side

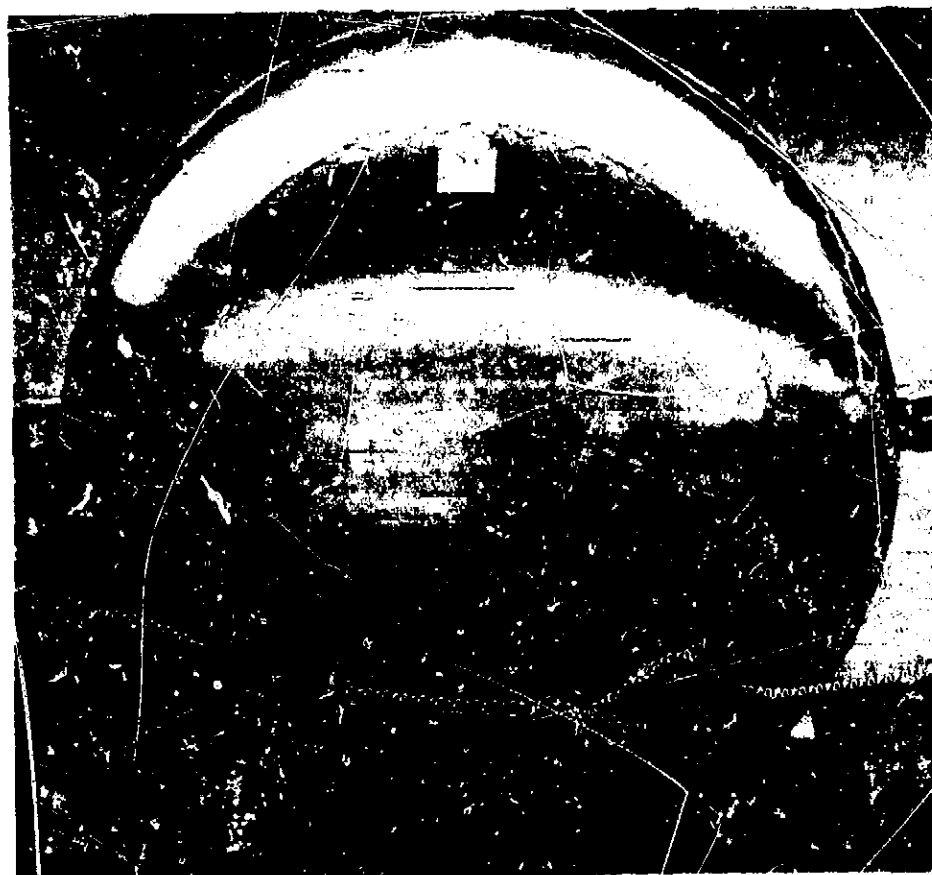


(b) Calorimeter Bottom

FIGURE III-5 ALUMINUM-FOIL-SYSTEM SPACER NETTING



(a) Calorimeter Side



(b) Calorimeter Bottom

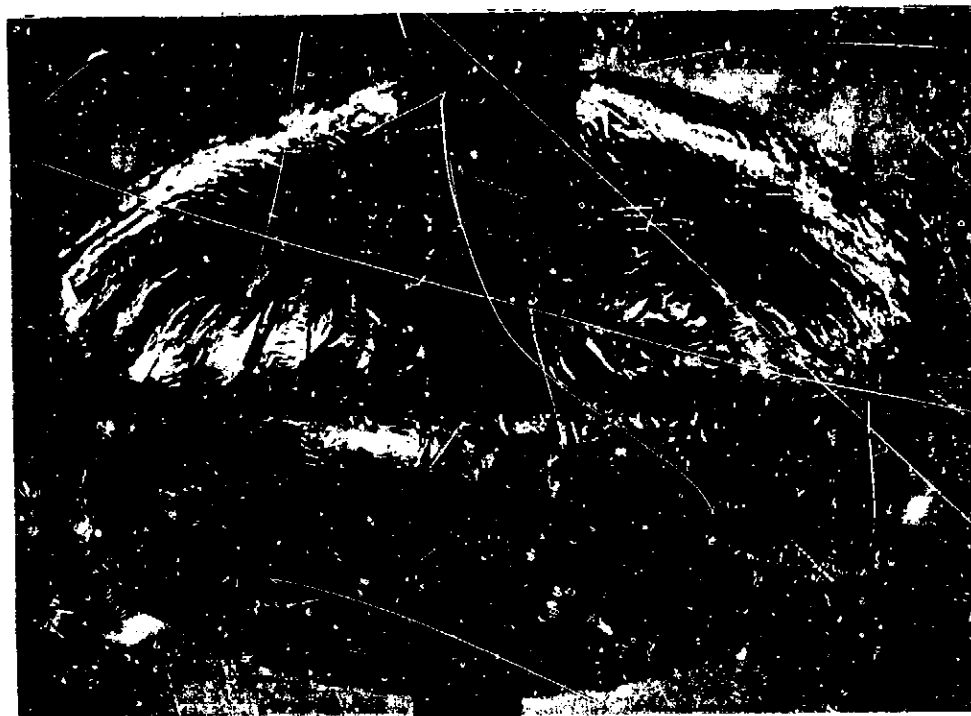
FIGURE III-6 NO. 4 ALUMINUM FOIL AND NO. 5 SPACER NETTING

C. Aluminized Polyester Film

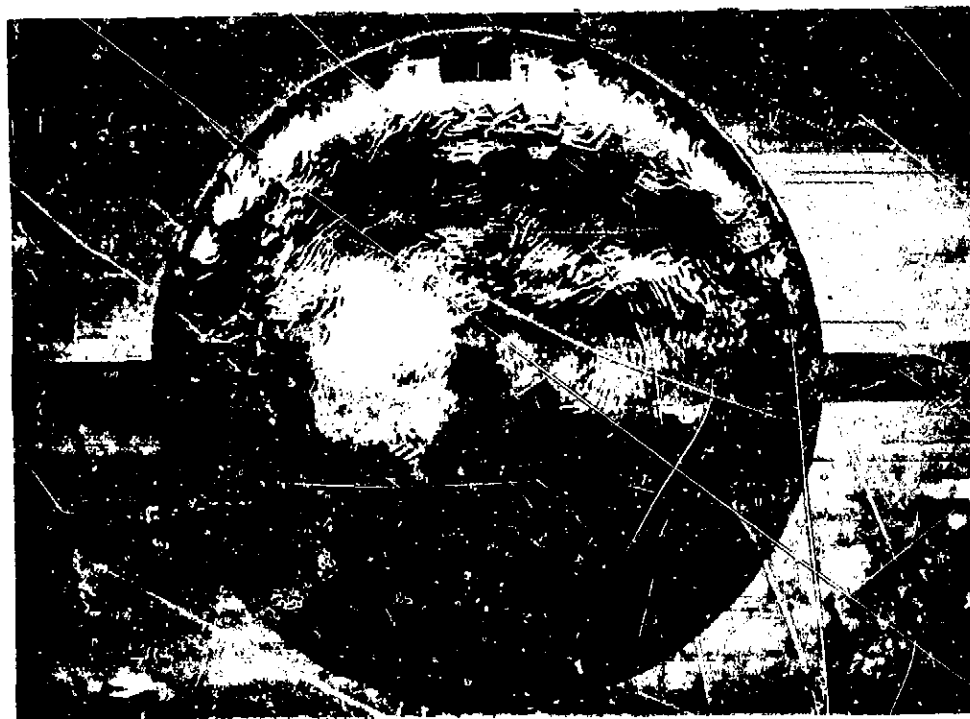
The second insulation system to be tested consisted of five shields of aluminized mylar foils, 0.00025 inch thick, spaced from each other with vinyl-coated, 1/8-mesh, glass fiber netting. When properly aluminized, the small gauge, low density, and low thermal conductivity of polyester film make it well suited to application in the range of temperatures of 100°F and below. Further, the material was selected for the test insulation on the second tank because of the large amount of heat flux data available from tests performed with the thermal conductivity apparatus. Where possible, the principal characteristics of the aluminized mylar system, i.e., spacer materials, foil and spacer dimensions, were made identical to those of the aluminum system in order to make the comparison between these two systems more direct. The final configuration of the aluminized polyester film insulation is shown in Figure III-7.

The aluminized mylar foils for the top and bottom of the vessel were formed from nonstretched circles 47-1/4-inches in diameter. The bottom circle was slit radially from the edge at 16 equidistant locations with slit lengths alternating between 8 and 20 inches. The circle forming the top of the calorimeter tank was slit in a similar fashion, except that slit lengths alternated between 6 and 8 inches. All segments of all foil layers were oriented with the aluminized surface facing the warm boundary.

While our attempts to stretch-form the heads into spherical segments proved successful, we did not use this method, because alteration of the mylar-radiation characteristics and/or thinning of the aluminization layer



(a) Calorimeter Side



(b) Calorimeter Bottom

FIGURE III-7 ALUMINIZED-POLYESTER FILM NO. 5
FOIL AND NO. 6 SPACER NETTING

III-19

could result, and the insulation system could be degraded. The details for applying the foils on the cylindrical section of the vessel and for applying the spacers were the same as those discussed above for the aluminum insulation system.

The foil layers became discontinuous at the top of the calorimeter vessel in the vicinity of the vent support. The edges of the shield system were in direct view of the lower end of the vent support. The warm shields could have channeled heat into the calorimeter tank. This was avoided through the use of an edge guard which was attached to the neck shield and was, in turn, shorted to the cold guard. The edge guard may produce an apparent improvement in the insulation performance, because heat escaping the edges is directed into the guard. The edge-guard details are shown in Figure III-8.

Secondary to measurement of the calorimeter heat leak was the measurement of the temperature distribution in the foil system. This was accomplished with copper-constantan thermocouples which were attached to selected foils at the locations shown in Figure III-9.

The thermocouples were prevented from interacting with the insulation system through the use of small-diameter lead wires and a thermocouple lead guard. The thermocouples were fabricated from No. 40 B & S wire gauges (0.0031 inch). The guarding was provided by the vent support shield shown in Figure III-8. The shield was insulated with the same number and type of foils as used on the calorimeter vessel. The thermocouples exited the calorimeter test insulation at the neck edge and passed

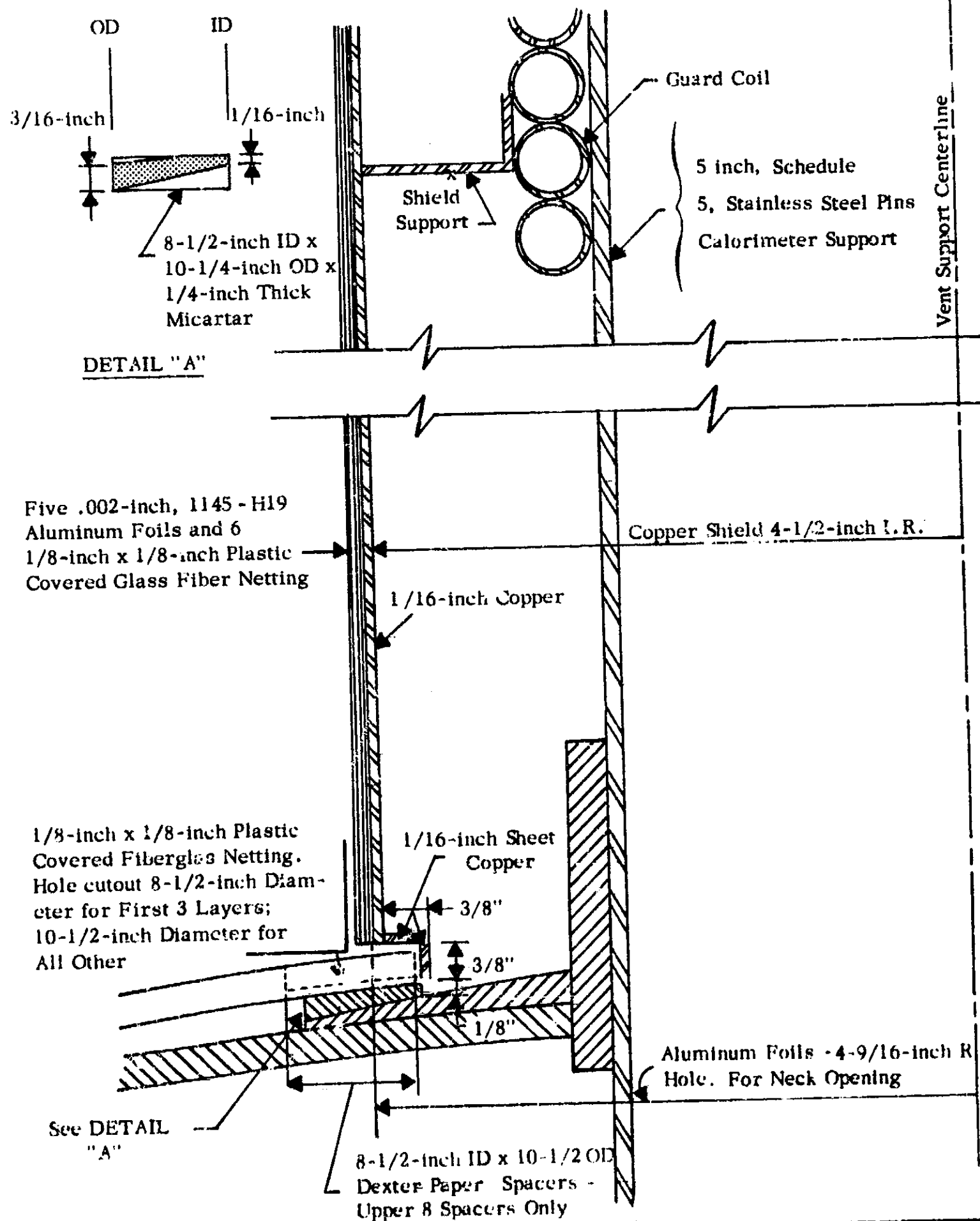
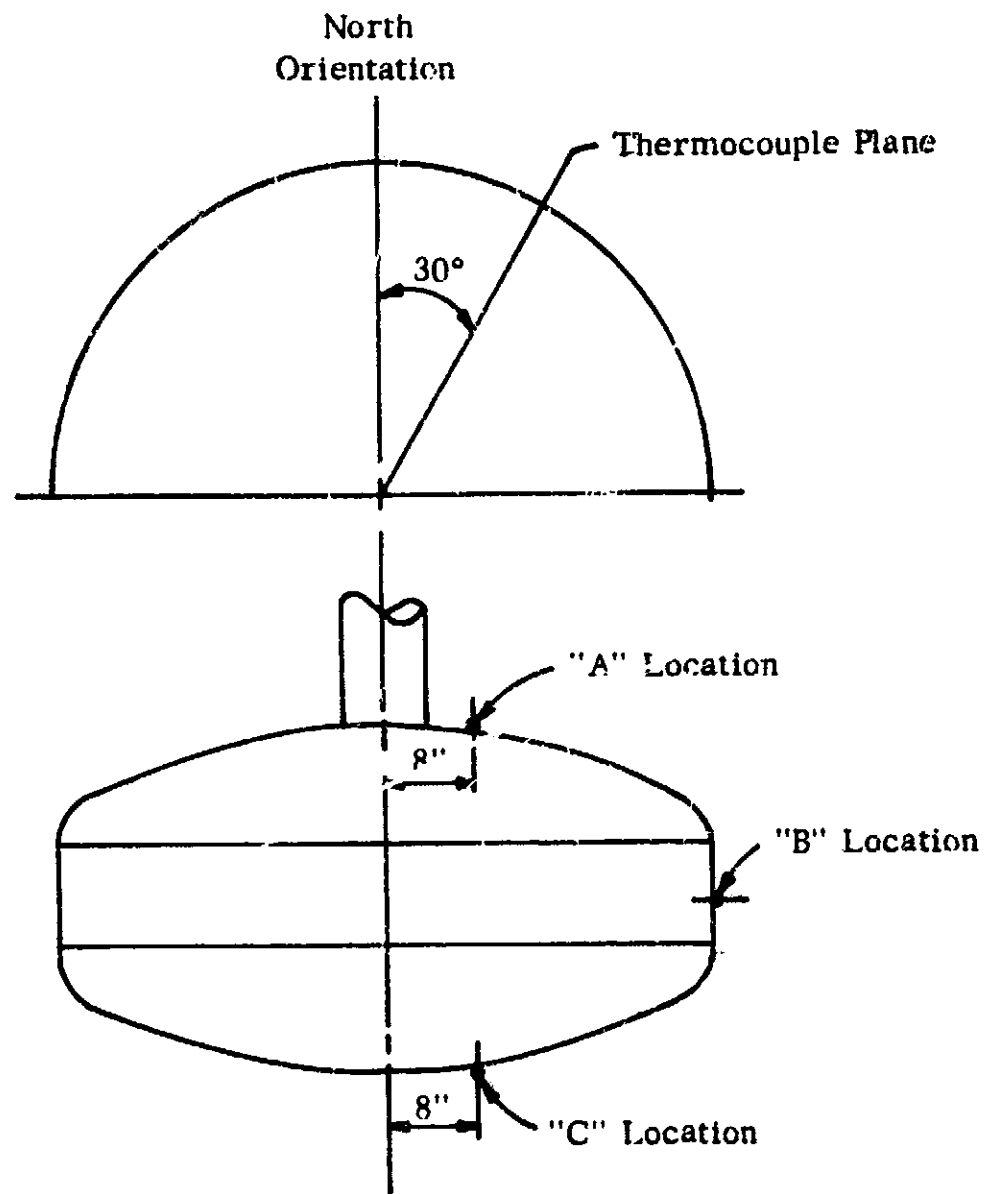


FIGURE III-8 TEST INSULATION EDGE GUARD AND VENT SUPPORT (RADIATION SHIELD)



X Thermocouple Identification

Note: IC and IB of Aluminum Shield System Inoperative.

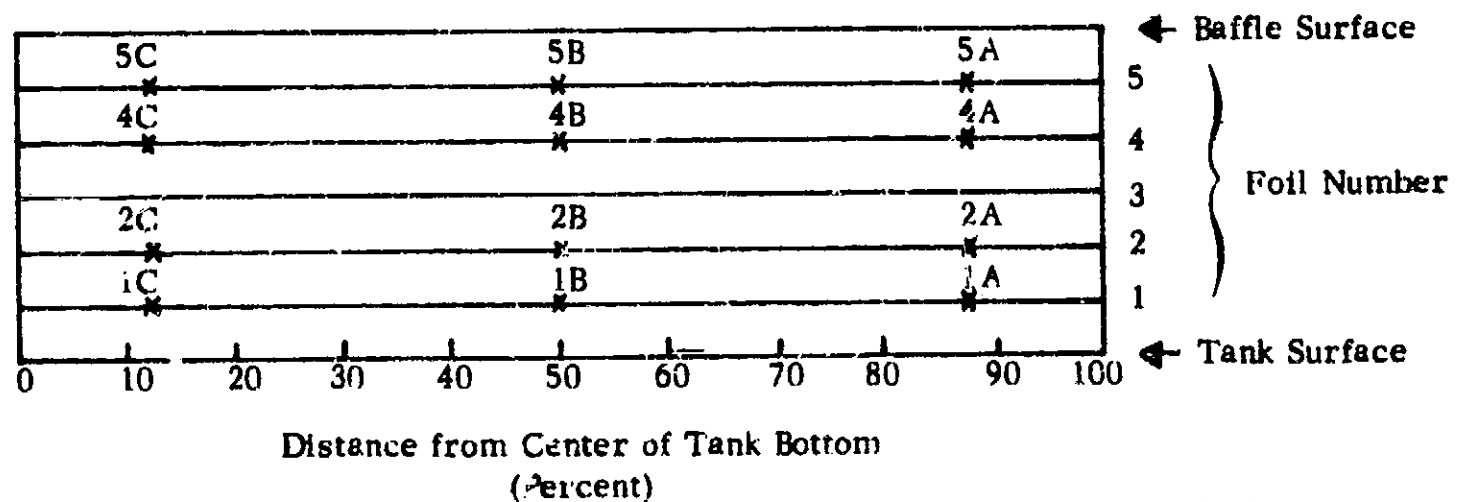


FIGURE III-9 INSULATION SYSTEM, THERMOCOUPLE LOCATIONS

into the neck shield insulation at corresponding depths. (See Figure III-10.) The couples exited the neck shield insulation and connected to the vacuum feed-through on the support flange.

Because of the similarity of the neck and calorimeter insulations as well as the source and sink temperatures, both temperature distributions were nearly the same. Thus, any heat conducted from the vent support flange would be distributed in the neck shield insulation and slightly alter its temperature gradient. At the same time the thermocouples would achieve temperature equilibrium with their respective shields prior to passing to the test insulation. As a result of the guarding and the small wire diameter used, the heat conducted through the thermocouple leads to the test insulation was estimated to be of the order of 0.1 BTU/hr.

D. Test Facility

At the start of this program it had been intended that the calorimeter tank be maintained at 37°R through the use of liquid hydrogen. To this end the hydrogen facilities at the J-3 cell, NASA/Plum Brook station, were adapted for use with the calorimeter. However, at the completion of the modification work the facility was requisitioned and used for a high-priority NASA research effort, and it could not be made available to this program in time to conduct the planned multilayer insulation tests prior to expiration of the contract.

As an expedient, an existing facility at Arthur D. Little, Inc., Cambridge, was adapted for use with the calorimeter to obtain limited data at liquid nitrogen temperatures. An equipment and instrument test

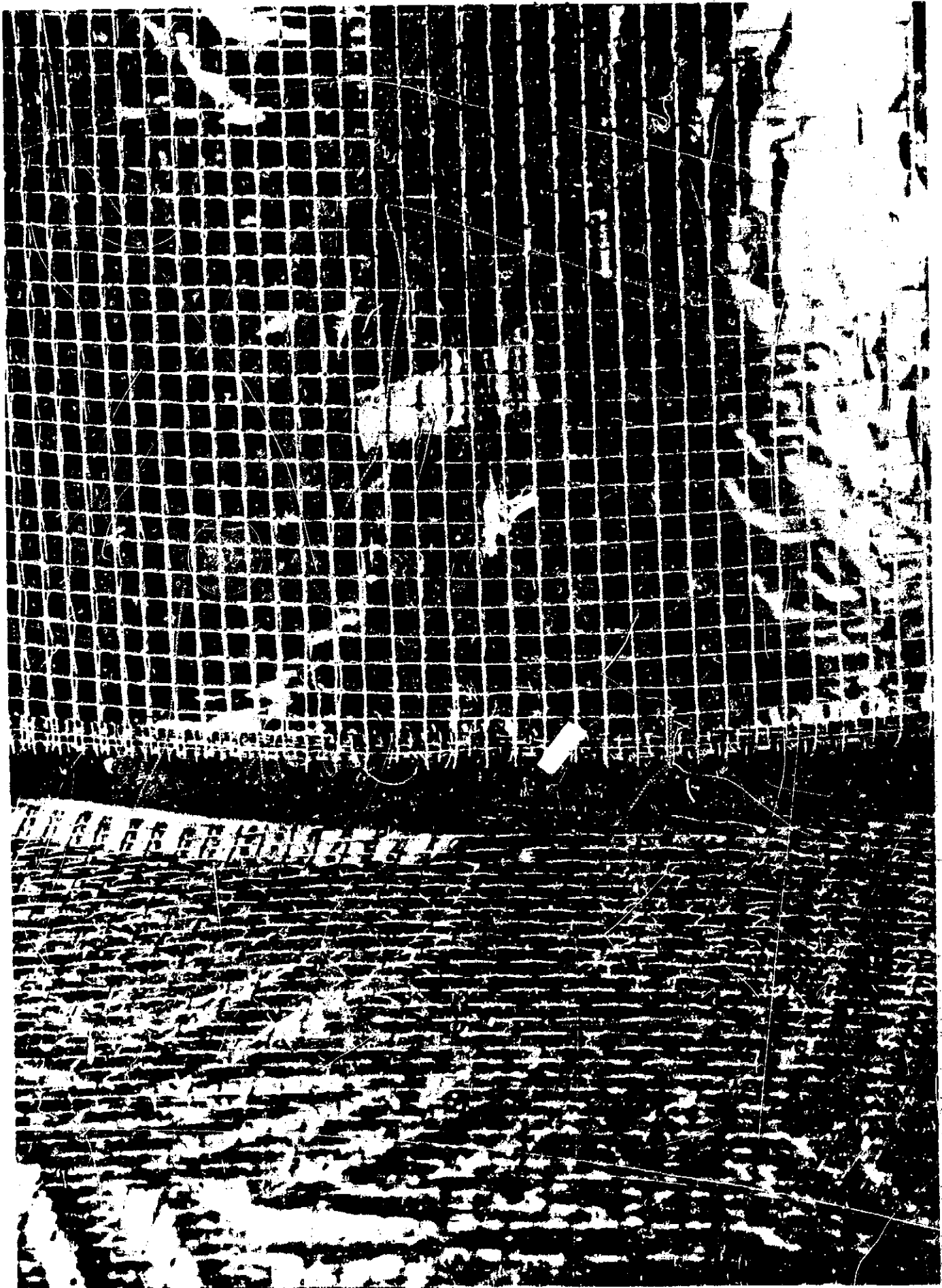


FIGURE III-10 THERMOCOUPLE LEAD WIRES - EXIT OF INSULATION SYSTEM

for the Cambridge facility is given in Table III-II. The wall of the chamber was used as the warm boundary radiation source instead of a controlled temperature baffle system similar to that provided in the Plum Brook J-3 facility.

The use of nitrogen in the Cambridge facility resulted in a considerably less hazardous operation than the J-3 operation. Thus, local hand operation of all functions and local instrument readout resulted in a greatly simplified system.

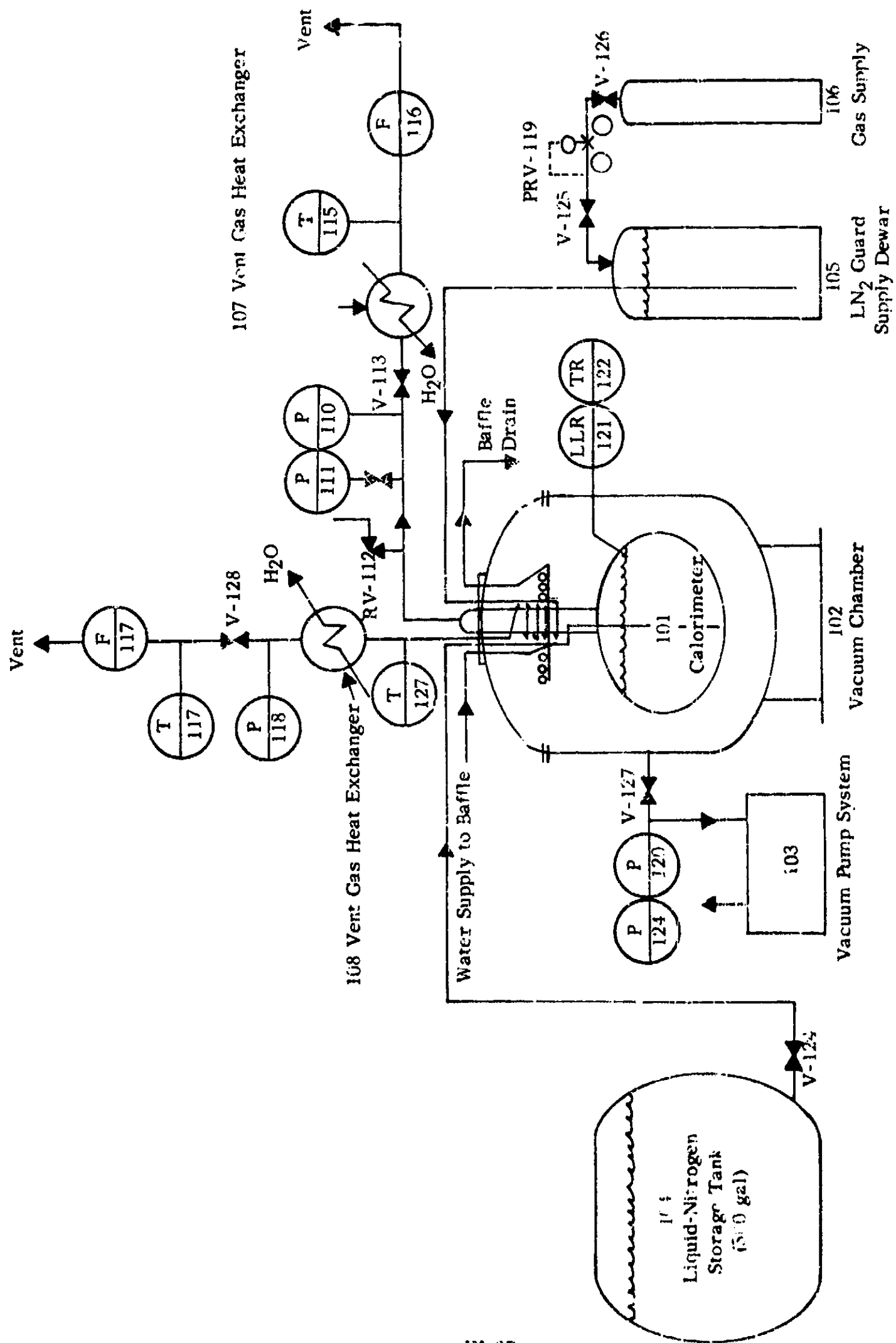
The facility consisted of a 5-foot diameter vacuum chamber, 4-inch diffusion and fore-pump system, 500-gallon liquid nitrogen supply tank, liquid nitrogen cold guard system, and calorimeter vent system. These are all identified in the flow schematic shown in Figure III-11.

The vacuum chamber was fabricated from carbon steel. Access to its interior was provided through the upper head, which was flanged but not bolted. (See Figure III-3.) External pressure and a neoprene O-ring were used to vacuum seal the flange joint. The interior of the chamber was coated with optical black to produce a high emissivity surface. A dynamic chamber vacuum of less than 1×10^{-5} torr was maintained with a 4-inch diffusion and fore-pump system. The calorimeter was flange mounted into the chamber head in identical fashion to the mounting in the J-3 facility.

The function of the cold guard mounted on the calorimeter vent line was to prevent the heat that was conducted down the vent line from the support flange from ever reaching the calorimeter tank. The "shorting" of this heat leak was accomplished through the use of a copper coil

TABLE III-II
EQUIPMENT AND INSTRUMENT LIST
CAMBRIDGE TEST FACILITY

<u>Item No.</u>	<u>Description</u>
101	Calorimeter
102	Vacuum Chamber
103	4-inch Diffusion & Fore-Pump System
104	Liquid Nitrogen Supply - Calorimeter
105	Liquid Nitrogen Supply - Cold Guard
106	High Pressure Nitrogen Gas Supply
107	Vent Gas Heat Exchanger - Calorimeter
108	Vent Gas Heat Exchanger - Cold Guard
109	
P1-110	Pressure Indicator, 0-30 psia
P1-111	Manometer, 0-50 inches water
RV-112	Relief Valve, 2-inch, 5 psig set pressure
V-113	Globe Valve, 2-inch
T-114	Mercury Thermometer
T-115	Mercury Thermometer
F-116	Gas Flow Meter, 0.1 ft ³ /revolution, wet test
F-117	Gas Flow Meter, dry type, American Meter Type 25B
P-118	Pressure Gauge, 0-25 psig
PRV-119	Pressure Regulating Valve
P-120	Vacuum Gauge, 0-30 psia
LLR-121	Liquid Level Capacitance Meter
TR-122	Foil Temperature Recorder
V-123	Instrument Line Valve
P-124	Vacuum Gauge
V-125	Gas Line Valve
V-126	Cylinder Valve
T-127	Guard Gas Exit Temperature, Thermocouple



III-27

Arthur D. Little, Inc.

FIGURE III-11 FLOW SCHEMATIC OF ARTHUR D. LITTLE, INC., TEST FACILITY

thermally bonded to the vent, which received a separate supply of liquid nitrogen. The heat was carried away by the vaporized nitrogen.

The cold guard was supplied from a 100-liter commercial dewar that was pressurized from a high pressure gas supply (Figure III-11). The cold guard temperature was maintained at a level a few degrees above the calorimeter temperature to prevent recondensation of the calorimeter vent gases. The cold guard vent gases were brought to room temperature by an air-warmed heat exchanger. The pressure, temperature, and flow quantity of this gas stream, as well as the cold guard temperature, were monitored to assure proper performance of this system.

The calorimeter vent gas was brought to room temperature in an air-warmed heat exchanger. The stream flow was measured with a wet test meter. The temperature and pressure of the stream at the meter inlet were measured so that appropriate corrections to the flow quantities could be made.

When the calorimeter was placed into the vacuum chamber, the following principal steps were taken to place the system in operation:

1. The chamber was slowly and uniformly evacuated from atmospheric pressure to approximately 0.25 inch of mercury over a period of one hour. This rate was based on a conservative estimate of the pressure gradient within the foil system that would avoid the possibility of damaging the system.
2. Next, the chamber pressure was reduced to approximately 10^{-4} mm Hg over a period of 24 hours while the chamber, insulation, and other surfaces were outgassing.

3. The calorimeter was then filled from the 500-gallon liquid nitrogen supply tank. When the calorimeter was full, the transfer line was disconnected from the calorimeter, and the calorimeter filling connection was blanked off.

4. Subsequently, the cold guard dewar was pressurized from the high pressure gas supply, and the vent gas rate was set by throttling valve V-128.

5. During and after the approach to temperature equilibrium of the insulation system, we measured the following data:

- a. Calorimeter vent gas flow, F-116.
- b. Calorimeter vent gas temperature, T-115.
- c. Calorimeter vent gas pressure, P-111.
- d. Local barometric pressure.
- e. Guard vent temperature, T-127.
- f. Guard vent temperature, T-117.
- g. Guard vent pressure, P-118.
- h. Guard vent flow, F-117.
- i. Chamber vacuum, P-124.
- j. Chamber wall temperature.
- k. Shield temperatures.

E. Auxiliary Equipment

In the early months of the program we acquired certain support equipment to be used with the calorimeter. The principal items in this group include the calorimeter mounting fixture, dummy tank, and shipping container.

A mounting fixture for positioning the calorimeter tank while the insulation was being applied was deemed necessary. The insulation system is easily degraded if severely compressed or struck with any objects. To minimize such contacts, a fixture was designed that would grip the calorimeter flange and position any portion of the tank surface in any desired orientation. This fixture is shown in Figure III-12.

The design and fabrication of the calorimeter occupied a significant portion of the program period. To initiate development of the insulation system as soon as possible after the start of our program, we fabricated a steel "dummy tank" having dimensions almost identical to those of the calorimeter vessels. This vessel is shown in Figure III-12 assembled into the mounting fixture.

During shipment between the Arthur D. Little, Inc., facility in Cambridge, and the NASA/Lewis facility at Plum Brook, the insulated calorimeter must be completely protected from contact with foreign objects and oil and other contaminants that would degrade the insulation. We have designed a shock mounted container, shown in Figure III-13, that will support the calorimeter by its flange and completely enclose it. The container is mounted on a pallet to facilitate handling with a fork-lift truck.

IV. Experimental Results

A. Experimental Program

At the initiation of the insulated tank program, a series of seven tests at liquid hydrogen temperatures were planned within the current contract period. These tests are identified in the Third Quarterly

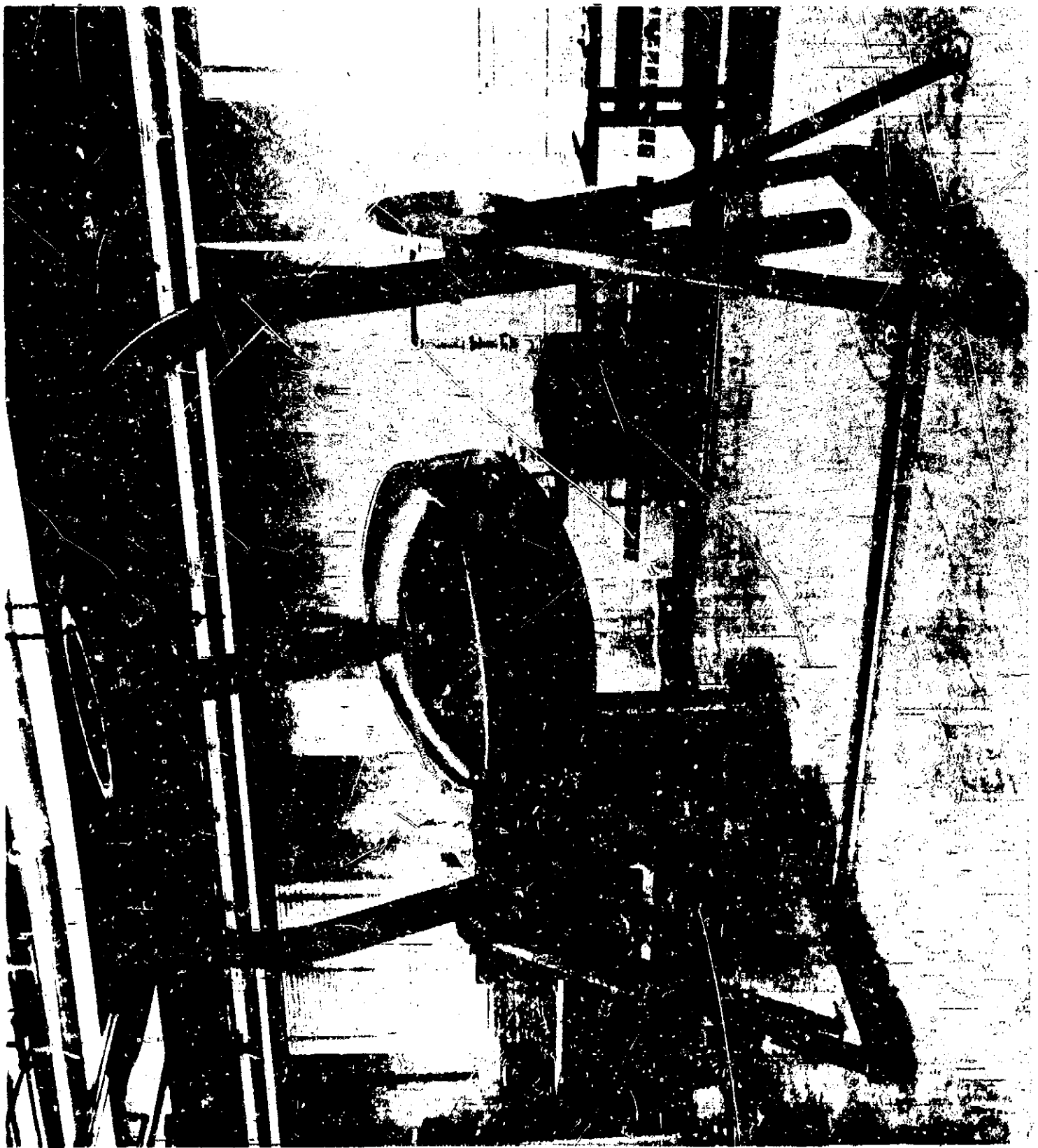


FIGURE III-12 DUMMY TANK AND MOUNTING FIXTURE

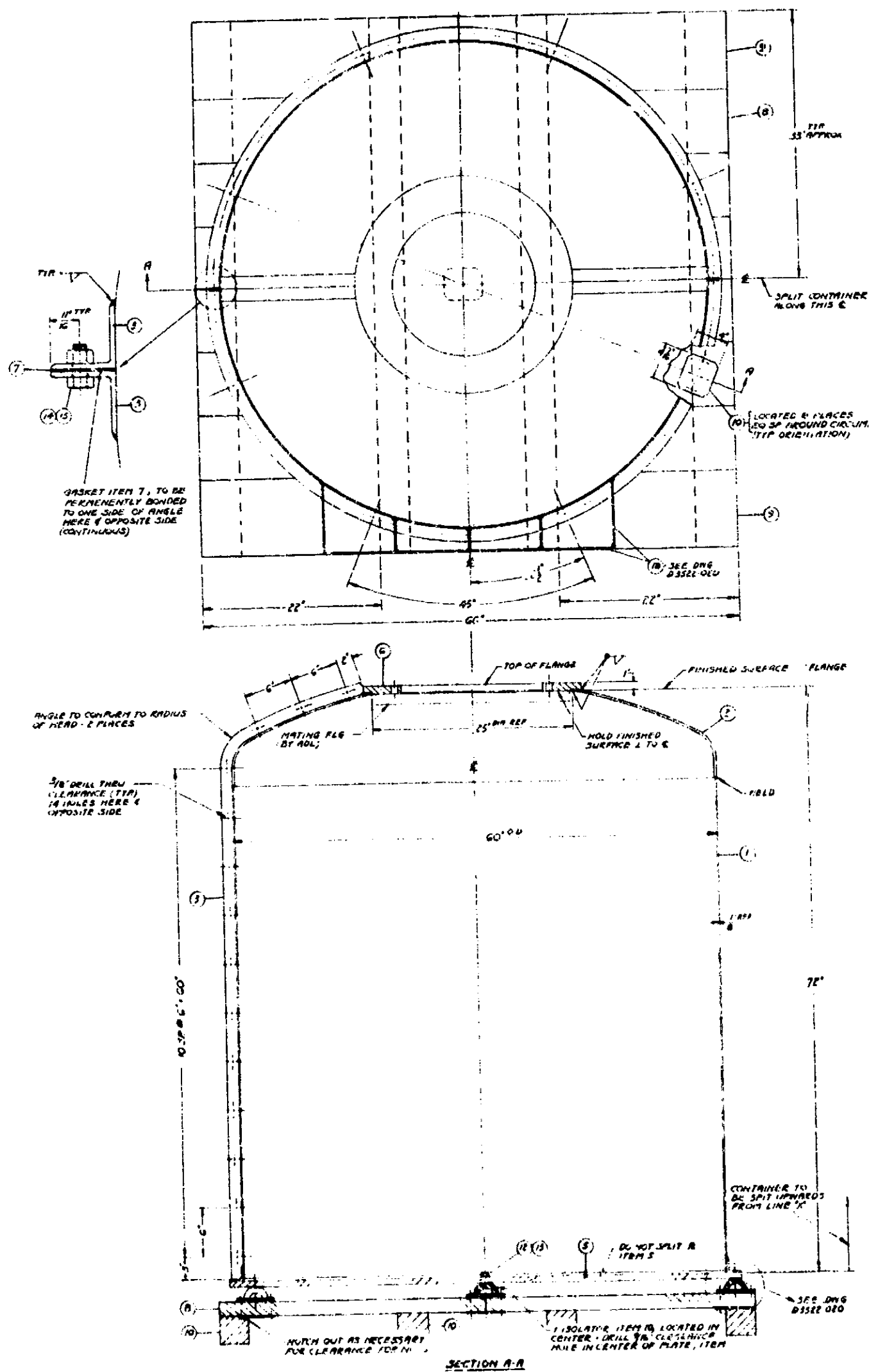


FIGURE III-13 SHIPPING CONTAINER

Progress Report and included tests on a system incorporating aluminum radiation shields and on a system incorporating aluminized polyester film radiation shields. The heat transfer performance of each was to be measured with and without simulated gaps and structural penetrations in the insulation system. Because of continued interference, by other programs, in the scheduled use of the J-3 facility at the Plum Brook station, all tests originally planned were cancelled. The test objectives of the program were subsequently limited to tests that could be obtained with liquid nitrogen at Arthur D. Little, Inc.'s, facilities in Cambridge.

The two systems tested have been described in a previous section and the principal characteristics listed in Table III-I. The aluminum foil system was tested in the period June 27 to July 3. The second system was tested in the period September 24 to 30. In each case the insulated calorimeter tanks were mounted into a 5-foot diameter vacuum chamber as shown in Figure III-3. With the chamber evacuated to a pressure of less than 10^{-5} mm Hg and with liquid nitrogen in the calorimeter tank, we measured the quantity and rate of vaporized nitrogen and also the distribution of temperature within the shields. The liquid nitrogen bath within the calorimeter tank maintained the cold boundary uniformly at -320°F , while the warm boundary, formed by the chamber wall, was maintained at room temperature by room air convections.

B. Measured Heat Flux

The total heat rate to the calorimeter insulation over a given data interval is related to the boil-off in the following manner. Three factors contribute to the boil-off of liquid nitrogen from the calorimeter

tank. The first two are heat leaks and consist of the heat flow through the insulation system and the heat flow through the calorimeter support system. These two cannot be distinguished from one another readily except when the latter is minimized by appropriate design and system operation. The third contributor is the change in the barometric pressure which becomes reflected in changes in calorimeter ullage pressure. The liquid nitrogen bath becomes a heat reservoir that stores heat when the pressure is rising and releases heat with a decline in pressure. Changes in the stored heat quantities must be accounted for, as they promote changes in the vent gas quantities.

The total heat rate comprising heat leaks and pressure changes is computed from the total nitrogen gas mass vented in the data interval and the latent heat of vaporization of liquid nitrogen. The gas mass is computed from the integrated volume measurement of the calorimeter vent gas stream and its temperature and pressure at the metering point. An hourly heat flow rate is next computed based upon the length of the data interval.

When the barometric pressure does not change over the data period, the computed heat-flow rate is also the rate corresponding to the insulation and support heat leak. In Test No. 1, the barometric pressure remained constant through the test period. Test No. 2 was conducted under conditions of rapidly varying atmospheric conditions and pressure. The measured heat flow was corrected from the computed value of heat storage or heat release in the following manner. The average mass of the liquid bath during the data interval was established from the liquid-level

measurement, tank-volume calibration, and liquid density. The increase or decrease in the saturation temperature of the bulk liquid at the end of the data interval as compared to that at the beginning is determined from the change in the calorimeter ullage pressure, which is a function both of the local barometric pressure and the pressure loss in the vent system. From the change in the bulk temperature and the liquid specific heat at saturation, the total heat energy stored or released during the data interval was computed and converted into an hourly rate. Any heat stored during the data interval was added to the heat flow determined from the calorimeter boil-off; a release of heat during the data interval was subtracted. The corrected values for the total heat flow are presented in Tables III-III and III-IV for Tests Nos. 1 and 2, respectively.

The data for the aluminum foil system are presented in Table III-III. The test was divided into eight data periods in which the guard temperature remained relatively constant. A depletion of liquid or gas in the guard supply system (see Figure III-11) produced these many interruptions. The changes in guard temperature level were the result of the attempt to economize on the liquid supply; the system flow would be set for a guard temperature of about -310°F , but when left unattended it always achieved a higher equilibrium temperature. Thus, if anything, the resulting computed total heat flow is higher at the higher guard temperature than that due to the insulation only, because of the contribution of the support heat leak which cannot be accurately defined.

TABLE III-III

TANK INSULATION PROGRAM

TEST NO. 1 ALUMINUM FOIL SYSTEM

Insulation System: Five aluminum radiation shields, .002 inches thick spaced with 1/8 mesh, vinyl coated, fiberglass screen .020 inches thick. See Table III-I for complete details.

Penetration and/or Gaps: None

Boundary Condition: Cold Boundary Warm Boundary
Temperature (ave) -320°F 74 - 90°F
Emissivity 0.97 0.97

Tank Surface Area: 38.14 ft²

Test	Data Period		Test Duration (hrs)	Average Vac (mmHg)	Guard Temp (°F)	Total Heat Flow (BTU/hr)	Measured Average Heat Flux		Chamber Temp (°F)	Adjusted Heat Flux (BTU/hr ft ²)
	Date & Time	Date & Time					(BTU/hr ft ²)	(1)		
1-A	6-28/1730	6-29/0150	8.33	0.53x10 ⁻⁵	-286	24.4 (1)	0.640	(1)	82	0.628
1-B	6-29/0215	6-29/1135	9.33	0.35x10 ⁻⁵	-245	15.1	0.396		75	0.412
1-C	6-29/1700	6-30/0010	7.17	0.34x10 ⁻⁵	-205	14.8	0.388		74	0.406
1-D	6-30/0100	6-30/1200	11.00	0.20x10 ⁻⁵	-20 (6)	23.5 (2)	0.616	(2)	77	0.633
1-E	7-1/0115	7-1/1315	12.00	0.35x10 ⁻⁵	-205	18.1	0.475		83	0.465
1-F	7-1/1750	7-2/0915	15.42	0.45x10 ⁻⁵	-248	14.5	0.380		87	0.363
1-G	7-2/1210	7-2/1645	4.59	0.47x10 ⁻⁵	-307	16.2	0.442		90	0.413
1-H	7-2/1600	7-2/2300	7.00	0.55x10 ⁻⁵	-309	13.5	0.364		86	0.349

Calculated ave. heat flow for periods B,C,D,E,F and G = 15.1 BTU/hr
Calculated ave. heat flux for periods B,C,D,E,F and G = 0.50 BTU/hr ft²

- (1) Not included in calculation of average value, insulation still cooling down.
- (2) Not included in calculation of average value because guard coolant was depleted.
- (3) Vacuum chamber wall assumed to be in equilibrium with room environment.
- (4) Adjusted to warm boundary temperature of 80°F.
- (5) Temperature noted is actually the guard vent gas temperature which is higher than the guard temperature based on data obtained in Test No. 2.
- (6) Based upon data from calorimeter Test No. 2.

TABLE III-IV

TANK INSULATION PROGRAM

TEST NO. 2 ALUMINIZED POLYESTER FILM SYSTEM

Insulation System: Five aluminized polyester film (NRC) radiation shields, 0.0025 inch thick, spaced with 1/8 mesh, vinyl coated, fiberglass screen 0.020 inch thick. Uncrinkled polyester film placed on tank with aluminized surface facing warm boundary. For complete details see Table III-1.

Penetrations and/or Gaps: None

Boundary Conditions: Cold Boundary Warm Boundary
 Temperature (ave) -320°F $60-73^{\circ}\text{F}$ (ave)
 Emissivity 0.97 0.97

Tank Surface Area: 39.45 ft^2

Test	Data Period		Test Duration (hrs)	Average Vac (mmHg)	Guard Temp ($^{\circ}\text{F}$)	Total Heat Flow (BTU/hr)	Heat Flux (BTU/hr ft^2)	Chamber Temp ($^{\circ}\text{F}$)	Adjusted Heat Flux (2) (BTU/hr ft^2)
	Date & Time	Date & Time							
2-A	9-25/0100	9-25/1630	15.5	0.15×10^{-5}	-314	40.3	1.02	60	1.19
2-B	9-25/1900	9-26/1930	24.5	0.15×10^{-5}	-317	40.0	1.01	76	1.04
2-C	9-26/2000	9-27/2315	27.25	0.20×10^{-5}	-222 & -158	51.8	1.31	75	1.36
2-D (1)	9-27/2315	9-30/0900	57.75	0.30×10^{-5}	-25	51.3	1.30	73	1.37

(1) Cold guard cooled by calorimeter boil-off only, no cold guard coolant flow.

(2) Adjusted to warm boundary temperature of 80°F .

The measured average heat flux through the insulation system was computed from the total heat flow and the area of calorimeter surface, assuming that the support heat leak is zero. As will be discussed later, this assumption is very good when the guard temperature is maintained below -300°F . A new guard system used in Test No. 2 assured this condition except when changed intentionally. However, for Test No. 1 there is no choice but to accept the heat flux as that passing through the insulation, except for Tests 1-A and 1-D. In Test 1-A, the measured foil temperatures indicate that the insulation system had not fully achieved temperature equilibrium until near the end of the data period. Test 1-D was performed intentionally without any guard flow, and the neck heat leak must, therefore, be significant.

The average temperatures of the chamber where the tests were performed are also listed in Table III-III. As can be seen, these average temperature values vary from test to test. Further, we assumed that the vacuum-chamber shell was in equilibrium with the room air. Measurements of the chamber wall and room ambient temperature during Test No. 2 indicate this assumption is good to within about 4°F . Thus, the warm boundary temperature varied from approximately 74°F to approximately 90°F .

Considering an ideal case where radiation is the sole mode of heat transfer, a change of 5°F in the warm boundary temperature results in a 3.5% change in heat transfer rate at the temperature levels under consideration. As will be pointed out later, the data indicate that

radiation is the principal heat transfer mode. Thus, in order to appropriately compare the heat transfer data obtained in one data period with that of a second data period, it appears reasonable that comparison be accomplished at a single warm boundary temperature. We have chosen to compare all heat fluxes at a warm boundary temperature of 80°F , using the fourth-power temperature difference of the Stefan-Boltzmann radiation equation to make the adjustment from the experimental boundary conditions. These adjusted values are presented in the last column in Table III-III.

A plot of heat flux vs guard temperature does imply a trend of higher heat leak at the higher guard temperatures. This is shown in Figure III-14 for Tests 1-A through 1-J. At guard temperatures below -240°F , the mean heat flux, weighted in terms of the test duration, appears to remain nearly constant at a value of 0.38 BTU/hr ft^2 . At higher values of the guard temperature, the heat fluxes computed from the vent gas appear to increase almost linearly to an equivalent value of 0.65 BTU/hr ft^2 which is obtained when the guard is not provided with coolant.

Note that in Test No. 1 the guard temperature levels were established from the temperature of the guard vent gas. From the data obtained in Test No. 2, where the temperature of both the guard and guard vent gas were measured, we determined that the guard was approximately 40°F or less below the vent gas temperature except when there was no coolant flow or very little coolant flow. With no coolant flow the guard in Test No. 2 achieved a steady state temperature of -20°F when the vent gas thermocouple indicated a temperature of about 70°F . Thus, in presenting the data for Test No. 1 in Figure III-14, the guard vent gas temperatures are used as guard temperatures except for Tests 1-D and 1-J, where the temperature used is that measured in Test No. 2.

Arthur D. Little, Inc.

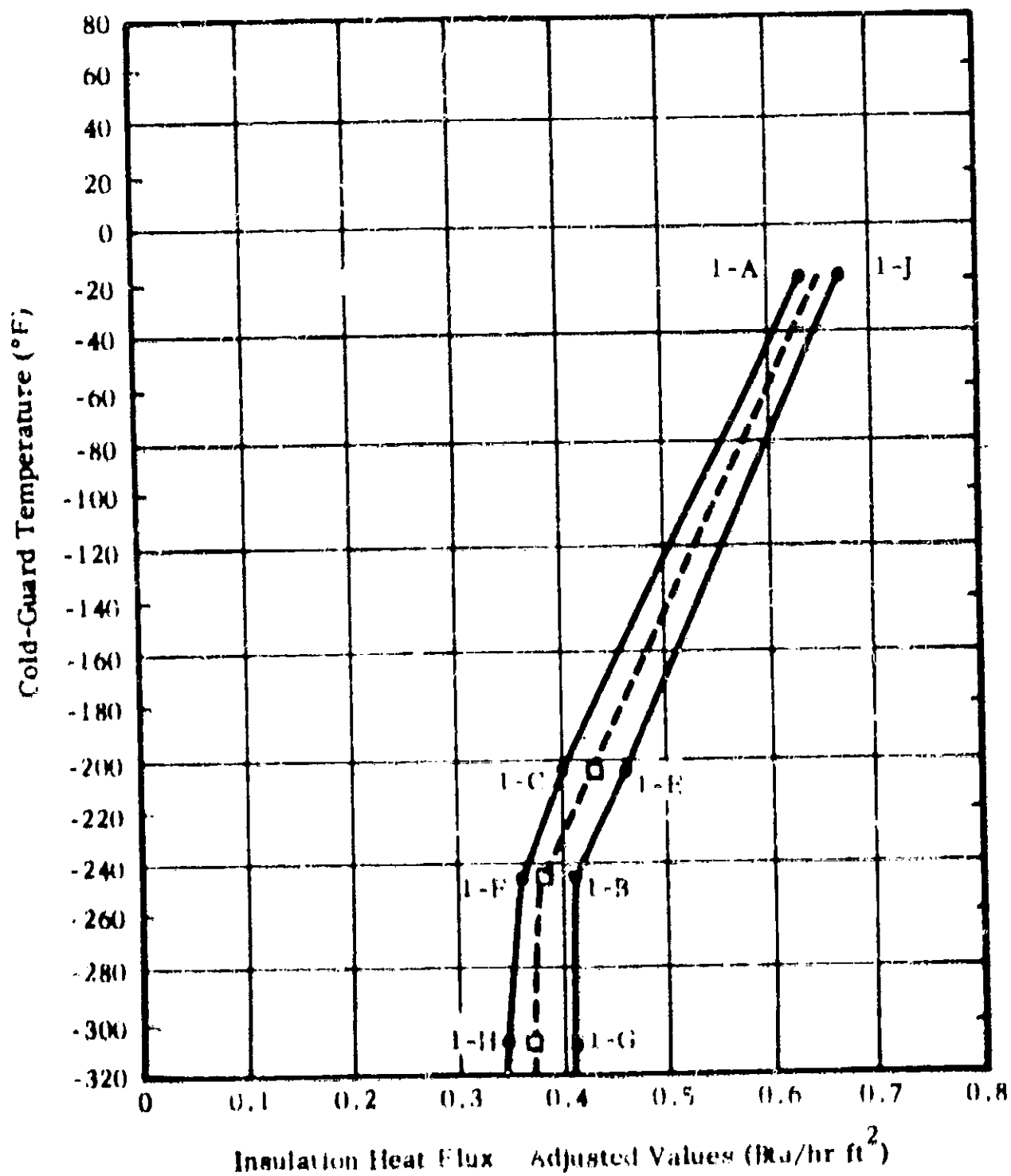


FIGURE III-14 INSULATION HEAT FLUX VS COLD-GUARD TEMPERATURE - ALUMINUM-RADIATION SHIELD SYSTEM

I
2

In order to compare the results of these tests with those obtained with the thermal conductivity apparatus, we computed a weighted and adjusted average heat flux value of $0.402 \text{ BTU/hr ft}^2$ for Tests 1-B, C, E, F, G, and H. Further we normalized the thermal conductivity apparatus data with respect to warm boundary temperature, number of radiation shields, and warm and cold boundary emissivity. The normalized values are presented in Table III-V for 14 tests along with the originally reported heat flux values and other pertinent data. With one exception the tank calorimeter flux is lower than those obtained with the thermal conductivity apparatus. This is an unusual result in view of the much greater complexity of the tank insulation system.

For several reasons, no attempt has been made to compute the thermal conductivity of the insulation system. The insulation thickness is not uniform. For example, at the knuckle radii on the tank heads, the insulation build-up is about $1/16$ inch for each layer of aluminum and spacer netting. Second, the top and bottom of the calorimeter tank are not perfect spherical segments. The aluminum foils and netting are, therefore, spaced away from the tank at certain locations. Third, it is extremely difficult to measure the distance that the outer foil is displaced away from the tank. In view of the probable wide variation in thickness and difficulty of measurement any reported thermal conductivity values for the tank systems would be misleading.

The data obtained with the aluminized polyester film radiation shields are presented in Table III-IV. Considerably improvement in the length of the data periods as well as improved guard temperatures was achieved

TABLE III-V

THERMAL CONDUCTIVITY APPARATUS DATA

Test No.	Test Date	Shield Data	Spacer Data	Press. (torr)	Source		Sink		Exp. Heat Flux	Adjusted Heat Flux	References
					Temp (°F)	E	Temp (°F)	E			
1005	Sep-Nov 62	10, AL	11, vinyl-coated glass fiber screen 1/8"x1/8" mesh	1x10 ⁻⁵	41	0.3	-320	0.1	0.32	0.89	Sep-Dec Quart, P28
(1)											
2004	Sep-Nov 62	Same as 1005	Same as 1005	1x10 ⁻⁵	64	0.3	-320	0.1	0.23	0.532	Sep-Dec Quart, P28
(1)(2)											
3000	Sep-Nov 62	Same as 1005	Same as 1005	9x10 ⁻⁵	57	0.3	-320	0.1	0.23	0.557	Sep-Dec Quart, P28
(1)(2)											
1032	15 Oct 62	10, AL, H-19 .002" He	11, glass fiber mat, 0.008" thick 50% perforations	3x10 ⁻⁵	61	0.2	-423	0.1	0.20 and 0.80	0.460	Sep-Dec Quart, P17
3005F	9 Feb 63	10, AL, H-19	Same as 1005	1x10 ⁻⁵	37	0.3	-320	0.9	0.18	0.495	Jan-Mar Quart, P77
(1)(3)											
2014	15 May 63	Same sample as 3005F	Same sample as 3005F	<5x10 ⁻⁵	37	0.3	-320	0.1	0.18	0.512	Apr-Jun Quart, P48
(1)(3)											
1044	13 Jun 63	Same Sample	Same Sample	<5x10 ⁻⁵	37	0.3	-320	0.1	0.21	0.60	Apr-June Quart, P48
(1)(3)											
2013d	28 Mar 63	10AL, 0.001" tk.	10 glass fiber paper, .003" thick	1x10 ⁻⁵	45	0.03	-423	0.3	0.2	0.497	Apr-Jun Quart, P30
(4)											
1049c	11 Sep 63	10, AL, H-19 0.002" thick	11, vinyl coated glass fiber screen 1/8"x1/8" mesh		67	0.3	-320	0.9	0.24	0.555	Sep (3, Monthly P7

Arthur D. Little, Inc.

TABLE III-V (continued)

Test No.	Test Date	Shield Data	Spacer Data	Press. (torr)	Source		Sink		Exp. Heat Flux		Adjusted Heat Flux	References
					Temp (°F)	E	Temp (°F)	E	BTU/hr ft ²			
1049d	11 Sep 63	Same as 1049c	Same as 1049c		68	0.3	-623	0.9	0.21	0.458		Sep 63, Monthly P7
20261	12 Sep 63	10, AL	11, glass fiber mat .014" thick	$<1 \times 10^{-5}$	69	0.3	-423	0.9	0.099	0.216		Sep 63, Monthly P8
2027a	16 Sep 63	10, AL	11, glass fiber cloth .004" thick, 3 per spacer	$<1 \times 10^{-5}$	69	0.3	-423	0.9	0.24	0.506		Sep 63, Monthly P9
3028g	5 Sep 63	6, AL, H-19 0.002" thick	7, CTL, 11% support area	$<5 \times 10^{-5}$	66	0.3	-320	0.9	0.31	0.416		Sep 63, Monthly P10
1043h	28 May 63	10, AL 0.001" thick	11, glass fiber paper .003" thick	2.4×10^{-5}	56	0.3	-423	0.1	0.23	0.558		
1032	30 Oct 62	20, crinkled Al-mylar, 2 per foil, back to back	11, vinyl coated glass fiber screen, 1/8"x1/8" mesh	10^{-5}	66	0.2	-320	0.1	0.5	1.38		Sep-Dec, Quart, P16
2005	26 Oct 62	60, mylar 1/4 mil, Al one side crinkled	61, glass fiber cloth, .001" thick	10^{-5}	62	0.2	-320	0.1	0.7 and 0.35	4.88		Sep-Dec Quart, P21
3001	30 Oct 62	50, 1/4 mil mylar, Al one side, crinkled	none	$<10^{-5}$	54	0.2	-320	0.1	0.089	1.30		Sep-Dec Quart, P20

TABLE III-V (continued)

Test No.	Test Date	Shield Data	Spacer Data	Press. (torr)	Source		Sink		Exp. Heat Flux	Adjusted Heat Flux	References
					Temp (°F)	E	Temp (°F)	E			
1033	1 Nov 62	10, 1/4 mil mylar, Al one side, crinkled	11, glass filter mat, .006" thick 50% perforation	10^{-5}	54	0.2	-423	0.1	0.6 and 0.3	0.75	Sep-Dec Quart, P25
2008P & I	4 Jan 63	95, 1/2 mil mylar, Al one side	96, fabric	$<10^{-5}$	48	0.3	-423	0.1	0.47 and 0.13	4.06	Jan-Mar Quart, P69
1036A Company P	10 Jan 63	20, 1/4 mil mylar, Al one side crinkled	none	$<10^{-5}$	47	0.3	-320	0.1	0.8	4.2	Jan-Mar Quart, P73

NOTES:

- (1) Calorimeter calibrations.
- (2) Same test article used in Tests 2004 and 3000; similar insulation used in Test 1005.
- (3) Same test article used in Tests 3005P, 2014, and 1044.
- (4) Bottom radiation shield was in contact with warm plate.

through the use of a revised guard system. In these tests both the guard and chamber temperatures were measured directly with thermocouples and continuously recorded. The basic heat transfer information was obtained in Tests 2-A and 2-B with the guard maintained at -314°F and -317°F , respectively. In order to evaluate the heat leak to the calorimeter through the support system, we operated in Test 2-C with a restricted flow of guard coolant and in Test 2-D without any guard coolant. As evident from the data, the total heat flow increased a maximum of 30% under these conditions.

The heat flux data obtained in Test No. 2 has been normalized to a warm boundary temperature of 80°F . The adjusted heat flux value for Tests 2-A and 2-B give a weighted average value of 1.1 BTU/hr ft^2 . This value is approximately 20% below the normalized value obtained in Test 1032 on a comparable insulation system and about 30% greater than the normalized lowest value obtained in Test 1033 with glass fiber mat, 0.008 inch thick, perforated 50%. Data obtained with the thermal conductivity apparatus on four other aluminized polyester film systems are presented for comparison in Table III-V. It should be noted that these systems are different from the one tested with the tank calorimeter.

C. Radiation Shield Temperature Distribution

The temperatures of the radiation shields at select locations were continuously recorded during the progress of the calorimetric measurements on the multilayer insulation. These data are of great importance for inferring what are the principal heat transfer modes of the tested systems and for showing up imperfections in the application techniques.

The analysis of the temperature data was simplified by the use of high emissivity coatings that were applied to the source and sink boundaries. Both the vacuum chamber inner surface and the calorimeter tank outer surface were coated with 3M Brand Velvet Coating No. 9564 optical black, for which we have previously measured a total hemispherical emissivity of 0.97. When boundary emissivities are large (by a factor of 10 or greater) in comparison to the radiation shield emissivities the value of radiant heat flux component is determined primarily by the radiation shield performance. A low emissivity on the boundaries cannot be known accurately while its effect on the value of the radiant heat flux is significant, especially for a 5-shield system. The high emissivity coating on the warm boundary is of particular importance as the effect of the ratio of the insulation area to chamber wall area on the heat transfer between the two surfaces is made negligible.

The location of thermocouples within each insulation system is shown in Figure III-9. All except for thermocouples 1B and 1C on the aluminum system, which were made inoperative during fabrication of the insulation, performed well.

The measured shield temperatures are presented in Figures III-15 and III-16 for the aluminum and aluminized polyester film systems, respectively. In Figure III-16, two things are immediately apparent. First, the "A" thermocouples on all shields read significantly lower temperatures than "B" and "C" thermocouples. Second, the shield temperatures actively responds to vacuum chamber temperature, particularly in late afternoons, when a portion of the chamber was in direct sunlight. This effect points up the need for providing good temperature control of the warm boundary.

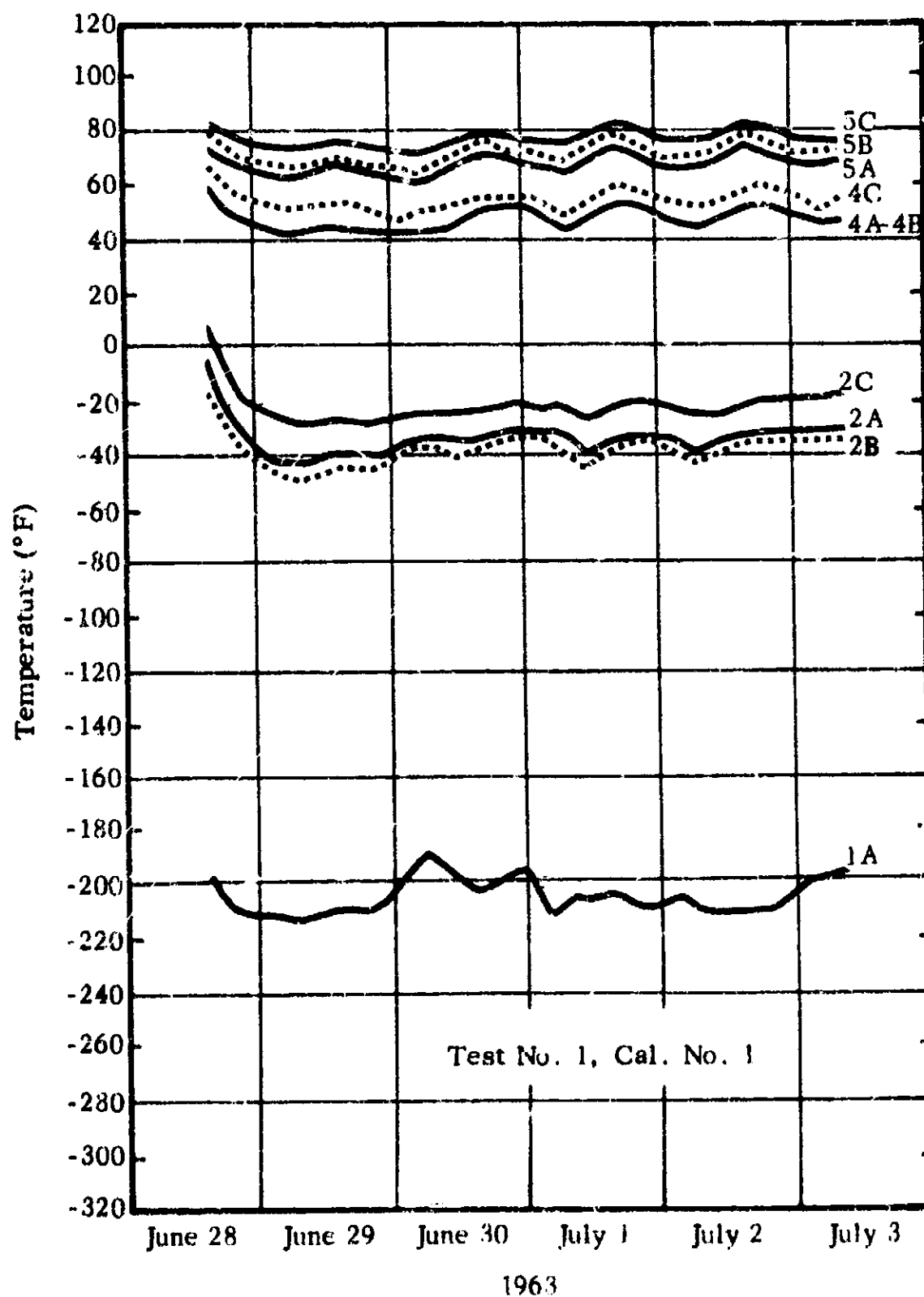


FIGURE III-15 ALUMINUM-FOIL SYSTEM FOIL TEMPERATURE DISTRIBUTION

Note: Refer to Figure III-9 for thermocouple locations.

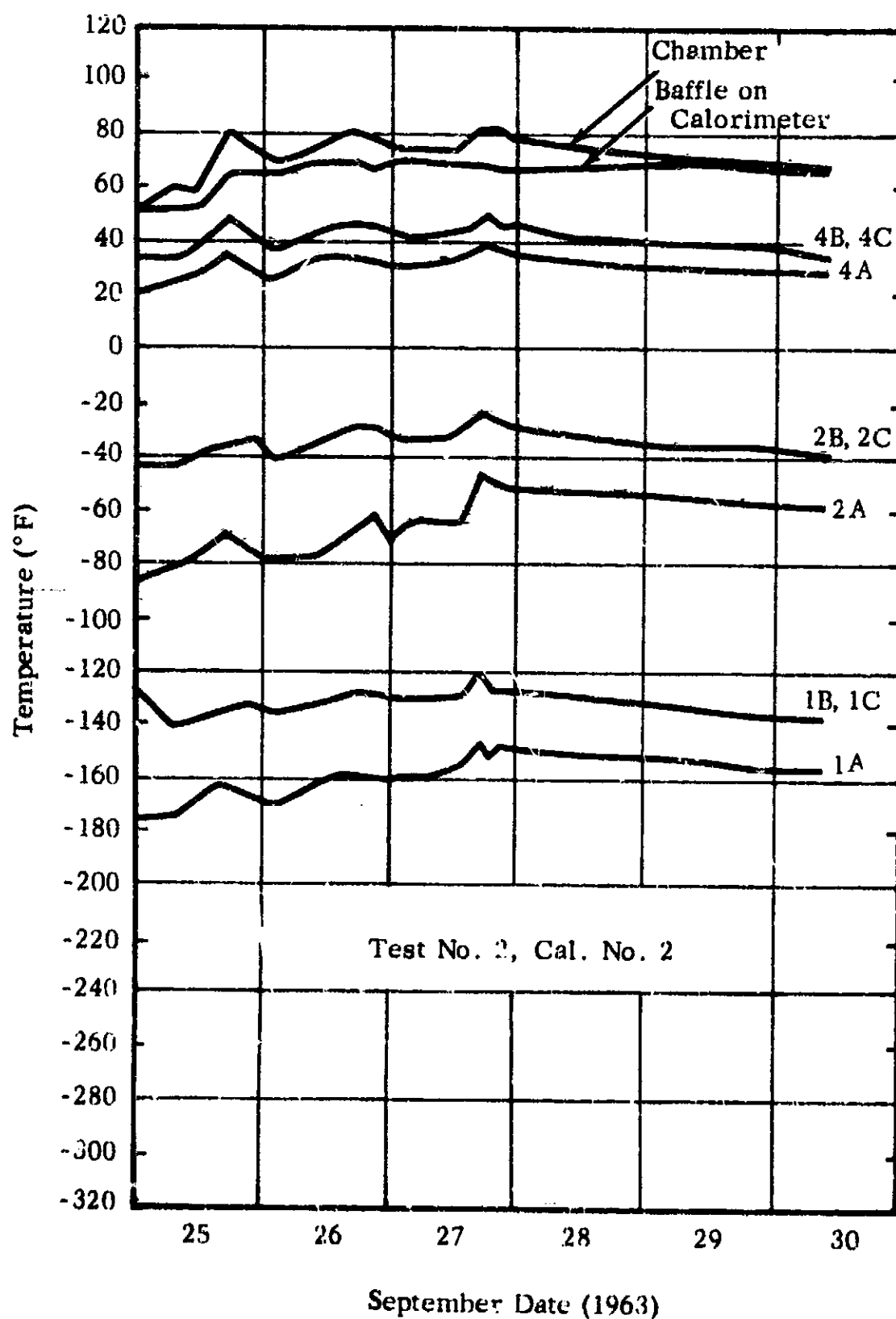


FIGURE III-16 ALUMINIZED-POLYESTER-FILM
SYSTEM--FOIL TEMPERATURE
DISTRIBUTION

Note: Refer to Figure III-9 for thermocouple location.

From the average boundary conditions and the measured heat fluxes the average apparent shield emissivities were computed. Average values of 0.0254 and 0.069 were obtained for the aluminum and aluminized film, respectively. Then through use of these emissivities the theoretical shield temperatures were determined. The computed temperatures are compared in Figures III-17 and III-18 with the experimentally determined temperatures for the two systems under consideration here. The periods for which the data is presented were selected on the basis of the lowest guard temperature achieved. Tests 1-G and 1-H were used for the aluminum shield system, and Test 2-B was used for the aluminized film system.

Radiation shields 2, 4 and 5 of the aluminum system are generally higher in temperature than the computed values. Considering only the radiation-heat-transfer mode, a decrease in shield emissivity with increasing temperature would promote this effect. Though not accurately established, there is an experimental as well as theoretical basis for the proportionality between emissivity and absolute temperature of aluminum and other metallic radiation shields. Were it not for the varying warm boundary conditions and the many interruptions in the test due to loss of the guard supplies, a correlation of the temperature and emissivity would be attempted.

However, in addition the single thermocouple on No. 1 foil shows a shield temperature which is on the average about 55°F below the computed value for this shield. A thermal short between No. 1 shield and the calorimeter could promote an effect similar to the one noted. While no electrical continuity existed between the two during fabrication of the insulation system, subsequent movement of the calorimeter could have

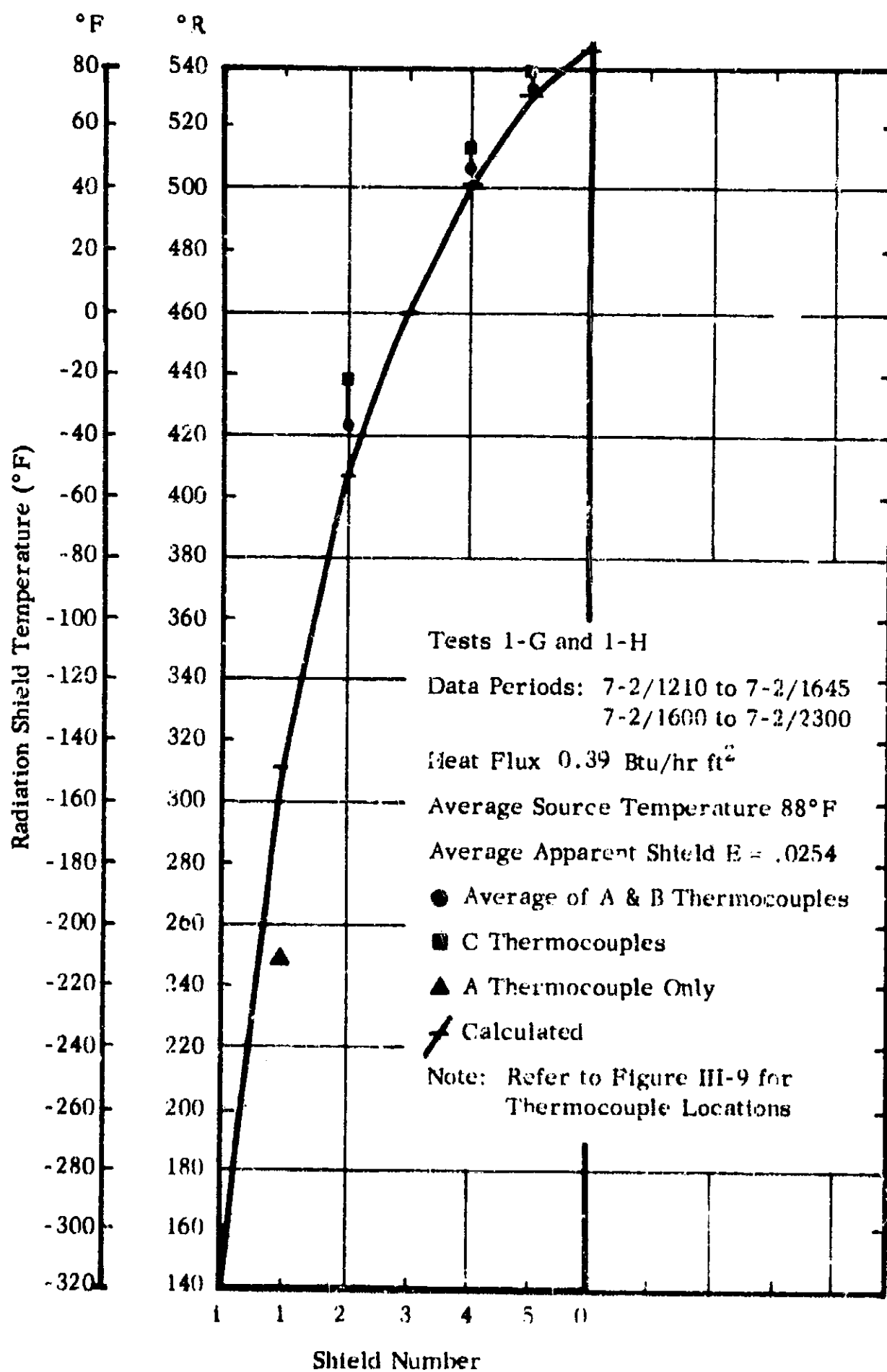


FIGURE II-17

RADIATION-SHIELD TEMPERATURE DISTRIBUTION--FIVE-FOIL ALUMINUM SYSTEM

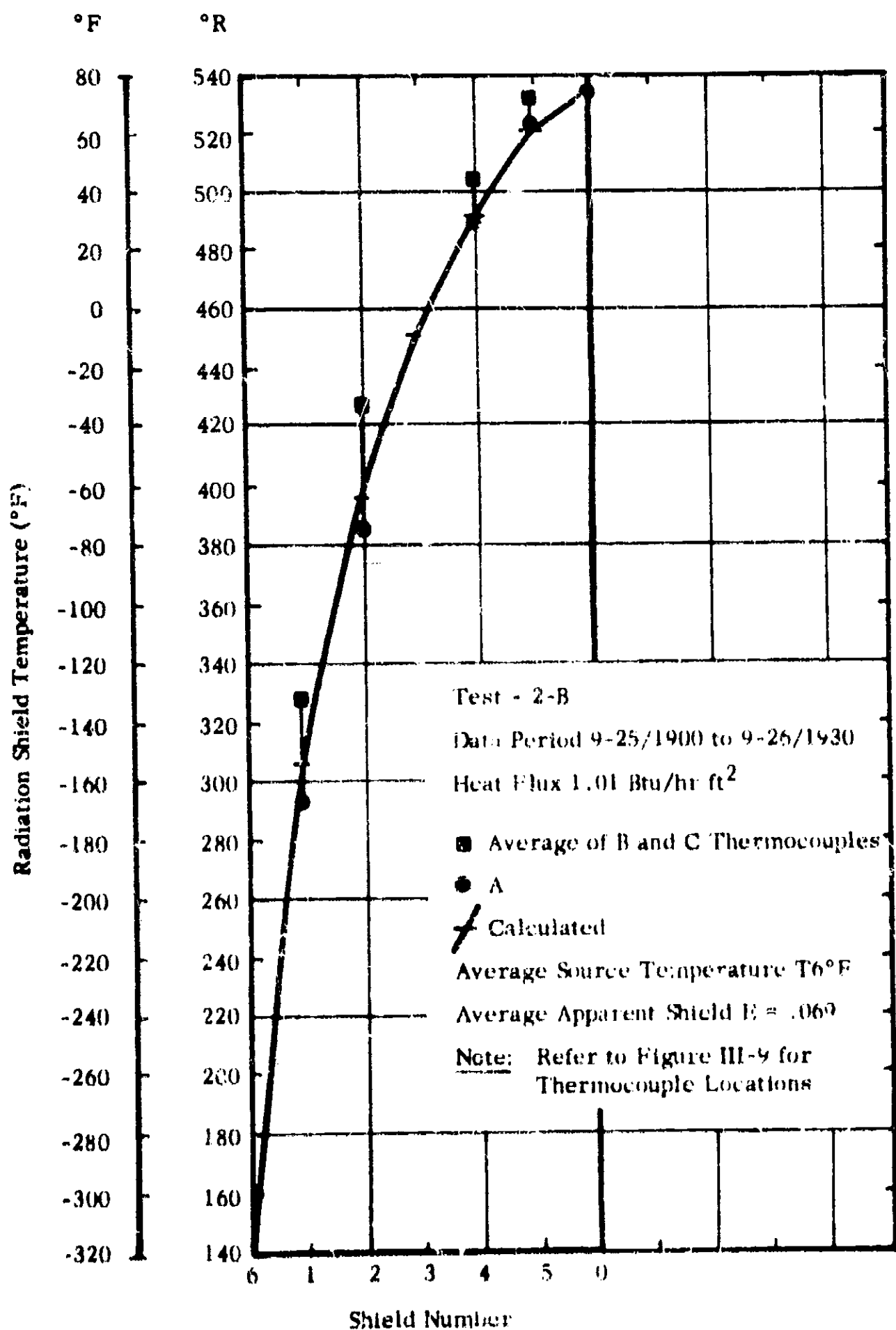


FIGURE III-18

RADIATION SHIELD TEMPERATURE DISTRIBUTION FIVE-FOIL ALUMINIZED-POLYESTER-FOIL SYSTEM

resulted in a short either at the pin locations (cylindrical portion of the tank, see Figure III-4) or at the edges of the aluminum foil. A sliver attached to the foil may have contacted the calorimeter tank. Foil No. 1 is not currently accessible and, therefore, an electrical continuity check to demonstrate shorting cannot be performed. It is to be noted that a short did exist, after fabrication of the insulation system, between shields No. 3 and 4. As the temperature of shield No. 3 is not measured, we cannot determine the magnitude of its effect. However, judging from the heat transfer performance of this insulation system and the measured temperature of shield Nos. 2 and 4, we surmise that the thermal shorting is of small value.

The shield temperatures at the "A" location in the vicinity of the neck edge are very close to the computed values and both are significantly lower than the "B" and "C" location temperatures. Order-of-magnitude estimates indicate that the loss of radiation from the shields through the edge to the neck support may account for the lower temperature near the edges. It must be noted that the edge guard (see Figure I-1-8) does not actually guard the first layers of the insulation system, because a space must be allowed between the guard and calorimeter to prevent thermal shorting of the two. While the guard will produce the same effect as the neck when it is at -300°F , an opposite effect should result when it is warmed as in Test 2-C and 2-D; i.e., the "A" temperature should rise higher than the "B" and "C" location temperature; because of radiation directed into the edges. However, this opposite effect did not take place. We expect to pursue several approaches to explain the observations, one of which includes the calibration of all the thermocouples that are accessible.

In all that has been stated thus far, little mention has been made of effect of the spacer and molecular conduction effects. We have assumed that negligible values have been accorded to these except for the weak short existing between No. 1 aluminum shield and the calorimeter.

For example, spacer and molecular conduction have two effects: first, they increase the unit heat transfer rate of the insulation; and second, they alter the temperature distribution of the radiation shields. With regard to the former, the heat flux measured with the aluminum shields is what would be predicted from a consideration of the radiation component alone, provided that account was taken of the decrease in emissivity with temperature. Molecular conduction has the effect of reducing the temperature difference between radiation shields. For example, if molecular conduction accounted for 10% of the heat flow between No. 1 shield and the calorimeter, the foil temperature decrease would be about 15°F in either system. This would be brought about by a residual gas pressure of about 0.3×10^{-4} mm Hg in the aluminized film system and 0.13×10^{-4} mm Hg in the aluminum shield system. While we did not measure the interstitial pressure, the chamber pressure was maintained about one magnitude lower than either of these values. In the aluminum system, if molecular conduction had resulted in a low No. 1 foil temperature, then molecular conduction would have caused a similar reduction in the No. 2 shield temperature. In Figure III-19, the heat flow due to molecular conduction is presented as a function of residual gas pressure (nitrogen) and the differential temperature between shields.

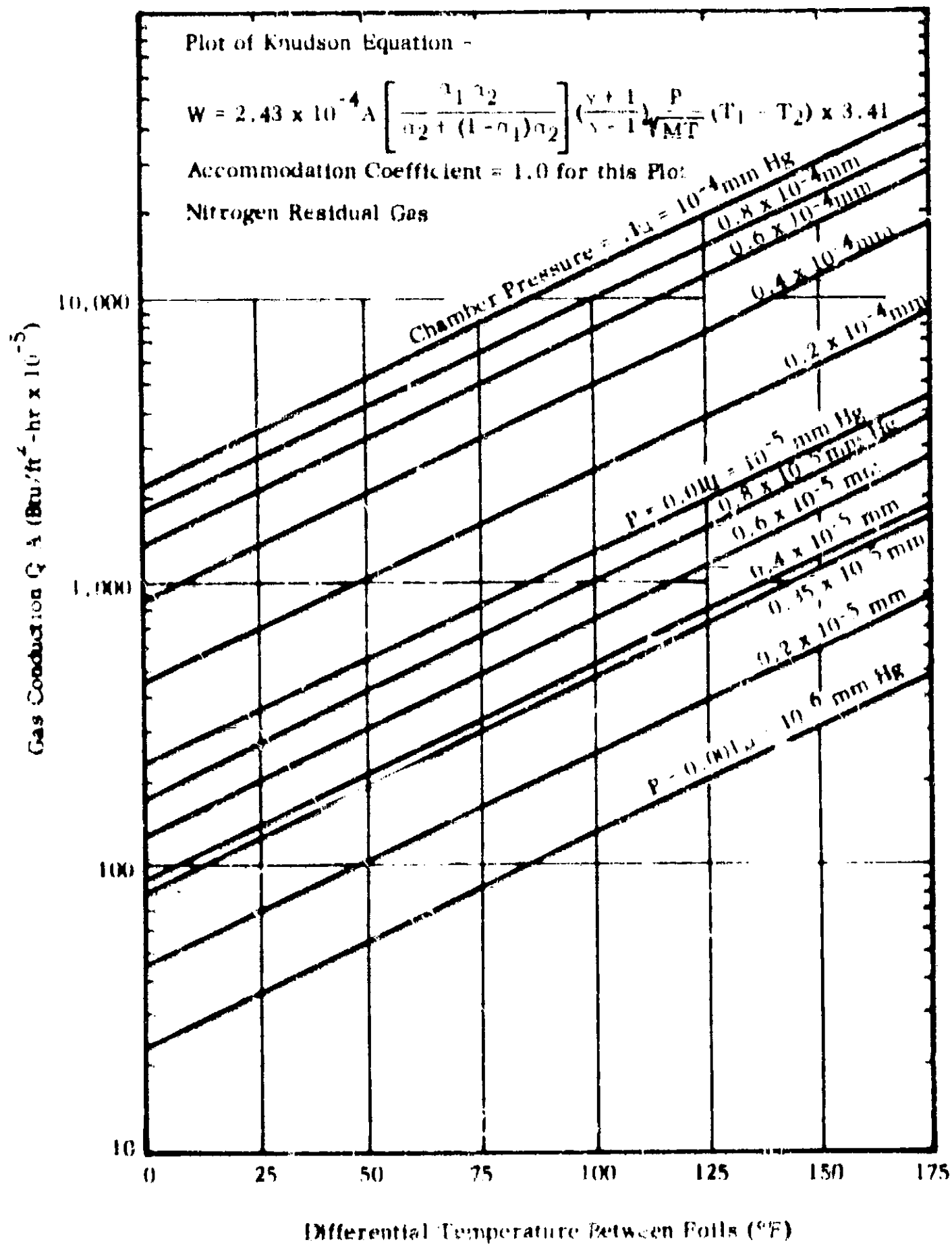


FIGURE III-19

RESIDUAL GAS HEAT TRANSFER

D. Application of Insulation

Several comments can be made at this time with respect to the relative difficulty of mounting the two multilayer insulation systems reported here. Generally, the aluminum is more difficult to cut than the mylar. Cutting of the aluminum produces slivers and pointed edges which must be carefully inspected and removed. Aluminum is less difficult to mount upon the tank and adjust into proper position than the mylar. However, once the mylar is located, the next layer of nettings can be sewed together without fear of creating strong thermal shorts, as is the case with aluminum shields.

Generally, the aluminum system was more difficult to apply to the calorimeter than was the aluminized polyester film system, as reflected in the greater elapsed time and manpower required for its installation.

V. Conclusions

1. Through the use of zores and/or pressure forming of the foils and spacers, multilayer insulations can be accurately conformed to segments of spherical and cylindrical surfaces.

2. By careful application of the foils and netting, heat transfer results comparable with those measured with the thermal conductivity apparatus are obtainable.

3. The measured temperature distribution in the radiation shields conforms generally to the theoretical distribution when radiation is the sole mode of heat transfer.

4. Thermal conduction due to the presence of the spacer and residual gas appears to be small for the systems and conditions tested.

5. From our experience it appears that aluminum radiation shields of 0.002-inch thickness may require more manpower and lapsed time to form and apply to the tank system than are required to form and apply 1/4-mil aluminized polyester film.

6. The 5-foil aluminum radiation shield system gave heat flux values nearly one-third the values obtained with the 5-foil aluminized polyester film. However, the computed $K \rho$ are nearly the same, i.e., 2.25×10^{-4} and 2.85×10^{-4} BTU-lb/hr ft⁴ °F for the aluminum and aluminized polyester systems, respectively based on calculated insulation thickness.

7. The results obtained thus far give promise that significant information applicable to future space-vehicle programs can be obtained with our current approach.

PART IV

EFFECT OF METEOROID BUMPER DEBRIS ON MULTILAYER INSULATION

TABLE OF CONTENTS

	<u>Page</u>
Estimate of Stand-off Distance	IV-2
Minimum Weight Considerations	IV-3
Description of Tests	IV-3
Sabot Separation and Low Velocity Debris	IV-4
Vaporization of Pellet and Bumper	IV-7
Neutron Activation Analysis	IV-13
Recommendations	IV-17

LIST OF TABLES

		<u>Page</u>
Table IV-1	Multilayer Insulation Sample Description	IV-5
Table IV-2	Sublimation Energy of Plastic and Some Common Metals	IV-10

LIST OF FIGURES

		<u>Page</u>
Figure IV-1	Test Facility	IV-6
Figure IV-2	Target	IV-8
Figure IV-3	Impact of Plastic Pellet on Plastic Bumper to Vaporize Pellet	IV-11
Figure IV-4	Impact of Magnesium Pellet on Bumpers of Various Densities to Vaporize Pellet	IV-14
Figure IV-5	Impact of Magnesium Pellet on Gold Bumper to Vaporize Pellet	IV-15
Figure IV-6	Impact of Magnesium Pellet on Lead Bumper to Vaporize Pellet	IV-16

IV. EFFECT OF METEOROID-BUMPER DEBRIS ON INSULATION

The velocity of meteoroids is generally such that on impacting a thin sheet of material the meteoroid and the portion of the sheet punched out by the meteoroid are sublimed. Behind the thin sheet the vaporized debris expands. The momentum of the meteoroid will remain in the vaporized debris, but the momentum per unit area of cross section parallel to the bumper will diminish as the vaporized cloud expands. This permits one to expose a surface behind the thin sheet at such a stand-off distance that the surface can withstand the impulsive loading due to this diminished momentum density. This is the concept of the meteoroid bumper for protection of space vehicles first proposed by Whipple and discussed in some detail in our report of June, 1963.⁽¹⁾

During the latter half of this contract period, a program was initiated to investigate the effect of the debris from meteoroid-bumper interactions on multilayer insulation. The purpose of this program was to determine experimentally the mode of failure of the insulation when impacted by the debris and to determine the minimum "stand-off distance" that results in no damage to the insulation.

(1) "Meteoroid Bumper Protection for Space Vehicles: Tentative Design Criteria," R. H. Johnston, D. A. Knapton, and D. Lull, to NASA, Report No. 65008-05-01.

Estimate of Stand-off Distance

Our initial efforts were to estimate the minimum stand-off distance between bumper and insulation that results in no damage to determine whether this distance was at all reasonable. These estimates were to be used in experimental tests to follow.

The meteoroid bumper debris imparts an impulsive temperature and pressure to the insulation. Only the impulsive pressure was believed to have a significant effect. Failure due to this pressure could be a fracture of the outer layer or layers of insulation, or a compression and deformation of the insulation to the point at which there is little recovery and a marked increase in thermal conductivity. The latter was determined to be the most probable mode of insulation failure. The strength of the outer layer of insulation appeared to be greater than the ability of the multilayer system to resist deformation. Based on this mode of failure, the minimum stand-off distance, S , was shown to be approximately:

$$S = 1.25 \left(\frac{I}{F_m} \right)^{1/2} \left(\frac{c}{\rho t} \right)^{1/4} \quad (1)$$

where I is the total impulse of the incoming meteoroid, F_m is the maximum static compressive loading the insulation will withstand with no appreciable increase in conductivity upon recovery, c is the compressibility or "spring constant" of the insulation, and ρ and t are the density and thickness of the outer layer of insulation. ⁽²⁾ Applying this relationship

⁽²⁾ "Second Quarterly Progress Report", to NASA, Report No. 55008-00-02.

to a cislunar flight with an exposure of 10^5 ft²-days and a requirement to avoid meteoroid damage with a probability of 0.99, it was estimated that a minimum stand-off distance of about 10 inches would be required. This was not considered unreasonable.

Minimum Weight Considerations

It can be seen from Equation 1 that if a protective skin is added to the insulation, the density and/or thickness may, in effect, be increased and the stand-off distance decreased. This reduction in stand-off distance will result in a reduction in meteoroid-bumper weight when considering curved surfaces. The weight reduction, however, has been shown to be generally offset by the additional weight of the protective skin, assuming the weight of the supports for the bumper in space is a small fraction of the bumper weight. (3)

Description of Tests

A series of tests was planned for a hypervelocity impact range at McGill University. Their purpose was to determine experimentally the minimum stand-off distance between a bumper and several different types of multilayer insulation, and the mode of failure of the insulation. Since the addition of a protective skin could result in a weight penalty, the tests were to be conducted with no protective skin. Tests were to consist of firing pellets at samples of each type of insulation behind a bumper. The spacing between the bumper and insulation was to be varied to determine the minimum spacing that resulted in no damage to the insulation. Damage was to be assessed visually with perhaps a limited number of thermal conductivity measurements in the X-apparatus.

(3) "Third Quarterly Progress Report", to NASA, Report No. 65008-00-03.

Four types of insulation were selected for the tests and are listed in Table IV-1. It was estimated that 6 or 7 shots would be required to determine the minimum stand-off distance for each type. In order to (1) assure complete vaporization of the pellet and bumper, (2) utilize a pellet with a typical meteoroid mass, and (3) achieve a minimum stand-off distance that was practical and within the test range capabilities, a 1/16-inch diameter spherical plastic pellet, a pellet velocity of 30,000 feet per second, and a 0.005-inch plastic bumper were selected. Tests were to be conducted at a pressure of less than 50 microns. Test samples 18 inches square and a sample mounting device were fabricated. A sketch of the test range and mounting device is shown in Figure IV-1.

From this test program, the minimum stand-off distance for each insulation corresponding to one meteoroid momentum (I) was to be determined. Assuming the impulsive loading on the insulation is an exponential function of stand-off distance ($S^2 \propto I$), the stand-off requirement for all incoming meteoroids that are vaporized upon impact could then be estimated and the design of a bumper insulation system made more rational.

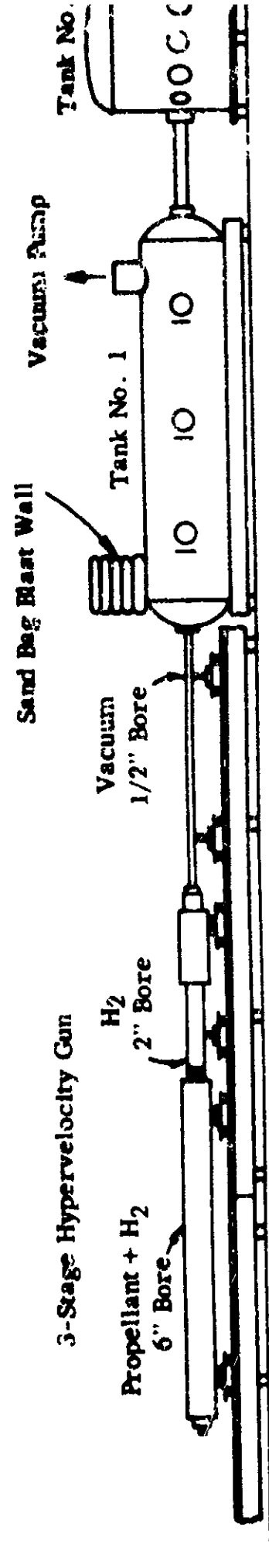
Sabot Separation and Low Velocity Debris

The test program was scheduled for August but was delayed and not accomplished in this contract period for two main reasons. First, difficulty was encountered in separation the sabot from the projectile. The final stage of the McGill hypervelocity light-gas gun has a 1/2-inch bore. Since we were interested in firing a projectile of much smaller size, it was necessary to mount the projectile on a 1/2-inch diameter

TABLE IV-1

MULTILAYER INSULATION SAMPLE DESCRIPTION

1. Ten radiation shields of 0.002-inch thick soft aluminum (Alcoa 99.45), bright on two sides, and ten spacers of 0.02-inch thick resin coated fiberglass mesh, grid dimensions 1/8 x 1/8 inch (Owens Corning Corporation).
2. Twenty radiation shields of 0.0005-inch thick soft aluminum (Alcoa 99.45), bright on one side, and twenty spacers of 0.003-inch thick polyester fiber spacers (Dexter paper).
3. Ten radiation shields of 0.00025-inch thick crinkled polyester film, aluminized on one side (NRC), and ten spacers of 0.003 inch thick polyester fiber spacers (Dexter paper).
4. Twenty radiation shields of 0.00025-inch thick crinkled polyester film aluminized on one side (NRC).



- Tank No. 1 3' Diameter x 15' Long
3 Ports for Velocity Measurement
- Tank No. 2 4-1/2' Diameter x 4-1/2' High
12 6" Diameter Windows for Observations
at 30 Degree Intervals

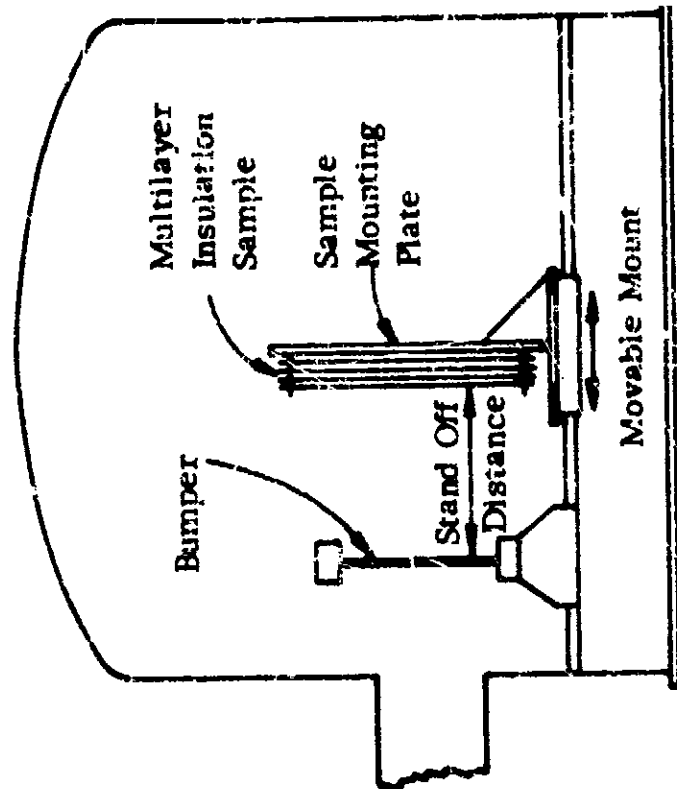


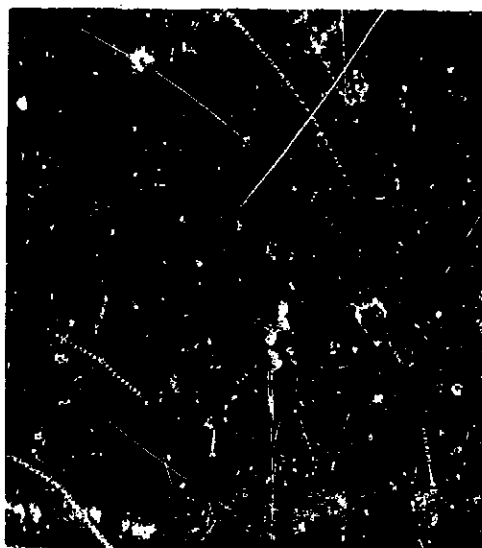
FIGURE IV-1 TEST FACILITY

carrier, or sabot, and fire both, separating the sabot and deflecting it off-course away from the target area after it left the muzzle. Second, difficulty was encountered in preventing low velocity debris from being carried with the projectile downrange to the target. It was necessary to eliminate this debris so as not to obscure the damage to the target due to the projectile.

At the end of this contract period, a technique had been developed which appeared to correct both difficulties. This consisted of holding a section of the range between the gun and the target tank at an elevated pressure (about 30 mm Hg) and using a segmented sabot. The drag on the sabot in passing through this section of the range appeared to be sufficient to separate the segments and deflect them off-course along with deflecting other low velocity debris away from the entrance to the target tank. The section of the range at the elevated pressure was isolated from the remainder of the range at a vacuum by diaphragms which were ruptured by squibs before passage of the sabot projectile. Other techniques for separation, such as petal sabots, ramps, etc., are being investigated by McGill.

Vaporization of Pellet and Bumper

During a few of the test firings that were conducted to perfect sabot separation and eliminate the low velocity debris, it was possible to observe the effect of pellet-bumper debris on a surface behind the bumper. Figure IV-2 is a photograph of damage to a cardboard surface located about 4-inches behind a 0.005-inch plastic bumper which is hit by a 1/8-inch plastic sphere at about 24,000 feet per second. This was an isolated



Pellet	1/8-Inch Diameter Plastic
Bumper	0.005-Inch Plastic
Stand-Off	4 Inches
Velocity	24,000 Ft/Sec
Pressure	Less than 50 microns

FIGURE IV-2 TARGET

case when sabot separation was achieved and only a small amount of low velocity debris hit the bumper with the pellet. The damage to the cardboard appeared to be due primarily to pellet-bumper debris and not low velocity debris.

As can be seen from the photograph, damage to the surface appears to have been caused by a spray of very fine particles. This observation led us to question whether or not it was possible to achieve complete vaporization with plastic pellets and bumpers within the capabilities of the McGill range. Plastic had been recommended early in the program as the material most suitable for the tests.

The sublimation energy of various metals that might possibly be used as a pellet or bumper material is listed in Table IV-2.⁽⁴⁾ Also listed in this table is an estimate of the sublimation energy of polycarbonate plastics based on commonly accepted bond energies. The low value was based on the conservative assumption that the vaporized debris consists of carbon dioxide, water, and benzene. The high value assumes complete atomization. In either case, the value would exceed that of many of the metals.

The velocity required to vaporize a plastic pellet and plastic bumper is shown in Figure IV-3 for various specific-heat ratios (γ) and

(4) "Selected Values of Thermodynamic Properties of Metals and Alloys",
Hultgran, Orr, Anderson, and Kelley.

TABLE IV-2

SUBLIMATION ENERGY OF PLASTIC AND SOME COMMON METALS

<u>Material</u>	<u>Density (grams/cc)</u>	<u>Sublimation Energy (kilocalories/gram)</u>
Plastic (Polycarbonate)	1.20	1.8 - 14.3
Magnesium	1.74	1.45
Beryllium	1.80	8.68
Aluminum	2.70	2.77
Titanium	4.50	2.65
Zinc	7.14	0.478
Tin	7.29	0.608
Iron	7.87	1.78
Nickel	8.85	1.75
Copper	8.89	1.27
Molybdenum	10.21	1.63
Silver	10.50	0.630
Lead	11.34	0.225
Gold	19.31	0.443
Platinum	21.38	0.690

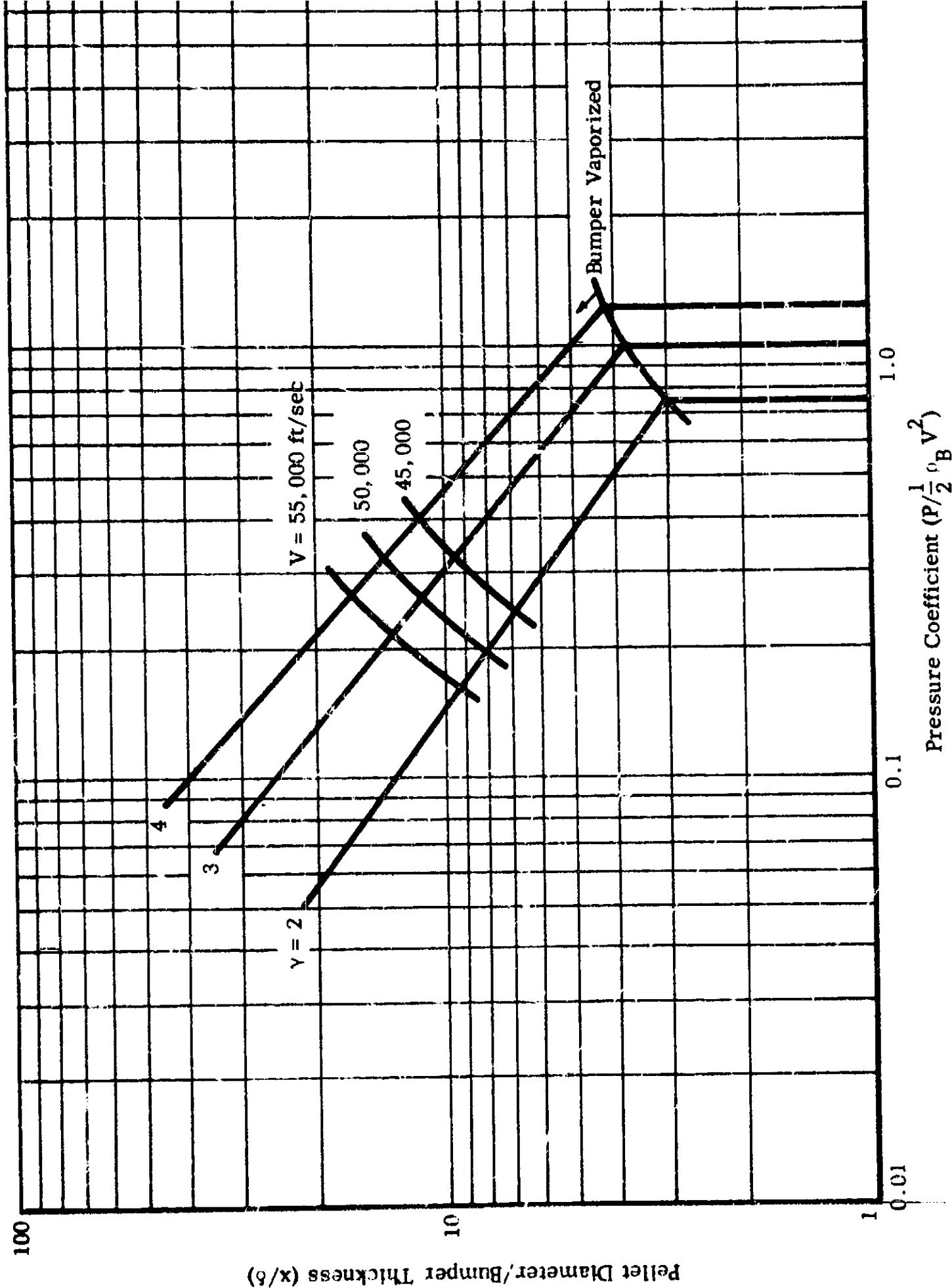


FIGURE IV-3 IMPACT OF PLASTIC PELLET ON PLASTIC BUMPER TO VAPORIZE PELLET

pellet-diameter-to-bumper-thickness ratios (x/δ). The sublimation energy of plastic is assumed to be 1.8 kilocalories per gram. The curves are based on the results of a one-dimensional treatment of the meteoroid-bumper interaction by McGill University.⁽⁵⁾

In preparing the curves it was assumed that vaporization occurs when the increase of free energy across the shock wave in the pellet and bumper equals the sublimation energy of the plastic. As can be seen from the figure, a 1/16-inch plastic pellet will not vaporize upon impacting a 0.005-inch plastic bumper ($x/\delta = 12.5$) unless the pellet velocity is greater than 53,000 feet per second, assuming a specific heat ratio (γ) of 3. This velocity is well beyond the capabilities of all light gas guns.

In searching for a combination of pellet and bumper materials that could be expected to vaporize within the velocity capabilities of the McGill range, we directed our attention away from plastics to the common metals listed in Table IV-2 for which experimental data on sublimation energy exists. The pellet material should first be of low density. This allows the use of large pellets to facilitate velocity measurement without the total pellet weights inhibiting attainment of high gun velocities or necessitating stand-off distances between bumper and insulation which exceed the capabilities of the test range. The lightest metal in

(5) "On the Impact of Pellets with Thin Plates: Theoretical Considerations", Part I and Part II, to NASA, by G. V. Bull, Report Nos. 63270-03-01 and 65008-05-03.

Table IV-2 is magnesium. Using the theory developed at McGill, the length of pellet vaporized for different specific heat ratios (γ), bumper-to-pellet-density ratios (ρ_B / ρ_P), and velocities (V) has been plotted in Figure IV-4. Since the theoretical work is based on a one-dimensional model, we desire a pellet-diameter-to-bumper-thickness ratio of 20 or more. From Figure IV-4 we would expect that a pellet with a diameter 20 times the bumper thickness would vaporize within the velocity capability of the test range if the bumper-to-pellet-density ratio were about 10. Referring again to Table IV-2, gold and lead have the lowest sublimation energies of those metals that are about 10 times as dense as magnesium. From Figures IV-5 and IV-6, a magnesium pellet and a gold or lead bumper will vaporize, assuming a specific heat ratio of greater than 3 and a pellet-diameter-to-bumper-thickness ratio of 20, if the pellet velocity is greater than 28,000 feet per second (gold bumper) or 24,000 feet per second (lead bumper). Lead is the better bumper material for shots at insulation because it is cheaper and more available and vaporization occurs at a lower velocity.

Neutron Activation Analysis

A magnesium pellet and gold bumper could be useful, however, in analyzing the flow pattern of the vaporized debris. If an aluminum witness plate were mounted behind the bumper, some of the debris would be vacuum-deposited on the plate, and the nature of the impact pattern could be investigated by means of neutron activation analysis. By this technique it would be possible to determine (1) where the bumper material impacted, (2) where the pellet material impacted, (3) whether the debris rebounded on impact thereby doubling the impulsive loading, and (4) whether the debris was completely sublimed.

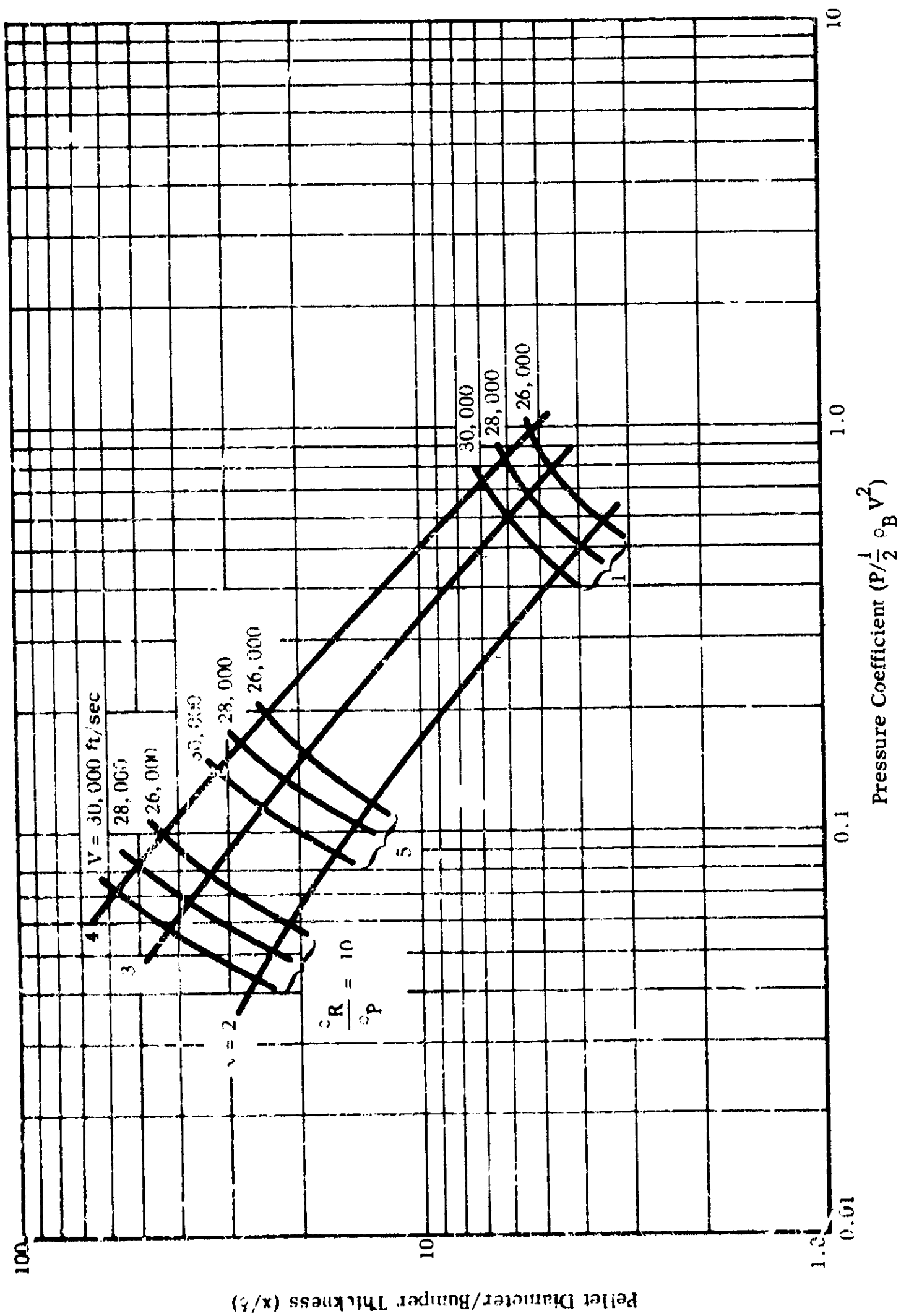


FIGURE IV-4 IMPACT OF MAGNESIUM PELLET ON BUMPERS OF VARIOUS DENSITIES TO VAPORIZE PELLET

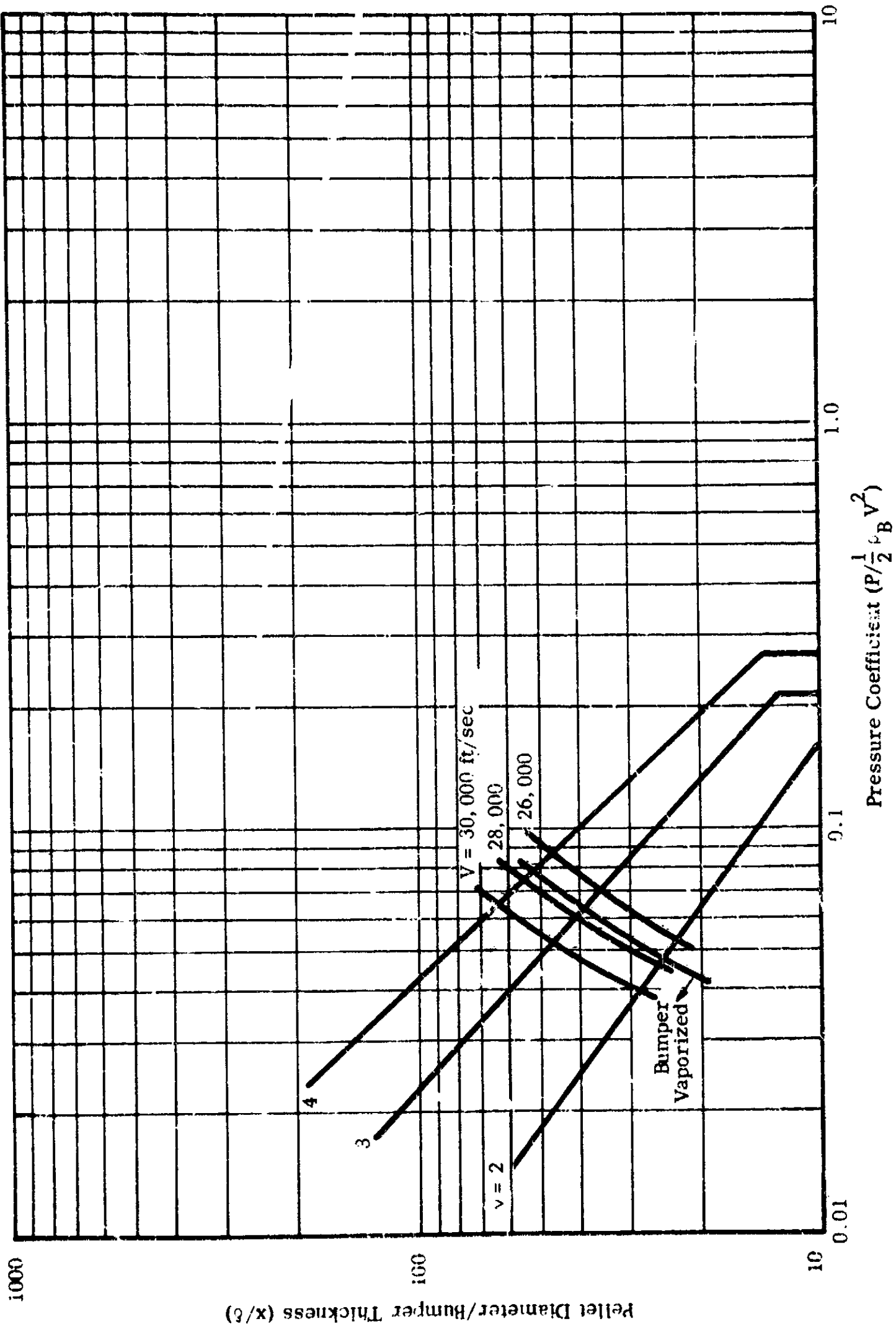


FIGURE IV-5 IMPACT OF MAGNESIUM PELLET ON GOLD BUMPER TO VAPORIZED PELLET

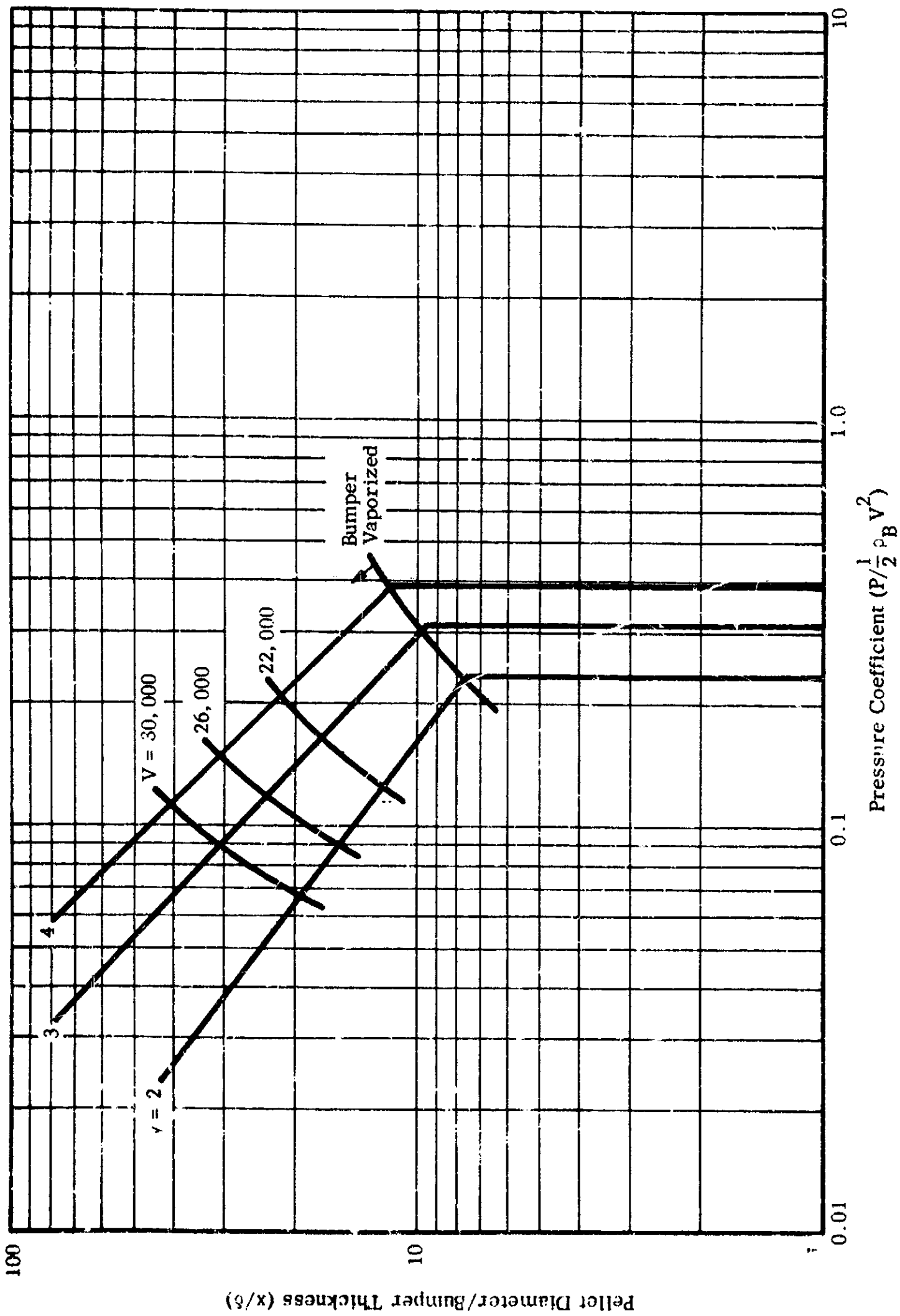


FIGURE IV-6 IMPACT OF MAGNESIUM PELLET ON LEAD BUMPER TO VAPORIZE PELLET

4

The neutron activation analysis would involve irradiation of the aluminum witness plate in a nuclear reactor after impact of the debris. By counting the irradiated witness plate soon after irradiation and again several weeks later, the contours of deposition for both gold and magnesium could be obtained. The gold would be counted at an early time and the magnesium after several weeks of storage.

Incomplete vaporization would result in a nuclear "hot-spot" on the witness plate. The precision of absolute counting would be such that it would be possible to determine whether most of the debris adhered to the witness plate or most of the debris rebounded on impact.

Recommendations

We feel that there still exists a need for the test program originally planned and scheduled for this contract period but delayed because of difficulties with the test range. It is recommended that it be rescheduled as soon as possible (upon development of a successful sabot separation technique).

Upon completion of the tests that have been outlined, it is recommended that the program be extended to cover additional types of insulation. It is also recommended that the pellet-to-bumper-density ratio, pellet shape, pellet mass, pellet velocity, and angle of impact be varied within the capabilities of the test range to determine their effects on bumper insulation stand-off distance.

It is further recommended that the technique of neutron activation analysis be explored to investigate the flow pattern of the pellet-bumper debris.

NOTE:

Before publication of this final report, McGill has reported a technique that appears to yield sabot separation with reasonable reproducibility. NASA has granted a contract time extension to permit partial accomplishment of the test program as originally planned. We will issue an addendum to this section of our final report upon completion of a limited number of shots to publish the results obtained.

PART V

MECHANICAL TEST PROGRAM ON A SPECIFIC MULTILAYER
INSULATION SYSTEM

Arthur D. Little, Inc., has conducted a short program on load-bearing insulation material. Although this program was not conducted with our program for the National Aeronautics and Space Administration, the results are pertinent to the problem of storage of cryogenic propellants in space and are, therefore, included in this final report on Contract No. NASw-615.

The results reported in this section (Section V) of this report were generated under a separate program, and are not part of the work performed on Contract No. NASw-615.

TABLE OF CONTENTS

	<u>Page</u>
Introduction	V-1
Static Tests	V-2
Dynamic Tests	V-8
Prototype Dewar	V-11
Thermal Performance of the Insulation	V-16

LIST OF FIGURES

<u>Figure No.</u>	<u>Title</u>	<u>Page</u>
V-1	Displacement vs. Mechanical Load	V-3
V-2	% Deflection of Preloaded Sample Referred to Free Height Vs. Mechanical Pressure	V-5
V-3	% Deflection of Preloaded Sample Referred to Free Height Vs. Mechanical Pressure	V-6
V-4	% Deflection Referred to Free Height Vs. Mechanical Pressure	V-7
V-5	Dynamic Behavior of Insulation Discs	V-10
V-6	Prototype Dewar	V-13
V-7	Prototype Dewar	V-14
V-8	Prototype Dewar	V-15

V. MECHANICAL TEST PROGRAM ON A SPECIFIC MULTILAYER INSULATION SYSTEM

Introduction

As a part of a test program to determine the mechanical properties necessary for the design of a high performance cryogenic system, we have located and tested a material which fills the dual function of insulation and mechanical support in cryogenic applications. The potential importance of load bearing insulation derives from the unavoidably high heat leak of existing mechanical support methods. In the case of vessels constructed with discrete supports, the total heat leak through these supports is approximately 3 times that through the insulation despite the approximate 200:1 ratio in cross-sectional heat transfer area between these two heat paths.

The insulation which was subjected to the tests described in this section was constructed of alternate layers of NRC-2 crinkled, aluminized-mylar radiation shields, and silicone-impregnated fiberglass spacers. The spacer material tested in this capacity was that fabricated by Cincinnati Testing Laboratories, (CTL), P. O. Box 227, Cincinnati 15, Ohio. The CTL material separates the radiation shields and provides the compressive strength of the insulation.

The evaluation of an insulation system for use as a dewar support should include a determination of its response to the anticipated range of environmental conditions. Mechanical test series were, therefore, conducted on the spacer material for both dynamic and static loading modes.

Based upon the information derived from these preliminary tests, a prototype spherical dewar was fabricated and subjected to vibration testing. These tests yielded information which permit description of the dynamic behavior of the inner vessel of a spherical dewar.

Although these tests were specific to the design of the system under consideration, we believe that the results obtained may be of general interest to other contractors concerned with similar problems.

Static Tests

A program of static tests was conducted to establish the relation between the mechanical load imposed upon the spacer material and its thickness variation. To facilitate these tests, an apparatus was constructed which permitted the sequential placement of a number of calibrated weights upon a stacked sample of spacer material wafers held in a vacuum environment, with simultaneous observation of the stack height. Provision was made to permit automatic re-cycling of the test machine so as to obtain an estimate of the repeatability of mechanical performance over a large number of cycles. Readings were taken as the weights were added and again as they were removed, providing an estimate of the material hysteresis.

Test Procedure

The first set of tests was conducted on 1-inch diameter specimen disks fabricated from approximately .070-inch thick sheet material (designated A). A stack consisting of 20 layers, without interleaved mylar, were used and the results are plotted in Figure V-1. The second set of tests was performed on spherical sections, i.e., disks cut from

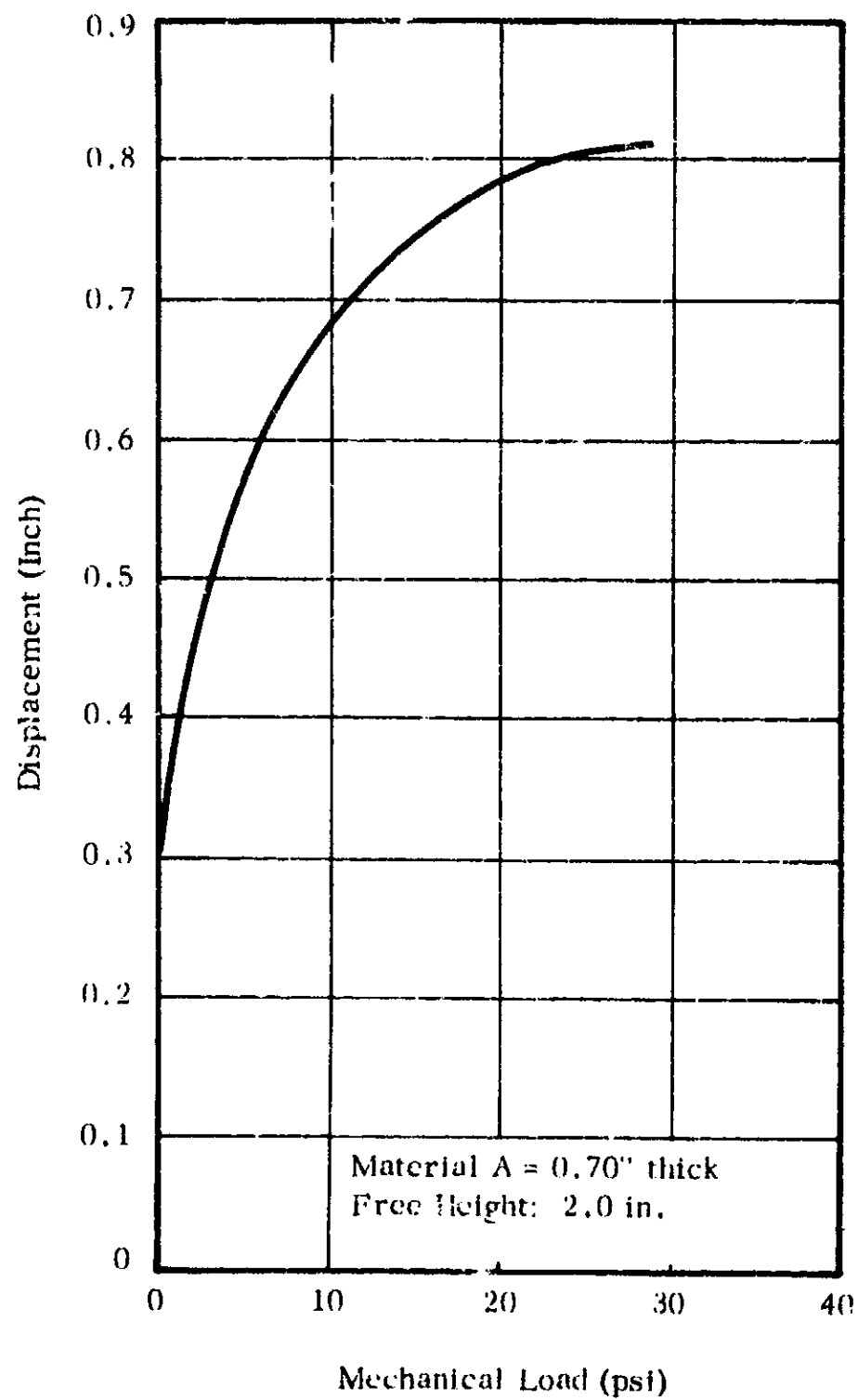


FIGURE V-1 DISPLACEMENT VS
MECHANICAL LOAD

insulation initially fabricated on production equipment in the form of spherical triangles suitable for application to a 29-inch diameter spherical cryogenic vessel. Again, aluminized mylar was not interleaved. Separate tests were conducted with stacks consisting of 24, 32, and 36 layers for the purpose of determining hysteresis behavior and the average load/deflection characteristic. Because the read-out device was not sufficiently accurate to determine the hysteresis behavior, only the average of these tests are presented in Figure V-2.

A third set of tests was conducted with interleaved aluminized mylar. Free height of the spacer/insulation stack varied over the range 0.7, 1.5, and 2.3 inches, (with corresponded, for the material thickness employed, to 9, 19 and 30 layers of insulation). It is interesting to note that difficulty was experienced as a result of a tendency of the insulation layers to slip, because of the decreased friction coefficient of mylar on fiberglass. For those tests conducted using small specimen cross-sectional area, this tendency to slip could not be overcome until the mylar layers were deleted.

Test Results

The effect of pre-load is illustrated in Figure V-3. For purposes of comparison, the behavior of a sample under a zero pre-load condition is illustrated in Figure V-4.

The effect of free height on the load/deflection characteristic of this material is shown in Figure V-2. If the material behaved in accordance with Hook's law, the characteristic at each free height would be the same. The fact that the results are not coincident illustrates that this material does not display a linear stress/strain relationship.

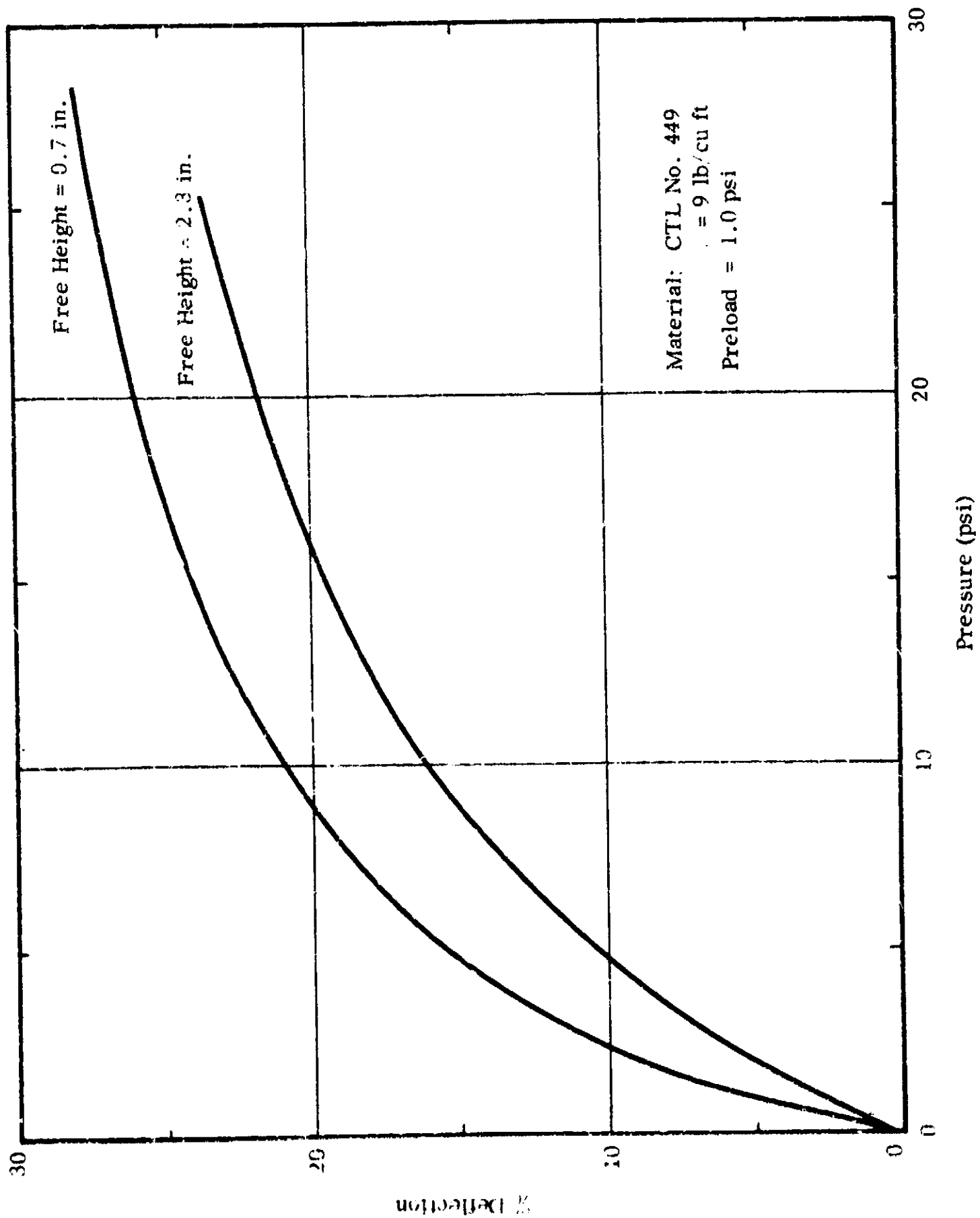


FIGURE V-2 DEFLECTION OF PRELOADED SAMPLE REFERRED TO FREE HEIGHT
VERSUS MECHANICAL PRESSURE

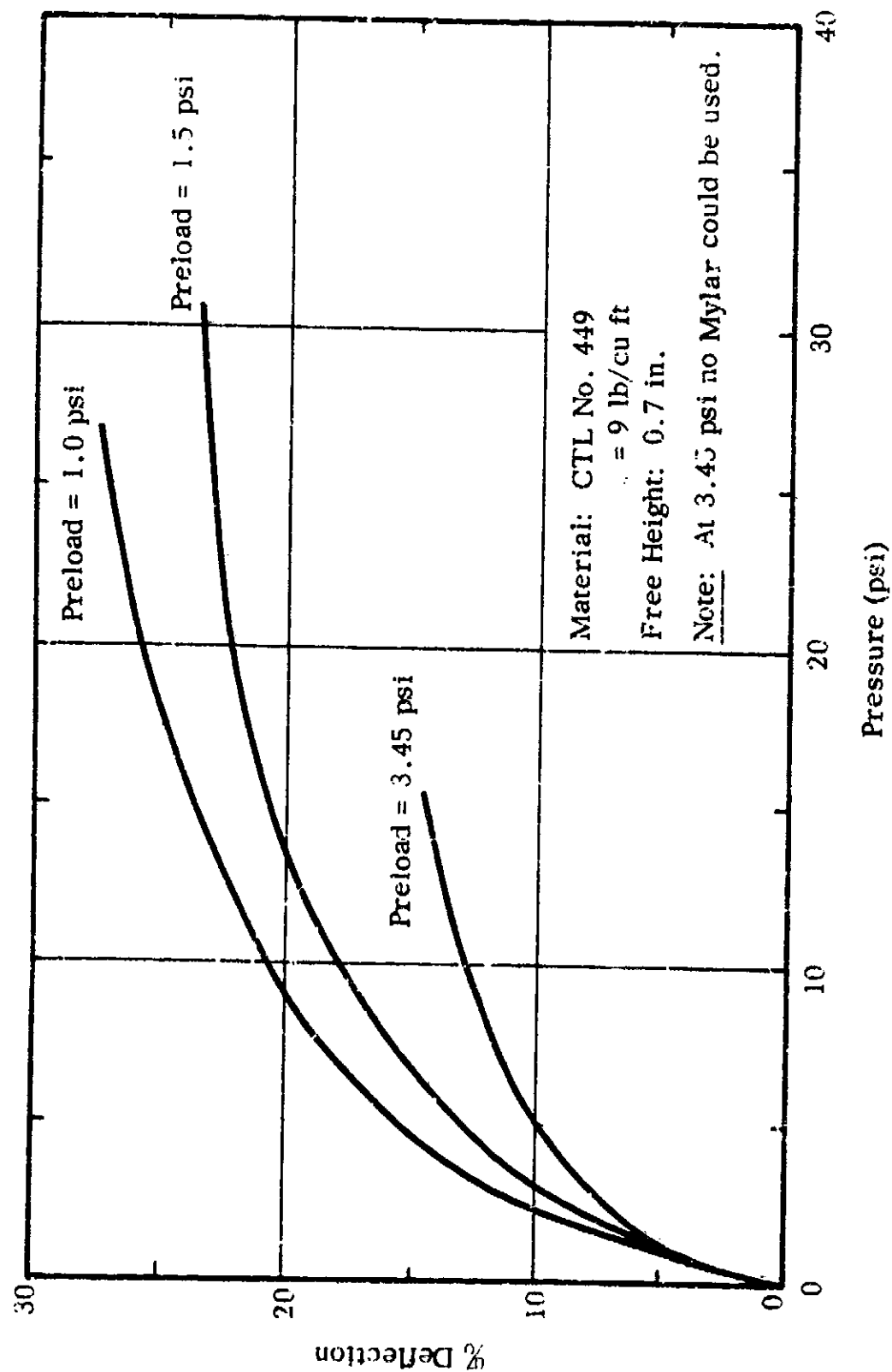


FIGURE V-3 DEFLECTION OF PRELOADED SAMPLE REFERRED TO FREE HEIGHT VERSUS MECHANICAL PRESSURE

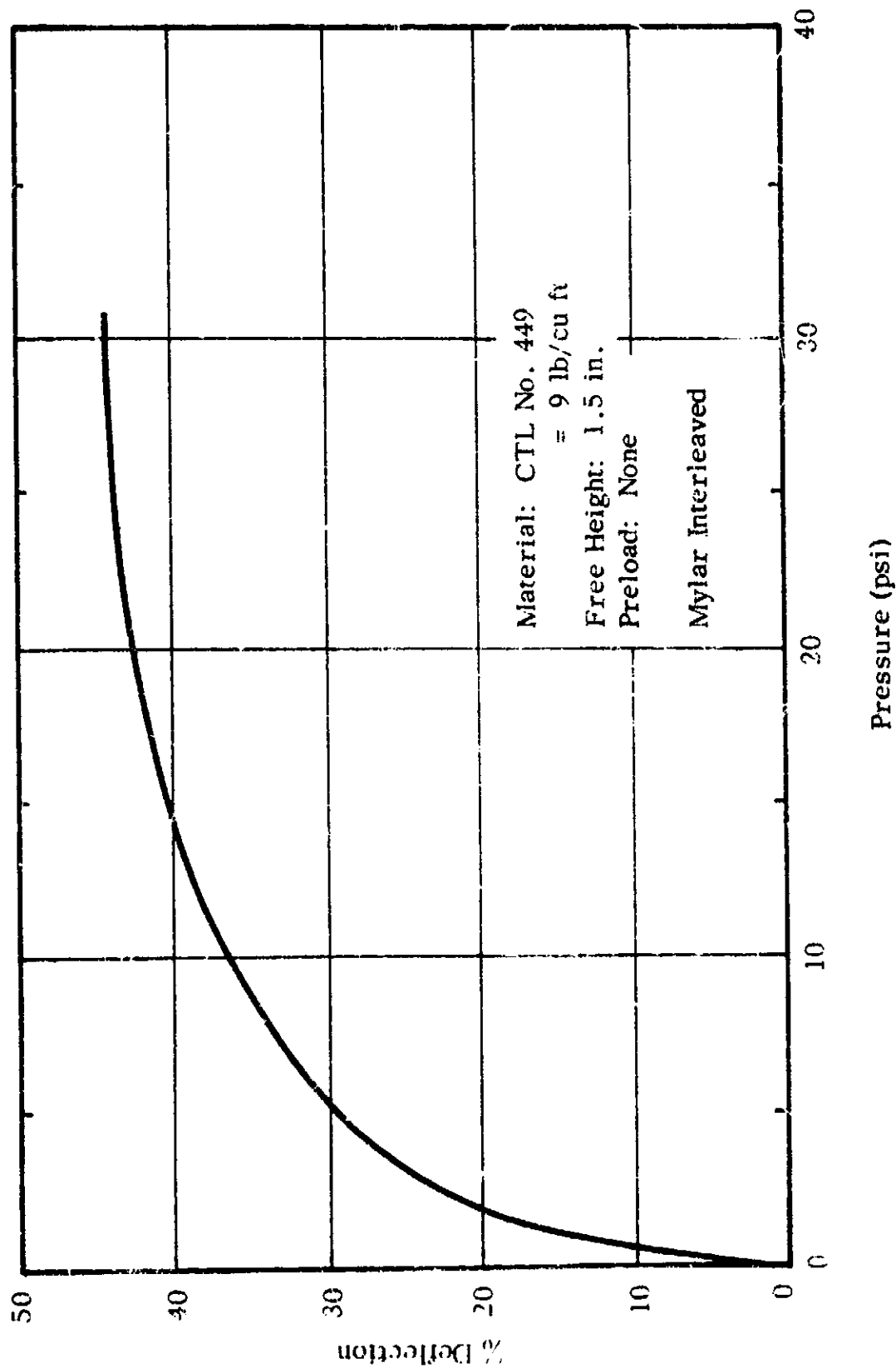


FIGURE V-4 % DEFLECTION REFERRED TO FREE HEIGHT VERSUS MECHANICAL PRESSURE

The tests described in this section were conducted over a relatively brief period of time utilizing simple test apparatus; the test results were required to meet a demanding schedule for prototype dewar fabrication. A number of these tests should be repeated with more refined test apparatus, particularly in the area of deflection measurement, to permit a careful appraisal of the hysteresis characteristic of the material.

Dynamic Tests

The dynamic behavior of the CTL/mylar insulation was initially determined by use of a special vibration test fixture in which an instrumented seismic mass was held between two opposed stacks of insulation. To closely simulate the behavior of an actual dewar in this two-dimensional test rig, the size of the seismic mass and/or the cross-sectional area of the insulation pads were varied to produce the same range of mechanical loading which could be anticipated for a full-sized dewar. The test fixture was constructed so as to permit maintenance of vacuum conditions around the insulation material during the test.

Insulation

Insulation specimens were cut from 0.070-inch thick, 29-inch diameter spherical triangles in the form of disks of 2-inch and 3-1/2-inch diameter. Holes were cut in the disks to correspond to guide rod locations. The insulation specimens consist of 20 layers of CTL material interleaved with NRC-2. The free height of each stack was then 1.6-inch for all tests.

Experimental Parameters

During the test series, mechanical pressure and the insulation pre-load were maintained as the independent variables. In the following paragraphs we define the pressure on the insulation as that induced by the seismic mass; and the pre-load as that induced by compressing the insulation between the two halves of the test assembly. This differentiation is required because the pressure represents the load resulting from a filled dewar resting on the insulation, while the pre-load results from compression of the insulation between the outer and the inner vessels of the dewar during assembly. During the test series, pressure was adjusted by variations in the seismic mass and/or the insulation cross-sectional area.

Experimental Results

A considerable mass of data was collected and later discarded as being unreliable because of the questionable behavior of the seismic mass. Typical results of the successful tests conducted with the final configuration are shown in Figure V-5, which describes the behavior of a simulated, filled, 18-inch LH₂ dewar. It may be readily seen that one principal point of resonance was observed (typical of all tests). This primary resonant frequency was found to occur in the range 30 to 60 cps; with many of the samples exhibiting a second resonance at a higher frequency around 600 cps. As might be expected, the primary resonant frequency was observed to increase with increasing pre-load.

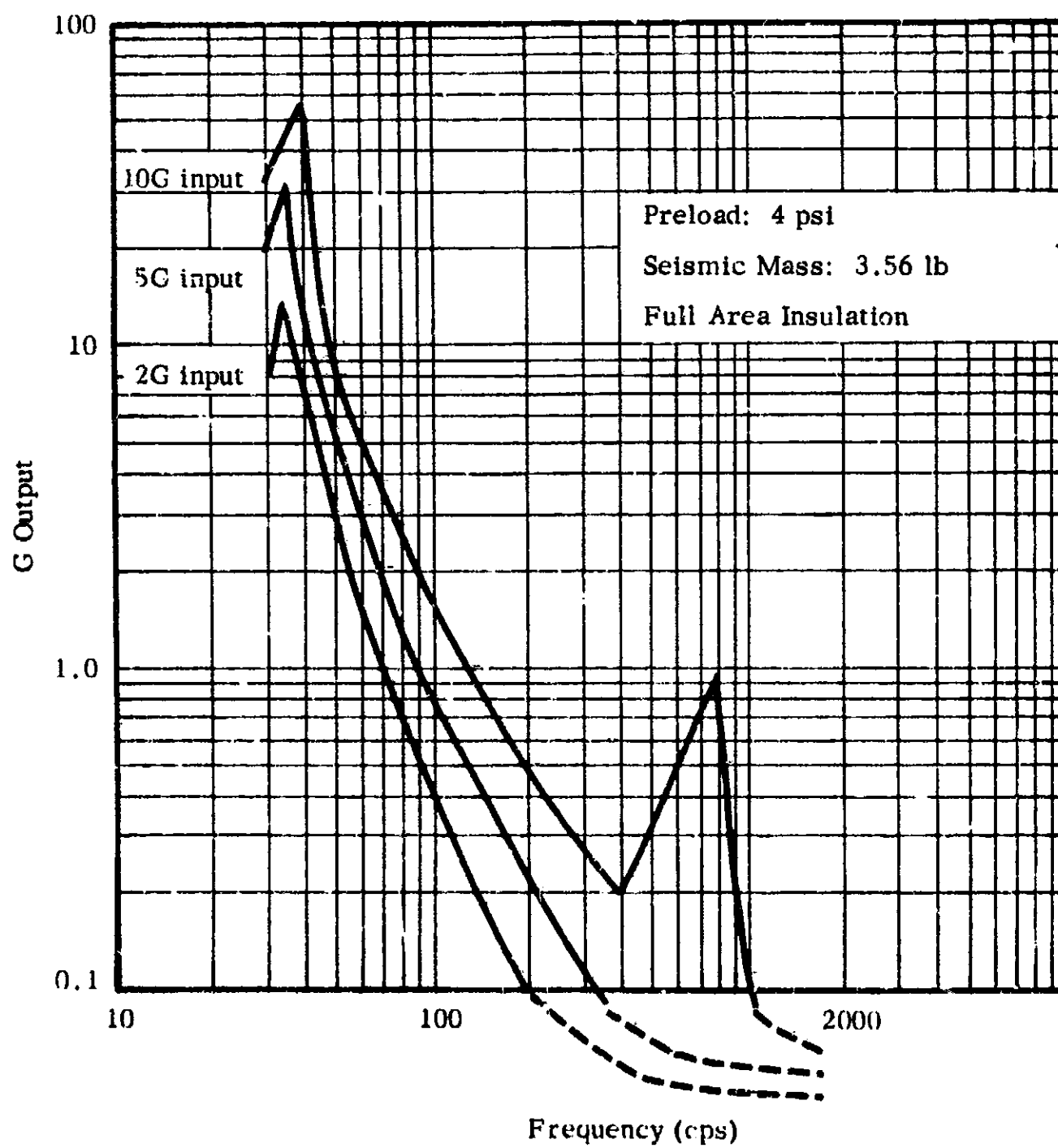


FIGURE V-5 DYNAMIC BEHAVIOR OF INSULATION DISCS

Prototype Dewar

On the basis of data obtained from the previously described test series, a prototype spherical dewar was designed, fabricated and subjected to vibration testing. The vessel was fabricated at the Arthur D. Little, Inc., Santa Monica experimental facility and consisted of a 1/4-inch thick, 29-inch O.D. stainless steel inner vessel, and a .070-inch thick, 31-inch I.D. stainless steel outer vessel. The insulation was comprised of spherical triangles of CTL fiberglass spacer material (No. 449) alternating with 1/2-mil aluminized mylar radiation shields (NRC-2). Prior to final assembly, the spacers were perforated with a circular hole cutter in such a manner to remove 50% of the spacer area while leaving the remaining material in a uniform radially-registered array. Six spherical triangles formed one complete spherical spacer layer; a total of 20 of which comprised the insulation array. The radius of curvature of each of these pre-formed spherical segments was chosen so as to accommodate the dimensional variation between the inner and the outer shells. A 15 psi insulation pre-load was adopted, but the assembly technique employed (which consisted of "shoe horning" the two outer vessel halves over the insulation using a special assembly fixture) left some question as to the accuracy of this figure. Subsequent calculation, based upon test results suggests that the actual pre-load was close to 12 psi. The empty weight of the inner vessel is approximately 200 lbs.

The objective of this test series was to determine the location of the resonant frequencies and the amplification factors at resonance over a wide range of vibration inputs, and with the vessel filled with LN₂. Mechanical failure of an external component early in the dynamic test

operation precluded testing with LN_2 . However, the assembly was tested in the empty configuration as well as in a water filled condition. With the empty dewar the following levels were tested.

<u>Frequency (cps)</u>	<u>Level (+ G)</u>	<u>Duration/Cycle (Minutes)</u>
5-2000-5	5	10
5-2000-5	2	10
5-2000-5	1	10

The results of these tests are described in Figures V-6 and V-7. Two principal points of resonance were observed, the primary one between 35 and 70 cps and increasing in frequency with decreasing G level input. A secondary resonance was observed at 550 cps in all tests.

When filled with water, the test dewar was subjected to the following input levels:

<u>Frequency (cps)</u>	<u>Level (+ G)</u>	<u>Duration/Cycle (Minutes)</u>
5-2000-5	5	10
20-2000-20	10	10
40-2000-40	15	8.5

The increasing spring mass resulting from the addition of water had two observable effects on the resonance points. The resonant frequency is decreased slightly while the amplification decreases substantially. The results of the first run of the series are presented in Figure V-8. The behavior observed in this test series is compatible with the assumption that small dynamic loads imposed on a spherical vessel are carried in

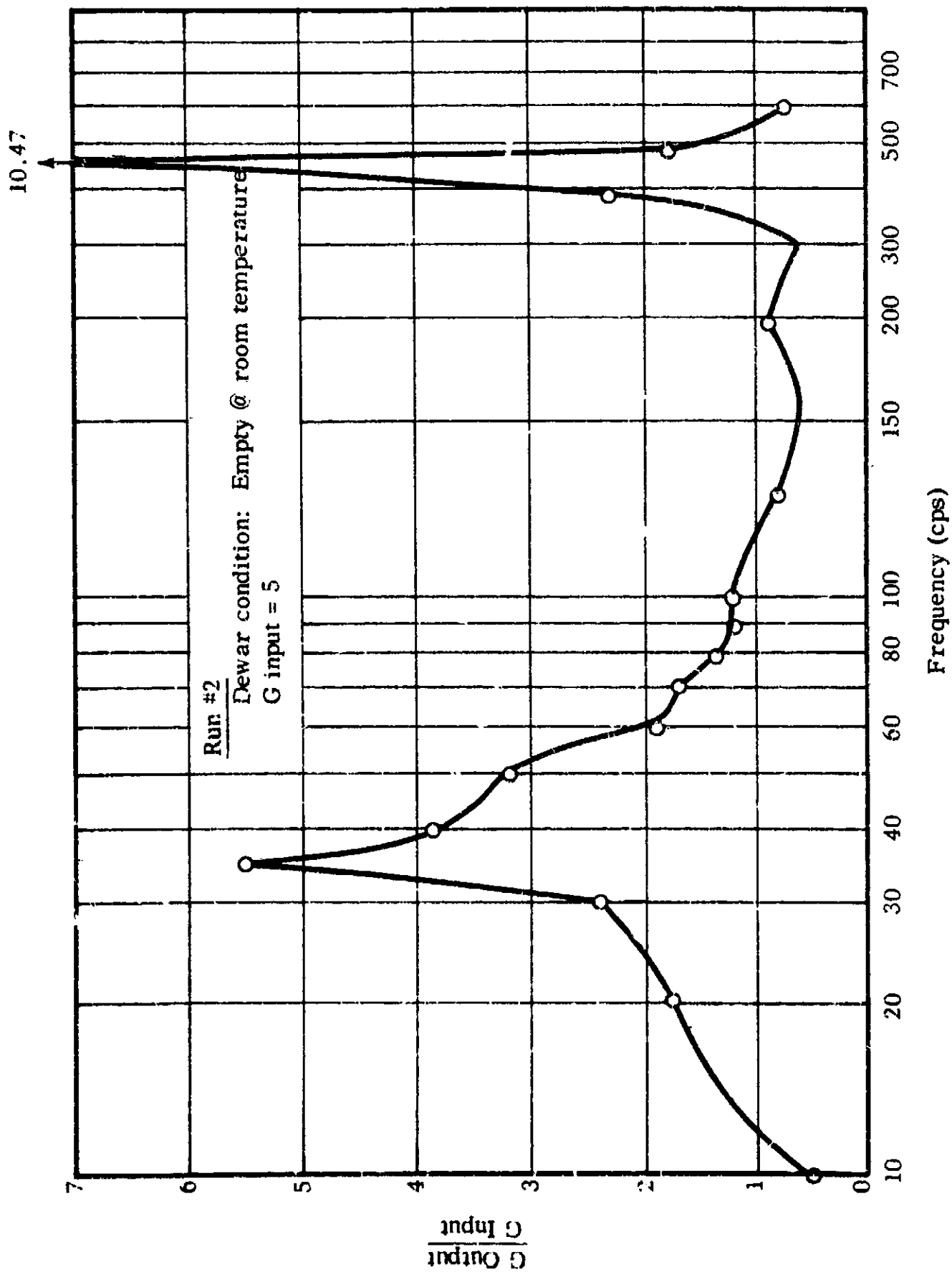


FIGURE V-6 PROTOTYPE DEWAR

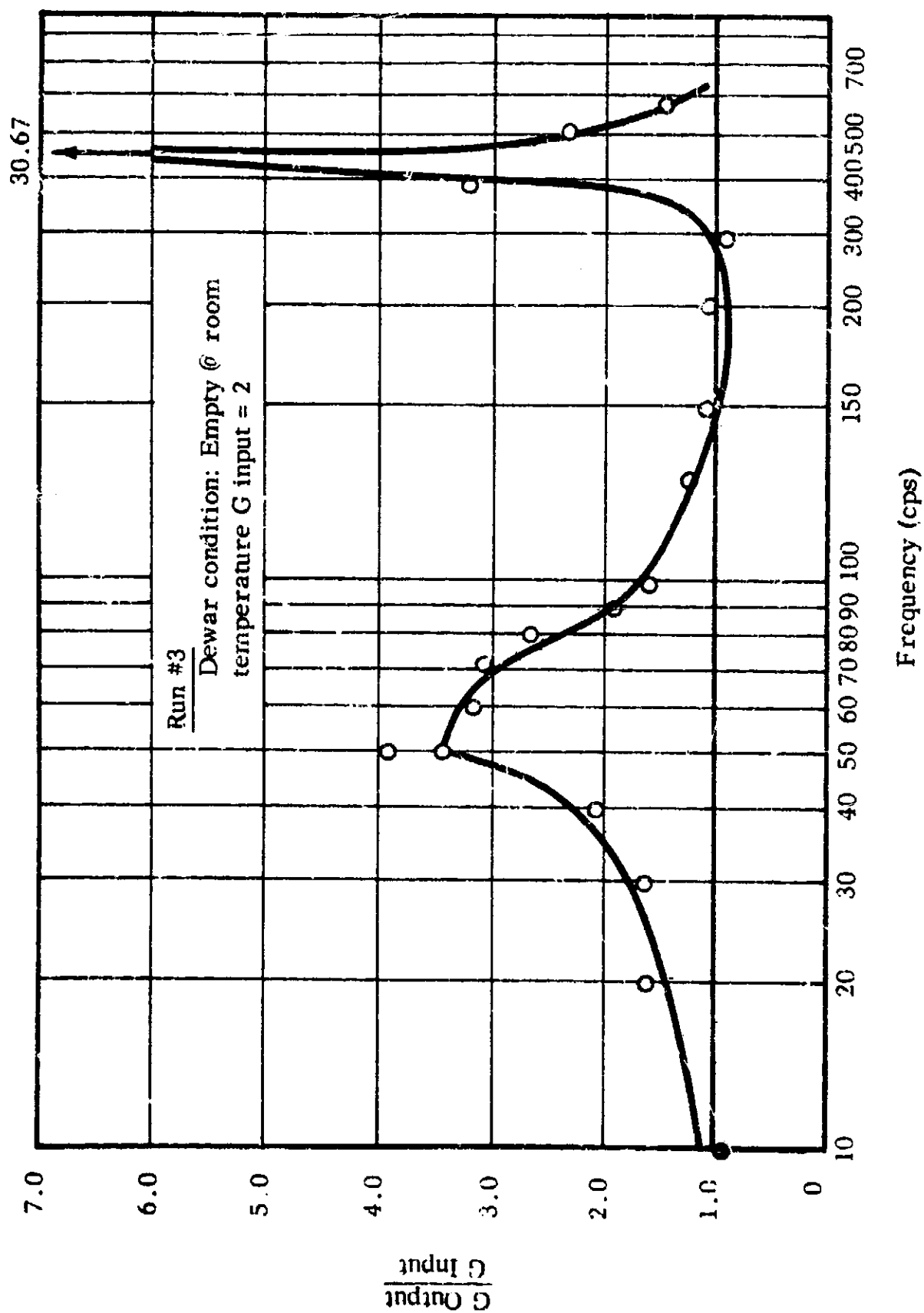


FIGURE V-7 PROTOTYPE DEWAR

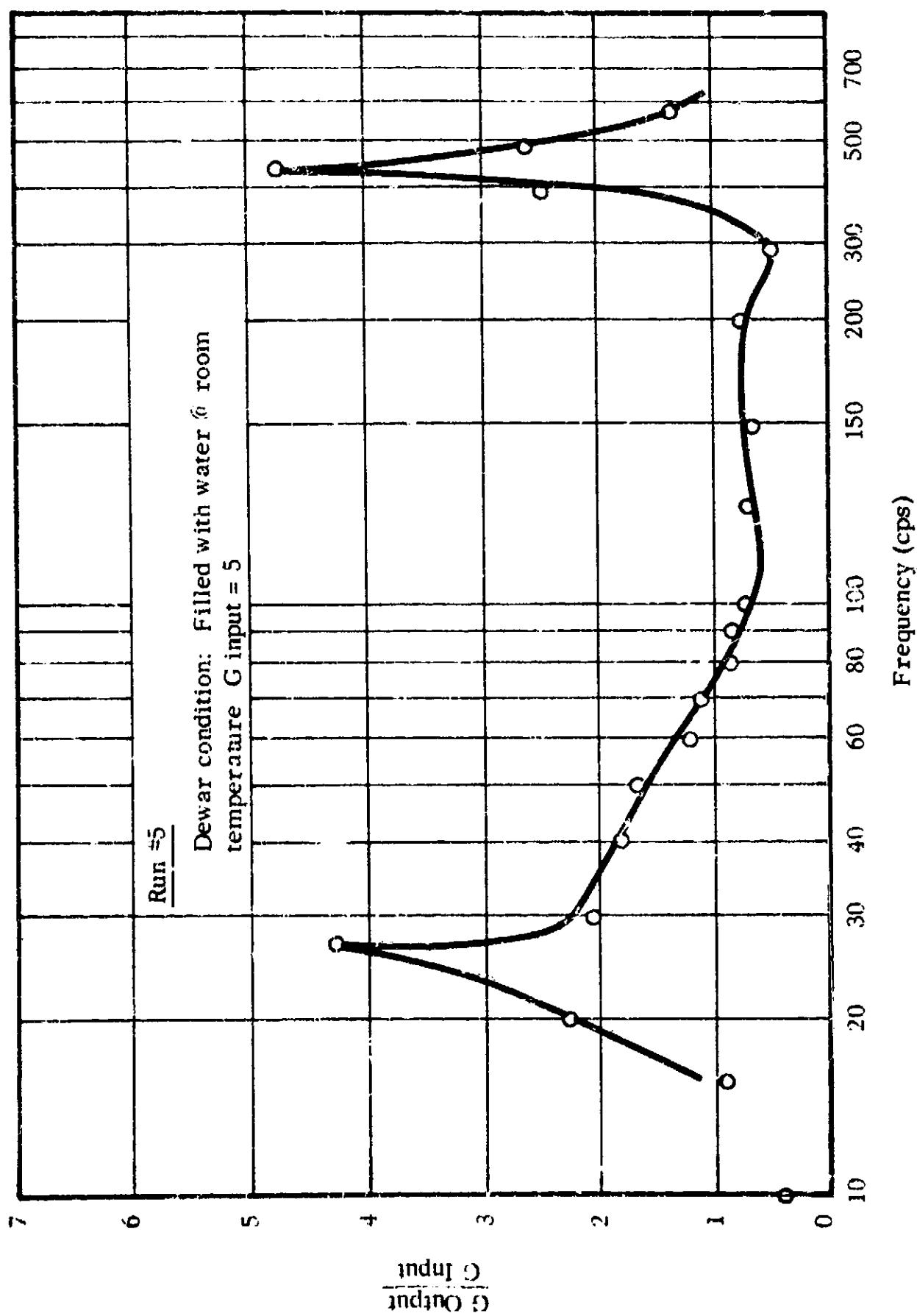


FIGURE V-8 PROTOTYPE DEWAR

compression near the axis of vibration, and in shear by the insulation at the circumference of the vessel furthest from the axis of vibration. With increased loading, relative motion between insulation layers introduces sliding friction at the circumference of the vessel which contributes little to the major support of the dewar provided by the insulation in compression near the vibration axis; but which produces appreciable coulomb-damping which serves to limit the relative motion between the two vessels.

Upon completion of the test series and disassembly of the test article it was noted that the fill and vent line connections between inner and outer vessels had failed, apparently as a result of rotational displacement of the inner vessel with respect to the outer vessel filling the insulation space with water. In addition to this failure, it was further noted that the gross motion imposed upon this assembly (as the result of high G inputs and excessive weight due to the water fill) produced an abrasion and almost complete removal of the aluminized coating on the mylar where it contacted the spacer material.

Thermal Performance of the Insulation

It was intended originally to measure the thermal performance of the prototype dewar after completion of the dynamic tests. In preparation for these thermal tests, samples of the CTL spacer material and NRC-2 aluminized mylar were tested in a flat plate calorimeter to determine the thermal conductivity of the proposed insulation system.

The spacers were perforated to achieve 60% open area, while the mylar was perforated with a random pattern of 1/8-inch diameter holes on 2-inch centers to permit rapid pump down and outgassing of the system. Calorimeter

measurements, with the same loading on the insulation as would be used in the prototype dewar, yielded values of 4×10^{-3} BTU-inch/hr-ft² - °F for the thermal conductivity of the insulation.

Other insulation samples, perforated for 76% open area of the spacer material, yielded thermal conductivity values of 3.25×10^{-3} BTU-in/hr-ft² - °F under identical test conditions.

The prototype dewar was tested to determine its thermal performance prior to the dynamic tests. Temperature equilibrium was achieved 14 hours after filling the inner vessel with liquid nitrogen. The thermal conductivity of the insulation system, determined from the measured boil-off, was calculated to be 4.3×10^{-3} BTU-in/hr-ft² - °F: very close agreement with the results obtained in the flat plate calorimeter.

No thermal test could be performed after the dynamic vibration tests.

During assembly of the prototype dewar, no particular care was taken to protect the insulation while making the final girth weld in the outer vessel, and no backup ring had been provided for this weld joint. On disassembly after the dynamic tests, it was noted that severe charring of the outer spacer material had occurred in a band about 4-inches wide contiguous to the girth weld. In spite of this damage, the thermal performance of the dewar in the initial tests agreed closely with predicted performance.

PART VI

ABSTRACTS OF REPORTS ON THE SPACE ENVIRONMENT

VI. ABSTRACTS OF REPORTS ON THE SPACE ENVIRONMENT

Our reports on the space environment were published under the initial contract and, therefore, are treated only briefly herein.

Arthur D. Little, Inc., Report No. 63270-05-01 ASTIA No. AD 263-476

Date: July 1961 OTS \$8.10

Title: Principles for the Calculation of Radiation Dose Rates in
 Space Vehicles

Author: Robley D. Evans

Abstract:

Methods are developed for computing the radiation dose rates in a space vehicle due to its exposure to any arbitrary spectrum of incident protons or of electrons. The analysis takes into account the angular distribution of the incident protons and electrons and the angular distribution of the electron bremsstrahlung. The distribution with depth in the propellant is determined for the dose rate due to protons, for the dose rate due to electron bremsstrahlung, and for the deposition of stopped protons. Whereas the dose rates for monoenergetic protons or electrons are maximum at the surface of the propellant, the deposition of protons has its minimum at the surface and increases linearly with depth up to the range of the protons. The radiation dose rate is developed in parametric form as a function of the number and energy of incident mono-protons over the energy domain from 10 Mev to about 1000 Mev (Figure P-8) and of electrons over the energy domain from 10 kev to about 1000 kev (Figure B-8). These parametric curves of dose rate per incident particle versus the kinetic energy of the incident particle provide a flexible method for calculating

the total dose rate due to any assumed spectrum, by folding in the spectral distribution and intensity as the final step. For the case of protons, the maximum surface dose rate depends primarily on the total number of protons striking the surface, and only slightly on their energy, so long as their energy is sufficient for them to clearly penetrate the surface medium. Illustrative calculations are carried out for the Freden and White spectrum of protons and for the Walt et al. spectrum of electrons incident on thin-walled stainless steel vehicles carrying liquid H₂ or liquid O₂. The numerical results for O₂ would be closely similar to those for biological materials.

Arthur D. Little, Inc. Report No. 63270-02-01

ASTIA No. AD 266-034

Date: September 1961

OTS \$9.10

Title: The Space Environment and Its Interactions with Liquid Propellants
and Their Storage Systems

Author: Norman M. Wiederhorn

Abstract:

The storage of liquid propellants on the surface of the moon or in space vehicles, which are in orbit or interplanetary flight, presents a series of unusual problems. In view of this, NASA established a program to elucidate the problem areas and provide engineering approaches to their solution. Arthur D. Little, Inc., under Contract No. NAS5-664, has been participating in this program. Our objectives are to define the mechanisms that affect the storage of propellants, to investigate systems to obviate or minimize deleterious effects, and to determine the magnitude of losses and penalties associated with various systems. In order to accomplish

this, it is necessary to have a quantitative statement of those factors in the space environment that can produce significant effects in storage systems.

The following sections are devoted to a discussion of the pertinent factors of the space environment that influence the storage of liquid propellants in space and the mechanisms whereby these may interact with a liquid propellant or its storage system. In addition to this discussion, an extensive bibliography, including abstracts, is contained in this report. This bibliography provides a survey of the space environment, which is a prerequisite to the consideration and study of any interaction or effects which might occur in the environment of space.

Arthur D. Little, Inc. Report No. 63270-05-02

Date: September 1962 Office of Scientific and Technical Information
NASA
Attn: Code AFSS-AD
Washington, D.C. 20546

Title: The thermal and Ionizing Radiation Aspects of the Storage of
Self-Heating Liquid Propellants in Space

Author: Norman M. Wiederhorn and Jay H. Vreeland

Abstract:

This report emphasizes various potential problems related to the storage in space of high-energy liquid propellants and provides a method for obtaining meaningful answers regarding the significance of such problems. The methodology is set up and examples are worked out, from which it is often possible to draw general conclusions. In some instances, however, it will be necessary to repeat the calculations for the specific propellant of interest. The authors discuss the thermal aspect of problems

associated with the storage of such "self-heating liquids" on the basis of work concerned with earth storage conditions. They consider both homogeneous and heterogeneous reactions, as well as factors that may influence the behavior of propellants in a space environment. In particular, the report concerns an evaluation of the potential hazard posed by the energetic particulate radiations in space.

PART VII

ABSTRACTS OF REPORTS ON THE EVALUATION OF METEOROID
BUMPER PROTECTION SYSTEMS

VII. ABSTRACT OF REPORTS ON THE EVALUATION OF METEOROID
BUMPER PROTECTION SYSTEMS

The major portion of the theoretical work on the solution of the meteoroid problem has been conducted by McGill University, under sub-contract to Arthur D. Little, Inc., and detailed reports have been issued previously. The McGill University final report is in preparation and will be issued when available.

Arthur D. Little, Inc. Report No. 63270-03-01 ASTIA No. AD 273-236

Date: January 1962

OTS #3.60

Title: On the Impact of Pellets with Thin Plates Theoretical
 Considerations - Part I

Author: Gerald V. Bull

Abstract:

This note outlines the results of a short theoretical investigation into the impact of pellets with thin plates at very high velocities. In order to render the problem tractable to analysis, a model has been assumed which allows use of essentially one-dimensional theory to predict both the impact shock-induced conditions and the subsequent expansion flow, although the latter state has been treated subsequently as a general axisymmetric three dimensional flow. The problem has been considered in three phases.

The first phase is the shock-induced impact states, which for thin bumper plates permits one-dimensional theory to be reasonably applicable. Based on the concept of the strong shock wave, it is seen that the initial impact-induced states may be expressed readily in terms of impact velocities, initial density ratios, and the polytropic gas exponent in the shocked states.

The second phase as discussed in this note results from the extremely high temperatures generated on impact. The resultant radiative loss mechanisms result in considerable reduction in the thermodynamic states from which expansion occurs. Detailed treatment of this phase will appear in subsequent notes.

The third phase, the break up of the pellet into an expanding particle cloud, has been approached in this note from the restricted point of view of one-dimensional shock and rarefaction waves interacting with a cylindrical rarefaction. This non-stationary wave system tends to accelerate the outer-material, essentially redistributing the initial kinetic energy of the pellet. Only brief consideration into the boundaries of this flow has been made in the present note. Subsequent detailed treatment of the expanding flow phase will be presented in the near future.

Arthur D. Little, Inc. Report No. 65008-05-01

Date: June 1963

Office of Scientific and Technical Information
NASA
Attn: Code AFSS-AD
Washington, D.C. 20546

Title: Meteoroid Bumper Protection for Space Vehicles Tentative Design
Criteria

Authors: Reed H. Johnston, David A. Knapton and David Lull

Abstract:

In this report the authors present their initial attempt at pulling together some of the details which pertain to meteoroid protection and to present some of the very tentative information concerned with meteoroid protection in such a form that the engineering implications are more easily appreciated. The purpose of the report is to provide a perspective which

may aid the structure designer in evaluating and overcoming the meteoroid hazard - to facilitate communication among structure engineers, meteor physicists, and hypervelocity physicists to recognize areas where their contributions can provide the structure engineer with the information he must have to carry out a detailed design of the meteoroid protection systems. The authors direct their major attention in this report towards the design of meteoroid protection for spacecraft by means of "meteor bumpers". A description of the meteoroid environment is given along with the discussion of meteoroid bumpers and the physics of meteoroid bumpers. The reaction on the protected surface is described. Incorporation of the bumper in the vehicle design, structural considerations and conceptual designs are included.

Arthur D. Little, Inc. Report No. 65008-05-02

Date: August 1963

Office of Scientific and Technical Information,
NASA

Attn: Code AFSS-AD

Washington, D.C. 20546

Title: A Sequentially Interrogated Meteoroid Penetration Sensor

Author: Reed H. Johnston

Abstract:

Direct observation of penetration through skins of thickness comparable to that used in vehicle construction would require exposure of excessively large areas for unacceptably long periods. A compromise to the problem of obtaining reliable information on the hazard of meteoroid impact on large space vehicles is described in this report. This compromise consists of designing a sensor appropriate to the permitted payload in which the areas

of various exposed thicknesses are so chosen that one may expect the numbers of penetrations through the three or four different thicknesses to exhibit relatively small statistical variation. The author presents a detailed design of a sensor for obtaining data on meteoroid hazard appropriate for detecting a penetration through a sheet of exposed material as well as an alternate approach. Diagrams and illustrations are included.

Arthur D. Little, Inc. Report No. 65008-05-03

Date: October 1963 Office of Scientific & Technical Information
NASA
Attn: Code AFSS-AD
Washington, D.C. 20546

Title: On the Impact of Pellets with Thin Plates: Theoretical
Considerations - Part 2

Author: D. A. J. Miller, W. H. Friend and C. L. Murphy

Abstract:

The theoretical analysis of the impact of pellets with thin plates and the resulting expansion flow is presented in this report. The analysis is based on the impact model discussed in Part 1 of this report by Gerald V. Bull (Report No. 63270-02-01). The short-term expansion of the plasma, the interaction between shock and rarefaction waves and the long-term expansion are investigated in some detail. Engineering design data for the protection of a space vehicle from meteoroid impacts are presented on the basis of the theoretical calculations carried out on the impact model. Results of an experimental program designed to check the predictions of this theory are reported in a companion paper, 65008-05-04 (to be published). A brief sketch of the nature of the required changes is indicated at the conclusion of this paper.

In addition to the reports described above, Arthur D. Little, Inc., initiated a theoretical and experimental study on the effects of meteoroid-bumper debris on multilayer insulations. The purpose was to determine the mode of failure of the insulation when impacted by the debris and to determine the minimum spacing between the bumper and insulation, or "stand-off distance", that results in no damage to the insulation. Although we have not been able to conduct the experimental phase of the investigation during this period, we strongly recommend that the test program be conducted. Further details of this study are included in this report.